Comprehensive Analysis of Glomerular Endothelial Cell MicroRNA Expression to Identify Diabetic Kidney Disease Biomarkers

Melissa Jayne Thomas

Thesis presented for the Degree of Master of Philosophy (Medicine)

June 2020

Division of Infection & Immunity

School of Medicine, Cardiff University

Acknowledgements

Greatest thanks to my fiancé and parents for their endless encouragement, support, love, and guidance.

Thank you to my supervisors and members of the WKRU, and to KESS2 and BBI Solutions for funding this project.

Summary

In accordance with worldwide trends for obesity, physical inactivity and an ageing population, the prevalence of diabetes mellitus is predicted to continue rising. Of those affected, it is estimated that 40% will develop diabetic kidney disease (DKD) (Jha *et al.* 2013; Alicic *et al.* 2017). DKD is the leading cause of end-stage renal disease and is a major contributor toward increased mortality in diabetes patients (Jha *et al.* 2013). Detection of urinary microalbuminuria forms the basis of current DKD progression monitoring, but prognosis is complicated since not all microalbuminuric patients progress to overt nephropathy. Numerous biomarkers have been assessed for utility in DKD, but none have demonstrated the specificity and sensitivity required to predict individual DKD patient outcomes. MicroRNAs (miRs) are ubiquitously expressed short noncoding RNAs that regulate the expression of most protein coding genes in the human genome. Urinary miRs represent a promising novel source of non-invasive biomarkers, that are rapidly and precisely detected by RT-qPCR (Beltrami *et al.* 2015). Recently, Beltrami *et al.* (2018) identified elevated detection of urinary miR-126, miR-155 and miR-29b in DKD, and demonstrated increased miR-126 in conditioned medium from cultured glomerular endothelial cells (GEnCs) in response to conditions mimicking the *in vivo* DKD environment. The work described in this thesis expanded these observations by conducting TaqMan Low Density Array (TLDA) expression profiling of 377 GEnC miRs from the same *in vitro* DKD model. A number of differentially expressed cellular and extracellular miRs were identified in response to hyperglycaemia and tumour necrosis factor-alpha (TNF-α) treatments. *In silico* analysis revealed the enrichment of biological pathways involved in TGF-β signaling, regulation of collagen expression, and cytoskeletal modulation. Further work will be required to determine the relevance of these alteration in miR expression *in vivo*.

Word Count: 31,851

Publications relating to thesis

Thomas, M. J., Fraser, D. J., & Bowen, T. (2018). Biogenesis, Stabilization, and Transport of microRNAs in Kidney Health and Disease. Non-coding RNA, 4(4), 30. https://doi.org/10.3390/ncrna4040030

This review examines evidence for the hypothesis that signaling between nephron regions may be mediated by microRNAs and discusses the possibility that this signaling process might mediate pathological effects.

Table of Contents

List of Figures

List of Tables

List of Abbreviations

AGEs - Advanced glycation end products

Ago2 - Argonaute 2

BCA - Bicinchoninic Acid

cDNA - Complementary DNA

ciGEnC - Conditionally immortalized Glomerular Endothelial Cell

CKD - Chronic kidney disease

Ct - Threshold cycle

DCT - Distal convoluted tubule

DKD - Diabetic kidney disease

DMSO - Dimethyl Sulfoxide

ECM - Extracellular matrix

EDTA - Ethylenediaminetetraacetic acid

eGFR - Estimated glomerular filtration rate

ESRD - End stage renal disease

EV - Extracellular vesicle

FBS - Foetal bovine serum (FBS)

GAG - Glycosaminoglycans

GBM - Glomerular basement membrane

GEnC - Glomerular Endothelial Cell

GFB - Glomerular filtration barrier

GFR - Glomerular filtration rate

GO term - Gene Ontology Term

HDL - High-density lipoprotein

HK-2 - Human Kidney-2

hTERT - human telomerase reverse transcriptase

HUVEC - Human umbilical vein endothelial cell

IGF-1 - insulin-like growth factor 1

MiR - MicroRNA

MiRNP - MicroRNA ribonucleoprotein complex

mRNA - messenger RNA

NO - Nitric oxide

NTA - Nanoparticle Tracking Analysis

PBS - Phosphate buffered saline

PCT - Proximal convoluted tubule

PEC - Parietal epithelial cell

PECAM1 - Platelet And Endothelial Cell Adhesion Molecule 1

PKC - Protein kinase C

Pre-MiRs - Primary-miR

qPCR - Quantitative polymerase chain reaction

RAAS - Renin-Angiotensin-Aldosterone System

RNA - Ribonucleic acid

RNAase - Ribonuclease

ROS - Reactive Oxygen Species

RQ - Relative Quantification

RT - Reverse Transcription

SDC4 - Syndecan-4

SV60LT - Simian Virus large 40 tumour antigen

TGF-β - Transforming Growth Factor beta

TLDA - TaqMan Low Density Array

TNF-α - Tumour Necrosis Factor-alpha

VEGF - Vascular Endothelial Growth Factor

VEGFR2 - Vascular Endothelial Growth Factor Receptor 2

vWF - von Willebrand factor

Chapter 1 - Introduction

1.1 MicroRNAs

1.1.1 Overview of microRNAs

MicroRNAs (miRs) are short, single-stranded, non-coding RNAs, which post-transcriptionally regulate gene expression. MiRs were first identified in *Caenorhabditis elegans* in 1993 (Lee *et al.* 1993; Wightman *et al.* 1993) and have since been found in algae, viruses, plants, invertebrates, and vertebrates (Lee and Ambros 2001; Griffiths-Jones *et al.* 2008; Moran *et al.* 2017). MiRs play roles in a vast array of biological processes, including developmental timing, cell differentiation, proliferation, and apoptosis. Underlying their importance in maintaining homeostasis, disrupted miR regulation in humans can cause immune diseases, developmental disorders, cardiovascular diseases, and malignancies (Vasudevan 2012; Ha and Kim 2014).

Most commonly, miRs suppress messenger (m)RNA expression, through interactions with mRNA 3'-untranslated regions (3'-UTRs; Ha and Kim 2014). Some controversial findings have suggested that miRs may also activate gene expression (Vasudevan 2012).

1.1.2 MiR biogenesis, and mechanisms of action

The genomic DNA sequences giving rise to miRs are most often located within introns of protein-coding genes, but can also be found within the exons of genes, or within intergenic regions (Rodriguez *et al.* 2004). MiR sequences found within, and in the same orientation as the host gene, are transcribed along with the primary transcript by the same promoter (Rodriguez *et al.* 2004; Ying *et al.* 2010). Intergenic miR sequences are believed to be transcribed by their own promoters, although the workings behind this assumption are unclear (Lagos-Quintana *et al.* 2003; Rodriguez *et al.* 2004; Monteys *et al.* 2010).

MiR loci often occur in clusters, from which they may be co-transcribed. Post-transcriptional regulation also applies to the miR transcripts themselves, meaning that a given miR or cluster of miRs can be transcribed, with only certain miR transcripts reaching maturity, whilst the rest are suppressed. An example of this is the miR-100~let-7~miR-125 cluster. The three miRs are co-transcribed, but the let-7 miR is suppressed post-transcriptionally in embryonic stem cells and some cancer cells (Ha and Kim 2014).

Once transcribed by RNA polymerase II, the primary transcript derived from the miR encoding region is known as a pri-miR. Pri-miRs, generally exceed 200 nucleotides in length, but are cleaved into 60-70 nucleotide base long hair-pin precursor miRs (pre-miRs) by the microprocessor multiprotein complex, a dimer composed of RNAse III enzyme Drosha, and double-stranded RNA binding protein Pasha/DGCR8 (Ha and Kim 2014) (Figure 1).

Pre-miRs are exported from the nucleus into the cytoplasm by the protein Exportin-5. Once in the cytoplasm, pre-miRs are processed by another RNAse III enzyme known as Dicer. Dicer cleavage results in a miR/miR* duplex, approximately 22 nucleotides in length. This duplex consists of a guide strand and a passenger strand (denoted here by an asterisk). The passenger strand is degraded when the duplex divides, and the guide strand associates with several RNA binding proteins, including argonaute 2 (Ago2), to form the microribonuclear protein (miRNP) complex known as the RNA-induced silencing complex (RISC) (Ha and Kim 2014) (Figure 1).

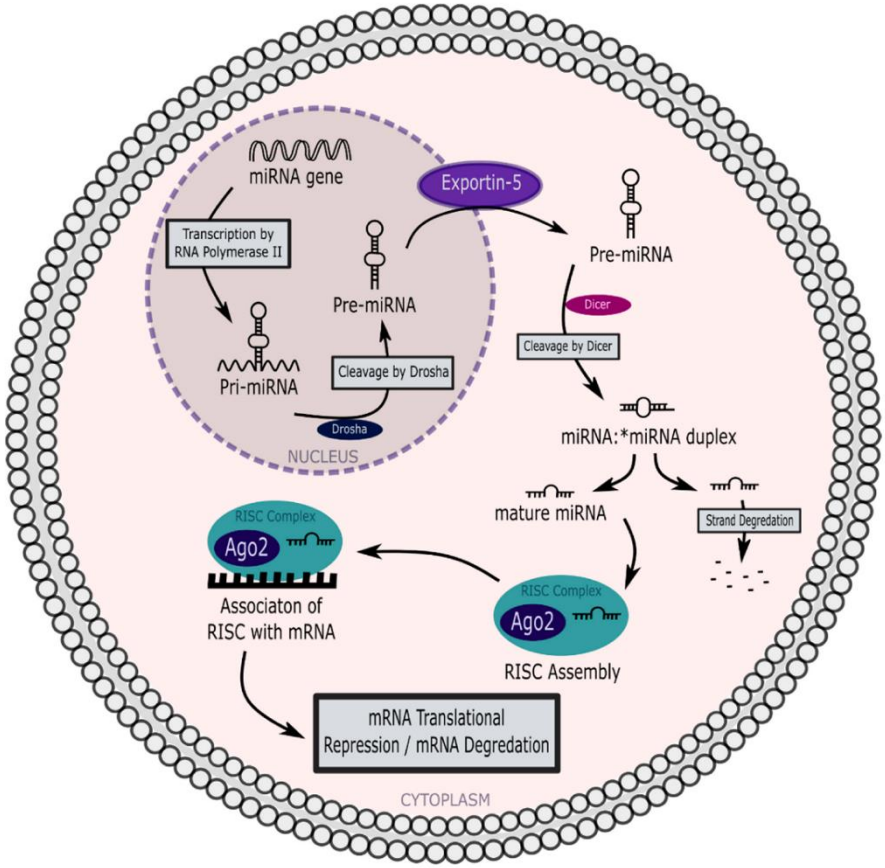

Figure 1: MicroRNA synthesis, and mechanisms of gene silencing. RISC - RNA-induced silencing complex. Ago2 - Argonatue 2. Image from Thomas *et al.* (2018)

The exact ways in which a miR silences a target gene are currently not fully understood (MacFarlane and R. Murphy 2010). A miR with full complementarity with its target mRNA is thought to employ a method of cleavage and subsequent degradation of the mRNA target as a means of silencing. MiRs will act as a guide, promoting the recognition of target mRNAs by the RISC complex. In the majority of cases, RISC recognition points are a sequence of 2-8 bases, present on the 3'-UTR of the target mRNA (Barutta *et al.* 2018). Most often, miRs are not fully complementary to their target mRNA, and so employ a method of translational inhibition to achieve the same outcome (MacFarlane and R. Murphy 2010). Although translational repression is usually followed by mRNA degradation, there are instances where a repressed mRNA can undergo translation re-activation (Barutta *et al.* 2018).

Interaction of miRs with their mRNA targets is dependent on a number of recognised factors, including the subcellular location of the miR, the ratio of miRs to their target mRNA strands, and the affinity of the miR to its target mRNA strand (O'Brien *et al.* 2018). A single miR can regulate hundreds of different gene transcripts, and can affect several cellular pathways (Trionfini *et al.* 2015).

1.1.3 MiR Cellular Release, Transport, and Uptake

Extracellular miRs have been reported in most bodily fluids, including blood, urine, cerebral spinal fluid, saliva, semen, and breast milk (Cogswell *et al.* 2008; Mitchell *et al.* 2008; Hanke *et al.* 2010; Kosaka *et al.* 2010; Wang *et al.* 2011; Gallo *et al.* 2012). However, methods of miR extracellular transport are not fully understood, and neither are the methods by which they protect themselves from degradation outside of their cellular origins.

Intracellularly, there is evidence that miRs are selectively shuttled between regions of the cell, to control specific mRNA expression (Makarova *et al.* 2016). Extracellularly, miRs may be transported in number of different ways (Figure 2). Valadi and colleagues (2007) were the first to discover the presence of miRs within exosomes released by mast cells. Since then, extracellular miRs have been reported as encapsulated within extracellular vesicles including exosomes and microvesicles; and in association with high density lipoproteins and Ago2 proteins (Thomas *et al.* 2018) (Figure 2). Some studies have also reported the release of miRs within apoptotic bodies (Bergsmedh *et al.* 2001).

MiR uptake following exosome and microvesicular mediated transport, and subsequent biological activity, has been demonstrated in numerous studies. However less evidence supports the uptake of miRs associated with HDL and Ago2 (Thomas *et al.* 2018).

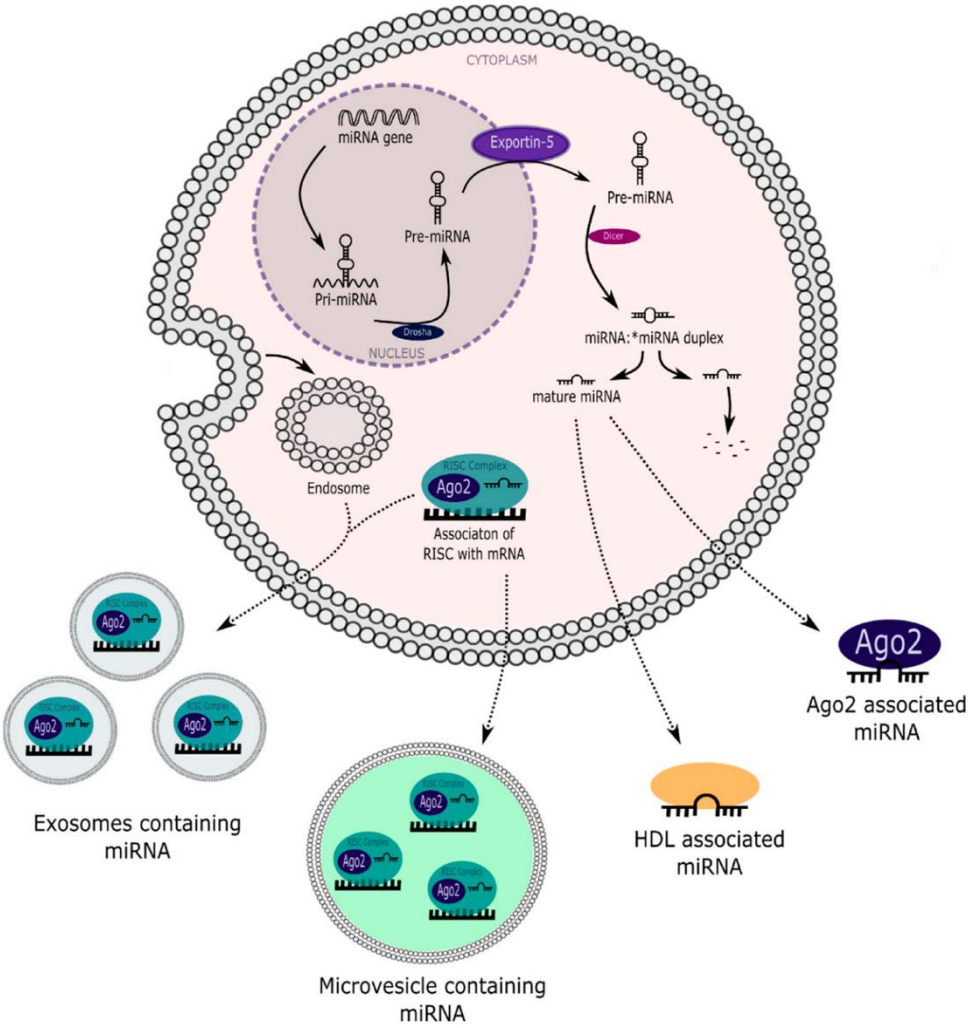

Figure 2: MicroRNA cellular release mechanisms. HDLs: high-density lipoproteins; pre-miRs: precursor miRs; pri-miRs: primary miRs. Image from Thomas *et al.* (2018).

1.2 The Renal System

1.2.1 Introduction to the renal system

The renal system in humans is comprised of the kidneys, ureters, bladder, and urethra (Chmielewski 2003). It is responsible for excretion of organic waste products from bodily fluids, and the elimination of these waste products from the body. The renal system also plays key roles in the maintenance of homeostasis, including fluid balance, pH regulation, and hormone production.

Urine is formed by the filtration of blood through the kidneys. Subsequently, urine is transported via peristalsis to the bladder, through hollow tubes of smooth muscle known as the ureters. The bladder is a spherical muscular organ, able to hold up to 500ml of urine in a healthy adult. Urine is temporarily stored in the bladder, until it's elimination from the body through the urethra (Chmielewski 2003).

Male and female renal systems vary in relation to the urethra. Males have an average urethral length of 22cm, along which four different regions are described in relation to their

location: the pre-prostatic urethra, prostatic urethra, membranous urethra, and spongy urethra. The female urethra is shorter, at approximately 5cm, and is not segmented according to anatomical position.

1.2.2 Anatomy and Physiology of the Kidney

The kidneys are a pair of bean-shaped vascular organs, located within the retroperitoneal space, either side of the spinal column. With respect to vertebral levels, the left kidney rests between T12 and L3, whereas the right kidney is situated slightly inferior due to displacement by the liver (Du *et al.* 2018). Both kidneys are angled between 30° to 50°, relative to the coronal plane (Sampaio 2000). In an average human adult-male, each kidney is approximately 12 cm in length, 6 cm in width, 2.5cm in thickness, and weighs between 120 to 170g (Chmielewski 2003).

Due to the highly vascularised nature of the kidneys, they require substantial protection. Each kidney is enclosed within a layer of fibrous connective tissue known as the renal capsule, which itself is covered by a protective layer of adipose tissue known as the renal fat pad (Sampaio 2000). Anchoring the kidneys to their surrounding structures is the renal fascia. The renal fascia is a dense fibrous layer of connective tissue which encapsulates the kidneys and their closely associated adrenal glands. The renal fascia itself fuses with the peritoneum, and muscles of the body wall. Additionally, the anatomical position of the kidneys below the ribcage offers further protection (Chmielewski 2003).

Internally, each kidney consists of an outer region known as the renal cortex, and an inner region known as the renal medulla. Extensions of connective tissue from the renal cortex into the renal medulla form structures known as renal columns. Renal columns separate the renal medulla into renal pyramids, and themselves provide a framework for the entry and exit of vessels into the cortex. A renal pyramid and its surrounding renal cortex is termed a renal lobe. The apex of each renal pyramid, known as a renal papilla, is where urine is emptied into a minor renal calyx. Minor calyces converge into major calyces, which further merge into the renal pelvis. Urine flows from the renal pelvis, into the ureter, and is transported to the bladder (Figure 3).

The renal hilium refers to the medial indentation of the kidney, which is the point of entry for the renal artery, lymphatics, and nerves; and the point of exit for the renal vein, lymphatics, nerves, and ureters (Figure 3).

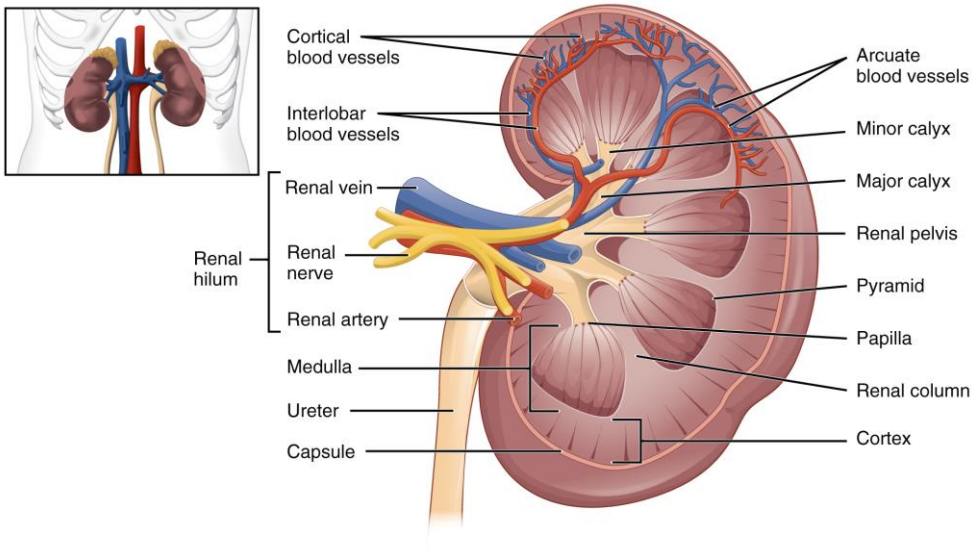

Figure 3: Illustrated diagram of left human kidney. Image from BC Faculty

The kidneys are heavily vascularised, receiving approximately 20% of total cardiac output (Chmielewski 2003). Blood arrives through the renal arteries (branching from the abdominal aorta) and exits through the renal veins (which lead onto the inferior vena cava).

1.2.3 Anatomy and Physiology of the Nephron, and associated components

The functional unit of the kidney is the nephron, which is a long tubular structure spanning the renal cortex and medulla. Nephrons function to filter the blood of waste and toxins, and maintain homeostatic balance of water and solutes. Each kidney contains approximately 1.3 million nephrons. Each nephron is comprised of the following regions: The Bowman's capsule, which is intimately associated with the glomerulus in the renal corpuscle; the proximal convoluted tubule (PCT); the loop of Henle; the distal convoluted tubule (DCT) and the collecting duct (Figure 4).

Blood is filtered as it passes though fenestrations in glomerular endothelial cells, followed by the glomerular basement membrane, and then between the foot processes of podocytes. The ultrafiltrate produced following this filtration passes sequentially through the sections of the renal tubule, with each section mediating its own selection of secretions and reabsorptions between the ultrafiltrate and the peritubular capillaries.

Two types of nephron exist: superficial cortical nephrons; and juxtamedullary nephrons. The former have their glomeruli in the outer cortex of the kidney, and have shorter loops of Henle; whereas the latter have larger glomeruli, present near the corticomedullary border, with longer loops of Henle which extend further into the medulla.

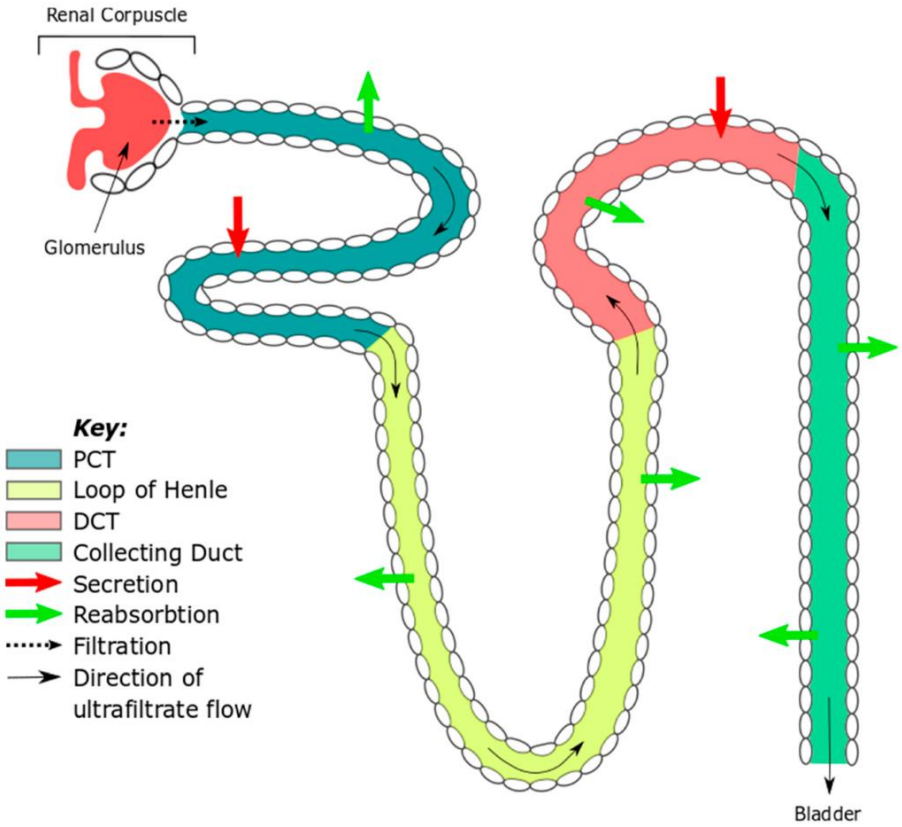

Figure 4: The nephron - the functional unit of the kidney. Colours are used to highlight each nephron domain. Direction of ultrafiltrate flow is shown with black arrows, bold arrows signify secretion of waste products (red) and solute reabsorption (green). PCT, proximal convoluted tubule; DCT, distal convoluted tubule. Image from Thomas *et al*. (2018).

1.2.3.1 The Renal Corpuscle, and the Glomerular Filtration Barrier (GFB)

The renal corpuscle consists of the glomerulus, and the Bowman's capsule (Figures 4 and 5). The glomerulus refers to the cluster of capillaries located at the cupped end of a nephron. The cupped end of the nephron itself is known as the Bowman's capsule. The renal corpuscle contains the three components of the glomerular filtration barrier (GFB): the glomerular endothelial cells, glomerular basement membrane, and podocytes (Figure 5). The glomerular filtration barrier as a whole is selectively permeable – allowing water and other small solutes through, but remaining relatively impermeable to larger molecules, such as the large protein albumin (Deen *et al.* 2001). The exact role of each GFB component is unclear, although it appears likely that their roles in size and charge filtration selectivity overlap, complementing each other to a large degree.

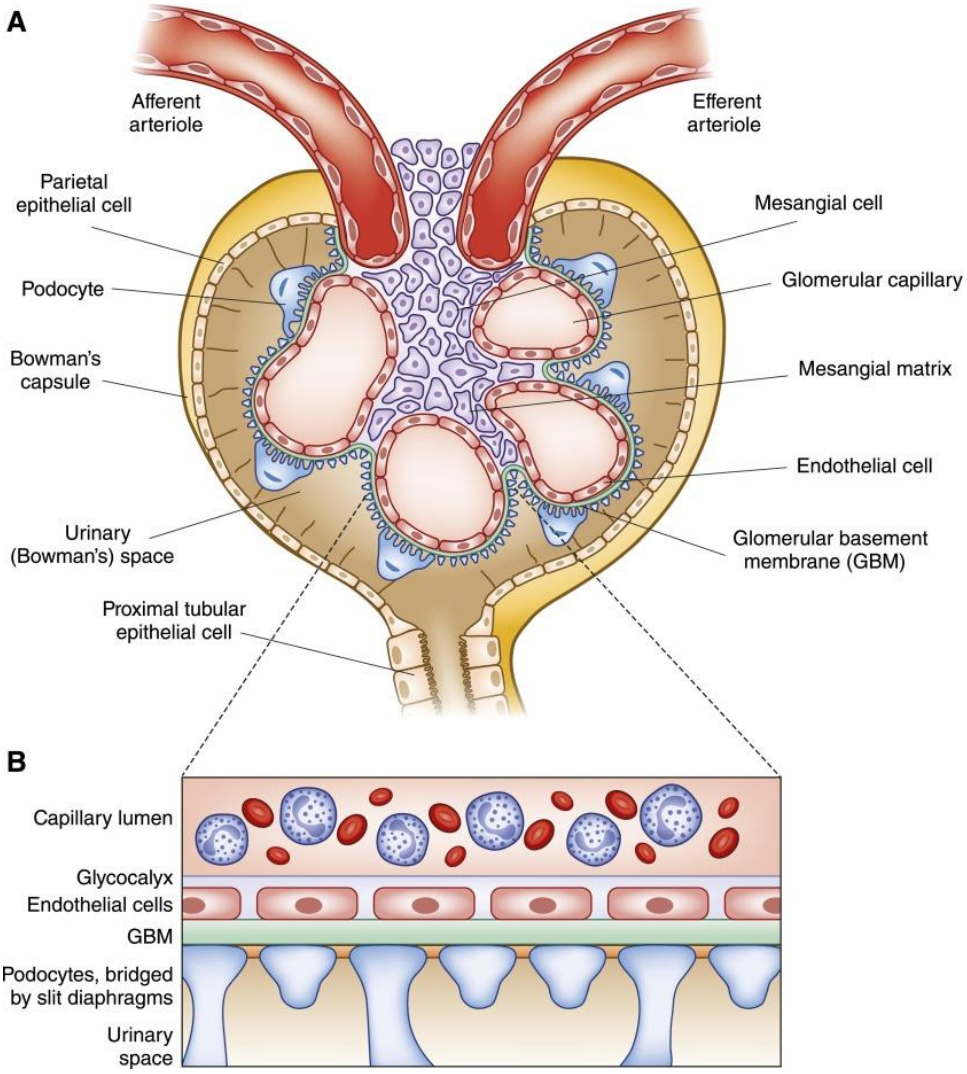

Figure 5: Illustration of the glomerular region and glomerular filtration barrier. A) Illustration showing renal corpuscle, with associated afferent and efferent arterioles. B) The glomerular filtration barrier, consisting of three components: the glomerular endothelial cells, glomerular basement membrane, and podocytes. Image from Kitching and Hutton (2016).

1.2.3.2 Glomerular Endothelial Cells

The luminal aspect of the glomerulus is lined by specialist endothelial cells called glomerular endothelial cells (GEnCs). GEnCs create a delicate fenestrated endothelial layer that forms the first barrier of the glomerular filter. GEnCs have specialised characteristics that allow them to function as highly efficient filters. Two key characteristics are i) GEnC fenestrations and ii) the glycocalyx.

GEnC Fenestrations

Fenestrations are transcytoplasmic holes through the endothelial cytoplasm that are found in organs requiring a high rate of exchange between intracellular and extracellular regions (Satchell and Braet, 2009) (Figure 6). Historically the study of GEnC fenestrations has been challenging due to a lack of suitable cell models and the necessity of electron microscopy

for their visualisation (Satchell and Braet, 2009). Current evidence suggests that GEnC fenestrations are unique when compared with other endothelial cell fenestrations due to the absence of a diaphragm and retention of basal lamina (Satchell and Braet, 2009).

Under homeostasis, fenestration of the GEnCs appear between 60 - 80nm in diameter (Satchell and Braet 2009). GEnC fenestrations are typically located away from the cell body, in the most attenuated regions of cell cytoplasm.

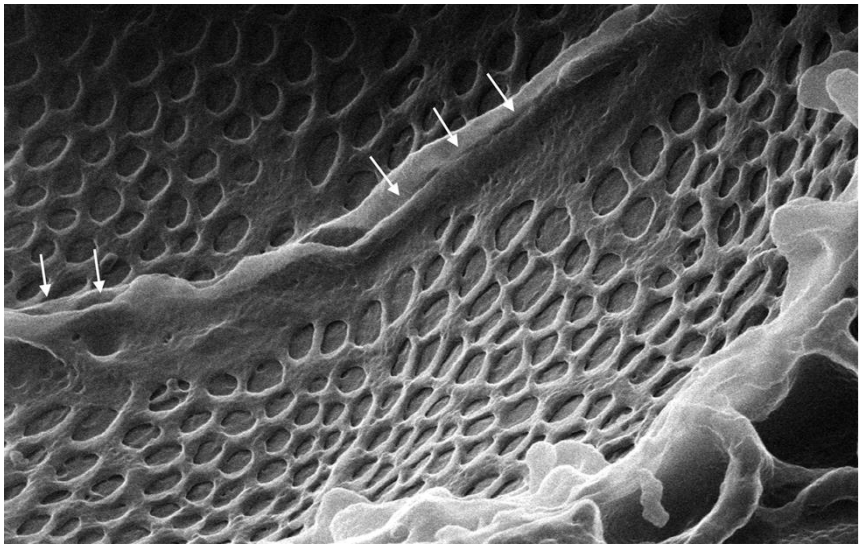

Figure 6: Luminal view of two adjacent rat GEnCs, showing circular fenestrations present over their entire surface area. White arrows signify location of tight junction between glomerular endothelial cells. Image obtained using high resolution helium ion scanning microscopy. Image adapted from Rice *et al.* (2013)

VEGF is thought to be the key inducer of GEnC fenestrations, and an essential component in their maintenance (Satchell and Braet 2009). VEGF signalling in GEnCs is believed to act through VEGF receptor 2 (VEGFR2), which is expressed early in their development and into maturity. It is thought to originate from nearby epithelial cells during GEnC development, and by podocytes throughout their maturity (Satchell and Braet 2009).

Since GEnC fenestrations are significantly larger than the size of circulating proteins, it was previously believed that GEnCs did not contribute directly to the filtration of macromolecules. This assumption was challenged when the GEnC glycocalyx was identified and its role in the filtration barrier's charge selectivity was recognised (Maezawa *et al.* 2015).

The GEnC Glycocalyx

GEnCs, and their fenestrations, are coated in a 200-400nm thick gel-like mesh called the glycocalyx (Singh *et al.* 2011). All endothelial cells possess glycocalyces, which vary in thickness and composition depending on vascular location (Alphonsus and Rodseth 2014). The glycocalyx can be described as a layer of membrane-associated proteoglycans,

glycosaminoglycans (GAGs), glycoproteins, glycolipids, and plasma proteins (Pries *et al.* 2000).

Proteoglycans consist of a protein core to which negatively charged chains of glycosaminoglycans are attached. Proteoglycans attached to the endothelial cell membrane form the core glycocalyx structure (Liew *et al.* 2017). Five types of GAG side-chains attach to proteoglycans. The most prominent GAGs present in the glycocalyx are heparan sulfate, which accounts for 50-90% of total GAG abundance, chondroitin sulphate, dermatan sulphate, keratin sulphate, and hyaluronic acid (Singh *et al.* 2011; Liew *et al.* 2017). Hyaluronic acid binds water molecules and is responsible for the viscous, gel-like nature of the endothelial glycocalyx. (Reitsma *et al.* 2007).

The endothelial glycocalyx is biologically inert, but interacts dynamically with plasma constituents such as proteins and soluble GAGs, which themselves are physiologically active (Alphonsus and Rodseth 2014). The layer of plasma constituents embedded in the glycocalyx is referred to as the endothelial surface layer, and these constituents are present in equilibrium with their respective plasma concentrations (Satchell and Braet 2009).

The glycocalyx functions in the regulation of endothelial cellular signalling, as well as playing a role in endothelial permeability. It also is a transmitter of sheer-stress information to endothelial cells, thereby playing an important role in the control of vascular tone (Liew *et al.* 2017).

The glycocalyx has recently been identified as a key factor mediating selectivity as part of the GFB. The negatively charged glycocalyx is at least partly responsible for the restricted passage through the GFB of anionic molecules relative to the passage of size-matched uncharged molecules (Jeansson and Haraldsson 2006). Jeansson and Haraldson (2006) performed a study injecting GAG-degrading enzymes into mice, demonstrating a resultant increase in clearance rates of the negatively charged protein albumin. The same study also demonstrated that degradation of the endothelial surface layer increased glomerular endothelial wall permeability to albumin, but not to Ficoll, which is equivalent to albumin aside from bearing a neutral charge (Satchell and Braet 2009).

GAG synthesis can also be disrupted by hyperglycaemic conditions, providing a potential link between high glucose conditions and glycocalyx dysfunction (Singh *et al.* 2011).

Glomerular Basement Membrane

The second ultrafiltration barrier exists in the form of a mesh of extracellular proteins and is known as the glomerular basement membrane (GBM) (Figure 7). The four main proteinaceous components associated with the GBM are type IV collagen, laminins, fibronectins, and proteoglycans (Pollak *et al.* 2014). The GBM is organised into three distinct layers: the lamina rara interna (on the endothelial side); the central lamina densa; and the

lamina rara externa (on the podocyte side) (Figure 7). Each layer contains its own complement of structural molecules.

GBM components are synthesised by both GEnCs and podocytes, and the fusion of basement membranes produced by both cell types accounts for the GBM being more than twice the thickness of other human basement membranes (Miner 2012; Marshall 2016). Any pathological changes that occur to the GBM are therefore attributable to either GEnCs, podocytes, or both (Marshall 2016).

The importance of the GBM as part of the GFB is still debated, although its contribution to the charge and size selectivity of the GFB is widely accepted. Supporting its size selectivity characteristics, laminin-β_2 deficient mice show greater GFB permeability, which is noteworthy given that laminin-β_2 is a crucial GBM component (Jarad *et al.* 2006). Charge selectivity is supported by studies measuring the passage of tracers across the GBM, demonstrating that a negative charge reduced the rate of tracer passage (Bohrer *et al.* 1978). The importance of the GBM as part of the filtration barrier is further evidenced by the effects of genetic abnormalities affecting GBM components. For example, homozygous mutants of Type IV collagen genes COL3A4 and COL4A4 cause a condition known as Alport syndrome (Pollak *et al.* 2014). Loss of effective type IV collagens result in a thinning of the GBM and typically result in end-stage renal disease (Haas 2009).

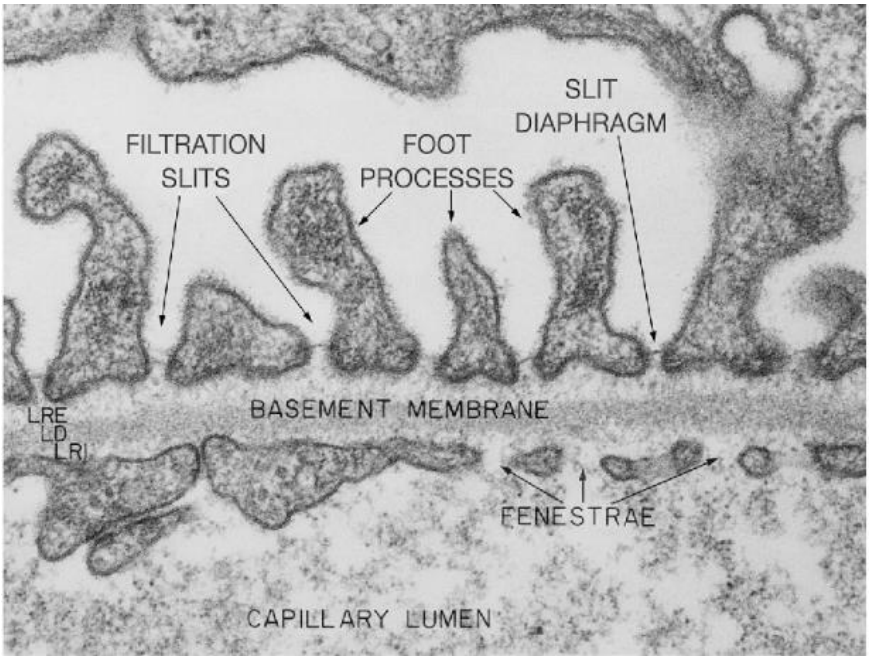

Figure 7: Electron micrograph of the glomerular filtration barrier, showing the three layers of the glomerular basement membrane. LRE= lamina rara externa; LD= lamina densa; LRI= lamina rara interna. Filtration slits, foot processes, and slit diaphragm each refer to podocyte components. Fenestrae refer to glomerular endothelial cell fenestrations. Image from Farquhar (2006).

1.2.3.3 Podocytes

The third and final barrier is formed by podocytes. Podocytes are specialised epithelial cells that rest on the GBM surrounding the glomerulus. The podocyte cell body branches out into several foot processes, which wrap themselves around the capillaries of the glomerulus (Pavenstädt *et al.* 2003) (Figure 8). The soles of these foot processes represent the podocyte's basal domain, and are fixed to the GBM. Between adjacent foot processes are filtration slits, which have a width of 30-40 nm (Pavenstädt *et al.* 2003). Ultrafiltrate must pass through these narrow filtration slits to enter the Bowman's capsule lumen (Pavenstädt *et al.* 2003). Podocytes are able to contract, narrowing the filtration slits, and thus reducing glomerular filtration rate (GFR; Arif and Nihalani 2013).

In disease, podocytes are susceptible to dedifferentiation along mesenchymal or epithelial pathways. Podocytes possess limited repair and regeneration abilities, and so their damage often leads to renal pathologies (Kitching and Hutton, 2016). There is limited evidence to suggest the exact role of podocytes as part of the filtration barrier, however the pathologies observed as a result of podocyte disruption point towards their critical importance. One of the first major studies to recognise the importance of podocytes in DKD pathology was that by Pagtalunan *et al.* (1997), which noted that reduced podocyte number correlated with albuminuria and a reduction in GFR in Pima Indians with type II diabetes. Since then,

numerous studies have also linked podocyte dysfunction with a range of pathologies, which have come to be known collectively as ‘podocytopathies’ (Singh *et al.* 2015).

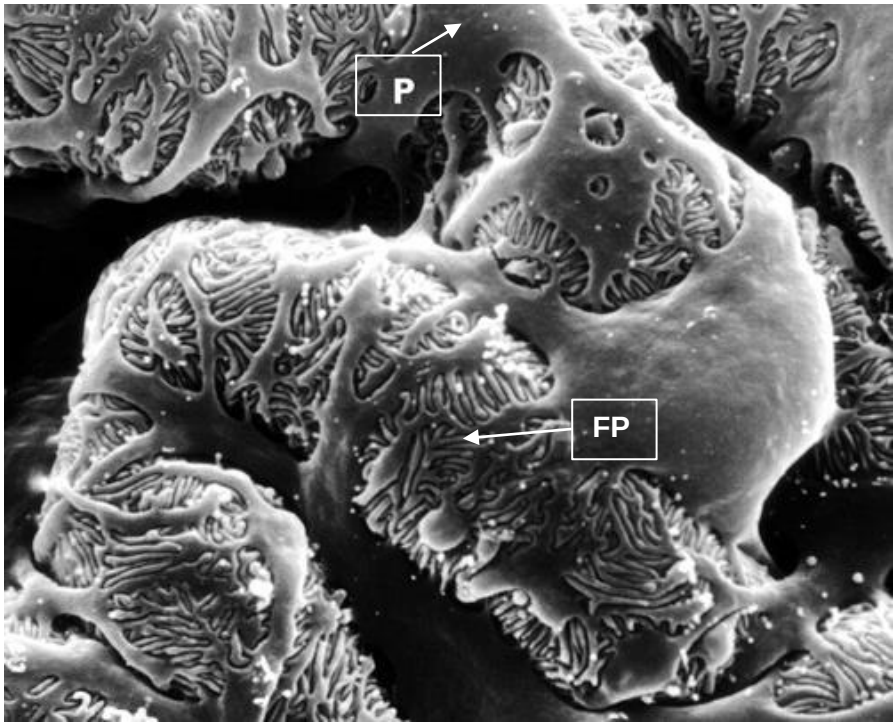

Figure 8: Scanning electron micrograph of rat glomerular capillaries. Urinary-side view, showing glomerular capillaries wrapped in podocyte foot processes. P=podocyte, FP= foot process. Image adapted from Pavenstädt *et al.* (2003).

1.2.3.4 Mesangial cells, and the mesangial extracellular matrix

Mesangial cells are also present in the glomerulus,, sitting between the glomerular capillaries and embedded in the mesangial extracellular matrix (ECM; Kurihara and Sakai, 2017) (Figure 5). Mesangial cells and their ECM contribute to the structural framework of the glomerulus, also providing a means of altering glomerular haemodynamic via cellular contraction and relaxation (Singhal *et al.* 1986; Kitching and Hutton, 2016). The healthy mesangial ECM contains a variety of components, including type III - VI collagens, heparin sulphate proteoglycans, and elastic fibre proteins including fibronectin and laminin. The composition of the ECM produced by mesangial cells changes in response to certain disease states, where certain disease stimuli result in ECM accumulation (Kitching and Hutton 2016). This disease state-specific mesangial ECM can also contain components not seen in the healthy state, such as collagen I (Pollak *et al.* 2014).

1.2.3.5 Glomerular parietal epithelial cells

Glomerular Parietal Epithelial Cells (PECs) form a monolayer which adheres to the urinary side of the Bowman’s capsule (Figure 5) (Gharib *et al.* 2014). PECs are derived from the same mesenchymal origins as podocytes, but unlike podocytes PECs maintain the ability to regenerate and proliferate (Kitching and Hutton, 2016). Some controversial evidence has suggested that PECs are able to differentiate into podocytes (Gharib *et al.* 2014; Miesen *et*

al. 2017). Activation of PECs through injury increases their migration, proliferation, and ECM production (Kuppe *et al.* 2019). Relative to other glomerular cells, comparatively little is known about the PECs (Ohse *et al.* 2009). The function of these cells remains unclear, with hypothetical roles including permeability barrier functions, albumin uptake in states of albumin overload, contraction, and mechanosensation (Ohse *et al.* 2009).

1.2.3.6 The renal tubule

Nephron segments distal to the renal corpuscle are referred to as the renal tubule. The renal tubule consists of the proximal convoluted tubule (PCT), the loop of Henle, the distal convoluted tubule (DCT), and the collecting duct system. The entire length of the nephron tubule is lined with tubular epithelial cells, which vary slightly between nephron regions while maintaining the general functions of secretion and reabsorbtion characteristic of the nephron tubule.

The PCT lies within the renal cortex in cortical nephrons, and near the corticomedullary border in juxtamedullary nephrons. The PCT is lined with simple cuboidal epithelial cells, which have brush borders that aid in the reabsorption of water and solutes, such as sodium chloride and sodium bicarbonate (Curthoys and Moe, 2014).

Tubular fluid passes from the PCT to the loop of Henle. The loop of Henle can be divided into two main sections: the descending limb, and ascending limb. Cortical nephron loops of Henle extend into the outer medulla of the kidney, whereas juxtamedullary nephron loops of Henle extend deep into the medulla (Figure 9). The loop of Henle functions as a counter current multiplier system, creating a high osmotic pressure in the medulla which promotes the reabsorption of water (Reeves *et al.* 2001).

The distal end of the loop of Henle joins with the DCT. The DCT is a short nephron segment that plays critical roles in the reabsorption of sodium chloride, secretion of potassium and maintaining physiological balance of calcium and magnesium (Subramanya and Ellison 2014). Several DCT functions are carried out through active transport. The epithelial cells of the DCT are rich in mitochondria, enabling sufficient ATP production for these active transport processes to take place (McCormick and Ellison, 2014).

Tubular fluid from the DCTs drains into a system of collecting ducts. Collecting ducts originate in the cortex, and extend into the medulla. Collecting ducts show varying permeability to water, relating to the concentration of antidiuretic hormone present, which is produced by the posterior pituitary gland in the brain in response to dehydration. An increased concentration of antidiuretic hormone increases the permeability of collecting ducts to water, and thus increases the reabsorption of water.

Urine exits the collecting ducts into the renal calyxes, then to the renal pelvis, and finally down the ureters to the bladder (Figure 3).

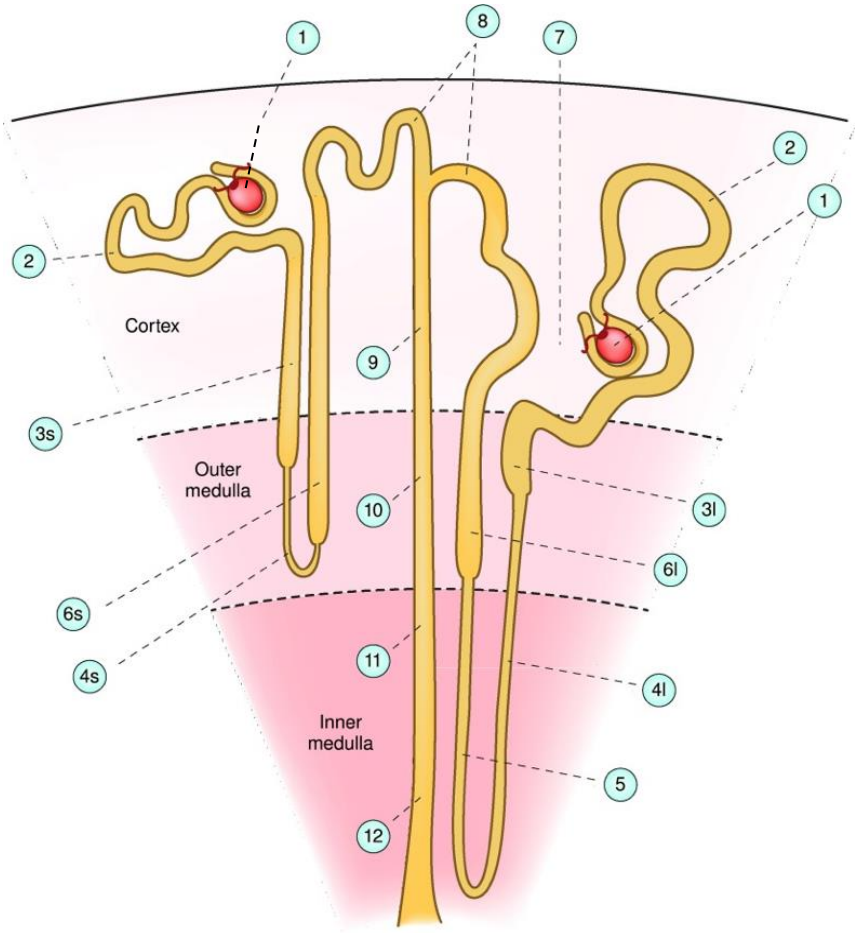

Figure 9: Illustration of cortical (left) and juxtamedullary (right) nephrons, demonstrating their locations relative to the renal cortex and medulla. 1) glomerulus; 2) proximal convoluted tubule; 3s) proximal straight tubule of cortical nephron; 3l) proximal straight tubule of the juxtamedullary nephron; 4s) thin descending limb of juxtamedullary nephron; 4l) thin descending limb of juxtamedullary nephron; 5) thin ascending limb; 6s) medullary thick ascending limb of cortical nephron; 6l) medullary thick ascending limb of juxtamedullary nephron; 7) macula densa; 8) distal convoluted tubule; 9) cortical collecting duct; 10) outer medullary collecting duct; 11) initial inner medullary collecting duct; 12) terminal inner medullary collecting duct. Image from Klein et al. (2011).

1.3 Communication between cells of the nephron

1.3.1 Evidence of intra-nephron communication

Multidirectional cross talk occurs between the various cells of the nephron. In this way it is believed that an initial insult to one cell type can cause nephron-wide disruption. Some instances of cell-to-cell communication in the nephron have been linked to a specific cellular mediator, but in most cases, the exact mechanisms of communication remain unclear. MiRs are however believed to be an important route of cell-to-cell communication within the nephron (Thomas *et al.* 2018).

On first consideration, it seems intuitive that intra-nephron communication can only occur in the direction of ultrafiltrate flow, from proximal to distal nephron cells. This concept has however been shown to be untrue in some cases. Despite high flow-through volume, the large surface area of the GFB results in relatively low flow velocity. Consequently, molecules can travel some distance in the opposite direction of ultrafiltrate flow (Haraldsson *et al.* 2008). This allows for paracrine communication between distal to proximal nephron cells, when these cells are in sufficiently close proximity (Haraldsson *et al.* 2008).

As well as paracrine communication, glomerular cells communicate through gap-junctions, for example between interdigitating mesangial cells and GEnCs in the paramesangial region of the capillary loop (Fu *et al.* 2015).

One of the best supported examples of communication within the nephron exists between podocytes and neighbouring renal cells. Podocytes release factors essential for the growth, survival, and maintenance of other nephron cells. For example, podocytes release vascular endothelial growth factor (VEGF) into the developing and mature glomerulus, which is essential for GEnC growth, development, and survival (Sison *et al.* 2010). This has been demonstrated in studies where inhibition of VEGF secretion by podocytes results in defective development of maturing GEnCs, and injury of mature GEnCs (Eremina *et al.* 2006). VEGF-A is the specific VEGF isoform secreted by podocytes, and interacts with receptors VEGFR-1 and VEGFR-2 expressed by GEnCs (Fu *et al.* 2015). VEGF secreted by podocytes is also thought to have an autocrine effect, with podocytes also being found in some studies to express VEGFR-1 and VEGFR-2 receptors (Chen *et al.* 2004; Guan *et al.* 2006; Bertuccio *et al.* 2011).

Studies have shown that podocyte VEGF secretion is also essential for mesangial cell differentiation, survival, and migration. Eremina *et al.* (2006) demonstrated a complete failure of mesangial cell differentiation in mice with podocyte specific VEGF-A knockdown. Podocyte injury also induces mesangial cell proliferation (Saleem 2015).

Podocytes also secrete a class of growth factors known as angiopoietins. Podocyte angiopoietin-1 signals to GEnCs, promoting their survival, reducing endothelial

permeability, and regulating VEGF mediated effects (Gale and Yancopoulos 1999; Thurston *et al.* 2000).

Podocytes are reliant on nearby cells for their maintenance and survival (Saleem 2015). In particular, molecular signals from GEnCs and mesangial cells are essential for normal podocyte function. Mesangial cell injury has been shown to result in podocyte effacement and podocyte fusion, suggesting a form of communication exists between them (Saleem 2015). Additionally, endothelin-1, a small peptide which acts as a potent vasoconstrictor, is released by GEnCs and is thought to act on podocyte endothelin ET_A receptors, inducing contraction of the actin cytoskeleton, and loss of slit diaphragm proteins such as nephrin (Dhaun *et al.* 2012). The release of ET-1 from GEnCs is also thought to act on mesangial cells to induce mesangial cell contraction (Marsden *et al.* 1991).

GEnCs and mesangial cells also communicate through the release of platelet-derived growth factor B (PDGF-B) from GEnCs, which bind to platelet -derived growth factor receptor β (PDGFRβ), present on mesangial cells. Evidencing this, endothelial specific PDGF-B knockout mice show glomerular defects related to lack of proper mesangial cell development (Bjarnegard *et al.* 2004).

Tubuloglomerular cross talk also occurs within the nephron, whereby the tubules and glomeruli exchange molecular signals. It is known for example that GFR can be altered in response to varying tubular salt concentrations and flow rates (Singh and Thomson 2010). It is also now understood that tubular injury predisposes the glomerulus to injury, and that GEnC injury can promote tubulointerstitial fibrosis and tubular cell inflammation (Ballermann and Obeidat 2014; Wang *et al.* 2018). It therefore appears that signals of damage can be communicated and transferred between the glomerulus and tubular cells.

In summary, considerable evidence supports cross-talk between cells within the nephron, and this communication is essential for the normal renal cell function. As yet unknown mediators of intra-nephron communication may help clarify some kidney disease pathological mechanisms, perhaps including DKD. One recently noted class of mediators with potential to signal within the nephron are miRs. The evidence behind miRs as molecular mediators of intra-nephron communication are discussed in the following section.

1.3.2 Evidence of miR mediated intra-nephron communication

To build a hypothesis for signaling between nephron regions may be mediated by miRs, several conditions should be fulfilled: (i) miRs must be released by upstream cells into the ultrafiltrate; (ii) these miRs must be packaged protectively to reach downstream cells intact; (iii) these packaged miRs must be taken up by downstream recipient cells without functional inhibition.

i) MiR release by upstream cells into the ultrafiltrate

As discussed in section 1.1.3, the miRs released by renal cells may be encapsulated within extracellular vesicles (EVs) such as exosomes or microvesicles, or may be associated with high density lipoproteins or Ago2 proteins (Figure 2) (Beltrami *et al.* 2015; Thomas *et al.* 2018).

Proteomic profiling of human urinary exosomes containing miRs have found miRs originating from each of the following nephron regions/cells: podocytes, PCT, the thick ascending limb of Henle, DCT, the collecting duct, and transitional epithelia from the urinary drainage system (Pisitkun *et al.* 2004; Keller *et al.* 2007; Knepper and Pisitkun, 2007; Gonzales *et al.* 2009). MiR-containing microvesicles isolated from human urine are believed to originate most often from podocytes, tubular cells, and epithelial cells lining the urogenital tract (Wang and Sun, 2014; Pomatto *et al.* 2017). There is also some evidence supporting the presence of non-exosome associated miRs within human urine. For example, Beltrami *et al.* (2015) described the presence of AGO2-associated miR-16 and miR-192 in human urine using RNA-immunoprecipitation.

ii) Protective packaging of miRs to reach downstream cells intact

The above evidence strongly supports the release of miRs by renal cells into the ultrafiltrate. The next required prerequisite for miR-mediated intra-renal communication is the functional protection of these miRs within the ultrafiltrate before reaching their proposed target cells. The ultrafiltrate and urine contain endogenous RNA-degrading ribonucleases (RNAses) that degrade unprotected miRs. Indeed, Beltrami *et al.* (2015) demonstrated rapid degradation of exogenous *Caenorhabditis elegans* cel-miR-39 when spiked into human urine, compared to endogenous miR-16.

Such protective mechanisms depend on the manner of miR association with stabilising structures. As well as a means of miR release, EV encapsulation offers a suitable means of protecting miR cargo from endogenous RNA-degrading ribonucleases (RNAses) within the ultrafiltrate and urine (Turchinovich *et al.* 2016; Lu *et al.* 2018; Sanz-Rubio *et al.* 2018). Ago2 association is also thought to confer protection to miRs within the ultrafiltrate. Beltrami *et al.* (2015) demonstrated the stability of Ago2 associated miR-16 and miR-192 in human urine, which was substantially reduced following proteinase-K treatment.

Given evidence of sufficient miR protection within the ultrafiltrate, it is reasonable to assume that miRs have the ability to reach downstream nephron cells intact, and therefore potentially functional. The next consideration is therefore their ability to enter a given target cell.

iii) Uptake of functional miRs by downstream recipient cells

EV uptake by cells is a well-recognised biological phenomenon. Binding to a target cell is directed by membrane protein composition and recipient cell surface receptors. Internalisation occurs through membrane fusion, or through a process of endocytosis (Montecalvo *et al.* 2012; Mulcahy *et al.* 2014). To date however, there is relatively little evidence to support the uptake of functional miRs by cells of the nephron.

Exosomes, a subtype of EVs, transfer functionally active miRs between numerous cell types including dendritic cells, smooth muscle cells, HUVECs, and dermal microvascular cells (Zernecke *et al.* 2009; Zhang *et al.* 2010; Montecalvo *et al.* 2012). With specific reference to the kidney, an *in vivo* experiment exposed collecting duct cells and proximal tubular cells to urinary exosomes isolated from healthy individuals, demonstrating uptake and functional action of the miRs contained within (Gracia *et al.* 2017).

Similarly, functional miRs have been found to be transferred by the EV subtype of microvesicles, for example between monocytes and microvascular endothelial cells (Zhang *et al.* 2010). An experiment by Cantaluppi *et al.* (2012) intravenously injected rats with miR-containing microvesicles from endothelial progenitor cells. These microvesicles were subsequently found localised to within the rats' tubular cells, and the miRs contained within were deemed to have been functional.

Some evidence also supports the uptake of miRs associated with Ago2 by endothelial and cancer cells (Ferreira *et al.* 2014; Prud'homme *et al.* 2016) However, no strong evidence supports the uptake of Ago2 associated miRs by renal cells.

A study by Vickers *et al.* (2011) demonstrated that hepatocytes cultured with high density lipoprotein (HDL)-associated miR-375 demonstrated an 11.8 fold increase in miR-375 expression, suggesting uptake of the HDL-associated miRs. However, a study by Wagner *et al.* (2013) showed that HDL-associated miRs were not taken up by endothelial cells, smooth muscle cells, or peripheral blood mononuclear cells *in vivo*. To date, no significant evidence exists demonstrating the uptake of HDL-associated miRs in renal cells.

1.4 Diabetes Mellitus

1.4.1 Overview of diabetes

Diabetes mellitus, more commonly referred to as diabetes, is a metabolic disorder characterised by an impaired ability to either produce or respond to insulin, and which subsequently leads to elevated blood glucose concentrations (Ang, 2018). The global prevalence of diabetes is currently rising, and is expected to be the 7th leading cause of human death by 2030 (Zhou *et al.* 2016).

Type I diabetes refers to a condition where the pancreas produces insufficient insulin, whereas type II diabetes occurs when the body becomes resistant to the insulin produced,

and eventually can also continue into a lack of insulin production due to pancreatic exhaustion. Type II diabetes accounts for approximately 90% of diabetes diagnoses, with predisposing risk factors including obesity and physical inactivity.

Diabetes was recognised as a pathology as early as 1500 B.C, when the ancient Egyptians noted increased urination and weight loss in certain individuals (Polonsky, 2012). Since then, research has contributed to a greater understanding of the disease. Indeed, a diagnosis of diabetes previously predicted death within months, since when prevention and treatment have improved significantly. The pancreas, which produces insulin, is undoubtedly the key player in the initiation of diabetes. However, it is now widely recognised that there are a wide range of contributors to the diabetic pathology including the liver, muscles, kidneys, brain, adipose tissue, and gut (Brunton, 2016). Despite advances, a cure for diabetes has remained elusive, and much still remains unknown of the mechanisms underlying the pathology of diabetes and related disorders such as diabetic kidney disease.

1.4.2 Glucose regulation in health, and in diabetes

To understand the pathophysiology of diabetes, one must first understand the process of glucose regulation in health. Plasma glucose is usually kept within a relatively strict physiological range. Plasma glucose concentration is determined by two factors: the rate of glucose entry into the circulation, and the rate of glucose uptake from the circulation. Glucose entry into the circulation is principally determined by intestinal absorption, glycogenolysis, and gluconeogenesis; whereas glucose removal from the circulation is principally determined by cellular respiration, glycogenesis, and de novo lipogenesis (Aronoff *et al.* 2004).

In the fed state, the rate of gastric emptying is the main determinant of how quickly glucose from the breakdown of food enters the circulation through intestinal absorption. Following absorption, glucose concentration increases, stimulating the release and production of additional insulin. Insulin is a peptide hormone secreted by the β-cells of the pancreas, which initiates a series of pathways that each ultimately lead to the removal of glucose form the circulation and therefore the re-establishment of glucose homeostasis. Insulin promotes three key processes: the uptake of glucose into skeletal muscle and adipose tissue; the initiation of glycogenesis in the liver; and the suppression of glucagon secretion from pancreatic α-cells. Insulin is not secreted until blood glucose concentrations reach levels of 3.4mmol/l, and is secreted in increasing amounts as glucose concentration increases above this (Aronoff *et al.* 2004).

Amylin is a second peptide hormone that is co-secreted with insulin, by pancreatic β-cells. The physiological effects of amylin are similar to that of insulin, in terms of their concurrent purpose of decreasing blood glucose levels. Amylin mainly works to suppress glucagon secretion, and to slow gastric emptying, thereby slowing the absorption of glucose (Aronoff *et al.* 2004).

In a fasting state, glucose is still removed from the circulation by metabolic processes, and so to maintain the required narrow plasma glucose concentrations there must be a source of glucose entry into the circulation. The rate of glucose entry into the plasma is determined mainly by processes occurring in the liver, known as glycogenolysis, and gluconeogenesis. Glycogenolysis refers to the breakdown of stored glycogen to produce free glucose; whereas gluconeogenesis refers to the formation of glucose from lactate and amino acids (Aronoff *et al.* 2004). Gluconeogenesis can also occur in the kidney, but only under state of severe starvation. During the first 8 to 12 hours of fasting, glycogenolysis is the primary method of glucose formation.

Both processes of glucose formation are initiated by the hormone glucagon, which is produced by the α-cells of the pancreas in response to low glucose concentration in the circulation. It is in this way that low glucose initiates a pathway leading ultimately to the release of glucose stores, and thus re-establishing glucose homeostasis.

The key pathology in diabetes types I and II is the lack of effective insulin availability. Therefore, when blood glucose increases following intestinal glucose absorption, there is no counter-action to promote the removal of glucose from the circulation. Additionally, a lack of insulin signalling prevents the suppression of glucagon, which allows the continuation of hepatic glucose production, further increasing blood glucose levels (Aronoff *et al.* 2004). Individuals with diabetes show impaired effective amylin production, which further compounds the effects of insulin deficiency (Scherbaum 2009).

1.5 Diabetic Kidney Disease

1.5.1 Overview of diabetic kidney disease

DKD is a diagnosis given to patients with chronic kidney disease (CKD) as a direct result of diabetes, which develops in approximately 40% of individuals diagnosed with diabetes (Alicic *et al.* 2017). DKD was not widely described until the 1920s, when the implementation of successful insulin therapy resulted in diabetic patients living long enough to develop secondary complications (Cameron, 2006). Diabetes is the biggest contributor of CKD and end-stage renal-disease (ESRD) in the developed world. Furthermore, amongst patients who do not develop end-stage renal-disease, mortality from other DKD-related pathologies such as cardiovascular disease and infections is high (Pourghasem *et al.* 2015; Alicic *et al.* 2017).

Reduction in kidney function causes a range of complications, including fluid retention, anaemia, calcium and phosphate balance disturbances, bone diseases, and cardiovascular diseases (Weiner, 2009). ESRD can be defined as an irreversible decline in renal function, necessitating dialysis or transplant for survival (Abbasi *et al.* 2010).

The two most influential DKD risk factors in diabetic patients are chronic hyperglycaemia, and hypertension. Strict and early control of blood glucose concentration is a key factor in

reducing the risk of developing DKD in patients with diabetes types I and II (The UK Prospective Diabetes Study, 1998). Studies have also shown that patients with diabetes type II have a 15% increased risk of developing impaired kidney function when they had baseline systolic blood pressure readings of greater than 140 mmHg (Bakris *et al.* 2003). Other risk factors such as sex, race, dietary factors, family history, and genetic susceptibilities have also been reported (Yip *et al.* 1993; Alicic *et al.* 2017).

Despite treatment to control modifiable risk factors including hyperglycaemia and hypertension, a large proportion of diabetic patients still go on to develop DKD (Nathan *et al.* 2013). A more complete understanding of DKD pathology will identify new treatment targets, improving treatment efficacy and patient outcomes.

1.5.2 Clinical Monitoring and Progression

In clinical practise, albuminuria and estimated glomerular filtration rate (eGFR) are the most commonly used variables to monitor DKD progression (Cao *et al.* 2019). Albuminuria refers to the presence of albumin protein in the urine. Due to its size, albumin is not ordinarily present in the urine at significant concentration. Albuminuria therefore signifies damage to the GFB. Microalbuminuria is defined as albumin urinary excretion of 30 mg–300 mg/day, macroalbuminuria is defined as total albumin urinary excretion of >500 mg/day (Allali *et al.* 2012).

eGFR is calculated using blood creatinine concentration, age, weight, height, and defined values based on sex and race. It is based on the filtration efficiency of creatinine, a waste product present in the blood.

Patients with DKD are typically described to progress through sequential stages of glomerular hyperfiltration, microalbuminuria, macroalbuminuria, declining GFR, and ultimately ESRD. However, in clinical practise the progression of DKD can be less straightforward, particularly with type II diabetic patients, with studies recording patients with declined GFR who did not previously display albuminuria (Nosadini *et al.* 2000; MacIsaac and Jerums, 2011). Furthermore, many patients have been shown to regress from a state of microalbuminuria to normoalbuminuria (Araki *et al.* 2005).

1.5.3 Structural changes that occur as a result of DKD

A series of structural changes are observed in the kidney during the progression of DKD. These are typically recognisable from two years following diabetes diagnosis (Lai *et al.* 2004). There is significant overlap in the structural changes observed under type I and type II diabetic conditions, although patients with type II diabetes tend to show more heterogeneity in terms of the changes observed. It is presently unclear whether this heterogeneity is due to the common co-morbidities seen in type II diabetic patients (e.g. obesity), or whether these discrepancies represent different disease processes (Pourghasem *et al.* 2015).

Several widely recognised classification systems exist for grading the histopathological changes occurring in DKD. One internationally recognised classification system proposed by the Renal Pathology Society groups DKD severity by the extent of glomerular lesions in the following way (Tervaert *et al.* 2010):

- class I: glomerular basement membrane thickening
- class IIa: mild mesangial expansion
- class IIb: severe mesangial expansion
- class III: nodular sclerosis
- class IV: global glomerulosclerosis in >50% of glomeruli

The following structural changes will be discussed in more detail: Thickening of glomerular and tubular basement membranes; mesangial cell expansion and Kimmelstiel-Wilson nodules; size and number of glomeruli, and podocyte injury.

Thickening of the glomerular and tubular basement membranes

Thickening of the GBM is widely agreed to be one of the first structural changes observed in DKD. GBM thickening is only visible using electron microscopy, and is caused by ECM accumulation (Najafian *et al.* 2011). The GBM may thicken to approximately twice its normal thickness in advanced DKD, and thickening increases linearly with disease duration (Drummond *et al.* 2003; Najafian *et al.* 2011) (Figure 10). GBM thickening correlates positively with the rate of albumin excretion and negatively with GFR in type I diabetic patients (Toyoda *et al.* 2007). Thickening of the GBM has been reported to predict DKD initiation in normoalbuminuric patients with type I diabetes (Caramori *et al.* 2013). Together with increased GBM thickness, tubular basement membranes also thicken in DKD (Najafian *et al.* 2011)(Figure 10).

ECM accumulation is central to basement membrane thickening. ECM levels are determined by a delicate balance between deposition and degradation, processes largely managed by endothelial cells and podocytes (Mason and Wahab, 2003; Rodriguez *et al.* 2008).

Mesangial cell expansion, and Kimmelstiel-Wilson nodules

The earliest structural change detectable by light microscopy in biopsy samples is expansion of the mesangium. As with GBM thickening, mesangial expansion is due to accumulation of ECM components, and is typically seen 4-5 years after the onset of type I diabetes (Najafian *et al.* 2011) (Figure 10). The progression of mesangial expansion is non-linear, with a rapid increase seen approximately 15 years following diabetes onset, and this therefore has been proposed as the main lesion type correlating with DKD severity (Mauer *et al.* 1984; Mauer *et al.* 1992; Drummond *et al.* 2003). In type I diabetic patients, mesangial

volume correlates positively with rate of albumin excretion and negatively with GFR (Toyoda *et al.* 2007).

As disease progresses, nodules of mesangial ECM may appear that are known as Kimmelstiel-Wilson nodules. These nodules develop in around 25% of patients with advanced DKD, typically developing approximately 15 years following the onset of diabetes (Tervaert *et al.* 2010). Mesangial nodules are formed as a result of two pathological occurrences in the glomerulus: mesangiolysis and the formation of capillary microaneurysms. Mesangiolysis refers to breakdown of the mesangial matrix and degeneration of mesangial cells; microaneurysms refer to dilations of the glomerular capillaries, often appearing as a ballooning of these vessels. The injury caused as a result of these two occurrences, and subsequent attempts at repair, lead to the formation of Kimmelstiel-Wilson nodules (Alpers and Hudkins, 2011).

Podocyte injury

Podocyte loss, whether through detachment or apoptosis, is also a key structural feature of DKD (Najafian *et al.* 2011) (Figure 10). Electron microscopy visualises the effacement of podocyte foot processes in DKD, a process in which regions of the foot processes becoming flattened and lose their overall structure. Electron microscopy also reveals regions of GBM that have been stripped of their previously overlying foot processes (Najafian *et al.* 2011). Critically, podocytes display limited capacity for repair and regeneration (Najafian *et al.* 2011). The widths of podocyte foot processes correlate positively with albumin excretion rate, and negatively with GFR in type I diabetic patients (Toyoda *et al.* 2007). In type II diabetic patients with microalbuminuria or proteinuria the number and density of podocytes are decreased when compared with healthy controls (Najafian and Mauer, 2009). Reduction in podocyte numbers in type II diabetic patients also correlates with albuminuria and GFR decline (Pagtalunan *et al.* 1997).

Size and number of glomeruli

The size and number of glomeruli is also a factor associated with DKD progression, although it is unclear whether it is associated with a predisposition towards DKD or occurs as a result of DKD. A study comparing the number of glomeruli between type I diabetic patients at varying levels of disease progression found that patients with no or mid-severity DKD had the same number of glomeruli as matched healthy controls. However, patients with severe DKD had significantly fewer glomeruli than matched healthy controls (Bendtsen and Nyengaard 1992). The authors concluded that this could be due to a loss of glomeruli occurring as part of the DKD disease progress, or that type I diabetic patients starting with a lower number of glomeruli are more susceptible to the development of severe DKD (Bendtsen and Nyengaard 1992). Another study found that patients with larger glomeruli were more likely to develop DKD within fewer years of diabetes onset (Bilous *et al.* 1989).

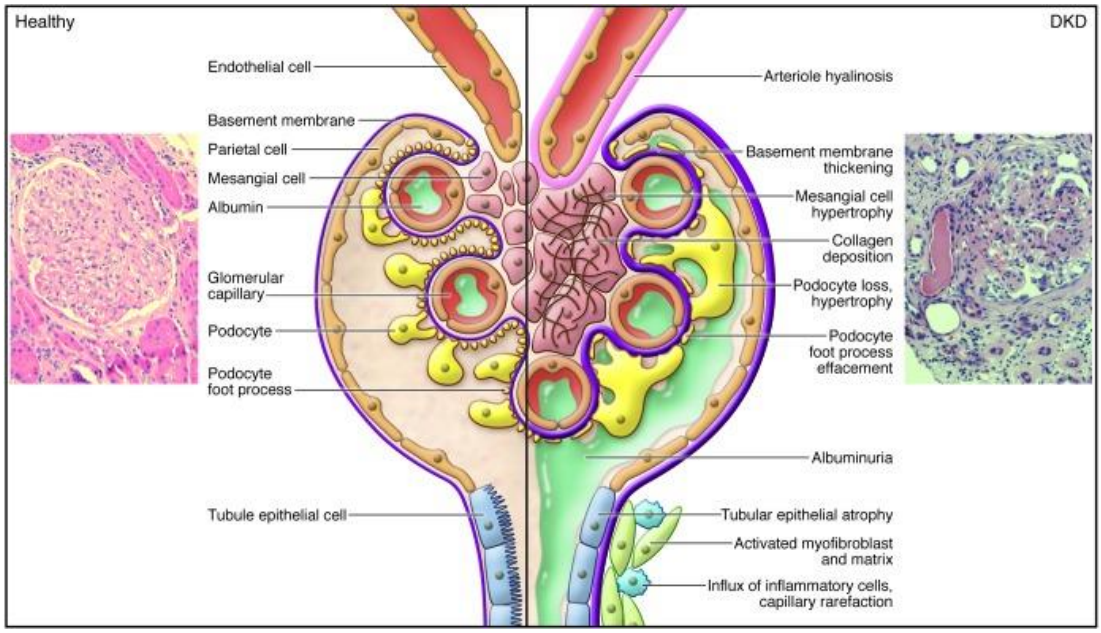

Figure 10: The effects of DKD on the renal corpuscle Reidy *et al.* (2014)

1.5.4 Pathogenic mechanisms of DKD

No complete picture of the specific cells, mediators, and timelines involved in the initiation and progression of DKD pathology currently exists. However, a substantial body of evidence suggests that hyperglycaemic insults experienced by GEnCs and podocytes are critical initiating factors. As described above, communication occurs between different cell types within the nephron. Therefore, an insult to one cell type may indirectly lead to insult of another cell type. This often results in a cycle of cellular damage, progressing the rate of renal function decline (Fu *et al.* 2015). Early detection and treatment are therefore critical clinical aims. It is conceivable that the known cellular and molecular mechanisms described above occur simultaneously, and form feedback loops of ongoing injury.

Central to the pathogenesis of DKD is the deleterious effect of hyperglycaemia on various kidney cells. DKD is most often observed in patients who have suffered with long-term diabetes and have a history of poor blood glucose level control. Broadly, the recognised factors associated with DKD pathology are haemodynamic, metabolic, or inflammatory in nature.

Chronically elevated serum glucose concentrations lead to a multitude of molecular changes that reportedly contribute to the development of DKD including the generation of advanced glycosylation end-products (AGEs), oxidative stress-induced cellular injury, RAAS overactivation, induction of inflammatory and fibrotic mediator production, and altered metabolic pathways (Barrera-Chimal and Jaisser, 2020).

The effects of hyperglycaemia can be seen long after normoglycemic conditions have been restored, for example in diabetic retinopathy. This demonstrates the lasting impact of

hyperglycaemic changes, which may be mediated by epigenetic changes resulting from high glucose concentrations (Anders *et al.* 2018).

Some of the key metabolic and hemodynamic factors believed to be initiation DKD factors are discussed below:

Overactivation of Protein Kinase C (PKC)

During states of hyperglycaemia, cells shuttle excess glucose into the hexosamine pathway, one of the final products of this pathway is the essential protein kinase C (PKC) co-factor. PKC is a serine-threonine kinase, which mediates a wide range of intracellular communications (Schrijvers *et al.* 2004). PKC activation induces expression of a range of genes relevant to DKD pathology including those encoding TGF-β, VEGF, collagen, fibronectin and nuclear factor-κB (NF-κB) (Brownlee, 2001; Trushin *et al.* 2003; Schrijvers *et al.* 2004; Tossidou *et al.* 2009).

Advanced Glycosylation End-products (AGEs)

In hyperglycaemia, excess glucose binds proteins through a non-enzymatic reaction. These glucose-bound proteins are initially reversible early glycosylation products, but later become irreversible advanced glycosylation end-products (AGEs) (Kobrin 1998). AGEs are formed at rates directly proportional to glucose plasma concentrations, and occur both extracellularly and intracellularly (Lapuz, 1997; Conserva *et al.* 2013). Extracellularly, AGEs bind ECM proteins, preventing their degradation and leading to their build-up (Conserva *et al.* 2013). Intracellularly, AGEs bind to cellular receptors, consequently altering levels of certain cytokines, growth factors (for example TGF-β), free radicals, and modifying biologically important proteins (Lapuz, 1997; Conserva *et al.* 2013).

In rats with streptozotocin-induced diabetes, staining for AGEs was found to be increased in the glomerulus, with particular concentration within the GEnCs (Soulis *et al.* 1997).

AGEs cause increased expression of ECM genes, mesangial expansion, and the upregulation of TGF-β1 in non-diabetic mice and rats (Vlassara *et al.* 1992; Striker and Striker, 1996). Cellular cultures of GEnCs and mesangial cells have demonstrated that AGE-rich proteins have the ability to increase PKC activity, TGF-β1 expression, and the expression of genes encoding ECM proteins (Ziyadeh *et al.* 1998; S Chen *et al.* 2001; Su *et al.* 2017). A study by Chen *et al.* (2001) demonstrated how PKC signalling, and consequent TGF-β1 activation, stimulated GEnCs incubated with glycated-albumin to increase basement membrane collagen production. PKC was also shown to reduce the proliferative capacity of GEnCs (Sheldon, Chen *et al.* 2001).

In terms of clinical relevance, serum AGE levels predict early morphological renal damage associated with DKD (Berg *et al.* 1997).

Formation of reactive oxygen species

Hyperglycaemic conditions also increase intracellular reactive oxygen species (ROS) via dysregulation of the electron transport chain. ROS promote AGE formation, which further increase ROS accumulation in a feedback loop (Dieter *et al.* 2015). ROS activate PKC and transcription factor NF-κB, which mediate their own fibrotic and inflammatory effects. Additionally, the oxidative stress caused by the ROS formation has been proposed as one of the primary insults leading to DKD (Brownlee, 2001; Forbes and Cooper, 2013). The effects of ROS accumulation include oxidative stress, damage to proteins and DNA, and cell death. In renal cells, this results in kidney fibrosis and decline in renal function (Badal and Danesh, 2014).

Renin-Angiotensin-Aldosterone System (RAAS) overactivation

In addition to metabolic factors, haemodynamic factors also contribute to the development of DKD. One of the key haemodynamic factors is overactivation of the renin-angiotensin-aldosterone system (RAAS) (Velez, 2009). Chronic RAAS activation leads to increased intraglomerular pressure and causes tissue injury, fibrosis, inflammation, and the generation of ROS (Sochett *et al.* 2006; Mauer *et al.* 2009).

Glomerular Hyperfiltration:

Hyperglycaemia causes dilation of afferent arterioles directly, through inducing the release of vasoactive mediators such as insulin-like growth factor 1 (IGF-1), glucagon, nitric oxide (NO), VEGF, and prostaglandin (Lin *et al.* 2018).

Dilation of the afferent arterioles occurs through the effect of hyperglycaemia on tubular reabsorption rates. Hyperglycaemia induces the upregulation of sodium glucose cotransporter 2 (SGLT2) in the proximal tubules, resulting in increased reabsorption of glucose and sodium chloride. With decreased sodium chloride concentration reaching the macula densa cells of the distal tubules, dilation of the afferent arterioles occurs through a process of tubuloglomerular feedback (Tuttle, 2017). The combination of afferent arteriole vasodilation, and efferent arteriole vasoconstriction result in glomerular hypertension. Glomerular hypertension is believed to be the cause of glomerular hyperfiltration (Tonneijck *et al.* 2017).

Endothelial dysfunction is also thought to contribute to glomerular hyperfiltration. Endothelial cell injury is a major event in diabetes that leads to a host of cellular and molecular disruptions. In summary, hyperglycaemia, insulin resistance, and the complementary process of hyperinsulinemia are all known to cause endothelial dysfunction by mediating increased endothelial ROS production, activation of PKC, and production of advanced glycation end-products (Lin *et al.* 2018). These intracellular factors disrupt the normal biological processes of endothelial cells. In particular, hyperinsulinemia increases

endothelial cell production of endothelin-1, which is a potent vasoconstrictor causing glomerular constriction.

Inflammation

As discussed above, a number of processes initiated by chronic hyperglycaemia result in the initiation of an inflammatory response. One of the key inflammatory mediators in DKD is tumour necrosis factor-alpha (TNF-α). TNF-α is a pro-inflammatory cytokine, produced by macrophages and renal cells including podocytes, mesangial cells, epithelial cells and endothelial cells (Baud and Ardaillou, 1995).

The detrimental effects of TNF-α in the kidney were first described by Bertani and colleagues (1989) when they injected rabbits with TNF-α and noted the presence of inflammatory cells in the kidney, glomerular endothelial damage, and renal fibrin deposition within glomerular capillary lumens. Damage to the GEnCs was dose-dependent (Bertani *et al.* 1989).

We now know that TNF-α mediates a range of DKD responses, including the recruitment of inflammatory cells and enhanced GEnC adhesion, disruption of the glomerular permeability barrier, disruption of haemodynamic balance by stimulation of vasoconstrictive and vasodilatory factors and the induction of apoptosis in a range of cells including GEnCs (Topley *et al.* 1989; Kusner *et al.* 1991; Gómez-Chiarri *et al.* 1993; Baud *et al.* 1994; Soler *et al.* 1996; Mccarthy *et al.* 1998).

The release of TNF-α within the glomerulus is amplified by formation of ROS, platelet activating factors, or by the deposition of terminal complement proteins (C5b-9) (Baud and Ardaillou, 1995). In contrast, prostaglandins, and interleukins IL-6 and IL-10 dampen glomerular TNF-α secretion (Baud and Ardaillou, 1995).

1.6 Urinary miRs in diabetic kidney disease

1.6.1 The potential of urinary miRs in DKD

As discussed above, the most common clinically used measurements of DKD progression are albuminuria and eGFR. Both these measurements have their limitations, however. Studies have reported the absence of albuminuria in diabetic patients (Huang 2017) prior to onset of GFR decline, and albuminuria cannot identify which patients will progress to ESRD (Nosadini *et al.* 2000; Araki *et al.* 2005; MacIsaac and Jerums, 2011; Cao *et al.* 2019). Additionally, many patients regress from microalbuminuria to normoalbuminuria (Araki *et al.* 2005). Furthermore, eGFR calculations are often unreliable in the elderly due to increasing comorbidities (Odden *et al.* 2009).

Therefore the shortcomings of current prognostic/diagnostic methods means that an unmet need still exists for a biomarkers that can accurately predict the onset, and monitor the progression of, DKD.

Urinary miR biomarkers are of particular interest in the context of kidney disease, given the renal origin of urine. Additionally, urine samples can be obtained easily and safely, without pain, and at lower cost that blood samples (Jing and Gao, 2018). Such information would allow for the stratification of patients, and could be used to better inform treatment options and better distribute healthcare resources.

MiRs show aberrant expression profiles in a range of human conditions including cancers, viral infections, cardiovascular diseases, neurodegenerative diseases, diabetes, and kidney injury (Lawrie, 2013; Wang *et al.* 2016). Critically important in terms of their biomarker potential, miRs are excreted extracellularly, and appear present at detectable, stable concentrations within a range of body fluids including blood, urine, and saliva (Huang, 2017).

MiRs are present within human urine. MiR profiles in human urine are stable in health, and change under disease conditions (Nascimento and Domingueti, 2019). Urinary miRs show great potential as biomarkers in conditions ranging from urological cancers to cardiovascular disease (Mlcochova *et al.* 2015). Selected studies investigating urinary miRs as biomarkers of DKD are discussed below.

In previous work from the host laboratory for this study, Beltrami *et al.* (2018) profiled 754 miRs from DKD patient urine, and compared these to urine from healthy controls. Numerous miRs were upregulated in urine from DKD patients, among them were miR-126, miR-155, and miR-29b, demonstrating fold increases of 2.8, 1.8, and 4.6 respectively (Beltrami *et al.* 2018). Jia *et al.* (2016) also reported upregulated miRs associated with DKD pathology, and demonstrated a positive association between urinary miR-192 and increasing albuminuria in patients with type II diabetes.

Argyropoulos *et al.* (2013) conducted a longitudinal study of urinary miRs in patients with type I diabetes with varying levels of albuminuria. At the beginning of the study, those patients with persistent moderate to severe albuminuria showed reduced levels of miR-323b-5p, and increased levels of miR-122-5p and miR-429 compared with those patients with intermittent albuminuria of the same severity. In addition, the onset of moderate to severe albuminuria was associated with decreased levels of miR-323b-5p and increased levels of miR-429. Furthermore, nine miRs: miR-619, miR-486-3p, miR-335-5p, miR-552, miR-191, miR-1224-3p, miR-424-5p, miR-141-3p and miR-29b-1-5p showed increased expression in urine. Decreased urinary miR-221-3p was also detected in patients who developed DKD compared with those who did not develop the condition.

Another longitudinal study by Argyropoulos *et al.* (2015) compared expression profiles of 723 urinary miRs in patients with normoalbuminuria who went on to develop microalbuminuria with those who retained normoalbuminuria. Eighteen miRs were found to be associated with the development of microalbuminuria, including miR-105-3p, miR-1972, miR-28-3p, miR-30b-3p, miR-363-3p, miR-424-5p, miR-486-5p, miR-495 and miR-548-3p.

Zang *et al.* (2019) analysed 87 exosomal miRs from the urine of patients with type II diabetes and DKD, and compared results with age and gender matched controls from the urine of type II diabetic patients with normal renal function. This study reported significantly upregulated urinary miR-21-5p, miR-let-7e-5p and miR-23b-3p in the urine of type II diabetic patients with DKD compared to those with normal renal function. In contrast, miR-125b-5p expression was significantly downregulated under the same conditions.

Xie *et al.* (2017) also quantified exosomal urinary miRs and compared miR abundance between patients with type II diabetes who either had macroalbuminuria, or who did not have renal disease. The results of this study showed upregulation of miR-362-3p, miR-877-3p, and miR-150-5p, and downregulation of miR-15a-5p.

A significant proportion of studies investigating urinary miRs have focused exclusively on exosomal miRs. This method of study potentially overlooks the contribution of other miRs, such as those which are Ago2-bound. Another limitation of studies in this area are the generally low sample sizes, typically under 100 patients. This reduces result reliability, and is another potential reason why results from studies appear inconsistent.

1.6.2 Previous research highlighting GEnCs as source of miRs mediating DKD pathology

A very recently study by Hill *et al.* (2020) used fluorescence tracking to demonstrate the transfer of EVs containing miRs from GEnCs activated by high glucose or inflammatory conditions to podocytes. The uptake of EVs altered the cellular expression of 48 podocyte genes, demonstrating functionality of the EVs' genetic contents. EVs released by treated GEnCs altered podocyte gene expression significantly more than those from untreated GEnCs. Podocytes treated with EVs from both GEnCs treated with high glucose, and

GEnCs treated with inflammatory stimuli, showed a number of unique gene expression changes not present in podocytes treated with a singular type of EV. In addition to mRNA changes, miRs were differentially expressed in podocytes treated with EVs from treated GEnCs. EVs from GEnCs activated genes leading to increased mitochondrial stress, which subsequently increased ROS production. In addition, podocytes exposed to activated GEnC EVs demonstrated reduced VEGF secretion, and a signs of cytoskeletal injury. This study attributed mediation of reduced podocyte VEGF secretion to miR-200c-3p within the activated GEnC EVs. Interestingly, GEnCs treated with either the high glucose concentration or inflammatory stimuli released a similar number of EVs as untreated GEnCs, and those EVs contained a similar RNA concentration. However, EVs from GEnCs treated with high glucose concentrations did contain higher concentrations of protein.

Previous work from the host laboratory has also suggested the involvement of GEnC miR secretion in the pathology of DKD. Following findings of increased urinary miR-126, miR-155, and miR-29b in patients with DKD, Beltrami *et al.* (2018) sought to determine the potential source of these miRs within the nephron. Laser capture microdissection of renal biopsies were followed by RT-qPCR analysis, to determine the abundance of miRs in different regions of the nephron. This analysis revealed the presence of miR-155 in the glomeruli, proximal distal tubule, and distal tubules, whilst miR-126 and miR-29b were most abundant in glomerular extracts. Subsequent cell culture experiments demonstrated miR-126 and miR-29b enrichment in ciGEnCs, when compared with podocytes, proximal tubular epithelial cells and fibroblasts. Further *in vitro* experiments demonstrated significantly increased miR-126 and miR-29b in ciGEnCs conditioned medium in response to TNF-α and TGF-β1, respectively, under both 5 mM and 25 mM D-glucose concentrations.

Findings from Beltrami *et al.* (2018) suggested that cytokines associated with the initiation of diabetic injury influenced the miR output of GEnCs. In addition, this study demonstrated the suitability of conditionally immortalised GEnCs as models of GEnC behaviour. However, this study focused on a restricted number of miRs, and further work investigating a range of miRs was required to identify miR mediators of diabetic renal injury.

1.7 Thesis aims

Early diagnosis of renal injury in diabetes has clear and significant potential to improve patient outcomes by bringing forward treatment and disease management steps, thereby minimising tissue damage and loss of renal function. Prognostic biomarkers in later stage DKD that could stratify those patients that will progress to ESRD from those that will not require immediate treatment would also be extremely valuable. Such "personalised medicine" markers would inform clinical decisions to target intensive treatment, and would also have the potential to quantify the efficacy of existing and new disease treatments. Considering the burgeoning global numbers of diabetes patients, these markers would confer considerable societal and economic benefits.

Glomerular endothelial cell (GEnC) miRs that undergo expression changes in response to DKD-associated stimuli are potential mediators of diabetic renal injury and putative prognostic and/or diagnostic disease biomarkers. Previous work by Beltrami *et al.* (2018) showed increased urinary miR-126 and miR-29b in DKD patients. Using conditionally immortalised GEnCs (ciGEnCs) obtained from Dr Simon Satchell, University of Bristol, Beltrami *et al.* (2018) subsequently showed increased extracellular miR-126 and miR-29b in an *in vitro* DKD model incorporating hyperglycaemia and TNF-α. (Beltrami *et al*. 2018).

The work in this thesis is based on the hypothesis that cellular and extracellular GEnC miR expression changes in response to DKD stimuli can identify miRs that mediate renal injury, and that these miRs therefore represent potential disease biomarkers.

Using ciGEnCs from Dr Satchell's laboratory, the project aims were as follows:

1. Culture ciGEnCs and extract RNA from *in vitro* diabetes mellitus and DKD models
2. Profile and analyse ciGEnC cellular and extracellular miR expression in these models

Chapter 2 - Methodology

2.1 Cell culture

2.1.1 Human conditionally immortalised glomerular endothelial cells

The ciGEnC cell line utilised as part of this project was developed by Dr Simon Satchell's team at the University of Bristol. Following advice from Dr Satchell's group, the following cell culture conditions were maintained. Any variations are stated.

In T75 flasks, ciGEnCs were maintained in EGM-2MV media (Lonza) supplemented with the following (each from Lonza):

- 5% FBS
- 0.2 µg/mL hydrocortisone
- 10 ng/mL human FGF-B
- 20 ng/mL R3 IGF-I
- 1 µg/mL ascorbic acid
- 5 ng/mL Human EGF
- 9.5 mL GA 1000 (Gentamycin and Amphotericin B)
- 0.5 ng/mL VEGF (unless otherwise stated)

Fresh medium was supplied three times a week. Cells were passaged at approximately 70% confluence. For passage from a T75 flask, cell culture medium was aspirated from a flask of cells at the non-permissive temperature of 33°C , and cells washed in 10 mL of PBS (Sigma-Aldrich). PBS was subsequently removed, and replaced with 1 mL of trypsin EDTA (Trypsin EDTA 0.25%, Sigma-Aldrich), and 5 mL of PBS (Sigma-Aldrich). Cells were incubated for approximately 3 min at 37°C to detach cells from the flask surface, before the addition of 10 mL EGM-2MV medium and subsequent transfer of flask contents to a 50 mL Falcon tube. Detached cells were pelleted by 1,000 rpm centrifugation for 5 min at 20°C. The resultant cell pellet was resuspended in the required volume of EGM-2MV medium depending on intended use.

For freezing, cell pellets were suspended in a solution of:

- 50% EGM-2MV media (Lonza)
- 40% FBS (Gibco)
- 10% dimethyl sulphoxide (DMSO) (Sigma-Aldrich)

Cells were placed immediately in -80°C for a minimum of 24 h before transfer to liquid nitrogen storage. For thawing, cryovials were removed from storage and placed into water baths of 37°C for approximately 2 min. Contents of the cryovials were then added to 20 mL of EGM-2MV, and pelleted by 1,000 rpm centrifugation for 5 min at 20°C. The cell pellet was resuspended in an appropriate volume of EGM-2MV for intended future use.

For reseeding, cell pellets were resuspended in 10 mL of EGM-2MV medium, containing 5% FBS, and supplemented as described above. The cell suspension was placed into flasks of appropriate size depending on cell density, and incubated at 33°C.

Cells were grown to approximately 70% confluence in the appropriate vessel at 33°C, before being transferred to 37°C. Cells were left at this non-permissive temperature for 5 days before experimentation, to ensure full deactivation of the temperature sensitive SV60LT. Following 5 days at 37°C, cells were treated for 24 h in serum-deprived medium before applying treatment conditions. Serum-deprivation and treatment conditions were carried out at 37°C.

Gelatin coating of T75 flasks was used in an attempt optimise ciGEnC culture. Gelatin (Sigma-Aldrich, G1393, 2%) was removed from the refrigerator and left at room temperature for 30 min. Once at room temperature, 40 µL of gelatin was added to 4 mL of sterile water, and mixed by vortexing. For each T75 flask, 4 mL of geltain solution was pipetted onto the base of the flask, and the flask swirled gently to ensure even coverage. The flask was left unagitated for 30 min, following which excess gelatin solution was aspirated, and 5 mL of PBS (Sigma-Aldrich) was gently added to the flask. The flask was again gently swirled, before removal of PBS (Sigma-Aldrich). The flask was left for approximately 5 min to dry, before addition of any culture medium.

Both permissive and non-permissive temperatures were maintained within humidified incubators at 5% CO_2.

Following initial receipt of two T75 flasks of ciGEnCs from Dr Satchell's laboratory in 2013, cells were cultured by Dr Cristina Beltrami and stored under liquid nitrogen at the WKRU (formerly the Institute of Nephrology, Cardiff University).

The following vials of ciGEnCs were collected from the liquid nitrogen storage:

- ciGEnC – Cell Passage 28
- ciGEnC – Cell Passage 29
- ciGEnC – Cell Passage 31
- ciGEnC – Cell Passage 32
- ciGEnC – Cell Passage not recorded (x2)

Cells of passage 32 were determined to be unsuitable for use due to their poor growth and morphology (see section 3.3.1), and were therefore discarded. Cells of passage 28 were maintained in EGM-2MV medium (Lonza), supplemented as described in section 2.1.1. These cells are referred to throughout this text as Group A.

Additional ciGEnCs of passage 23 were kindly donated by Dr Simon Satchell's group at the University of Bristol. These cells were grouped into Group B and Group C. Both groups were cultured in EGM-2MV medium (Lonza) supplemented as described in section 2.2.1.1, with group B medium containing VEGF, and Group C medium excepting VEGF (Figure 11).

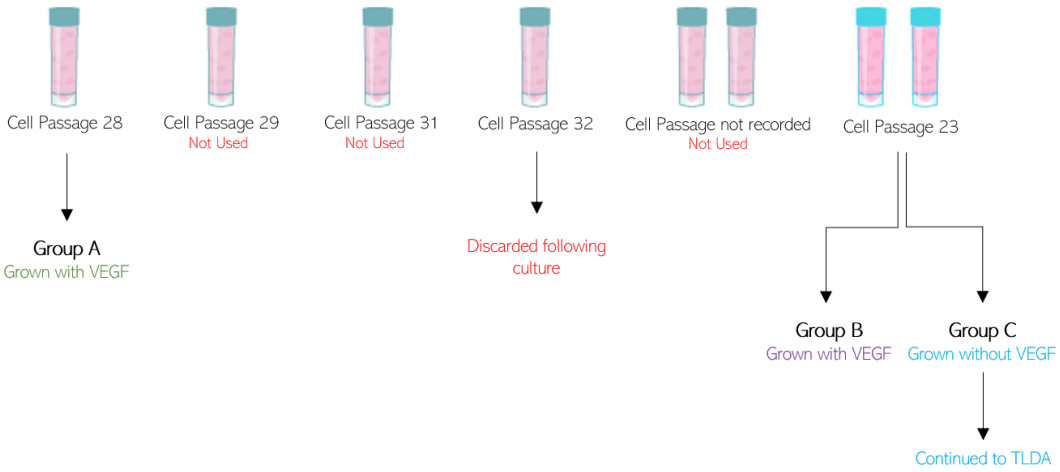

Figure 11: ciGEnC passage number and culture conditions.

2.1.2 hTERT- Human Umbilical Vein Epithelial Cells (hTERT-HUVECs)

Two cryovials of human telomerase reverse transcriptase (hTERT)-immortalized HUVECs were kindly donated by Professor Aled Clayton and Dr. Jason Webber from the Division of Cancer & Genetics, Cardiff University School of Medicine.

hTERT-HUVECs (hereafter called HUVECs) were cultured at 37°C in M199 (Sigma-Aldrich), supplemented with 20% FBS (Gibco) and maintained within humidified incubators at 5% CO_2.

hTERT-HUVECS were passaged at approximately 70% confluence. To passage cells from a T75 flask, medium was removed from the flask, and cells washed with 10 mL PBS (Sigma-Aldrich). Following aspiration of the PBS wash, 500 µL Trypsin (Trypsin EDTA 0.25%, Sigma-Aldrich) and 5 mL of PBS were added to the flask, which was subsequently incubated for approximately 4 min at 37°C. Following incubation, 4 mL of FBS (Gibco) was added to the flask in order to prevent further tryptic activity. Flask contents were transferred to a 50 mL falcon tube, and cells pelleted by 500 rpm centrifugation for 5 min at 20°C. The resulting cell pellet was resuspended in an appropriate volume of medium depending on intended use.

For freezing, cell pellets were resuspended in a solution containing:

- 70% M199
- 20% FBS
- 10% dimethyl sulphoxide (DMSO)

Resuspended cells were immediately stored at -80°C for a minimum of 24 hours, before transfer to liquid nitrogen. For thawing, cryovials were placed into a water bath at 37°C for approximately 2 min before mixing with a 20 mL solution of 80% M199 and 20% FBS. This cell suspension was transferred to a 50 mL falcon tube, and cells pelleted by 500 rpm centrifugation for 5 min at 20°C. Cell pellets were resuspended in a suitable volume of 80% M199 and 20% FBS depending on intended use.

For reseeding, cell pellets were resuspended in 10 mL of 80% M199 and 20% FBS. The cells suspension was placed into flask of appropriate size depending on cell density, and incubated at 37°C.

Cells were exposed to serum-deprived medium for 24 h prior to any experimental treatments.

2.1.3 Human Proximal Tubular Epithelial Cells (PTECs): Human Kidney-2 (HK-2) Cell Line

Human Kidney 2 (HK-2) cells are an immortalised human proximal tubular epithelial cell (PTEC) line produced through exposure of primary human proximal tubular epithelial cells to a recombinant retrovirus containing human papilloma virus-16 E6/R7 genes (Ryan *et al.* 1994).

Two cryovials of immortalised HK-2s were donated by Dr Lucy Newbury at Wales Kidney Research Unit (WKRU), Cardiff University.

HK-2s were maintained in a 1:1 solution of Hams F12 (Sigma), and Dulbecco's Modified Eagle's Medium (DMEM, Gibco), supplemented with the following:

- 10% FBS (Gibco)
- 20 mM HEPES ((4-(2-hydroxyethyl)-1-piperazineethanesulfonic acid, Gibco)
- 2 mM L-glutamine (Gibco)
- 5 µg/mL transferrin (Gibco)
- 5 ng/mL sodium selenite (Gibco)
- 0.4 µg/mL hydrocortisone (Gibco)

HK-2s were passaged at approximately 70% confluence. For culture from a T75 flask, cell culture medium was removed, and cells were washed with 10 mL of PBS (Sigma-Aldrich). Following removal of PBS wash, 500 µL Trypsin EDTA (Trypsin EDTA 0.25%, Sigma-Aldrich), and 5 mL of PBS were added to the flask, which was incubated for approximately 4 min at 37°C. Following incubation, 4 mL of FBS was added to the flask, the flask contents transferred to a 50 mL Falcon tube, and 500 rpm centrifugation carried out for 5 min at 20°C. The resulting cell pellet was resuspended in an appropriate volume of medium depending on intended use.

For freezing, the cell pellet was resuspended in a solution of the following:

- 45% 1:1 solution of Hams F12, and DMEM, supplemented as described above.
- 45% FBS
- 10% dimethyl sulphoxide (DMSO, Sigma-Aldrich)

Once resuspended in freezing medium, cells were immediately stored for a minimum of 24 hours at -80°C before transfer to liquid nitrogen. To thaw cells, cryovials were placed into a water bath at 37°C for approximately 2 minutes, before mixing with a 20 mL solution of the following:

- 90% 1:1 solution of Hams F12, and DMEM, supplemented as described above.
- 20% FBS

This cell suspension was transferred to a 50 mL Falcon tube, and cells pelleted by 500 rpm centrifugation for 5 min at 20°C. The cell pellet was resuspended in a suitable volume of the following solution, depending on intended use:

- 90% 1:1 solution of Hams F12, and DMEM, supplemented as described above.
- 20% FBS (Gibco)

The resulting cell suspension was transferred to a vessel of appropriate size, and incubated at 37°C.

Cells were exposed to serum-deprived medium for 24 h prior to experimental treatment.

2.2 Manipulation of cell culture conditions

Both ciGEnCs and HUVECs underwent 24 h of serum deprivation, directly prior to application of experimental treatments. For serum starving, the corresponding medium was used for each cell type, without FBS.

All treated cells were subjected to one of the following medium conditions for 24 h:

1) 5 mM Glucose (control condition)
2) 5 mM Glucose + 10 ng/mL TNF-α
3) 25 mM Glucose
4) 25 mM Glucose + 10 ng/mL TNF-α

2.2.1 Normoglycemic and hyperglycemic glucose concentrations

Normoglycemic (5 mM) and hyperglycemic (25 mM) concentrations of D-glucose were used for cell treatments.

The D-glucose concentration of both EGM-2MV (Lonza), and M199 (Sigma-Aldrich) was 5 mM glucose. The addition of 3.6 mg of D-glucose powder (Gibco) per mL of medium was required to give a final concentration of 25 mM D-glucose.

D-glucose powder was weighed under non-sterile conditions. Therefore, following addition of glucose powder and subsequent mixing, the medium was filtered through a 0.22 µm syringe filter (Sigma-Aldrich) under sterile conditions.

2.2.2 Tumour Necrosis Factor-alpha (TNF-α)

TNF-α (Sigma-Aldrich) was reconstituted from powder in sterile PBS (Sigma-Aldrich) to a storage concentration of 100 µg/mL, from which a stock solution of 10 µg/mL was created by further dilution in PBS (Sigma-Aldrich). To create a medium TNF-α concentration of 10 ng/mL, 1 µL of 10 µg/mL TNF-α stock solution was added per 1 mL of culture medium.

Following addition of TNF-α solution to culture medium, the solution was mixed thoroughly by inversion.

2.3 Cell viability assay AlamarBlue

Alamarblue is a cell viability reagent used to measure cell proliferation and metabolic activity. The Alamarblue assay involves the use of a non-toxic, cell permeable, non-fluorescent, blue dye called resazurin, which turns to a fluorescent pink dye called resorufin in response to metabolic activity. Therefore, the metabolic activity of cells can be deduced proportionally by the rate of colour change and fluorescence change of the dye.

Cells were incubated at 37°C for 60 min in fresh culture medium without serum, containing 10% (v/v) Alamarblue reagent (Bio-Rad, BUF012B). Following incubation, 100 µL samples of medium from each condition were transferred to wells of a 96-well black plate. For the control reading, medium without serum, containing 10% (v/v) Alamarblue reagent, was incubated in an empty dish for 60 min at 37°C, and treated in the same way there-after for analysis. Fluorescence was measured at 530-560nm excitation wavelength and 590nm emission wavelength. Each analysis condition was repeated in triplicate.

2.4 RNA extraction

2.4.1 RNA extraction from cell lines

Cells cultured in 12-well plates were lysed in 500 µL of TRI-Reagent (per well) and stored at -80°C until further analysis. When required, samples were defrosted at room temperature. Then, 100 µL of chloroform was added to each sample (per 500 µL TRI-Reagent used initially) and mixed thoroughly. Following 5 min room temperature incubation, 12,000*g* centrifugation was carried out for 15 min at 4°C. Samples were incubated at room temperature for 5 min before each aqueous phase was removed to a fresh collection tube and 250µL of 100% isopropanol was added. Samples were then vortexed, incubated at room temperature for 15 min, and RNA pelleted by 12,000*g* centrifugation for 10 min at 4°C. Pellets were washed 3 times in 500 µL of 75% ethanol, with 7,500*g* centrifugation for 5 min at 4°C following each wash. Finally, pellets were air-dried for 30 min, resuspended in 10 µL of nuclease-free water, and stored at -80°C.

The RNA concentration of each extract was analysed using a NanoDrop ND-1000 spectrophotometer (Sigma-Aldrich).

2.4.2 RNA extraction from cell culture medium

The Qiagen miRNeasy kit (Qiagen) was used to extract RNA from cell culture medium, with the modifications to the manufacturer's recommendations outlined below. 1 µg of carrier RNA (MS2 RNA, Roche) was added to 350 µL of conditioned medium, and 750 µL of QIAzol added thereafter. Following a 5 min room temperature incubation. 200 µL of chloroform was added to each sample, and mixed vigorously. Following 2 min room temperature incubation, 12,000*g* centrifugation was carried out for 15 min at 4°C.

The manufacturer's recommendations were followed from this point onward. The aqueous phase from each sample was transferred to a fresh collection tube, and 1.5 volumes of 100% ethanol were added, followed by thorough mixing. Samples were then transferred to RNeasy Mini columns at room temperature and centrifuged at 12,000*g* for 30 s. Flow-through was discarded, 700 µL of buffer was pipetted onto each column, and 12,000*g* centrifugation was carried out for 1 min at room temperature. Flow-through was again discarded, 500 µL of RPE buffer was pipetted onto each column, and room temperature centrifugation carried out for 2 min at 12,000*g*. Flow-through was discarded, and each column placed in a fresh collection tube before 1 min room temperature centrifugation at 12,000*g* to dry the membrane. Columns were then transferred to fresh sterile ultracentrifugation tubes, and 50 µL of RNAase-free water pipetted onto each column membrane. Samples underwent a final 1 min room temperature centrifugation at 8,000*g* for RNA elution. The RNA concentration of each extract was analysed using a NanoDrop ND-1000 spectrophotometer (Thermo Scientific), and samples were stored at -80°C.

2.5 RT-qPCR for mRNA detection

cDNA was generated using the High Capacity cDNA Reverse Transcription Kit (Cat. No 4368814, Thermo-Scientific). A reverse transcription (RT) master mix for each reaction was made up as follows

Reagent	Volume/reaction (µL)
Molecular biology grade water	3.7
10 x Reverse Transcription Buffer	2
100 mM dNTP	0.8
40 U/µL RNase Inhibitor (New England BioLabs® Inc)	0.5
MultiScribe Reverse Transcriptase	1
Random Primers	2

10 µL of master mix was added to 10 µL of RNA extract, pre-diluted to 50ng/µL with molecular biology grade water. The non-template control contained an equal volume of water instead of RNA. Solutions were mixed thoroughly.

The thermo cycler profile used was as follows:

- 10 min at 25°C,
- 2 h at 37°C,
- 5 s at 85°C,
- Cooling at 4°C

The resulting cDNA was diluted 1:3 with nuclease-free water.

A quantitative polymerase chain reaction (qPCR) master mix for each reaction was made up as follows

Reagent	Volume/reaction (µL)
Water	4.8
SYBR Green Buffer	10
Forward Primer	0.6
Reverse Primer	0.6

Primer sequences were as follows:

Primer	Sequence
SDC4 forward primer	CCTCCTAGAAGGCCGATACTT
SDC4 reverse primer	AGGGCCGATCATGGAGTCTT
GAPDH forward primer	AAGGTGAAGGTCGGAGTCAAC
GAPDH reverse primer	GGGGTCATTGATGGCAACAATA
PECAM1 forward primer	GAGCCCATTCACGTTTCAGTTT
PECAM1 reverse primer	TCCTTCCTGCTTCTTGCTAGCT
18sRNA forward primer	GTAACCCGTTGAACCCCATT
18sRNA reverse primer	CCATCCAATCGGTAGTAGCG

For each sample, 4 µL of cDNA was added to 16 µL of qPCR master mix, per reaction well of an Optical 96 Well Fast Plate (Applied Biosystems). Liquids were mixed thoroughly by pipetting, and the plate was sealed using MicroAmp Optical Adhesive Film (Applied Biosystems).

The qPCR reaction was carried out on ViiA7 Real-Time PCR System (Life Technologies) with the cycling parameters as follows:

- 94°C for 2 min,
- 40 cycles of 94°C for 15 s, and 60°C for 1 min,
- Cooling at 4°C

Ct values were calculated equal to the cycle number at which the threshold was reached. The expression of target genes was normalised to a control gene, and to a control treatment condition, using the comparative 2-ΔΔCt method (Vandesompele *et al.* 2008).

2.6 RT-qPCR for miR detection

The High Capacity cDNA Reverse Transcription Kit (Cat. No 4368814, Thermo-Scientific) was used for reverse transcription, using a specific primer for each miR.

RNA extracts were diluted with water to ensure concentration of 2 ng/µL prior to use.

An RT master mix for each reaction was made as follows:

Reagent	Volume/reaction (µL)
Water	4.25
10 x Reverse Transcription Buffer	1.5
100 mM dNTP	0.15
40 U/µL RNase Inhibitor (New England BioLabs® Inc)	0.1
MultiScribe Reverse Transcriptase	1
5x RT-primer specific for each miR	3

10 µL of master mix was added to 5 µL (equal to 10 ng) of RNA. The non-template control contained an equal volume of water instead of RNA.

The thermal cycler profile used was as follows:

- 30 min at 16°C,
- 30 min at 42°C,
- 5 min at 85°C,
- Cooling to 4°C.

The resulting cDNA was diluted 1:3 with nuclease-free water.

The qPCR master mix for each reaction was made up as follows:

Reagent	Volume/reaction (µL)
Water	5

Universal PCR Master Mix with No AmpErase UNG (Applied Biosystems)	10
Taqman miR assay, specific for each miR	1

Taqman miR assays used are as follows:

MiR	Catalogue Number
hsa-miR-191	Part number 4427975 Assay ID 002299
hsa-miR-155	Part. Number 4427975 Assay ID 002623
hsa-miR-126	Part. Number 4427975 Assay ID 002228
hsa-miR-29b	Part. Number 4427975 Assay ID 000413

16 µL of mater mix was added per reaction well of an Optical 96 Well Fast Plate (Applied Biosystems), followed by 4 µL of 1:3 pre-diluted cDNA. For the control wells, 4 µL of water was substituted for cDNA dilution. In each case, liquids were mixed thoroughly by pipetting, and the plate was sealed using MicroAmp Optical Adhesive Film (Applied Biosystems). The qPCR was performed on a ViiA7 RealTime PCR System (Life Technologies) using the manufacturer's recommended cycling parameters as follows:

- 10 min at 95°C,
- 40 cycles of 15 s at 95°C , and 1 min at 60°C

Ct values were calculated equal to the cycle number at which the threshold was reached. The expression of target genes was normalised to a control gene, and to a control treatment condition, using the comparative $2^{-\Delta\Delta Ct}$ method (Vandesompele *et al.* 2008).

2.7 Isolation and Analysis of Extracellular Vesicles (EVs)

2.7.1 Extracellular vesicle depletion of FBS

Prior to isolation of EVs from conditioned cell culture medium, FBS (Gibco) was processed to remove bovine EVs and thereby prevent addition of exogenous vesicles during cell culture.

FBS (Gibco) was syringed into quick-seal ultracentrifuge tubes (Beckman Coulter), which were sealed with a soldering iron. The tubes were loaded into a fixed-angle 70Ti rotor, secured with spacers, and 32,000 rpm ultracentrifugation proceeded for 18 h at 4°C.

Following ultracentrifugation, the FBS-filled tubes were removed, and pierced carefully. The tubes were emptied with care to avoid disturbing the EV pellet at the base of each tube. The EV-free FBS was filtered firstly through a 0.22 µm filter, and then through a 0.1 µm filter.

The EV-free FBS was then stored at -80°C until use.

2.7.2 EV Isolation

Ten T75 flasks of hTERT-HUVECs were cultured at 37°C, in M199 (Sigma-Aldrich), supplemented with 20% EV-free FBS (Gibco). Following 5 d of culture, the entire 10 mL of culture medium was extracted from each flask and pooled.

For removal of cells from the culture medium, pooled medium was centrifuged twice for 6 min at 400 *g*, 4°C, followed by a further 4°C centrifugation step for 15 min at 2,000 *g*. At each centrifugation stage, the cell pellet was discarded. The final supernatant was filtered through a 0.22 µm syringe filter, and stored at -80°C.

When required, the medium was defrosted and syringed into ultracentrifuge tubes. Tubes were ultracentrifuged for 90 min, at 4°C, at 32000 rpm. The pellet resulting from ultracentrifugation was resuspended in 50 µL of PBS, forming the EV-rich sample.

2.7.3 EV Quality Determinants

2.7.3.1 Bicinchoninic acid (BCA) assay

A bicinchoninic acid (BCA) assay was performed using the BCA Assay Protein Kit (ThermoFisher), to determine the protein concentration of the EV sample. A BCA assay is a colorimetric assay which relies on the reduction of Cu^{2+} to Cu^{1+} by protein in an alkaline medium, which reacts with BCA to form a purple coloured product. The formation of product is proportional to the amount of protein present, and therefore the amount of protein in a sample can be determined by measuring the rate of colour change.

To each well of a 96 well flat bottomed plate, 40 µL of BCA standard, or 1:8 diluted EV sample, was added. BCA reagent was prepared using manufacturer's recommended combination of reagents 'A', 'B', and 'C', and 50 µL of the solution was added to each well. Following incubation at 37°C for 35 min, the absorbance of each sample was measured at 562 nm in a PHERAstar microplate reader. The concentration (µg/mL) of protein in each sample was calculated by comparing sample absorbance with a standard curve.

2.7.3.2 Nanoparticle Tracking Analysis (NTA)

Nanoparticle Tracking Analysis (NTA) was conducted on aliquots taken from exosome isolates, to determine the size of particles within the sample. NTA involves the tracking and sizing of particles based on the principles of Brownian Motion.

EVs were diluted in 1 ml of filtered PBS. Filtered PBS was used as a control. NTA measurement conditions are given below:

- Temperature - 23.75 ± 0.5°C,
- Viscosity - 0.91 ± 0.03 cP,
- Frames per second - 25,
- Measurement time - 60 s

NTA was performed on NanoSight LM10 system (NanoSight Ltd), configured with a 405 nm laser, using a high sensitivity digital camera system (OrcaFlash2.8, NanoSight Ltd). Videos were collected and analysed using the NTA-software (version 2.3), with automatic settings for minimal expected particle size, minimum track length, and blur setting.

All recordings were taken in triplicate, and averages calculated.

2.7.3.3 Determination of exosome purity

The ratio of particles (per mL) to protein (µg/mL) was calculated to determine exosome sample quality. Webber and Clayton (2013) proposed this method, and advise that ratios of 3×10^{10} particles per µg of protein, or greater, can determined as high purity.

2.8 TaqMan Low Density Array

2.8.1 Reverse Transcription

Extracted RNA from three replicate experimental conditions were pooled by volume, and the resulting RNA was diluted to 7ng/µL. RNA was reverse transcribed using the Megaplex RT Kit (ThermoFisher, Product code 4399966, Human Pool A v2.1).

An RT master mix was created from the following components:

Reagent	Volume/reaction (µL)
MegaplexTM RTPrimers (x10, A card)	0.8
dNTPs with dTTP (100mM)	0.2
MultiScribeTM Reverse Transcriptase (50U/µL)	1.5
10 x RT buffer	0.8
$MgCl_2$ (25 mM)	0.9
RNase inhibitor (20U/µL)	0.1
Nuclease-free water	0.2

4.5 µL of RT master mix was added to 3 µL of RNA in a MicroAmp 8-Tube Strip which was incubated on ice for a minimum of 5 min before being placed in a thermocycler.

Thermocycler parameters were as follows:

- 40 cycles of: 2 min at 16°C, 1 min at 42°C and 1 sec at 50°C,
- 5 min at 85°C
- Cooling step at 4°C.

2.8.2 Pre-amplification

The resulting cDNA was preamplified using the TaqMan PreAmp Kit (ThermoFisher, 4391128).

A pre-amplification master mix was prepared as follows:

Reagent	Volume/reaction (µL)
TaqMan PreAmp Master Mix (2 x)	12.5
Multiplex PreAmp Primers (10 x)	2.5
Nuclease free water	7.5

22.5µL of pre-amplification master mix were added to 2.5µL of cDNA, and incubated on ice for 5 min before being placed on the thermocycler under the following conditions

- 10 min at 95°C
- 2 min at 55°C
- 2 min at 72°C
- 12 cycles of 15 sec at 95°C and 4 min at 60°C
- 10 min at 99.9°C
- Cool to 4°C

The resulting product was diluted with 75 µL of nuclease-free water per sample.

2.8.3 qPCR

A mater mix was prepared for the following:

Reagent	Volume/reaction (µL)
TaqMan Universal PCR Master Mix, no UNG	450
Nuclease free water	441
Pre-diluted pre-amplification product	9

100 µL of master mix was loaded into each well of a 384-well plate-based miR array (Thermofisher, 4398965, Card A), which had been previously incubated at room temperature for 15 minutes. The card was centrifuged at 1600 rpm for 2 minutes, and sealed. The card was run on a ViiA 7 real-time PCR system (ThermoFisher) using the following default thermal-cycling conditions:

- 50°C for 2 minutes
- 94.5°C for 10 minutes
- 40 cycles of 97°C for 30 seconds, the 59.7°C for 1 minute

The card layout is demonstrated in Figure 12, and the associated primer sequences are available at www.thermofisher.com.

Ct values were calculated using the comparative $2^{-\Delta\Delta Ct}$ method, with software provided by Thermo Fisher Cloud (Available at apps.thermofisher.com/apps/dashboard) (Vandesompele *et al.* 2008). Expression values were normalised using a global normalisation technique, following the standard settings on the Thermo Fisher Cloud Software.

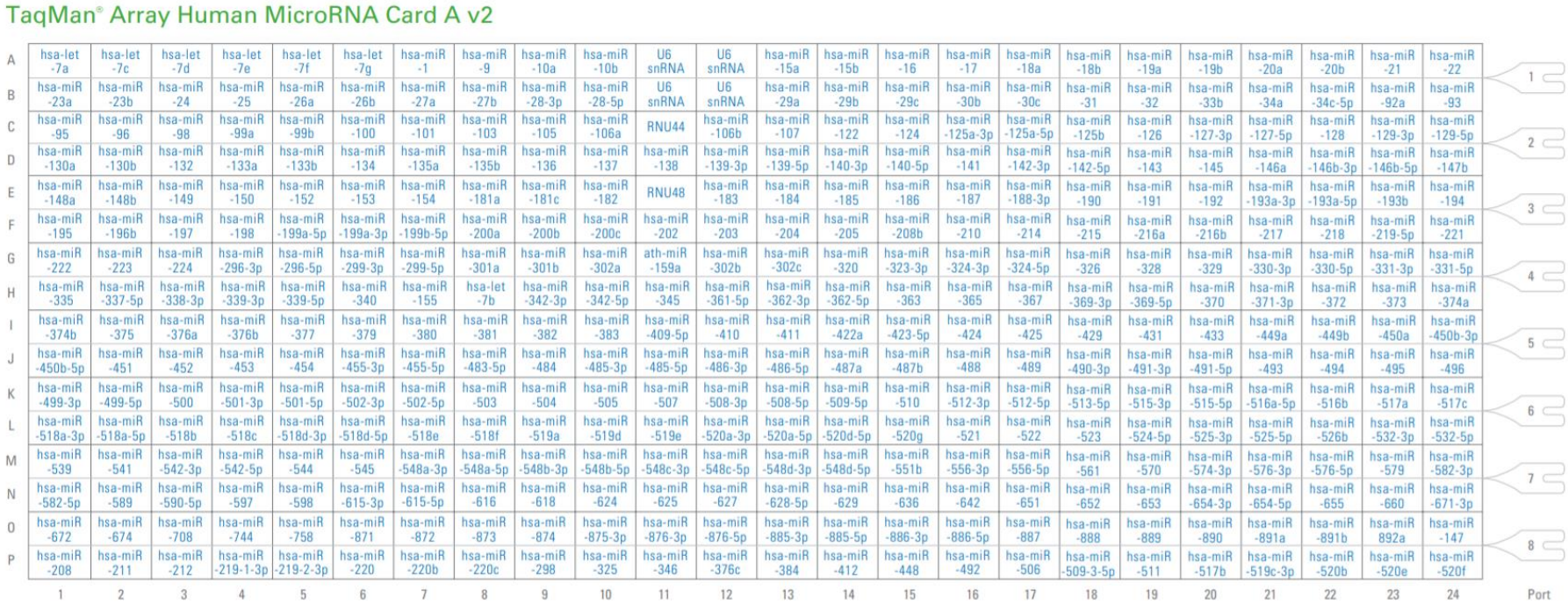

Figure 12: TaqMan Low Density Array (TLDA) card A (Thermo Fisher) assay layout

2.9 Statistical analysis

Microsoft Excel 2020 and GraphPad version 8 were used for all statistical analysis. GraphPad was used to generate graphical outputs.

For determination of miR-191 suitability as a control miR, individual one-way ANOVAs were performed on cellular and extracellular data (Figures 20, 21). A one-way ANOVA was also carried out on PECAM1 expression data (Figure 18).

A two-way ANOVA was performed to determine the effects of glucose concentration and TNF-α on the abundance of miR in a given sample. A post-hoc Tukey Test was performed if significant differences were identified. A simple main effect analysis was conducted where a significant interaction was found between the effects of glucose concentration and TNF-α presence (Figures 22-29).

Statistical analysis could not be conducted on TLDA data, due to lack of replicate results. Therefore, logarithmic relative quantification (log_2RQ) values were chosen as cut-offs to represent increased and decreased expression. $Log_2RQ > 1$ was determined to represent increased expression, whilst $Log_2RQ < -1$ was determined to represent decreased expression.

2.10 *In silico* analysis:

In silico analysis was conducted on TLDA results relating to the cellular and extracellular expression of miRs.

MiRs determined to be up or down regulated within each treatment condition were entered into MiR Data Integration Portal (MirDIP) Version 4.1.11.1, Database version 4.1.0.3 (available at http://ophid.utoronto.ca/mirDIP/) (Tokar *et al.* 2018). MirDIP is a tool which integrates 30 independent miR-target resources, including DIANA, miRbase, miRDB, mirTar, PicTar, and TargetScan. MirDIP provides an integrative score to each unique miR-target interaction, which is based on the combination of confidence measures given by each of the individual resources. This method of combining resources generates more accurate MIR-target predictions than the use of any singular resource (Tokar *et al.* 2018). Only the top 1% of miR-target predictions were extracted for further analysis.

Large lists of predicted gene targets were generated from the MirDIP analysis. To narrow down the list of potential targets, exclusion criteria were applied.

Genes predicted as targets of cellular miRs differentially expressed by ciGENCs were compared to a complete expression profile of GEnCs obtained from Sengoelge *et al.* (2014). Only genes appearing in the expression profile list and in the miR-target prediction list were continued to further analysis.

Genes predicted as targets of extracellular miRs demonstrating differential expression were compared with the expression profile of the nephron, obtained from the Human Protein Atlas (Thul and Lindskog 2018). Only genes present in the expression profile of the nephron, and in the miR-target prediction list, were continued to further analysis.

The 200 genes with the highest MiRDIP-generated prediction scores were selected for STRING analysis. For combined analysis of treatment conditions, genes predicted under all relevant treatment conditions had their prediction scored summed and ranked.

STRING (version 11.0) is a database which allows for computational prediction of protein-protein interactions (Szklarczyk *et al.* 2019). Genes entered into STRING are converted to their protein counterparts, and run through a collated database of protein-protein interaction information. For this analysis, evidence for protein-protein interaction was restricted to biochemical/genetic data; previously curated pathway and protein-complex knowledge; co-expression evidence, and text-mining based on co-citation. Only 'high-confidence' data was included. STRING is freely available at www.string-db.org/.

The g:GOSt tool as part of g:Profiler (version e99_eg46_p14_f929183) was used to perform the functional enrichment of gene lists (Raudvere *et al.* 2019). Entire predicted gene lists were entered into g:GOSt, and functionally enriched using custom background gene lists. For genes predicted as targets of extracellualr miRs demonstrating differential expression, the expression profile of the nephron was used a background gene list (Thul and Lindskog 2018). For genes predicted as targets of cellular miRs with differential expression, a GEnC expression profile was used a background gene list (Sengoelge *et al.* 2005). Enriched GO terms, KEGG pathways, and REACTOME pathways were outputted.

Functionally enriched GO terms were entered into REVIGO for removal of redundant GO terms, and the creation of tree maps to visualise related GO terms. REVIGO is available at www.REVIGO.irb.hr/ (Supek *et al.* 2011). REVIGO outputs 'parent GO term clusters', which typically have a number of related 'child GO terms' associated with them. Parent GO term clusters provide general broad annotation, whereas the associated child GO-terms provide more specific annotations.

Chapter 3 – Results I: Culture and RNA extraction from ciGEnCs in an *in vitro* DKD model using hyperglycaemia and TNF-α

3.1 Introduction

Glomerular endothelial cells (GEnCs) have historically been challenging to study due to difficulties maintaining their physiological phenotype under cell culture conditions (Satchell *et al.* 2006). In 2006, Dr Simon Satchell's research group at the University of Bristol developed conditionally immortalized GEnCs to address this issue (Satchell *et al.* 2006).

Satchell *et al.* (2006) described a process of sieving healthy human renal cortex tissue, and growth of the contents on culture plates coated with extracellular matrix components, and supplemented with growth factors. GEnCs were isolated from culture using an immunomagnetic bead selection technique. Using retroviral vectors, these primary GEnCs were transduced with temperature sensitive simian virus large 40 tumour antigen (SV60LT), and the catalytic subunit of human telomerase (hTERT). Previous research has shown a requirement for both these elements for successful immortalization of endothelial cells (Saleem *et al.* 2002). Cells successfully transduced with both SV40LT and hTERT were selected, and characterised extensively to confirm similarity to GEnCs derived from primary culture (Satchell *et al.* 2006). The SV60LT construct allows for ciGEnC proliferation at the permissive temperature of 33°C. Growth arrest and maturation of phenotype occurs at the non-permissive temperature of 37°C.

CiGEnCs were kindly donated by Dr Satchell for use in this study. The primary aim of this chapter is to culture healthy ciGEnCs, and investigate their miR-126, miR-155, and miR-29b expression in response to hyperglycaemia and TNF-α. These results will be compared to those of Beltrami *et al.* (2018).

Human umbilical vein endothelial cells (HUVECs) will also trailed as a potential ciGEnC alternative. HUVECs are widely used endothelial cells that are straightforward to obtain and maintain in culture (Baudin *et al.* 2007). In this study, HUVECs were investigated as a possible source of endothelial cells to compare with ciGEnCs with respect to miR expression in response to diabetic stimuli.

Two cryovials of human telomerase reverse transcriptase (hTERT)-immortalized HUVECs were kindly donated by Professor Aled Clayton and Dr. Jason Webber from the Division of Cancer & Genetics, Cardiff University School of Medicine. hTERT immortalization is conferred via forced expression of the hTERT catalytic subunit of the telomerase enzyme. This process prevents telomere-controlled senescence, the process of telomere shortening following each cellular division (Lee *et al.* 2004).

HUVEC miR-126 expression will be investigated, and compared with results of miR-126 expression from ciGEnCs.

In addition, exosomes will be extracted from HUVEC cell culture medium, and labelled for later experiments investigating their uptake by proximal tubular cells in culture.

3.2 Optimisation of ciGEnC culture, and observation of ciGEnC phenotype *in vitro*

3.2.1 Visual inspection of ciGEnC phenotype *in vitro*

Initially, ciGEnCs of passage numbers 28 and 32 were cultured to approximately 80% confluence at 33°C, before transfer to a non-permissive temperature of 37°C for 4 days. Cells were imaged at this point, and cellular morphology assessed visually to determine their viability. Cells of passage 28 and 32 were cultured in EGM-2MV medium, supplemented as described in section 2.1.1, with the inclusion of VEGF.

Cell Passage 32 ciGEnCs – Cultured cells appeared fibroblastic in nature following final culture at 37°C for 4 days (Figure 13). These cells were deemed unsuitable for experimentation and were therefore discarded.

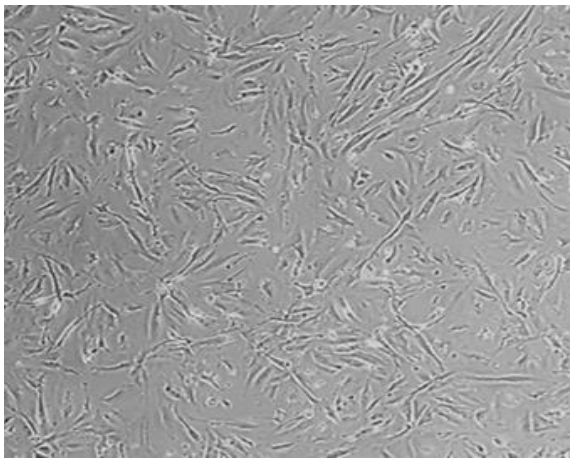

Figure 13: CiGEnCs of cell passage 32, cultured to approximately 80% confluence at 33°C, and transferred to a non-permissive temperature of 37°C for 4 days. Magnification x100.

Cell Passage 28 ciGEnCs – Relative to ciGEnCs at passage 32, ciGEnCs at passage 28 appeared to show the predicted, cobblestone appearance typical of endothelial cells, although some cells appeared atypically elongated (Figure 14). These ciGEnCs proliferated very slowly and cultures experienced a high rate of cell death. This was attributed to their relatively high passage number, and length of storage-time in liquid nitrogen. These cells were retained for further experiments, as alternative cells were not available at that time.

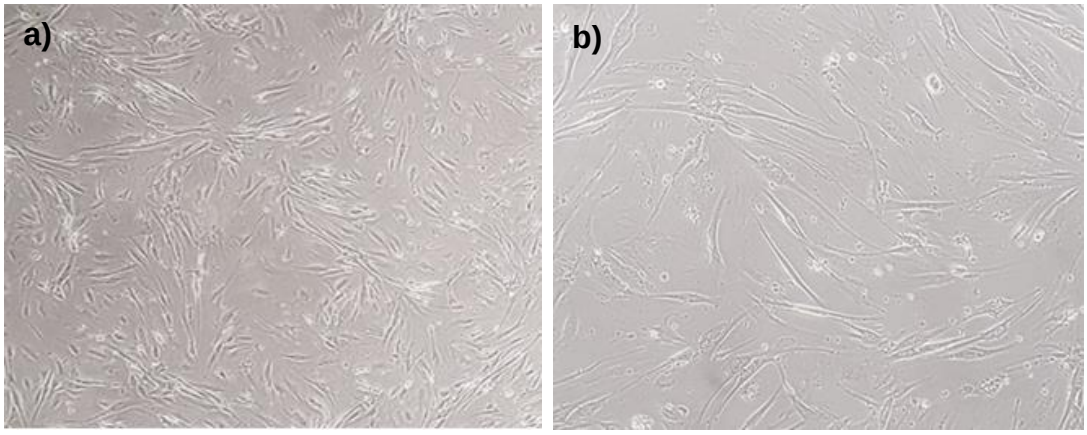

Figure 14: CiGEnCs of cell passage 28 (Group A), cultured to approximately 80% confluence at 33°C, before transfer to a non-permissive temperature of 37°C for 4 days. a) Magnification x 100, b) Magnification x 200.

Despite concerns over the suitability of the passage 28 ciGEnCs, cultures of these cells were maintained and treated, with results being analysed in comparison to preliminary data from the host laboratory in order to determine suitability for further experimentation (Beltrami *et al.* 2018). These cells will be referred to throughout this text as 'Group A'.

Following analysis of experimental data from Group A cells, it was decided that their increasingly fibrotic morphology, variable growth rates, and lack of consistency with preliminary data (see Results 3.4.2), made them unsuitable for further experimentation.

Dr Simon Satchell's group at the University of Bristol kindly provided a further two cryovials of ciGEnCs of passage 23. These passage 23 ciGEnCs were cultured in EGM-2MV medium (Lonza), supplemented as described in section 2.1.1, with the inclusion of VEGF. These will be referred to as "Group B" cells.

Relative to Group A, the growth and morphology of Group B ciGEnCs was less variable, the cells were more uniform in appearance and less fibrotic than Group A cells. It was however noted that some cells with a fibrotic appearance remained (Figure 15), and that results of experiments with passage 23 ciGEnCs were also not consistent with preliminary data from the host lab (Beltrami *et al.* 2018), (see Results 3.4.2).

Provision of gelatin coated flasks did not improve the appearance of the Group B ciGEnCs (Figure 15).

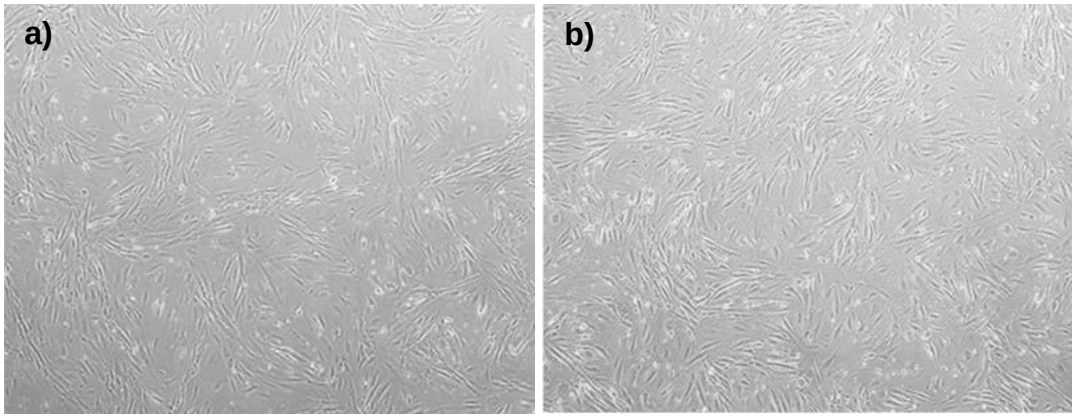

Figure 15: CiGEnCs of cell passage 23 (Group B), cultured to approximately 80% confluence at 33°C, then transferred to a non-permissive temperature of 37°C for 4 days. **a)** Cultured in uncoated T75 flask. **b)** Cultured in T75 flask pre-coated with gelatin. Magnification x 100.

It was noted that several published studies using ciGEnCs excluded VEGF from the EGM-2MV medium. This was also the case for cells used to generate the host laboratory data used to compare the results from the present study (Beltrami *et al.* 2018). It was therefore decided to attempt culturing P23 ciGEnCs in EGM-2MV medium free of VEGF. These cells will hereafter be referred to as “Group C” ciGEnCs.

Cells in Group C were uniform, appearing small and round, and bore the greatest similarity to images of the cells published previously (Figure 16) (Satchell *et al.* 2006). Following further tests, described below, carried out to establish their responses in comparison with previously published data, these Group C cells were then used in all subsequent experiments.

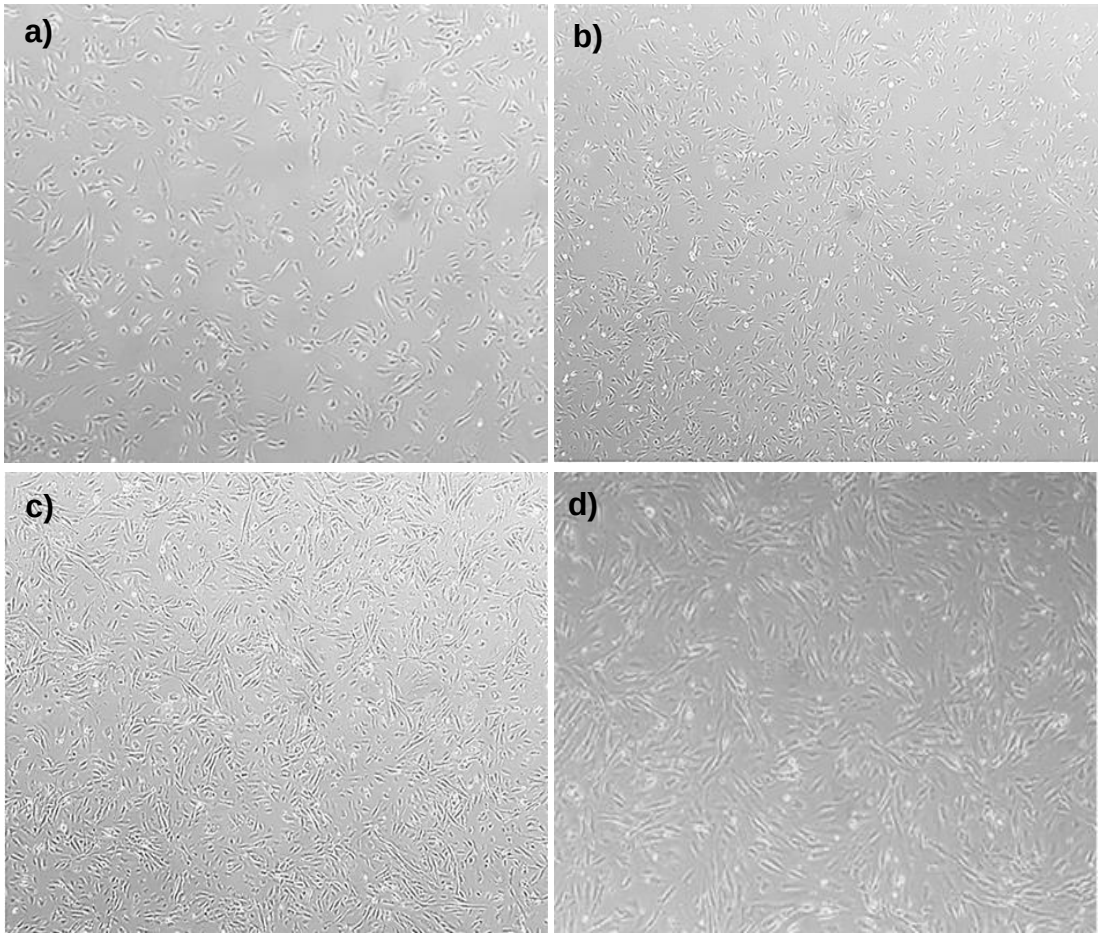

Figure 16: Group C passage 23 ciGEnCs, maintained in EGM-2V endothelial cell medium without VEGF, cultured to approximately 80% confluence at 33°C, then transferred to a non-permissive temperature of 37°C: **a)** Day 1, **b)** Day 2, **c)** Day 3 and **d)** Day 4. Magnification x100.

3.2.2 Molecular characterisation of ciGEnC

In addition to the above visual morphological analysis, Group C ciGEnCs were analysed further for previously reported responses. Previous research has shown that ciGEnCs respond to TNF-α stimulation by increasing expression of the transmembrane heparan sulfate proteoglycan, syndecan-4 (SDC4) (Satchell *et al.* 2006). To test for this predicted TNF-α response, Group C ciGEnCs were treated with 5mM glucose + 10 ng/mL TNF-α for 24 h. The resulting increase in SDC4 expression demonstrated that these cells were behaving as predicted (Figure 17).

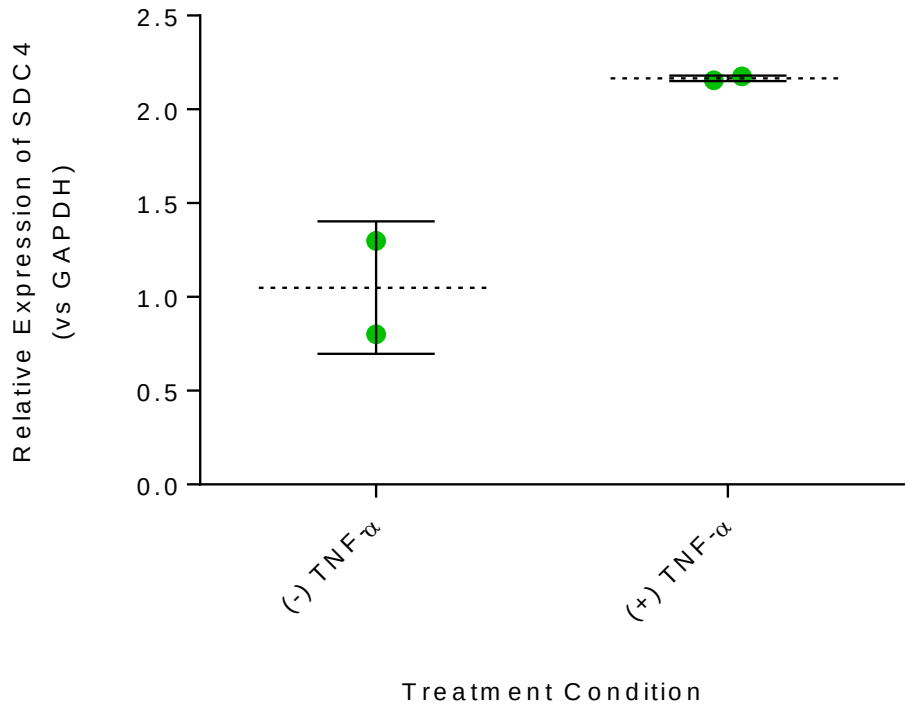

Figure 17: Group C ciGEnC SDC4 expression, relative to GAPDH..Group C refers to ciGEnCs cultured with EGM-2MV medium, without VEGF. (+) TNF-α (10 ng/mL, 24 h treatment) n=2, (-) TNF-α n=2. Symbols represent data points. Dotted lines represent mean, error bars represent standard deviation. SDC4 - Syndecan-4, GAPDH - Glyceraldehyde 3-phosphate dehydrogenase.

Following the above visual morphological analyses, expression of human platelet and endothelial cell adhesion molecule 1 (PECAM1) was analysed in ciGEnCs from Groups A, B, and C. PECAM1 is a recognised endothelial cell marker, therefore increased expression was predicted in endothelial cells compared to other cell types. PECAM1 expression was compared to that of proximal renal tubular epithelial cell type HK-2, and endothelial cell type human umbilical vein epithelial cells (HUVECs).

Although not statistically significant for each comparison, Figure 18 shows that Group C ciGEnCs exhibited the highest PECAM1 expression, supporting the visual evidence of their endothelial-like morphology. Interestingly, although from the same initial source and same passage number at time of experimentation, Group B and Group C cells showed different PECAM1 expression levels. This suggests that treatment with VEGF repressed endothelial characteristics in ciGEnCs, corroborating earlier morphological observations of these cells (see Results - 3.1.1)

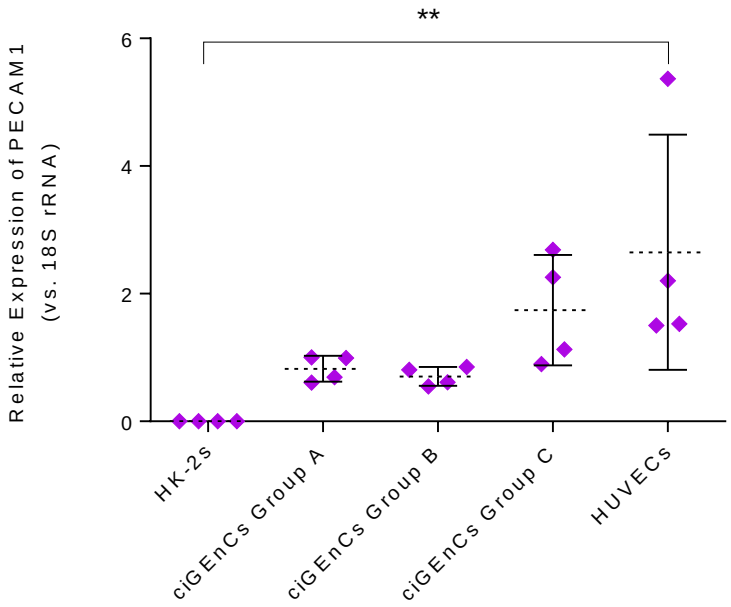

Figure 18: Scatter-dot plot showing expression of PECAM1 relative to 18S rRNA. Group A refers to passage number 28 ciGEnCs culture with EGM-2MV medium, including VEGF. Group B refers to P23 ciGEnC culture with EGM-2MV medium, including VEGF. Group C refers to ciGEnC culture with EGM-2MV medium, excepting VEGF. Symbols represent data points. Dotted lines represent mean, error bars represent standard deviation. Line above graph indicates groups with significantly different expression. One way ANOVA (n = 4) reveled statistical significance, F (4, 15) = 5.025, P=0.009. Tukey's multiple comparisons test indicated a significant difference between the mean PECAM1 expression of HK-2s and HUVECs (adjusted P= 0.0073**). **p<0.001. PECAM1 - human platelet and endothelial cell adhesion molecule 1, 18S rRNA – 18S ribosomal RNA.

3.3 Culture of HUVECs and observation of HUVEC phenotype *in vitro*

3.3.1 Visual inspection of HUVEC phenotype *in vitro*

Human umbilical vein endothelial cells (HUVECs) showed characteristic endothelial cell appearance upon seeding from prior liquid nitrogen storage (Figure 19). These cells expressed high levels of PECAM1, confirming retention of their endothelial phenotype (Figure 18).

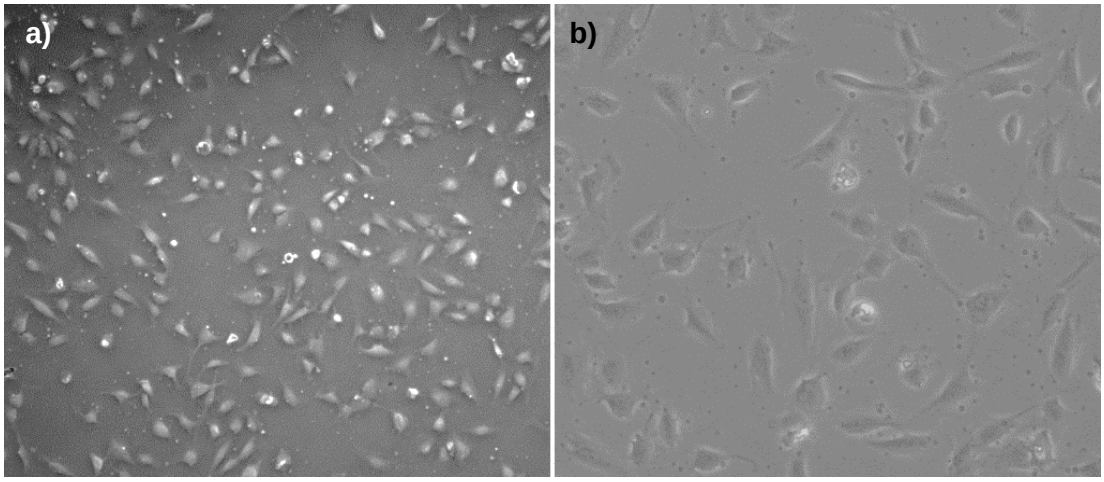

Figure 19: HUVECs following 4 days of culture in M199 supplemented with 20% FBS a) Magnification x100 b) Magnification x 200.

3.3.2 HUVEC Viability Assay

Alamarblue assays were carried out on HUVECs following a control treatment of 5 mM glucose and three experimental treatments: 5 mM glucose + 10 ng/mL TNF-α, 25 mM glucose, 25 mM glucose + 10 ng/mL TNF-α. Significantly increased metabolic activity was found in HUVECs under the 25mM glucose + 10 ng/mL TNF-α treatment compared to the control treatment condition (Table 1). It was determined that this difference could be accounted for by the normalisation of all readings to a control gene/miR.

Table 1: Alamarblue analysis, detailing mean fluorescence readings, and percentage fluorescence change relative to control treatment (5 mM glucose) (n = 3). One way ANOVA indicated a significant difference between groups $F(3, 8) = 6.076$, $P = 0.0185$. Subsequent Tukey's multiple comparisons test indicated a significant difference between the mean fluorescence reading of cells under the 5mM glucose condition, and the 25mM glucose + 10 ng/mL TNF-α treatment condition (adjusted P= 0.0147).

Cell Treatment	Average Fluorescence Units	Relative Percentage Fluorescence Change (%)
5mM glucose	26170.78	100
5mM glucose + 10 ng/mL TNF-α	30143.67	115
25mM glucose	32727.33	125
25mM glucose + 10 ng/mL TNF-α	35403.78	135

3.4 Exosome isolation, and determination of exosome sample purity

Following preparation of a HUVEC exosomal sample using methods described in section 2.7, BCA and NTA assays were carried out to determine sample purity, and concentration of exosomes.

Results of the BCA assay determined a protein concentration of 4316µg/mL in the purified exosome sample. Results of the NTA revealed an average concentration of particles per mL of 3.51 x 10^{11}. Combined, these results give a protein to particle ratio of 1:8.1 x 10^{7}. It was advised that the sample was not sufficiently concentrated for continuation to exosome labelling and uptake experiments as planned.

3.5 MiR detection

3.5.1 Identification of suitable control miRs

A suitable reference is essential for accurate calculation of RT-qPCR relative expression values for miRs. Ideally, this reference should be expressed stably across cells subjected to all treatment conditions.

Identification of suitable control for cellular and extracellular ciGEnC miR expression

The host laboratory previously identified that miR-191 was expressed at constant levels in urine samples from diabetic kidney disease patients and unaffected controls (Beltrami *et al.* 2018). MiR-191 was also used to normalise both cellular miR expression and extracellular miR data from ciGEnCs subjected to the same treatment conditions as in the current project (Beltrami *et al.* 2018). In the present study, miR-191 was therefore the first candidate miR investigated to normalise cellular and extracellular ciGEnC miR data.

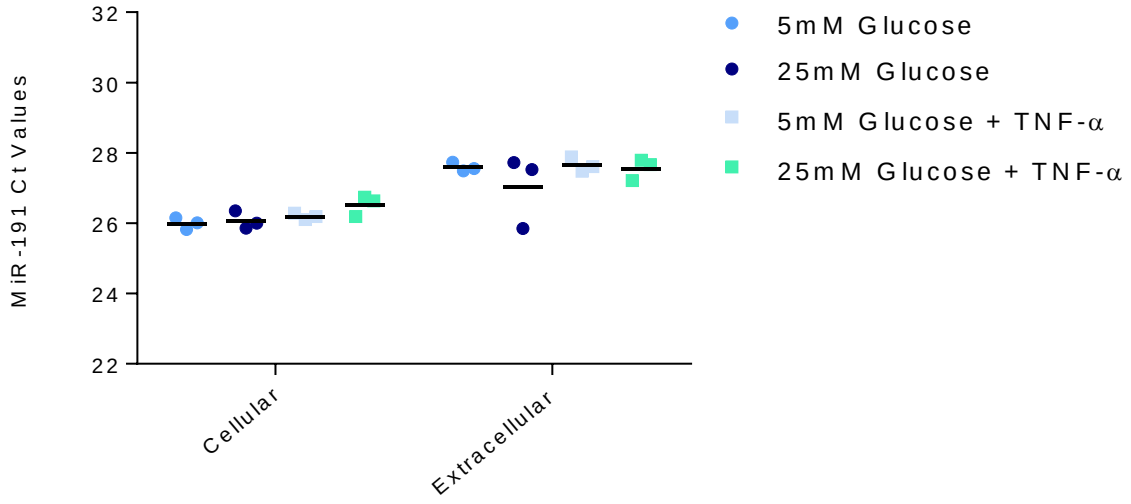

Figure 20: Cellular and extracellular miR-191 threshold cycle (Ct) values for Group C ciGEnCs. Group C refers to ciGEnC culture with EGM-2MV medium, without VEGF. Symbols represent data points and a key is provided. Bold lines represent mean values. One way ANOVA tests were carried out independently for cellular and extracellular data (n = 1), and revealed no significant difference in miR-191 Ct values between treatment conditions (P= 0.0673, P=0.5180, respectively).

Consistent cellular miR-191 expression, and extracellular detection was observed in Group C ciGEnCs under all treatment conditions (Figure 20). It was therefore decided to use this miR to normalise further.

Identification of a suitable control for cellular and extracellular HUVEC miR expression

Following the above, miR-191 was also considered first as a control miR to normalise HUVEC miR data. This transcript was found to be suitably stable across treatment conditions, both for cellular and extracellular miR detection, and was therefore used to normalise further experimental HUVEC cellular and extracellular miR (Figure 21).

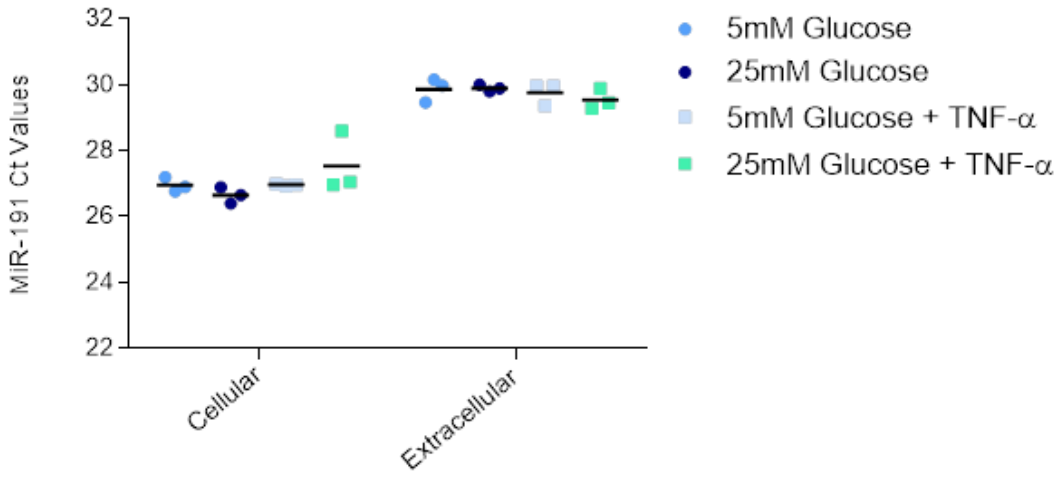

Figure 21: Cellular and extracellular miR-191 Ct Values for HUVECs. Symbols represent data points. Symbols represent data points and a key is provided. Bold lines represent mean values. One way ANOVA tests were carried out independently for cellular and extracellular data (n = 1), and revealed no significant difference in miR-191 Ct values between treatment conditions (P= 0.2361, P=0.5037, respectively).

3.5.2 Detection of cellular and extracellular ciGEnC miRs

All Ct values for the following analyses are recorded in appendix 1

Detection of extracellular ciGEnC miR-126

Since the host laboratory had previously investigated the cellular and extracellular expression of miR-126 under the same experimental conditions as the present study, this was the first miR analysed (Beltrami *et al.* 2018). Extracellular miR-126 expression was analysed for each ciGEnC group (A, B, and C).

Beltrami *et al.* (2018) reported increased detection of miR-126 in ciGEnC culture medium of cells treated with TNF-α in both 5 mM glucose and 25 mM glucose. These experiments were conducted in the absence of VEGF, the same medium composition used in the work described in this thesis to culture Group C ciGEnCs.

Data for Group A and C ciGEnCs concur with these previous data, with a statistically significant increase miR-126 in the culture medium of cells treated with 5mM glucose + 10 ng/mL of TNF-α (Figure 22 a, c). However, ciGEnCs from Group B did not show significantly different miR-126 expression following TNF-α treatment (Figure 22, b).

By contrast with the host laboratory's previous findings from Beltrami *et al.* (2018) significant changes in extracellular miR-126 detection were observed for Group A and C between 5 mM and 25 mM glucose treated ciGEnCs (Figure 22 a, c). Group A cells showed an increase in miR-126 medium detection in response to increased glucose concentration. This increase was present in both the (+) TNF-α, and (-) TNF-α conditions (Figure 22, a). Conversely, Group C cells exhibited a decrease in miR-126 medium detection in response

to treatment with an increased glucose concentration, which again was evident in both the (+) TNF-α, and (-) TNF-α conditions (Figure 22, c). Group B cell data supported the findings of Beltrami *et al.* (2018), demonstrating no significant differences in miR-126 medium detection in response to increased glucose concentration treatment (Figure 22, b).

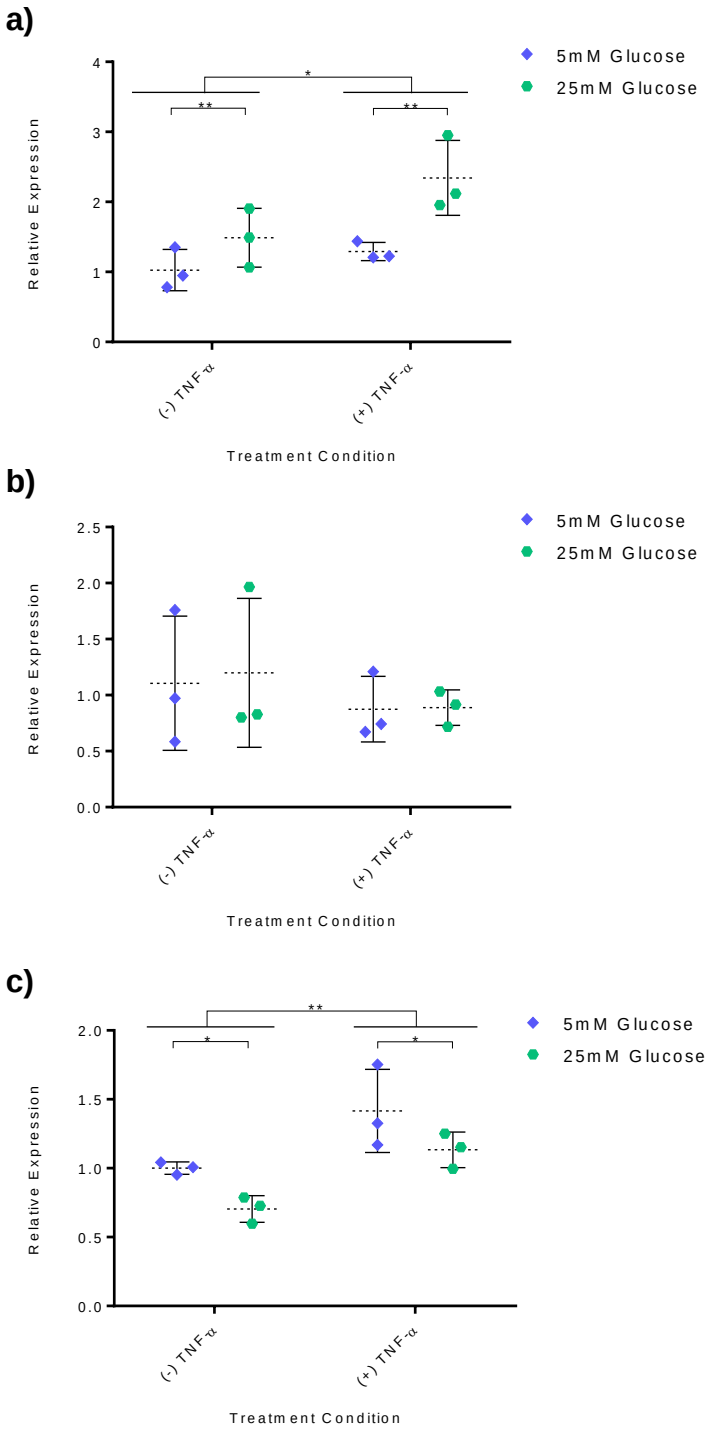

Figure 22: Detection of extracellular miR-126 in growth medium from Group A, B and C ciGEnCs cultured for 24 h. **a)** Group A ciGEnCs: passage >28 cells cultured in EGM-2MV medium including VEGF. Two way ANOVA: no interaction, cytokine factor p = 0.0328*, glucose factor p = 0.0083**. **b)** Group B ciGEnCs: passage >23 cells cultured in EGM-2MV medium including VEGF. Two way ANOVA: no interaction, cytokine factor p = 0.3550, glucose factor p = 0.8514. **c)** Group C ciGEnCs: passage >23 cells cultured in EGM-2MV medium without VEGF. Two way ANOVA: no interaction, cytokine factor p = 0.0028**, glucose factor p = 0.0198*. Data were normalized to endogenous control miR-191 and are presented as mean +/- standard deviation (n=1); * p<0.05, ** p<0.01.

Detection of cellular ciGEnC miR-126

Beltrami *et al.* (2018) showed no significant difference in miR-126 cellular expression between ciGEnCs cultured under different glucose and TNF-α conditions. These data do not concur with the data from this study (Figure 23).

Within group A, there was a significant interaction between glucose concentration and the presence or absence of TNF-α, $F(1,8) = 10.75$, $p = 0.0112$). Simple main effect analysis revealed ciGEnCs treated under the 5mM glucose concentration showed decreased miR-126 expression in response to TNF-α, whilst ciGEnCs treated with 25 mM glucose showed no significant difference in miR-126 expression in response to TNF-α (Figure 24).

Group B showed a significant decrease in miR-126 expression in response to both increased glucose concentration, and TNF-α treatment conditions (Figure 23, b).

Group C did not show any significant differences in miR-126 expression between glucose concentrations, however there was a trend towards decreased miR-126 expression in cells treated with TNF-α, compared with treatment without TNF-α ($p=0.0567$) (Figure 23, c).

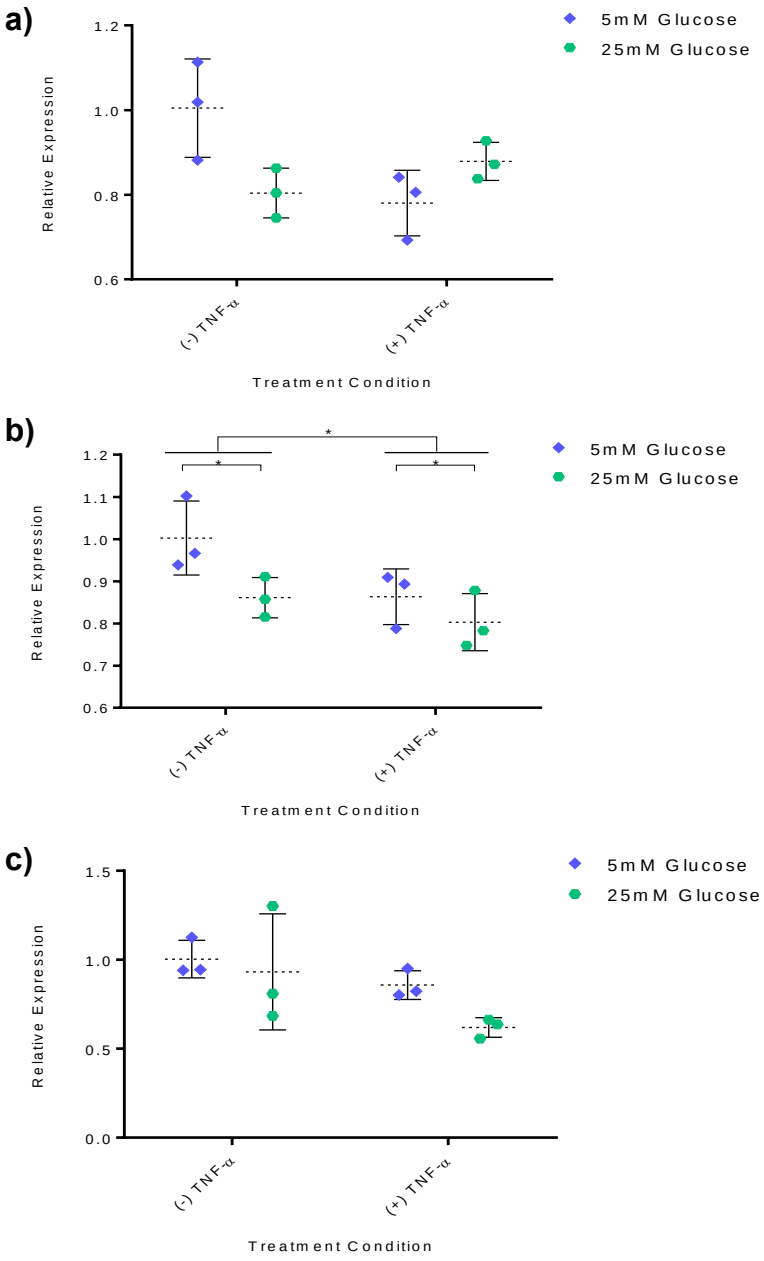

Figure 23: Detection of cellular miR-126 from Group A, B and C ciGEnCs cultured for 24 h. **a)** Group A ciGEnCs: passage >28 cells cultured in EGM-2MV medium including VEGF. Two way ANOVA: significant interaction p = 0.0112* (described in figure 24); cytokine factor p = 0.1396, glucose factor p = 0.2971. **b)** Group B ciGEnCs: passage >23 cells cultured in EGM-2MV medium including VEGF. Two way ANOVA: no interaction, cytokine factor p = 0.0377*, glucose factor p = 0.0345*. **c)** Group C ciGEnCs: passage >23 cells cultured in EGM-2MV medium without VEGF. Two way ANOVA: no interaction; cytokine factor p = 0.0567, glucose factor p = 0.1697. Data were normalized to endogenous control miR-191 and are presented as mean +/- standard deviation (n=1); *p<0.05, **p<0.01.

There was a significant interaction between glucose concentration and cytokine treatment conditions in Group A ciGEnCs (Figure 23, a). Simple main effect analysis was therefore carried out on miR-126 expression in this cell type. As shown in Figure 24, in 5 mM glucose miR-126 expression decreased in response to TNF-α treatment ($F(1,8) = 11.404$, $p = 0.010$). By contract in 25mM glucose, TNF-α treatment had no effect on miR-126 expression ($F(1,8) = 0.620$, $p = 0.454$).

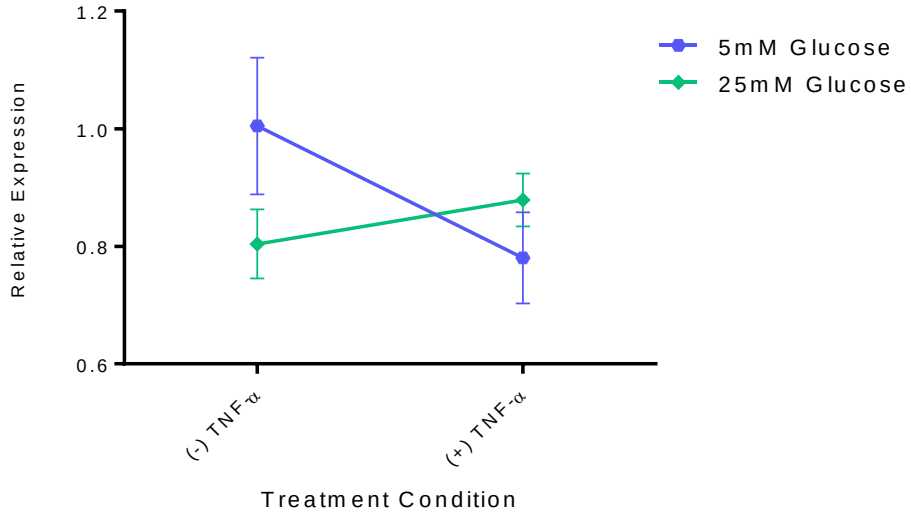

Figure 24: Simple main effect analysis for cellular expression of miR-126 in ciGEnCs. Group A passage >28 ciGEnCs cultured in EGM-2MV medium including VEGF. At 5 mM glucose, miR-126 expression was decreased in response to TNF-α treatment ($F(1,8) = 11.404$, $p = 0.010$). At 25 mM glucose, TNF-α treatment had no effect on miR-126 expression ($F(1,8) = 0.620$, $p = 0.454$). Adjustment for multiple comparisons: least significant difference. Data were normalized to endogenous control miR-191 and are presented as mean +/- standard deviation (n=1).

Detection of extracellular ciGEnC miR-155

Due to time constraints, cellular and extracellular RT-qPCR detection of miR-155 and miR-29b were carried out for Groups A and B ciGEnCs, but not Group C cells. In accordance with the data of Beltrami and colleagues (2018), Group A and B cells showed no significant differences in extracellular miR-155 medium detection (Figure 25 a, b).

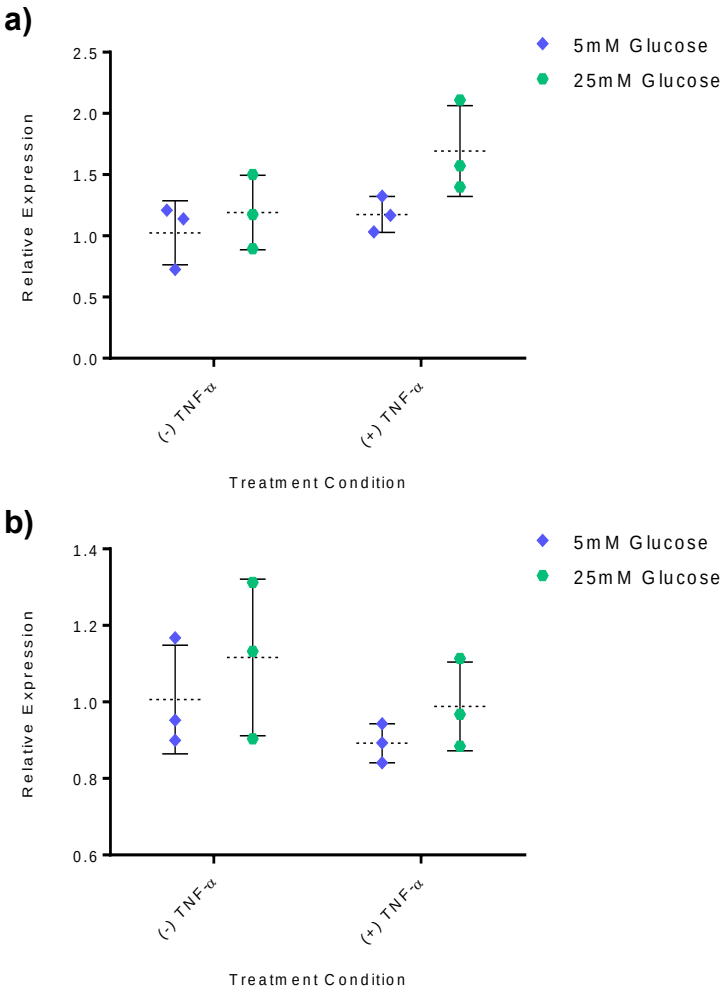

Figure 25: Detection of extracellular miR-155 from Group A and B ciGEnCs cultured for 24 h. **a)** Group A ciGEnCs: passage >28 cells cultured in EGM-2MV including VEGF. Two way ANOVA: no statistically significant interaction, cytokine factor p = 0.0803, glucose factor p = 0.0689 **b)** Group B ciGEnCs: passage >23 cells cultured in EGM-2MV medium including VEGF. Two way ANOVA: no statistically significant interaction, cytokine factor p = 0.1724, glucose factor p = 0.2372. Data were normalized to endogenous control miR-191 and are presented as mean +/- standard deviation (n=1).

Detection of cellular ciGEnC miR-155

In accordance with Beltrami *et al.* (2018) Group A ciGEnCs showed no significant changes in miR-155 cellular expression in response to any experimental condition. Conversely, ciGEnCs from Group B showed increases miR-155 cellular expression in response to TNF-α under both 5 mM and 25 mM glucose treatment conditions (Figure 26).

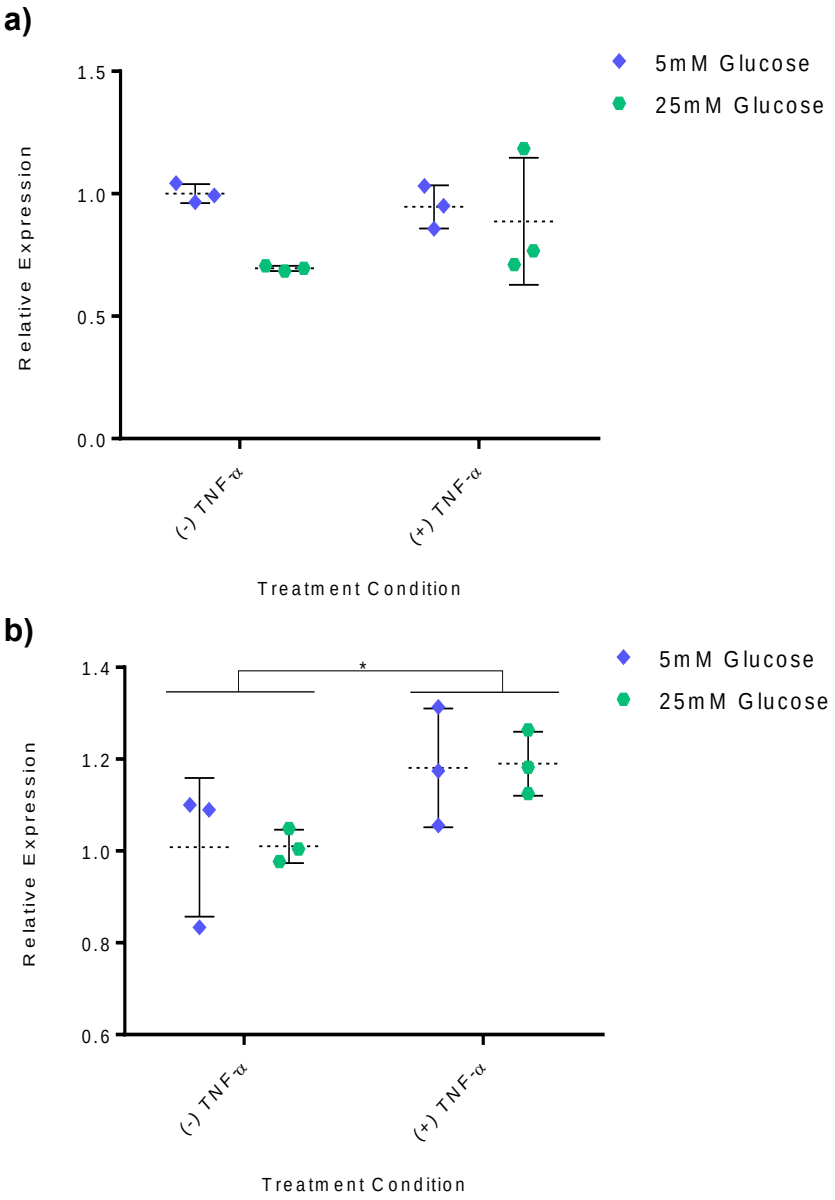

Figure 26: Detection of cellular miR-155 from Group A and B ciGEnCs cultured for 24 h. **a)** Group A ciGEnCs: passage >28 cells cultured in EGM-2MV medium including VEGF. Two way ANOVA: no statistically significant interaction, cytokine factor p = 0.4117, glucose factor p = 0.0519. **b)** Group B ciGEnCs: passage >23 cells cultured in EGM-2MV medium (Lonza), including VEGF. Two way ANOVA: no statistically significant interaction, cytokine factor p = 0.0210*, glucose factor p = 0.9318. Data were normalized to endogenous control miR-191 and are presented as mean +/- standard deviation (n=1); *p<0.05.

Detection of extracellular ciGEnC miR-29b

In accordance with results by Beltrami (2014), ciGEnC groups A and B showed no significant differences in miR-29b medium detection under either glucose or TNF-α treatment conditions (Figure 27).

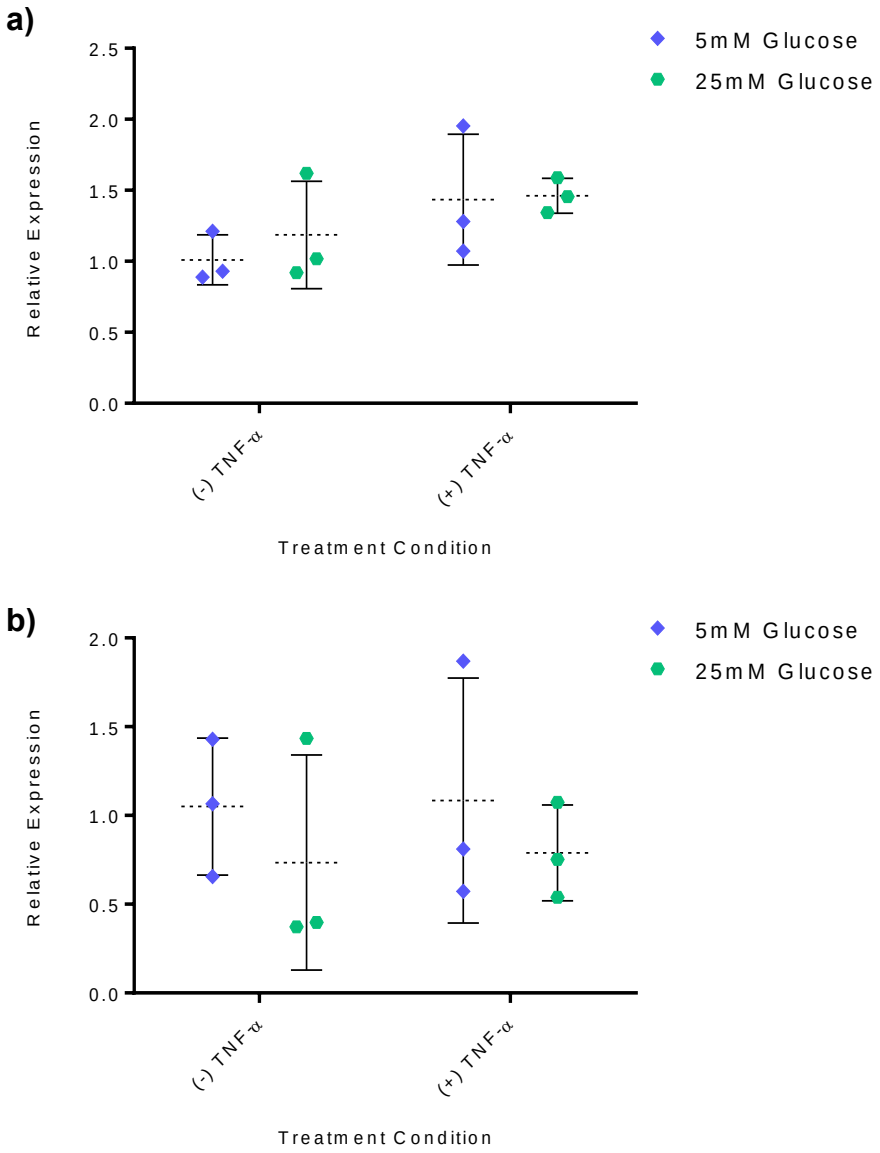

Figure 27: Detection of extracellular miR-29b from Group A and B ciGEnCs cultured for 24 h. **a)** Group A ciGEnCs: passage >28 ciGEnCs cultured in EGM-2MV medium including VEGF. Two way ANOVA: no statistically significant interaction, cytokine factor p = 0.0916, glucose factor p = 0.5938. **b)** Group B ciGEnCs: Group B ciGEnCs passage >23 ciGEnCs cultured in EGM-2MV medium including VEGF. Two way ANOVA: no statistically significant interaction, cytokine factor p = 0.8849, glucose factor p = 0.3347. Data were normalized to endogenous control miR-191 and are presented as mean +/- standard deviation (n = 1).

Detection of cellular ciGEnC miR-29b

Groups A and B showed no significant differences in miR-29b cellular expression levels under either glucose or TNF-α treatment conditions (Figure 28). These data is not in agreement with data from Beltrami (2014) which found a decrease in miR-29b cellular expression under both (+) TNF-α treatments, relative to the control treatment.

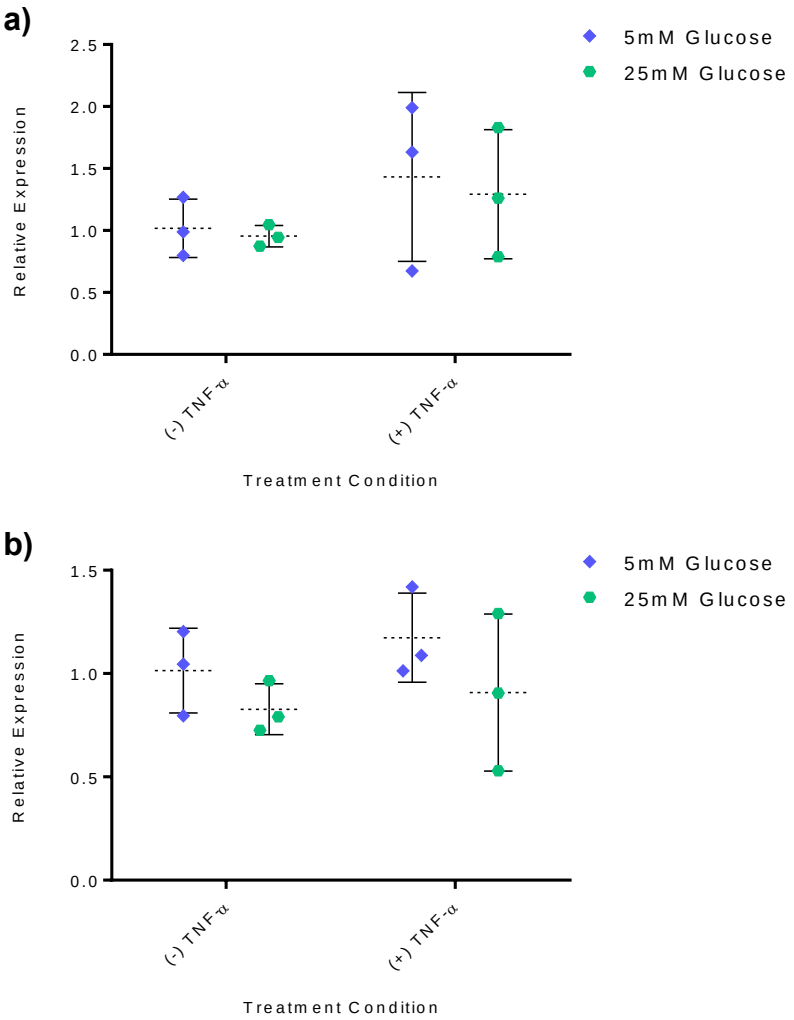

Figure 28: Detection of cellular miR-29b from Group A and B ciGEnCs cultured for 24 h. **a)** Group A ciGEnCs: passage >28 cells cultured in EGM-2MV medium including VEGF. Two way ANOVA: no statistically significant interaction, cytokine factor p = 0.1826, glucose factor p = 0.7045. **b)** Group B ciGEnCs: passage >23 cells cultured in EGM-2MV medium including VEGF. Two way ANOVA: no statistically significant interaction, cytokine factor p = 0.4287, glucose factor p = 0.1548. Data were normalized to endogenous control miR-191 and are presented as mean +/- standard deviation (n = 1); *p<0.05, **p<0.01.

3.5.3 Detection of cellular and extracellular HUVEC miRs

Detection of extracellular HUVEC miR-126

Significantly decreased miR-126 detection was observed in HUVEC culture medium following treatment with TNF-α under both 5 mM and 25 mM glucose treatment conditions (Figure 29). These findings are in contrast with those from all ciGEnC groups analysed in the present study (Figure 22).

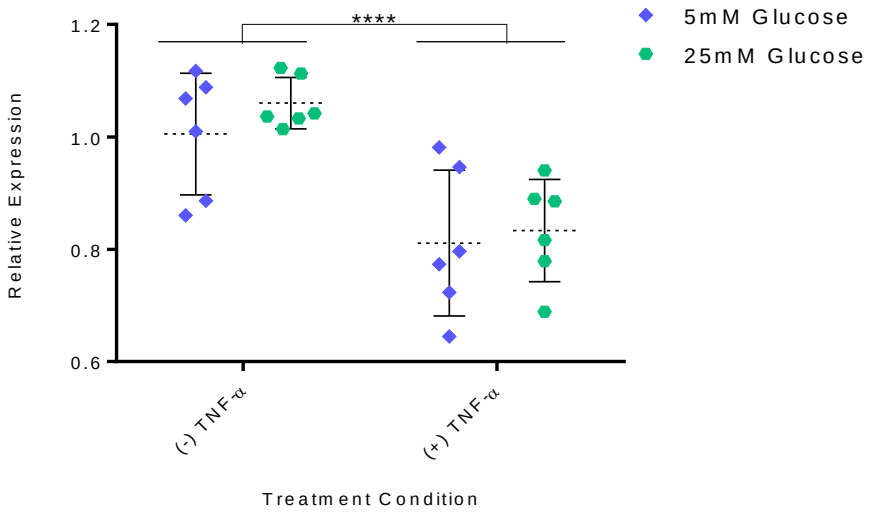

Figure 29: Detection of extracellular miR-126 from HUVECs cultured for 24 h. Two way ANOVA: no statistically significant interaction, cytokine factor p<0.0001****, glucose factor p = 0.3478. Data were normalized to endogenous control miR-191 and are presented as mean +/- standard deviation (n = 2); ****p<0.0001.

Detection of cellular HUVEC miR-126

A statistically significant decrease was observed in HUVEC miR-126 detection following TNF-α treatment under 5 mM and 25 mM glucose treatment conditions (Figure 30). These data contrasted with those for Group C ciGEnCs, which showed no significant differences in cellular miR-126 detection irrespective of culture conditions (Figure 23, c).

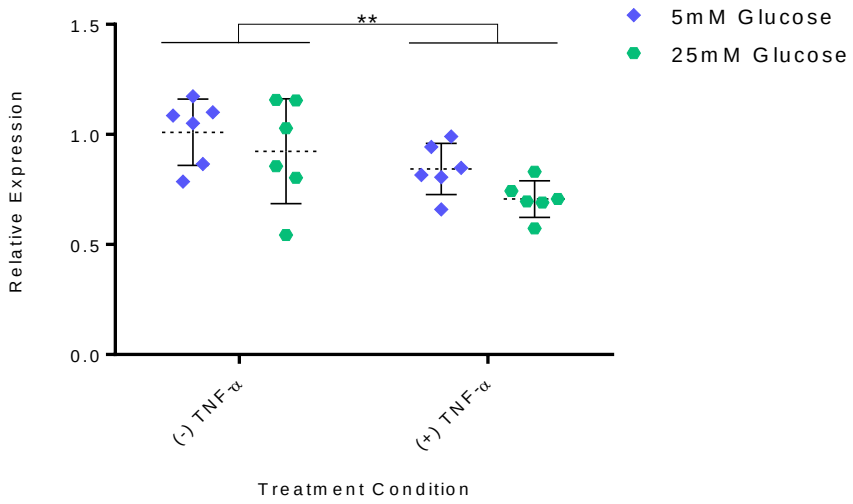

Figure 30: Detection of cellular miR-126 from HUVECs cultured for 24 h. Two way ANOVA: no statistically significant interaction, cytokine factor p < 0.0075**, glucose factor p = 0.0989. Data were normalized to endogenous control miR-191 and are presented as mean +/- standard deviation (n = 2); **p<0.01.

The above data for detection of miR-126 from HUVEC cells and culture medium presence emphasised their unsuitability as a replacement endothelial cell line for the GEnCs. Therefore, further experiments used only ciGEnCs.

3.6 Discussion

Evaluating ciGEnC use in in vitro disease models

In this study, ciGEnCs were used to investigate cellular and extracellular miR expression in response to stimuli known to be associated with diabetes mellitus and DKD. The inherent difficulties involved in isolating a single cell type's response to stimuli *in vivo* means that cell culture is a common starting point for most medical research. However, a cell culture model of a complex biological system is unlikely to accurately reflect all aspects of the *in vivo* environment accurately, and cells may respond differently to a stimulus in culture than *in vivo*. Nevertheless, numerous reports have shown that appropriate cell culture models can mimic key *in vivo* conditions, and relevant biological outcomes can be observed. Such outcomes have previoulsy paved the way for subsequent *in vivo* studies.

For the models used in this study, the principal points of consideration with respect to experimental validity include the similarity of *in vivo* GEnCs to ciGEnCs, and the degree to which the ciGEnC culture media used can mimic the *in vivo* diabetic/DKD environment.

The ciGEnC cells line used in this project were developed by Dr Simon Satchell's team at the University of Bristol. Primary GEnCs are notoriously difficult to maintain in culture, being prone to early onset senescence (Satchell *et al.* 2006). Consequently, GEnCs have historically been neglected as part of studies into DKD pathology. To counter this problem, Dr Satchell's team utilised a method of conditional immortalisation that had previously been

used to successfully create conditionally immortalised podocytes (Saleem *et al.* 2002). A similar approach of conditional immortalisation was also successful in the culture of alveolar bone marrow cells, breast microvascular endothelial cells, and fibroblasts, with each cell type proving to show characteristics similar to their respective primary cell lines (O'Hare *et al.* 2001; Salih *et al.* 2001).

Evaluation by Dr Satchell's team determined that ciGENCs created by their lab were morphologically consistent with primary culture GEnCs, being of a small size, homogeneous, and forming of 'cobblestone' monolayers up to at least passage 41 (Satchell *et al.* 2006). Further evidence of ciGEnC validity was provided by Satchell *et al.* (2006), through their use of a cDNA array to compare gene expression profiles of ciGEnCs and their primary counterparts. This investigation showed overall gene expression similarities between primary GEnCs and ciGEnCs, under both permissive and non-permissive temperature conditions. This evidence supports the use of ciGEnCs as a model of primary GEnCs. Furthermore, maintenance of endothelial cell-specific marker genes in the ciGEnCs under both permissive and non-permissive temperature conditions supported their suitability as a model of primary GEnCs (Satchell *et al.* 2006). The endothelial markers examined included PECAM1, vascular endothelial growth factor receptor 2 (VEGFR2) and von Willebrand factor (vWF). VEGFR2 and vWF demonstrated moderately increased expression in ciGEnCs compared with primary GEnCs. The increased expression of VEGFR2 in particular might represent an important inconsistency, given the importance of VEGF signalling in GEnC biology (Satchell *et al.* 2006).

On balance, Dr Satchell's ciGEnCs appear to be an appropriate alternative to the use of primary GEnCs. and have been used as such in numerous published studies including Reine *et al.* (2019), Beltrami *et al.* (2018), Ramnath *et al.* (2014), Byron *et al.* (2014), Singh *et al.* (2011), Boor *et al.* (2010), Hamer *et al.* (2012), and Tati *et al.* (2011).

Given the importance of these cells to the validity of this project, substantial attention was given to their successful culture in the WKRU laboratories, prior to the initiation of experimental treatments. One of the key factors affecting the apparent health of the ciGEnCs in culture was the addition of VEGF to the culture medium. The Bristol laboratory routinely cultures these cells with and without VEGF, depending in their intended use. At the beginning of this study VEGF was included in the growth medium, at WKRU this resulted in cells growing with an elongated phenotype. VEGF was therefore subsequently excluded from the culture medium in this study, and this also allowed for direct comparison of results with those of Beltrami *et al.* (2018).

The use of VEGF as a cell medium component was discontinued following culture of cells in Groups A and B. The ciGEnCs cultured without VEGF in Group C appeared to more closely resemble primary GEnCs in terms of visual morphology (Figure 16), and endothelial marker expression (Figure 18). The TNF-α response of ciGEnCs was also consistent with

results from Ramnath *et al.* (2014), providing further evidence that the cells were behaving as expected in culture (Figure 17).

Previous reports using these conditionally immortalised cells have varied in their use of VEGF in the cell culture medium. For example, Reine *et al.* (2019), Beltrami *et al.* (2018), Ramnath *et al.* (2014), Byron *et al.* (2014), and Singh *et al.* (2011) all excluded VEGF form the cell culture medium, whist Boor *et al.* (2010), Hamer *et al.* (2012), and Tati *et al.* (2011) included VEGF.

Since VEGF influences ciGEnC phenotype, its inclusion/exclusion in the culture medium should be consistent, unless it is an experimental variable. For the purposes of this project VEGF was excluded, as this resulted in the closest adherence to primary GEnCs with respect to cell morphology and endothelial marker expression (Satchell *et al.* 2006). However, studies have shown the importance of podocyte-secreted VEGF for the proper maintenance of GEnCs *in vivo*, with low levels of VEGF resulting in loss of fenestrations and decreased survival (Eremina *et al.* 2008; Veron *et al.* 2010). The apparent intolerance of ciGEnCs to VEGF could point towards another critical difference between ciGEnCs and GEnCs, which is potentially related to the aforementioned increased VEGFR2 expression.

Another important factor in the culture of ciGEnCs was the time permitted for differentiation at 37°C. Once again, studies using ciGEnCs have not been methodologically consistent, with culture at 37°C ranging from 24 hours (Kuravi *et al.* 2014) to 14 days (Tati *et al.* 2011). Cells progressively lost their small-round phenotype over time at 37 °C, but insufficient time at 37°C resulted in incomplete differentiation. Satchell *et al.* (2006) monitored the expression of the SV40LT antigen in ciGEnCs at the non-permissive temperature of 37°C, and showed a rapid reduction in the first 24 hours and over 30 times reduction at 5 days. This study concluded that ciGEnCs were quiescent following 5 days at 37°C. Following detailed discussions with the Satchell laboratory, the ciGEnCs in this study were used following 4 days at 37°C, to maximise differentiation time while preventing the development of a fibrotic phenotype.

Passage number was another critical component that influenced the behaviour of ciGEnCs in culture. Passage (P)32 cells used initially had a fibroblastic phenotype in culture, lacking the typical cobblestone appearance of endothelial cells. P28 ciGEnCs (Group A) appeared more endothelial-like in nature, but some fibroblastic characteristics remained. P23 cells (group B and C) were considerably less fibrotic that than P32 and P28 (Group A) cells. Group A and B cells (cultured under identical conditions) also demonstrated different miR responses under experimental conditions (Figure 22-27). Increased passage number is likely to explain some of this variation, and fibroblastic morphology, but the length of time in liquid nitrogen storage is also likely to have had a significant effect, as ciGEnCs of P32 and P28 had previously been stored for over 5 years. Satchell *et al.* (2006) determined that ciGEnCs showed a cobblestone appearance up to at least P41, but differences in

morphology and miR response of ciGEnCs were observed at different passage numbers. When time and opportunity permit, periodic comparison between lower passage ciGEnCs and primary GEnCs would be appropriate.

In a previous study by Ramnath *et al.* (2014), ciGEnCs SDC4 expression increased in response to TNF-α. In the present study, to test the response of cultured ciGEnCs to TNF-α, Group C cells were treated with 5mM glucose + 10 ng/mL TNF-α for 24 hours. The cells showed increased relative expression of SDC4, demonstrating the predicted response (Figure 17).

PECAM1 expression was then measured in group A, B and C ciGEnCs and compared to proximal tubular epithelial cells (PTECs) and human umbilical vein epithelial cells (HUVECs) as negative and positive controls, respectively (Figure 18). The highest PECAM1 expression was observed in Group C ciGEnCs, which supported observations of improved cell morphology relative to Group A and B cells. These finding both suggest that treatment with VEGF repressed endothelial characteristics in ciGEnCs.

In this project ciGEnCs were treated with stimuli reflecting the conditions these cells would be subject to *in vivo* in diabetes mellitus/DKD. The culture conditions used in this project represented two key components of the diabetic/DKD milieu: the high glucose concentration present in the hyperglycaemia that characterises diabetes mellitus, and the presence of TNF-α.

Like all *in vitro* models, there is a limit to which the culture protocol could replicate such complex and variable conditions, and other significant components from the diabetic/DKD milieu were absent. These include the importance of neighbouring cells, structural components and continuous fluid flow across the GEnC monolayer. Future studies might employ co-culture where the interactions between ciGEnCs and other renal cells, like podocytes, could be modelled. Additionally, culture methods of allowing continuous flow of culture medium across a ciGEnC monolayer could be used to mimic the flow of blood through the glomerular capillaries *in vivo*.

HUVECs as a GEnC model

HUVECs are commonly used as model endothelial cells that are relatively easy to maintain in culture. It was therefore investigated if HUVECs could be used as an endothelial cell line with which to compare the miR responses of ciGEnCs, by comparing the miR response of HUVECs and ciGEnCs treated under the same conditions.

The HUVECs used in this study appeared phenotypically normal: of uniform size and shape, and demonstrating the expected cobblestone appearance of cultued endothelial cells (Figure 19). These cells also expressed high levels of PECAM1, confirming retention of their

endothelial phenotype (Figure 18). Neither cellular nor extracellular miR-191 Ct values showed a significant difference between treatment conditions (Figure 21).

Significantly decreased miR-126 detection was observed in HUVEC culture medium following treatment with TNF-α under both 5 mM and 25 mM glucose treatment conditions (Figure 30). These findings are in contrast with those from all ciGEnC groups analysed in the present study (Figure 22).

Decreased cellular miR-126 expression was also observed in HUVECs following TNF-α treatment under both 5 mM and 25 mM glucose treatment conditions (Figure 29). These data contrasted with those for Group C ciGEnCs, which showed no significant differences in cellular miR-126 detection in response to any treatment condition (Figure 23c). Data from Group B ciGEnCs demonstrated decreased miR-126 cellular expression in response to TNF-α treatment, as seen in HUVECs. However, group B ciGEnCs also show decreased miR-126 cellar expression in response to increased glucose concentration, which was not seen in HUVECs (Figure 23b). Group A ciGEnCs under the 5 mM glucose condition demonstrated the same TNF-α induced decrease in miR-126 cellular expression as in HUVECs, although also demonstrated TNF-α-induced increase in miR-126 cellular expression under the 25 mM glucose condition (Figure 24).

These findings demonstrated clear differences in HUVEC and GEnC miR responses *in vitro*, and no further experiments were carried out on HUVECs in this project. These differences might reflect the specialist nature of the GEnCs, which are microvascular endothelial cells adapted specifically to perform the function of high volume filtration.

Exosome Isolation

The isolation of extracellular vesicles (EVs), including exosomes, from HUVEC culture medium was carried out under the expert guidance of Professor Aled Clayton from Cardiff University School of Medicine. This was carried out with the intention of then labelling purified exosomes and investigating their uptake by HK-2 cells, thereby modelling endothelial to proximal tubular epithelial cell EV-mediated communication in the nephron.

The protein to particle ratio method of determining sample purity was proposed by Webber and Clayton (2013). Their research demonstrates that a high purity exosome sample has a particle:protein ratio threshold of $>3 \times 10^{10}$ particles per µg of protein, and samples not meeting this criteria are unsuitable for further analysis. The exosome sample in this study, extracted from culture medium from 10 x T75 HUVEC culture flasks, contained 8.1×10^{7} particles per µg of protein, which was considered too low in purity for successful labelling and uptake experiments. Time-constraints did not allow for this experiment to be repeated with a larger quantity of culture medium.

ciGEnC TaqMan Assays

The miR TaqMan RT-qPCR assays performed for specific miRs generated some data that were inconsistent with those of Beltrami *et al.* (2018), despite the fact that the group C ciGEnCs were cultured under the same conditions as ciGEnCs in Beltrami *et al.* (2018).

Cellular miR-126 expression data from Group C ciGEnCs partially supported data from Beltrami *et al.* (2018), with no significant difference in response to increased glucose or TNF-α, although group C ciGEnCs did show a trend towards decreased miR-126 expression in response to TNF-α ($p = 0.0567$) (Figure 23c). Group A ciGEnCs also partially support Beltrami *et al.* (2018), demonstrating no change in cellular miR-126 expression in response to TNF-α at 25 mM glucose, however there was a significant decrease in miR-126 expression at 5 mM glucose (Figure 24). Group B ciGEnCs did not support Beltrami *et al.* (2018), demonstrating significant decrease in miR-126 expression in response to both TNF-α and 25 mM glucose (Figure 23b).

Group C ciGEnCs partially supported data from Beltrami *et al.* (2018), demonstrating increased extracellular miR-126 expression in response to TNF-α treatment (Figure 22c). Group A ciGEnCs demonstrated the same response to TNF-α treatment (Figure 22a). However, Groups A and C ciGEnCs also demonstrated a significant relationship between glucose concentration and miR-126 extracellular expression, which was not reported by Beltrami *et al.* (2018). Group B results differ from Beltrami *et al.* (2018), demonstrating no significant difference in miR-126 extracellular expression in response to TNF-α, although supported the observation of no significant change in miR-126 extracellular expression in response to 25mM glucose (Figure 22b).

TaqMan assay data supported Beltrami *et al.* (2018) for group A cellular miR-155 expression, with both reporting no significant expression changes in repose to either TNF-α or high glucose treatment conditions (Figure 26a). Group B cellular miR-155 expression also demonstrated no significant change in response to 25 mM glucose treatment but did demonstrate increased expression in response to TNF-α under both glucose conditions (Figure 26b). Extracellular miR-155 expression results from both groups A and B were in agreement with data from Beltrami *et al.* (2018), demonstrating no significant differences under any treatment condition. Due to time constraints, miR-155 and miR-29b were only assayed for group A and B ciGEnCs.

TaqMan assay data for miR-29b cellular expression were inconsistent with data from Beltrami (2014). CiGEnCs of Groups A and B demonstrated no significant difference under either 25 mM glucose or TNF-α treatment conditions, whilst Beltrami (2014) showed decreased miR-29b cellular expression in response to TNF-α. Extracellular expression miR-29b data for Groups A and B did concur with those of Beltrami (2014), with both demonstrating no significant change under either glucose or TNF-α treatment conditions.

The inconsistencies observed between the data collected in this study and those reported previously (Beltrami *et al.* 2018) could be attributed to a number of factors including GEnC phenotype. It is also possible that due to the small sample sizes of this study (n = 3) and Beltrami *et al.* (2018) (n = 4), it is not possible to extrapolate meaningful comparative data without carrying out further experiments. Indeed, to increase the reliably of statistical inferences, these results should be repeated with larger samples in future work.

Comparison with previously conducted urinary miR analysis

Since the primary focus of this project was the analysis of miRs as potential DKD biomarkers, TLDA results were compared with urinary analysis conducted by Beltrami *et al.* (2018), who profiled 754 miRs in pooled urine samples from 20 DKD patients. Beltrami *et al.* (2018), found significantly increased expression of 12 miRs, and decreased expression of 35 miRs, within the urine of patients with DKD compared with healthy controls.

None of the upregulated miRs found in the urine of DKD patients also demonstrated upregulated extracellular expression in this study. There were however several miRs downregulated in the urine of DKD patients that also demonstrated extracellular downregulation in this study.

MiRs -618, -200b and -362-3p demonstrated decreased extracellular expression in response to all three treatment conditions, supporting Beltrami *et al.* (2018) who demonstrated decreased miRs -618, -200b and -362-3p in the urine of DKD patients.

MiRs -885, -100, and -10a all demonstrated decreased extracellular expression in response to both 25mM glucose treatment conditions, which supports data by Beltrami *et al.* (2018), citing these same miRs as among those most significantly downregulated in DKD urine compared with urine from healthy controls.

Similarly, miR-576 showed decreased medium abundance in response to the 25mM glucose + 10 ng/mL TNF-α treatment condition, and was also among the most significantly downregulated miRs in DKD urine compared with healthy controls (Beltrami *et al.* 2018). MiR-576 was however found to be upregulated in the medium of the cytokine treatment condition.

Chapter 4 – Results II: Profiling and analysis of ciGEnC miR expression in an *in vitro* DKD model using hyperglycaemia and TNF-α

4.1 Introduction

Following results of the previous chapter, Group C ciGEnC miR expression will be analysed further by TLDA analysis, allowing for the simultaneous detection of 377 target miRs. This will build a more comprehensive view of cellular and extracellular ciGEnC miR expression in response to hyperglycaemia and TNF-α.

The term 'extracellular miR expression' is used throughout this document to indicate the detected extracellular presence of a miR.

Methods of *in silico* analysis will then be employed to identify potential gene targets of those differentially expressed miRs, and to identify biological processes and pathways associated with those targets.

4.2 TaqMan Low Density Array (TLDA)

4.2.1 TaqMan Low Density miR Array Exclusion Criteria

Following TLDA analysis, exclusion criteria were applied to narrow down the list of 381 miRs and identify those miRs that were most responsive to the presence of TNF-α and/or 25 mM glucose. These exclusion criteria were applied independently to TLDA data from ciGEnC cells and culture medium (Figure 31).

The first exclusion criterion was removal of the 4 control miRs: 3 endogenous control assays (RNU44-001094, RNU48-001006, U6 snRNA-001973) and 1 negative control assay (ath-miR159a-000338) (Figure 31). Since global normalisation was used, these controls were unnecessary for normalisation.

Secondly, miRs with either undetectable threshold cycle (CT) values or CT values >35 in 2 or more treatment conditions were excluded (Figure 31). Following these exclusions, 167 cellular and 165 extracellular miRs were removed from further analysis.

The final exclusion criterion was removal of any miRs for which no changes were detected in response to altered culture conditions (Figure 31).

For the purpose of this study, an upregulation was defined as a log relative quantification value (log_2RQ) of above 1, whilst a downregulation was defined as a log_2RQ of below -1. Implementation of this exclusion criterion resulted in the removal of 134 cellular and 109 extracellular miRs from further analysis.

The remaining miRs were arranged into groups according to the treatment conditions in which they changed (Figure 31).

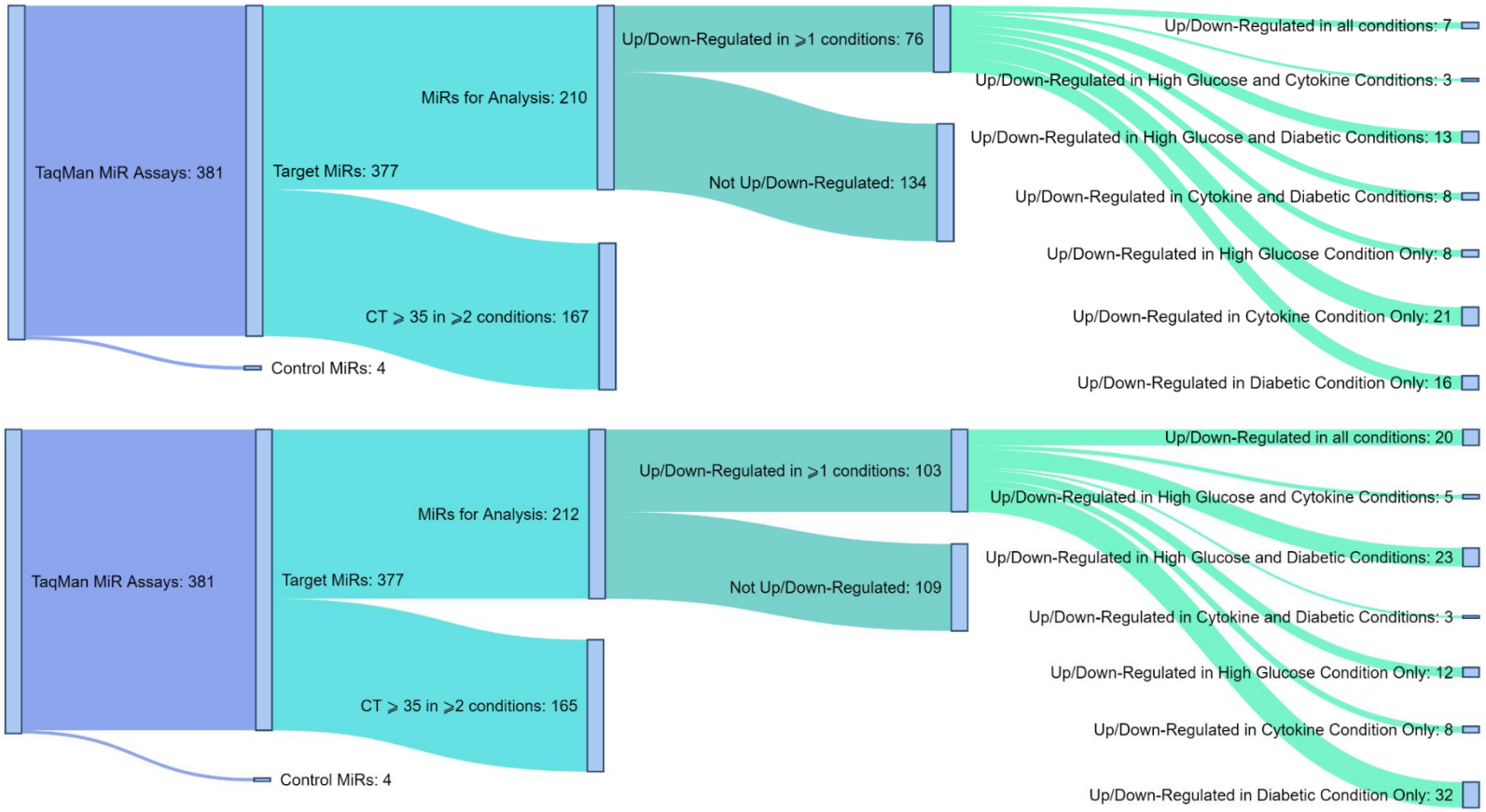

Figure 31: Diagrammatic representation of TLDA exclusion criteria applied to ciGEnCs, a) cellular expression, b) medium detection, under various treatment conditions. Results normalised by global normalisation. Relative gene expression analysed using comparative CT method. Upregulation defined as $\log_2 RQ>1$, and downregulation as $\log_2 RQ<-1$

4.2.2 Detection of cellular ciGEnC miRs by TLDA analysis

For each culture medium treatment, the numbers of cellular miRs that met the above expression upregulation or downregulation criteria are shown below (Figures 32-34).

Cellular ciGEnC expression

Under the 25 mM glucose treatment condition, 21 miRs were upregulated and 10 downregulated (Figure 32).

Under the 5mM glucose + 10 ng/mL TNF-α treatment condition, 14 miRs were upregulated and 25 downregulated (Figure 33).

Under the 25 mM glucose + 10 ng/mL TNF-α treatment condition, 29 miRs were upregulated and 15 downregulated (Figure 34).

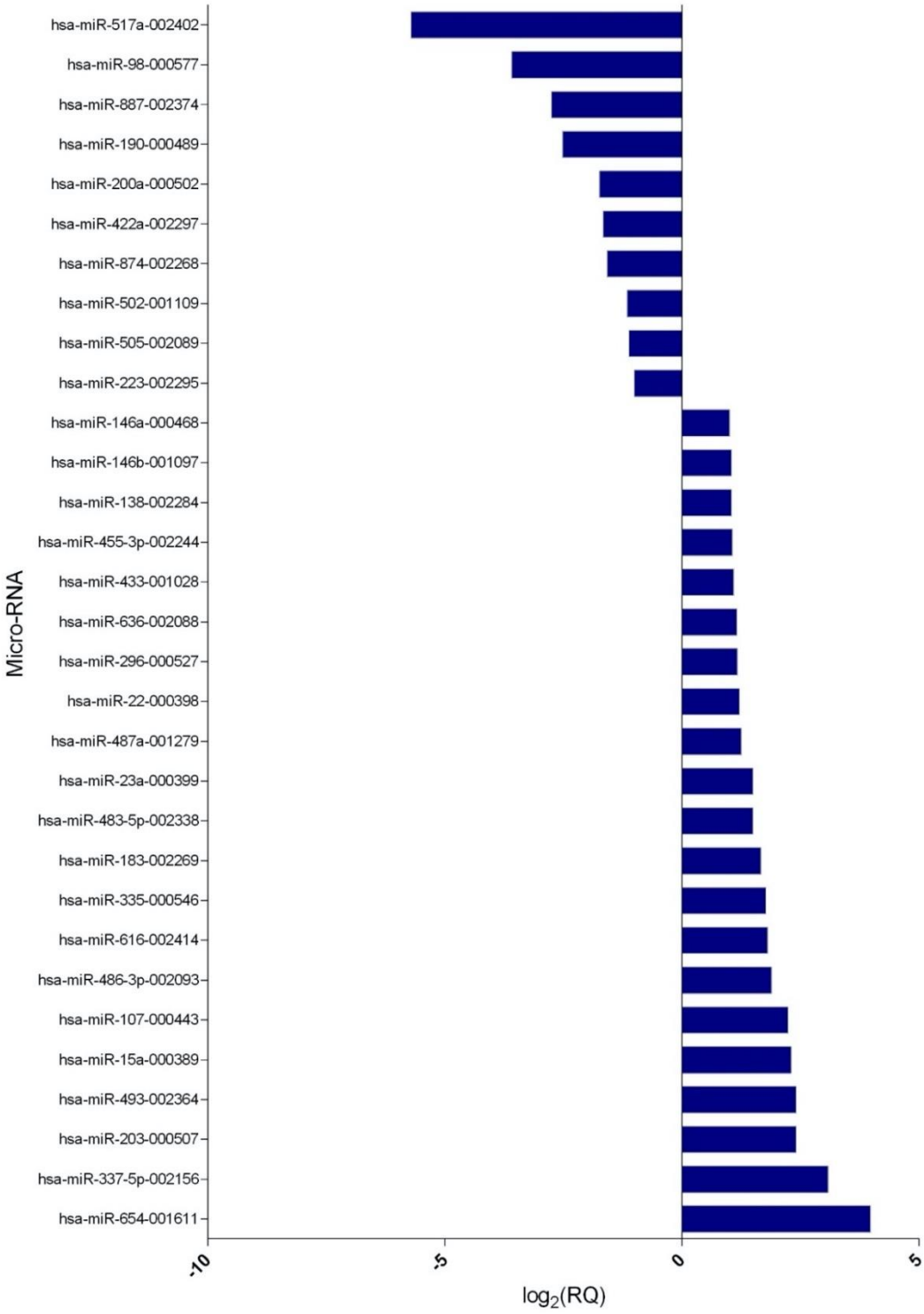

Figure 32: Altered cellular ciGEnC miR expression under the 25 mM glucose treatment condition. Upregulation defined as $log_2RQ>1$, and downregulation as $log_2RQ<-1$; global data normalisation (n = 1).

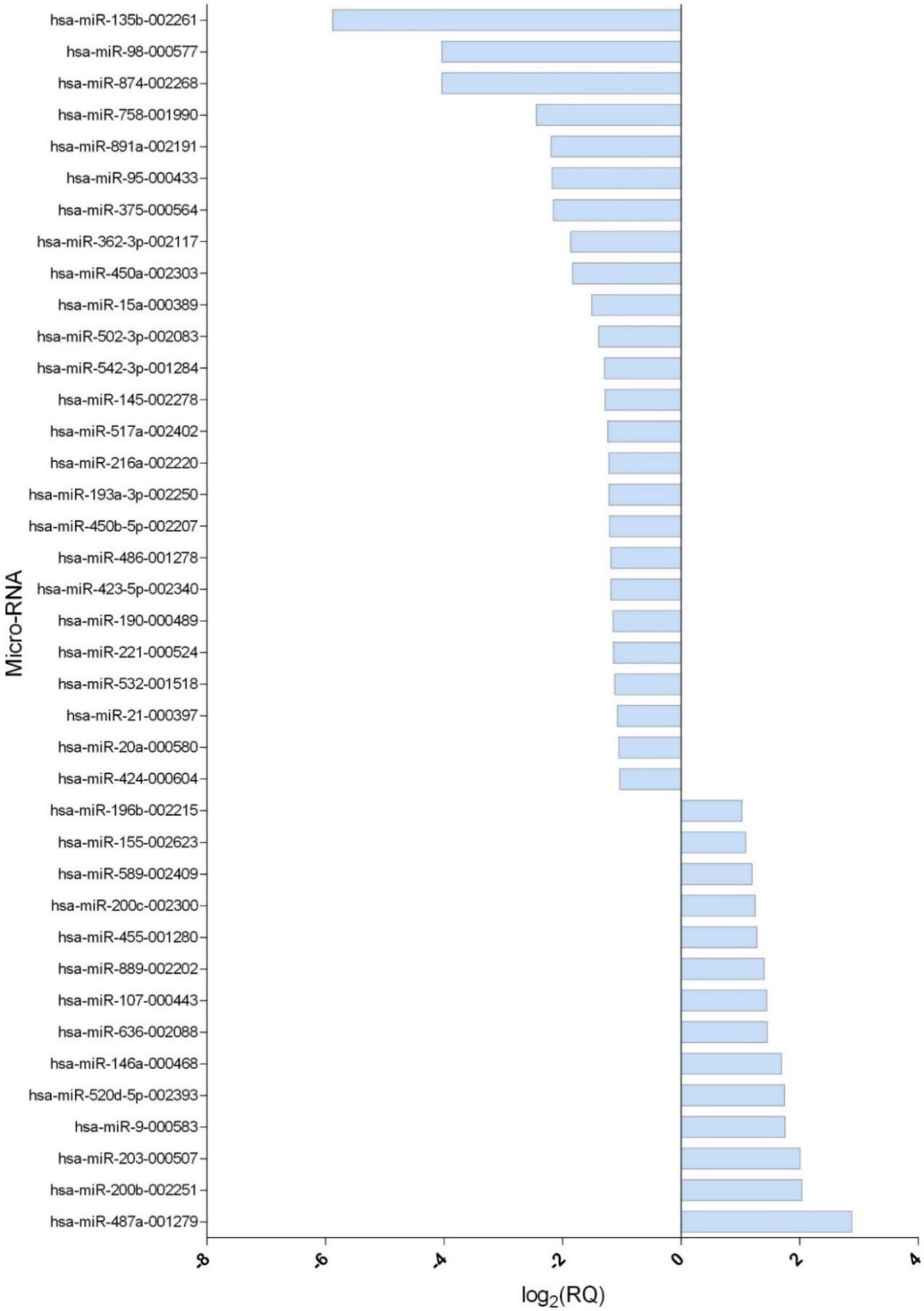

Figure 33: Altered cellular ciGEnC miR expression under the 5mM glucose + 10 ng/mL TNF-α treatment condition. Upregulation defined as $log_2RQ>1$, and downregulation as $log_2RQ<-1$; global data normalisation (n = 1).

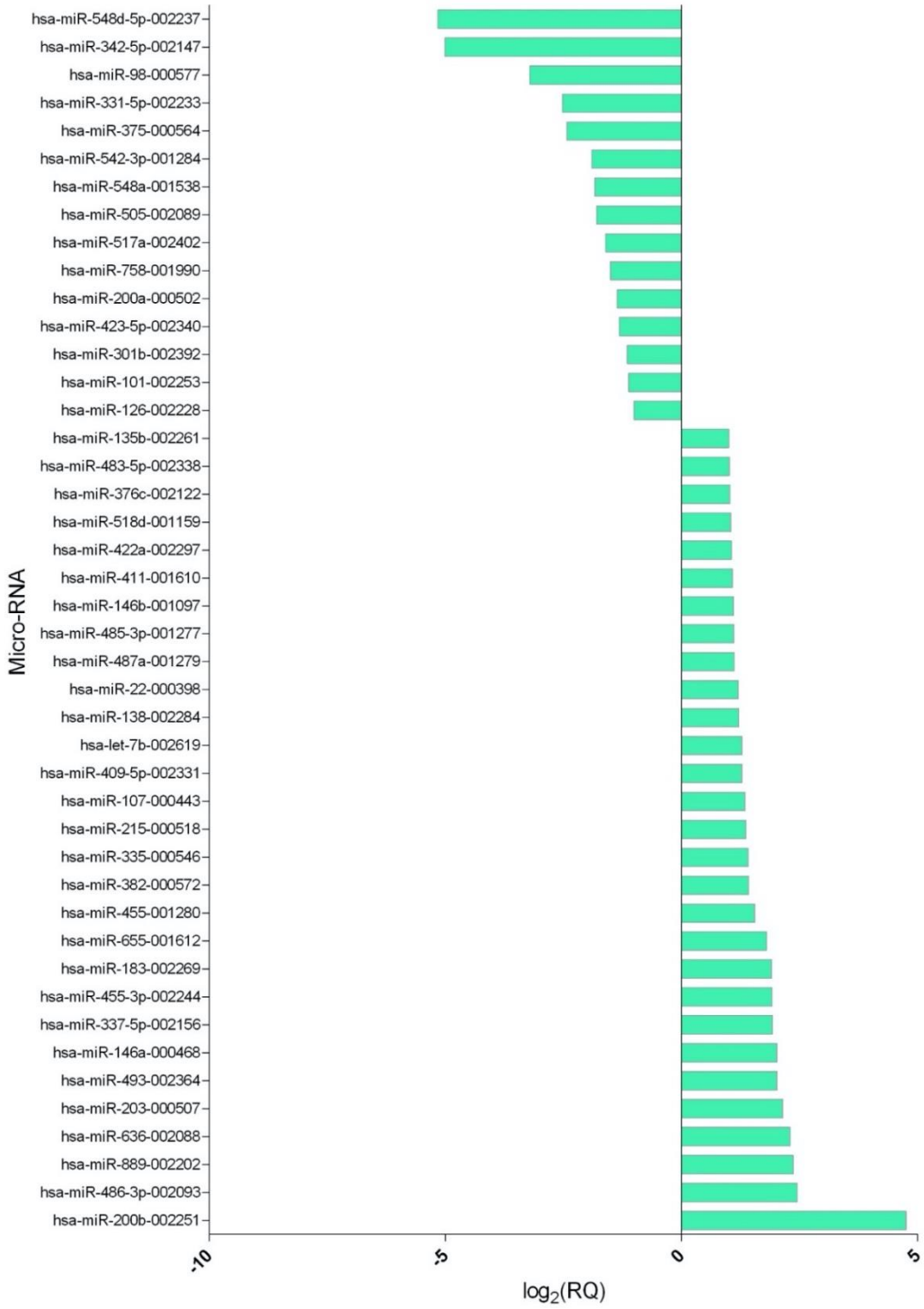

Figure 34: Altered cellular ciGEnC miR expression under the 25 mM glucose + 10 ng/mL TNF-α treatment condition. Upregulation defined as $log_2RQ>1$, and downregulation as $log_2RQ<-1$; global data normalisation (n = 1).

4.2.3 Detection of extracellular ciGEnC miRs by TLDA analysis

For each culture medium treatment, the numbers of extracellular miRs that met the above expression upregulation or downregulation criteria are shown below (Figures 35-37).

Extracellular ciGEnC expression

Under the 25 mM glucose treatment condition, 20 miRs were upregulated and 40 downregulated (Figure 35).

Under the 5mM glucose + 10 ng/mL TNF-α treatment condition, 11 miRs were upregulated and 25 downregulated (Figure 36).

Under the 25 mM glucose + 10 ng/mL TNF-α treatment condition, 60 miRs were upregulated and 10 downregulated (Figure 37).

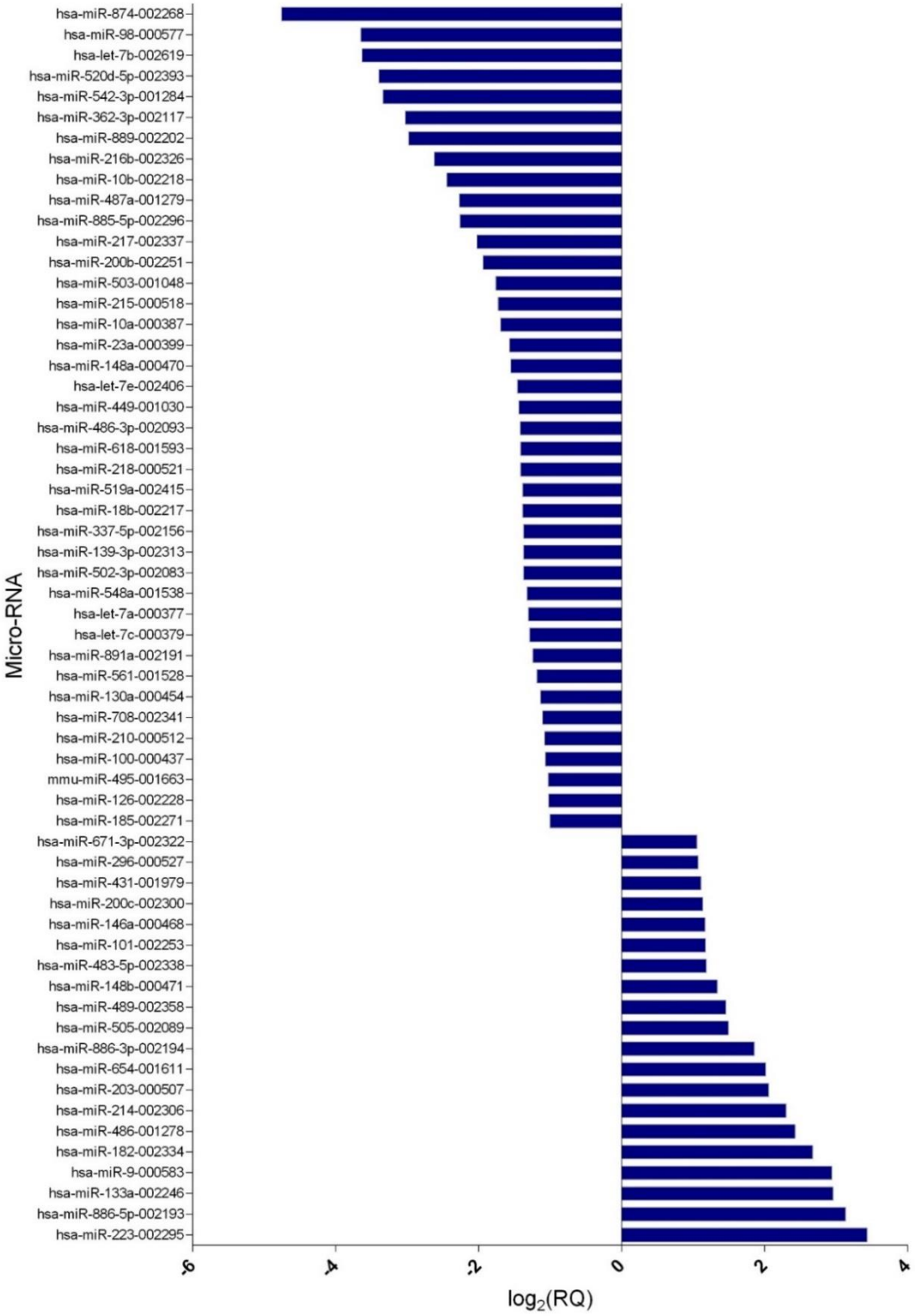

Figure 35: Altered extracellular ciGEnC miR expression under the 25 mM glucose treatment condition. Upregulation defined as $log_2RQ>1$, and downregulation as $log_2RQ<-1$; global data normalisation (n = 1).

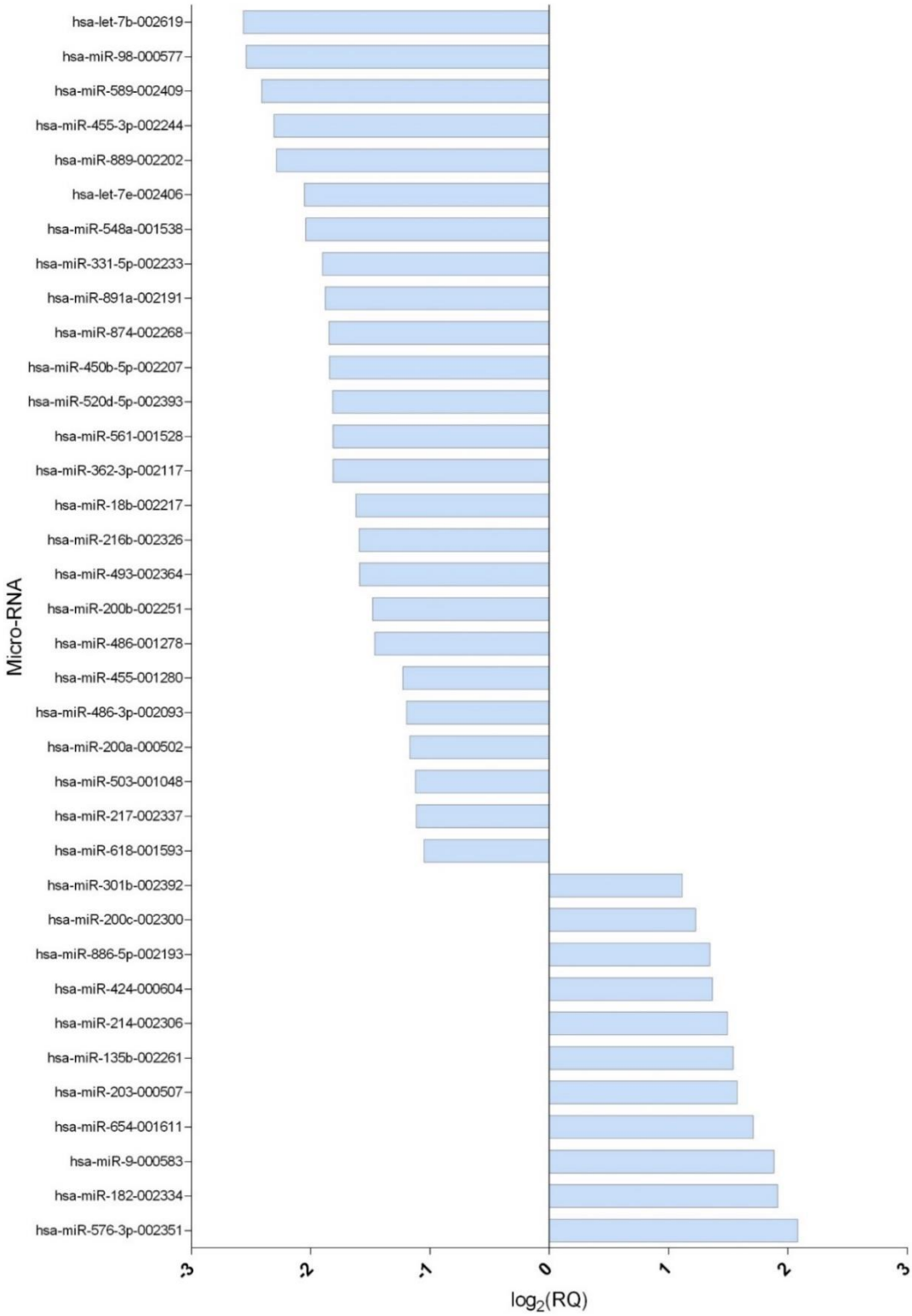

Figure 36: Altered extracellular ciGEnC miR expression under the 5mM glucose + 10 ng/mL TNF-α treatment condition. Upregulation defined as $log_2RQ>1$, and downregulation as $log_2RQ<-1$; global data normalisation (n = 1).

Figure 37: Altered extracellular ciGEnC miR expression under the 25 mM glucose + 10 ng/mL TNF-α treatment condition. Upregulation defined as $log_2RQ>1$, and downregulation as $log_2RQ<-1$; global data normalisation (n = 1).

4.2.4 Comparative analysis of altered ciGEnC miR expression

Comparative analysis of cellular miR expression in ciGEnCs under different treatment conditions

Differentially expressed cellular ciGEnC miRs were compared across experimental treatments. In total, 7 miRs were differentially expressed in all treatments, and the direction of effect for each miR was the same (Figure 38).

Of these 7, 5 were upregulated in all treatments: hsa-miR-636-002088, hsa-miR-203-000507, hsa-miR-146a-000468, hsa-miR-107-000443, hsa-miR-487a-001279; and 2 were downregulated: hsa-miR-517a-002402, hsa-miR-98-000577 (Figure 38).

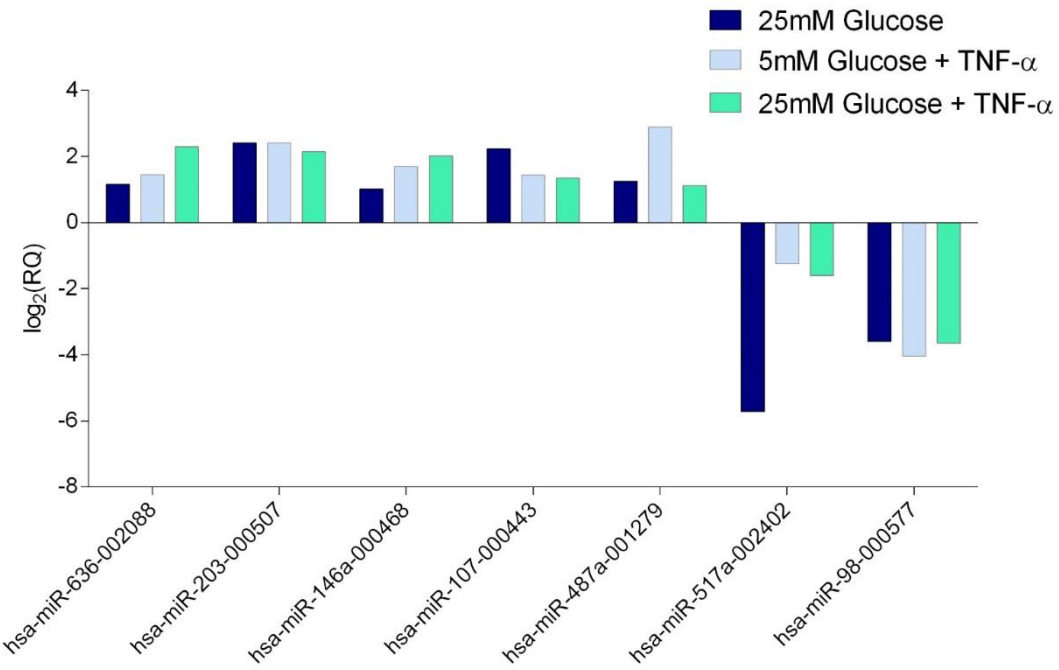

Figure 38: Altered expression of cellular ciGEnC miRs in all three culture treatments: 25 mM glucose, 10 ng/mL TNF-α, 25 mM glucose + 10 ng/mL TNF-α. Upregulation defined as $log_2RQ>1$, and downregulation as $log_2RQ<-1$; global data normalisation (n = 1).

A total of 13 miRs were differentially expressed under both 25 mM glucose and 25 mM glucose + 10 ng/mL TNF-α treatment conditions, with the direction of effect the same for 12 of these miRs (Figure 39).

Of these 13 miRs, 10 were upregulated: hsa-miR-337-5p-002156, hsa-miR-493-002364, hsa-miR-486-3p-002093, hsa-miR-335-000546, hsa-miR-183-002269, hsa-miR-483-5p-002338, hsa-miR-22-000398, hsa-miR-455-3p-002244, hsa-miR-138-002284, hsa-miR-146b-001097; 2 were downregulated: hsa-miR-505-002089, hsa-miR-200a-000502; and 1 was downregulated in 25 mM glucose, but upregulated in 25 mM + 10 ng/mL TNF-α: hsa-miR-422a-002297 (Figure 39).

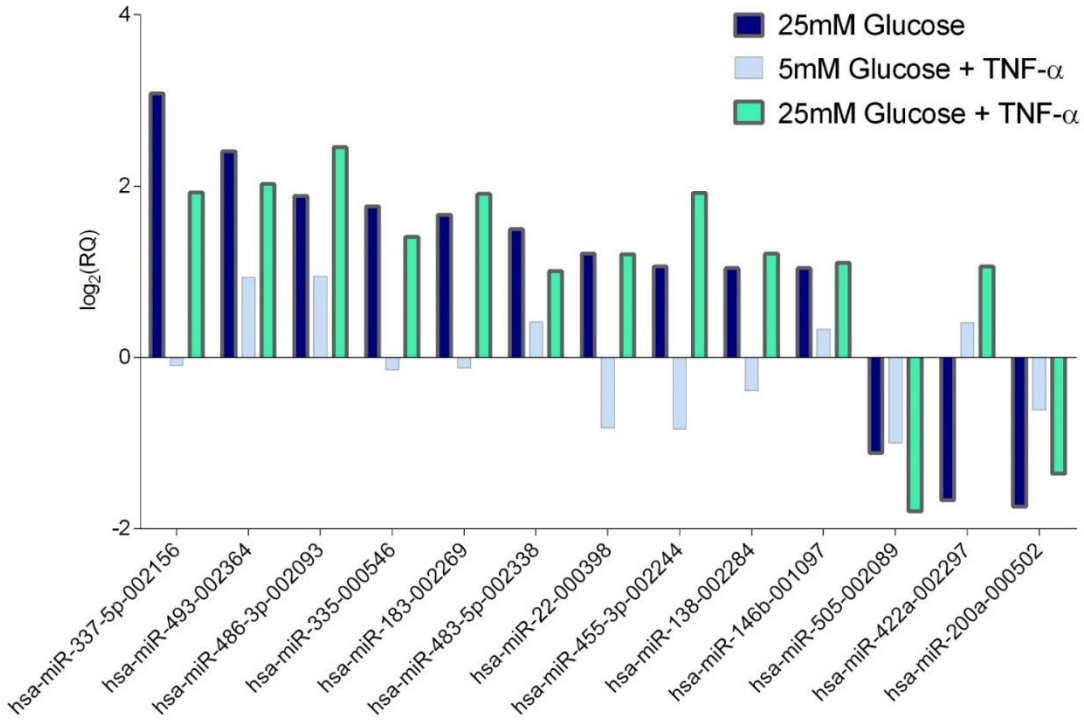

Figure 39: Altered expression of cellular ciGEnC miRs in 25 mM glucose and 25 mM glucose + 10 ng/mL TNF-α. Upregulation defined as $log_2RQ>1$, and downregulation as $log_2RQ<-1$; global data normalisation (n = 1).

Eight miRs were differentially expressed under both the 5mM glucose + 10 ng/mL TNF-α and 25 mM glucose + 10 ng/mL TNF-α treatment conditions. Seven miRs demonstrated the same direction of effect (Figure 40).

Of these, three were upregulated: hsa-miR-200b-002251, hsa-miR-889-002202, hsa-miR-455-001280; 4 were downregulated: hsa-miR-423-5p-002340, hsa-miR-542-3p-001284, hsa-miR-375-000564, hsa-miR-758-001990. Hsa-miR-135b-002261 was upregulated in 25 mM glucose + 10 ng/mL TNF-α, but downregulated in 5mM glucose + 10 ng/mL TNF-α (Figure 40).

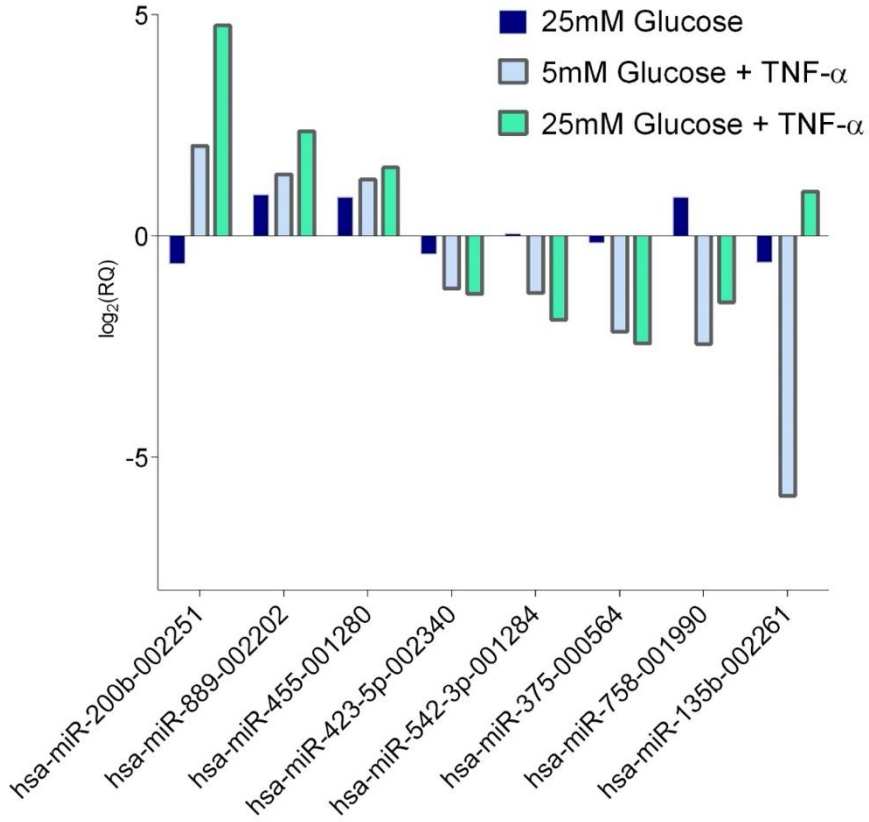

Figure 40: Altered expression of cellular ciGEnC miRs under 10 ng/mL TNF-α and 25 mM glucose + 10 ng/mL TNF-α treatment conditions. Upregulation defined as $log_2RQ>1$, and downregulation as $log_2RQ<-1$; global data normalisation (n = 1).

Analysis of cellular ciGEnC miR expression when classified by up- or down-regulation showed extensive overlap between treatment groups (Figure 41).

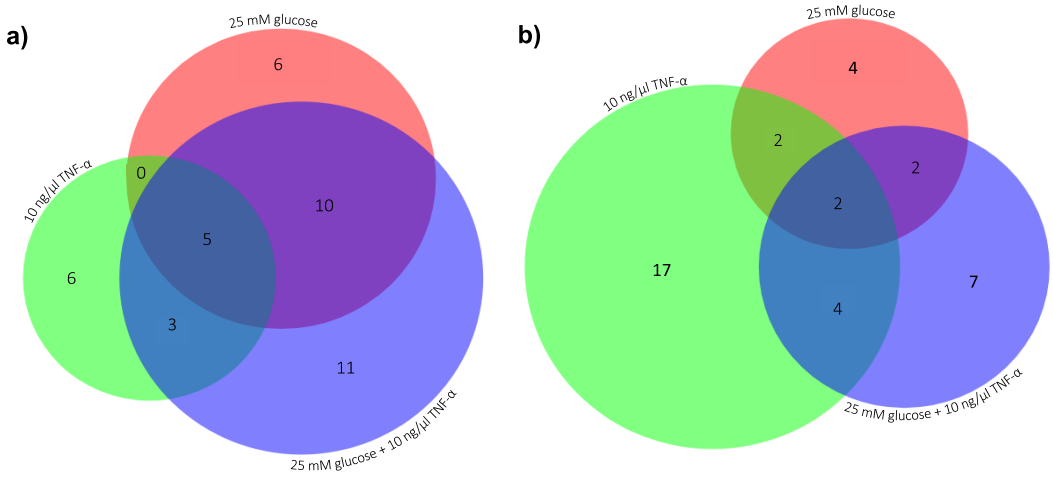

Figure 41: Proportional Venn Diagrams showing commonalities between **a)** upregulated cellular miRs and **b)** downregulated cellular miRs, under various treatment conditions. Upregulation defined as $log_2RQ>1$, and downregulation as $log_2RQ<-1$; global data normalisation (n = 1).

Comparative analysis of extracellular miR expression in ciGEnCs under different treatment conditions

Differentially expressed extracellular ciGEnC miRs were compared across experimental treatments.

In total, 20 miRs were differentially expressed in all three treatments, and the direction of effect for each miR was the same (Figure 42).

Of these, 5 miRs were upregulated under all treatment conditions: hsa-miR-886-5p-002193, hsa-miR-214-002306, hsa-miR-654-001611, hsa-miR-182-002334, hsa-miR-9-000583; and 15 were down-regulated under all treatment conditions: hsa-miR-362-3p-002117, hsa-miR-561-001528, hsa-miR-217-002337, hsa-miR-874-002268, hsa-miR-18b-002217, hsa-let-7e-002406, hsa-miR-618-001593, hsa-miR-548a-001538, hsa-miR-216b-002326, hsa-miR-200b-002251, hsa-let-7b-002619, hsa-miR-486-3p-002093, hsa-miR-889-002202, hsa-miR-503-001048, hsa-miR-891a-002191.

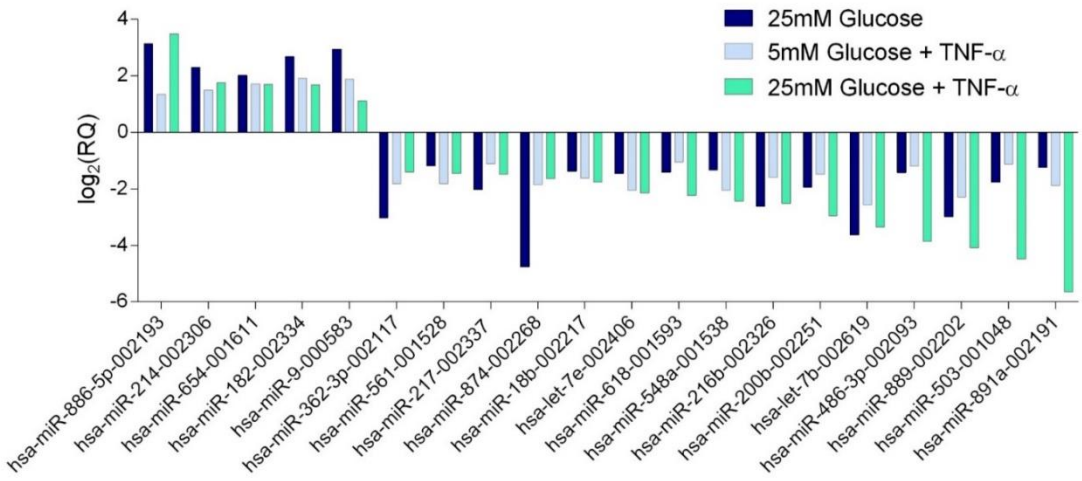

Figure 42: Altered expression of extracellular ciGEnC miRs under all three culture treatment conditions: 25 mM glucose, 10 ng/mL TNF-α, 25 mM glucose + 10 ng/mL TNF-α. Upregulation defined as $log_2RQ>1$, and downregulation as $log_2RQ<-1$; global data normalisation (n = 1).

A total of 23 miRs were differentially expressed under both 25 mM glucose and 25 mM glucose + 10 ng/mL TNF-α treatment conditions. All 23 miRs demonstrated the same direction of effect.

Of these, 5 were upregulated: hsa-miR-146a-000468, hsa-miR-431-001979, hsa-miR-296-000527, hsa-miR-886-3p-002194, hsa-miR-133a-002246; and 18 were downregulated: hsa-miR-23a-000399, hsa-let-7c-000379, hsa-miR-10b-002218, hsa-miR-130a-000454, hsa-miR-502-3p-002083, hsa-miR-337-5p-002156, hsa-miR-449-001030, hsa-miR-218-000521, hsa-miR-542-3p-001284, hsa-miR-487a-001279, hsa-miR-885-5p-002296, hsa-

miR-100-000437, hsa-miR-708-002341, hsa-miR-10a-000387, hsa-miR-519a-002415, hsa-miR-215-000518, hsa-miR-126-002228, hsa-miR-210-000512) (Figure 43).

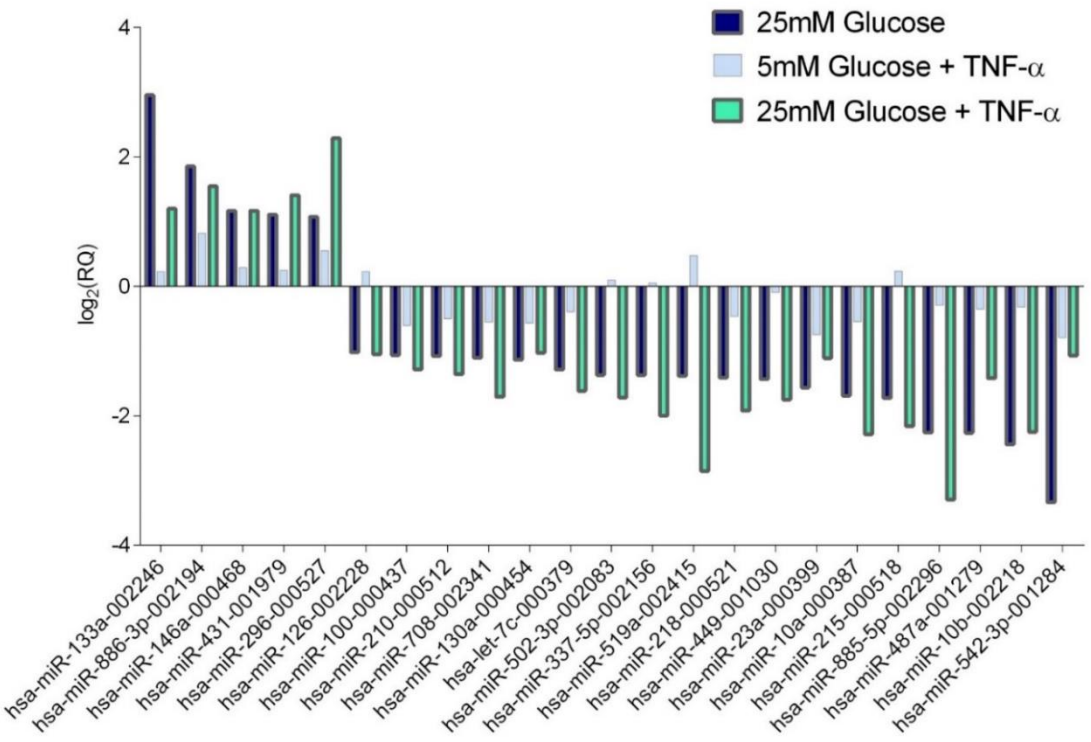

Figure 43: Altered expression of extracellular ciGEnC miRs under both 25 mM glucose and 25 mM glucose + 10 ng/mL TNF-α treatment conditions. Upregulation defined as $log_2RQ>1$, and downregulation as $log_2RQ<-1$; global data normalisation (n = 1).

Three miRs were differentially expressed under both 10 ng/mL TNF-α and 25 mM glucose + 10 ng/mL TNF-α treatment conditions. Two of these miRs demonstrated the same direction of effect.

One miR was upregulated: hsa-miR-135b-002261; 1 miR was downregulated: hsa-miR-589-002409, and hsa-miR-576-3p-002351 expression was upregulated in 5mM glucose + 10 ng/mL TNF-α, but downregulated in 25 mM glucose + 10 ng/mL TNF-α (Figure 44).

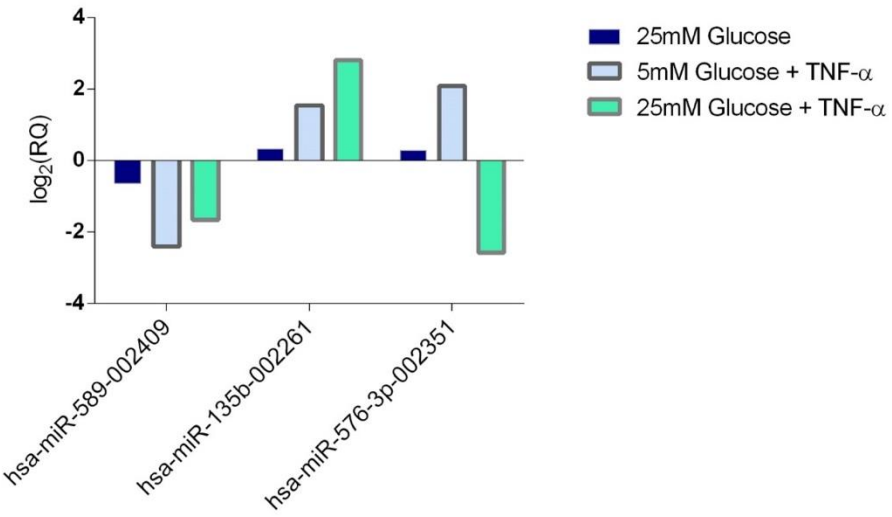

Figure 44: Altered expression of extracellular ciGEnC miRs under 10 ng/mL TNF-α and 25 mM glucose + 10 ng/mL TNF-α treatment conditions. Upregulation defined as $log_2RQ>1$, and downregulation as $log_2RQ<-1$; global data normalisation (n = 1).

Analysis of extracellular ciGEnC miR expression when classified by up- or down-regulation, showed extensive overlap between treatment groups (Figure 45).

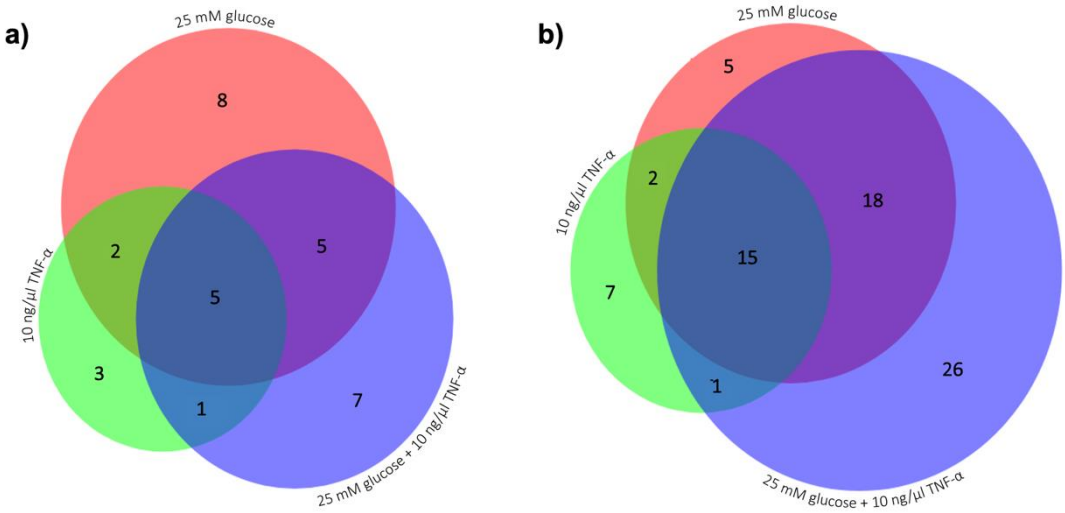

Figure 45: Proportional Venn Diagrams showing commonalities between **a)** upregulated extracellular miRs and **b)** downregulated extracellular miRs, under various treatment conditions. Upregulation defined as $log_2RQ>1$, and downregulation as $log_2RQ<-1$; global data normalisation (n = 1).

Comparison with previously conducted urinary miR analysis

Since the primary focus of this project was the analysis of miRs as potential DKD biomarkers, TLDA results were compared with urinary analysis conducted by Beltrami *et al.* (2018), who profiled 754 miRs in pooled urine samples from 20 DKD patients. Beltrami *et al.* (2018), found significantly increased expression of 12 miRs, and decreased expression of 35 miRs, within the urine of patients with DKD compared with healthy controls.

None of the upregulated miRs found in the urine of DKD patients also demonstrated upregulated extracellular expression in this study. There were however several miRs downregulated in the urine of DKD patients that also demonstrated extracellular downregulation in this study.

MiRs -618, -200b and -362-3p demonstrated decreased extracellular expression in response to all three treatment conditions, supporting Beltrami *et al.* (2018) who demonstrated decreased miRs -618, -200b and -362-3p in the urine of DKD patients.

MiRs -885, -100, and -10a all demonstrated decreased extracellular expression in response to both 25mM glucose treatment conditions, which supports data by Beltrami *et al.* (2018), citing these same miRs as among those most significantly downregulated in DKD urine compared with urine from healthy controls.

Similarly, miR-576 showed decreased medium abundance in response to the 25mM glucose + 10 ng/mL TNF-α treatment condition, and was also among the most significantly downregulated miRs in DKD urine compared with healthy controls (Beltrami *et al.* 2018). MiR-576 was however found to be upregulated in the medium of the cytokine treatment condition.

4.3 *In silico* analysis

4.3.1 Analysis of differentially expressed cellular and extracellular ciGEnC miRs

Differentially expressed cellular ciGEnC miRs were compared across treatment groups, and results visualised using a DiVenn diagram (Figure 46). This process was completed also for the corresponding for extracellular miRs (Figure 47).

Overlap in differentially expressed cellular ciGEnC miRs was observed in different culture treatments. The greatest number of commonly differentially expressed miRs was shared between 25 mM glucose and 25 mM + 10 ng/mL TNF-α, and 10 ng/mL TNF-α and 25 mM + 10 ng/mL TNF-α treatments. In total, 5 miRs were upregulated and 2 miRs were downregulated in all treatments. The fewest overlapping differentially expressed miRs were shared between 25 mM glucose and 10 ng/mL TNF-α treatments (Figure 46).

Substantial overlap was also observed between extracellular ciGEnC miRs in different culture treatments. Once again, the greatest number of commonly differentially expressed miRs was shared between 25 mM glucose and 25 mM + 10 ng/mL TNF-α, and 10 ng/mL TNF-α and 25 mM + 10 ng/mL TNF-α treatments. There was also a substantial overlap between miRs showing differential medium abundance under all three treatment conditions, with 5 miRs upregulated under all treatment conditions, and 15 miRs downregulated under all treatment conditions. Unlike the cellular expression results, there was not a high proportion of overlap demonstrated between the 5mM glucose + 10 ng/mL TNF-α and 25 mM + 10 ng/mL TNF-α treatment conditions. However, similarly to cellular expression

results there was not a high proportion of overlap between miRs differentially expressed under 25 mM and 10 ng/mL TNF-α treatments (Figure 47).

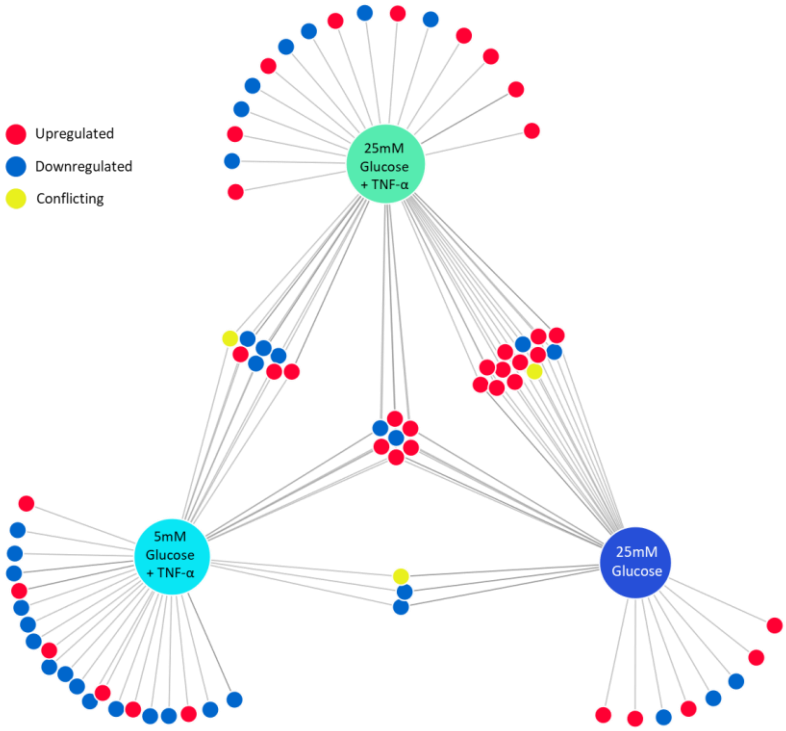

Figure 46: DiVenn diagram showing shared differentially expressed cellular miRs in ciGEnCs in treated with 25 mM glucose, 10 ng/mL TNF-α and 25 mM glucose + 10 ng/mL TNF-α.

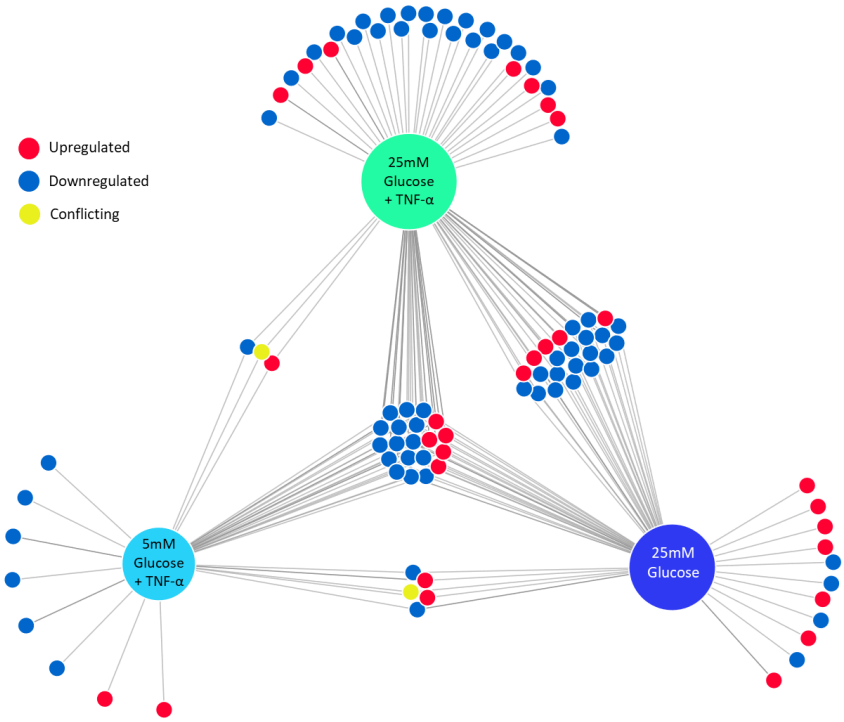

Figure 47: DiVenn diagram showing shared differentially expressed extracellular miRs in ciGEnCs in treated with 25 mM glucose, 10 ng/mL TNF-α and 25 mM glucose + 10 ng/mL TNF-α.

4.3.2 miRDIP analysis

MirDIP is a tool which integrates 30 independent miR-target resources, including DIANA, miRbase, miRDB, mirTar, PicTar, and TargetScan. MirDIP provides an integrative score to each unique miR-target interaction, which is based on the combination of confidence measures given by each of the individual resources. This method of combining resources generates more accurate MIR-target predictions than the use of any singular resource (Tokar *et al.* 2018). Only the top 1% of miR-target predictions were extracted for further analysis.

For data entry into mirDIP the ThermoFisher TLDA miR assignations used so far in this thesis were converted to their corresponding identification codes in miRbase (Appendix 2).

Differentially expressed miR data were entered into mirDIP to identify predicted target genes for each miR (Tokar *et al.* 2018). Due to the large volume of data generated during this analysis, only mRNAs within the top 1% of target predictions were included.

MirDIP predicted:

- 9,870 mRNAs were associated with differentially expressed cellular ciGEnC miRs in 25 mM glucose + 10 ng/mL TNF-α
- 9,224 mRNAs were associated with differentially expressed cellular ciGEnC miRs in 25mM glucose

- 9,857 mRNAs were associated with differentially expressed cellular ciGEnC miRs in 5mM glucose + 10 ng/mL TNF-α
- 11,443 mRNAs were associated with differentially expressed extracellular ciGEnC miRs in 25mM glucose + 10 ng/mL TNF-α
- 10,771 mRNAs were associated with differentially expressed extracellular ciGEnC miRs in 25mM glucose
- 9,739 mRNAs were associated with differentially expressed extracellular ciGEnC miRs in 5mM glucose + 10 ng/mL TNF-α

Shared predicted mRNA targets for differentially expressed ciGEnC miRs between different experimental culture treatments are shown in Figures 48 (cellular miR targets) and 49 (extracellular miR targets).

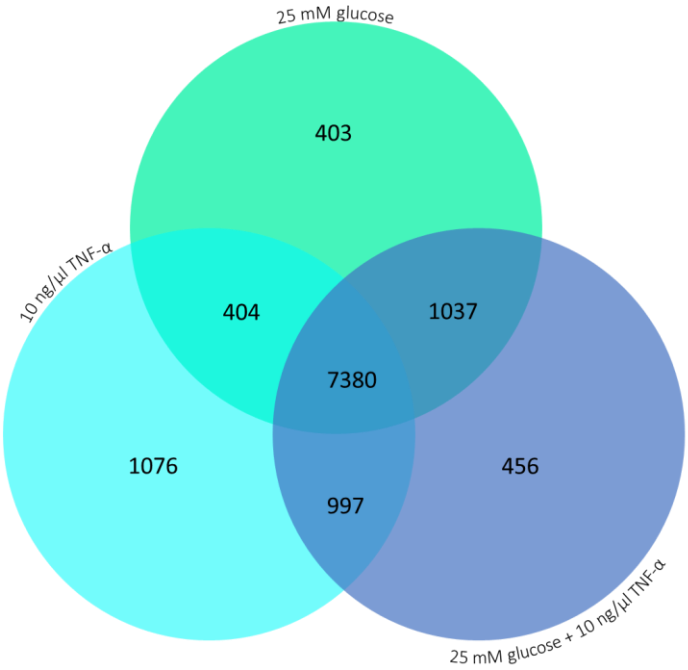

Figure 48: Venn diagram of predicted mRNAs targets for differentially expressed cellular ciGEnC miRs

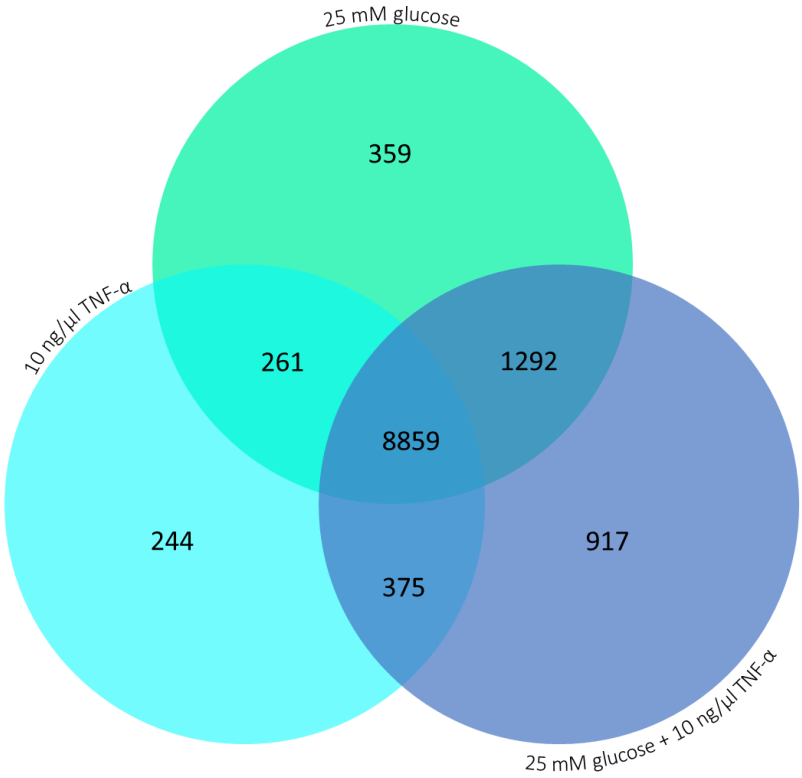

Figure 49: Venn diagram of predicted mRNAs targets for differentially expressed extracellular ciGEnC miRs.

In contrast to the corresponding outputs for differentially expressed ciGEnC miRs described above (Figures 46 and 47), by far the largest number of shared mRNA targets in Figures 48 and 49 were common to all three experimental culture treatments.

Cellular ciGEnC miR data from Figure 46 showed most sharing between the 25 mM glucose + 10 ng/mL TNF-α treatment, with 25 mM glucose and 10 ng/mL TNF-α + 5 mM glucose treatment conditions. Despite the fact that there were only 3 shared differentially expressed cellular miRs between 25 mM glucose and 5 mM glucose + 10 ng/mL TNF-α (Figure 46), there was a large overlap in the predicted mRNA targets for these treatments (Figure 48).

Extracellular ciGEnC miR data from Figure 47 showed most sharing between the 25mM glucose and 25 mM glucose + 10 ng/mL TNF-α treatment conditions, and between all three treatment conditions. These were also the treatment condition combinations sharing the greatest number of mRNA predictions (Figure 49). Comparatively few differentially expressed miRs (Figure 47) and mRNA targets (Figure 49) were shared between the 5 mM glucose + 10 ng/mL TNF-α and the other two treatment conditions.

4.3.3 GEnC-expressed cellular miR targets

The above analysis of cellular miRs generated approximately 10,000 potential mRNA targets for each treatment condition. To refine this analysis, these mRNA targets were then restricted to those 8540 genes expressed in glomerular endothelial cells, as defined in the comprehensive analysis of Sengoelge *et al.* (2014).

Limiting mRNA targets to those identified as GEnC-specific (Sengoelge *et al.* 2014):

- 2,327 mRNAs remained that were associated with differentially expressed cellular ciGEnC miRs in the 25mM glucose treatment condition (Appendix 3)
- 2,471 mRNAs remained that were associated with differentially expressed cellular ciGEnC miRs in the 5 mM glucose + 10 ng/mL TNF-α treatment condition (Appendix 4)
- 2,506 mRNAs remained that were associated with differentially expressed cellular ciGEnC miRs in the 25 mM glucose + 10 ng/mL TNF-α treatment condition (Appendix 5)

A venn diagram of the refined predicted cellular mRNA targets is shown in figure 50.

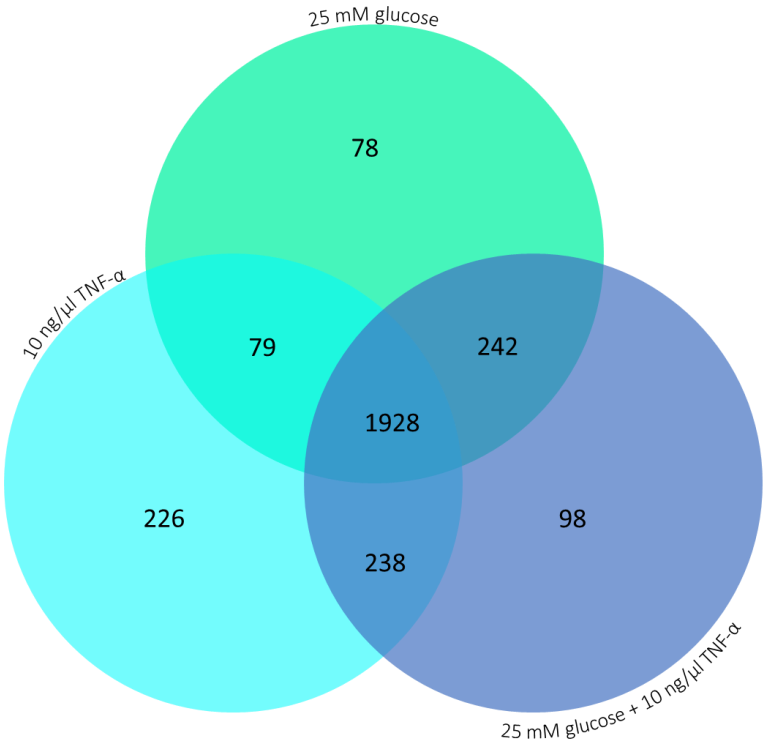

Figure 50: Venn diagram of predicted GEnC-expressed mRNA targets for differentially expressed cellular ciGEnC miRs following various experimental culture treatments.

4.3.4 Extracellular miR targets expressed in the nephron

A second refinement process was conducted for extracellular miR target predictions, in which the predicted mRNAs were restricted to those 7906 mRNAs expressed in the nephron, as defined by The Human Protein Atlas version 19.3 (The Human Protein Atlas).

Limiting mRNA targets to those identified as nephron-specific:

- 5,241 remained that were associated with differentially expressed extracellular ciGEnC miRs in 25 mM glucose treatment condition (Appendix 9)
- 4,849 remained that were associated with differentially expressed extracellular ciGEnC miRs in 5 mM glucose + 10 ng/mL treatment condition (Appendix 10)
- 5,535 mRNAs remained that were associated with differentially expressed extracellular ciGEnC miRs in 25 mM glucose + 10 ng/mL treatment condition (Appendix 11)

A venn diagram the refined predicted extracellular mRNA targets is shown in figure 51.

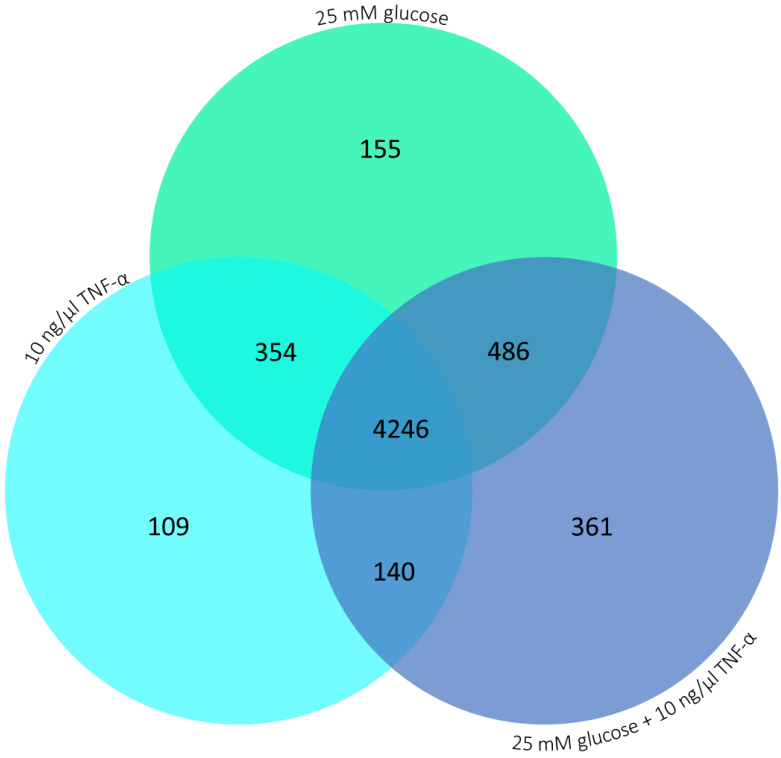

Figure 51: Venn diagram of predicted GEnC-expressed mRNA targets for differentially expressed extracellular ciGEnC miRs following various experimental culture treatments.

4.3.5 Functional enrichment of predicted gene lists

For analysis of predicted gene targets associated with miRs of differential cellular and extracellular expression, the following combinations of predicted gene targets were entered into g:Profiler for computation of functionally enriched GO terms, KEGG pathways, and REACTOME pathways:

i) mRNA targets present under all three treatment conditions (Appendix 6, 12)
ii) mRNA targets present under both 25 mM glucose and 25 mM glucose + 10 ng/mL TNF-α treatment conditions (Appendix 7, 13)
iii) mRNA targets present under both 10 ng/mL TNF-α and 25 mM glucose + 10 ng/mL TNF-α treatment conditions (Appendix 8, 14)

Each treatment condition was also analysed separately.

KEGG and REACTOME pathways are shown in tables 2-13, with their respective p-values.

GO terms were entered into REVIGO for summarisation, and the removal of redundant GO terms. Tree maps were created for visual depiction of GO term cluster results, and are presented in appendix 15-50.

Functional enrichment analysis of predicted genes associated with differentially expressed cellular miRs

Genes associated with cellular miRs expressed under all three treatment conditions (25 mM glucose + 10 ng/mL TNF-α, 25mM glucose, 5 mM glucose + 10 ng/mL TNF-α)

Considering those genes predicted to be associated with all three treatment conditions, the biological process GO term clusters showing highest enrichment were 'regulation of cellular component organisation', followed by 'anatomical structure development', and 'movement of cell or subcellular component' (Appendix 15). The cellular component GO term cluster with the highest enrichment was 'plasma membrane region', followed by 'cytoplasmic region' and 'cell projection' (Appendix 16). Within the molecular function class, the most enriched GO term cluster was 'cytoskeletal protein binding', followed by 'regulatory region nucleic acid binding', and 'RNA polymerase II transcription factor activity, sequence-specific DNA binding' (Appendix 17).

The KEGG term of highest enrichment was 'miRs in cancer', and the REACTOME pathway with the highest enrichment was 'signal transduction' (Table 2).

Table 2: KEGG and REACTOME pathways functionally enriched within the predicted gene list associated with ciGEnC cellular miR expression under all three treatment conditions (25 mM glucose + 10 ng/mL TNF-α, 25mM glucose, 5 mM glucose + 10 ng/mL TNF-α).

Pathway	Term Name	Term ID	P-Value
KEGG	MiRs in cancer	KEGG:05206	1.72E-06
KEGG	Proteoglycans in cancer	KEGG:05205	6.67E-05
KEGG	PI3K-Akt signaling pathway	KEGG:04151	0.000139
KEGG	Regulation of actin cytoskeleton	KEGG:04810	0.000515
KEGG	Focal adhesion	KEGG:04510	0.001001
KEGG	Prostate cancer	KEGG:05215	0.002491
KEGG	Pathways in cancer	KEGG:05200	0.004327
KEGG	Melanogenesis	KEGG:04916	0.004684
KEGG	Adrenergic signaling in cardiomyocytes	KEGG:04261	0.006924
KEGG	Adherens junction	KEGG:04520	0.024229
KEGG	Dopaminergic synapse	KEGG:04728	0.030231
KEGG	Human papillomavirus infection	KEGG:05165	0.04297
REACTOME	Signal Transduction	REAC:R-HSA-162582	1.65E-09
REACTOME	Signaling by Receptor Tyrosine Kinases	REAC:R-HSA-9006934	0.001229
REACTOME	L1CAM interactions	REAC:R-HSA-373760	0.003423

Genes associated with cellular miRs expressed under both 25mM glucose conditions (25 mM glucose + 10 ng/mL TNF-α, and 25mM glucose)

The biological process GO term clusters showing the greatest level of enrichment were 'positive regulation of biological process', 'anatomical structure development', 'protein phosphorylation', and 'cytoskeleton organisation' (Appendix 18). Under the cellular component GO term clusters, the terms showing greatest enrichment were 'plasma membrane part' followed by 'cytoskeleton' and 'cell protection' (Appendix 19). The molecular function GO term clusters of highest enrichment were 'cytoskeletal protein binding', 'transcription regulatory region DNA binding' and 'phosphatase activity' (Appendix 19).

The KEGG and REACTOME pathway terms showing greatest enrichment were 'Pathways in cancer' and 'Signal transduction' respectively (Table 3).

Table 3: KEGG and REACTOME pathways functionally enriched within the predicted gene list associated with ciGEnC cellular miR expression under both 25mM glucose treatment conditions (25mM glucose and 25mM glucose + 10 ng/mL TNF-α)

Pathway	Term Name	Term ID	P-Value
KEGG	Pathways in cancer	KEGG:05200	3.47E-05
KEGG	MiRs in cancer	KEGG:05206	0.000126
KEGG	MAPK signaling pathway	KEGG:04010	0.001683
KEGG	Dopaminergic synapse	KEGG:04728	0.001827
KEGG	Adrenergic signaling in cardiomyocytes	KEGG:04261	0.002492
KEGG	Prostate cancer	KEGG:05215	0.003323
KEGG	Ras signaling pathway	KEGG:04014	0.003941
KEGG	PI3K-Akt signaling pathway	KEGG:04151	0.004218
KEGG	Relaxin signaling pathway	KEGG:04926	0.004393
KEGG	Proteoglycans in cancer	KEGG:05205	0.012001
KEGG	Endocrine resistance	KEGG:01522	0.019441
KEGG	Breast cancer	KEGG:05224	0.022388
KEGG	Regulation of actin cytoskeleton	KEGG:04810	0.023026
KEGG	Melanogenesis	KEGG:04916	0.025297
REACTOME	Signal Transduction	REAC:R-HSA-162582	1.28E-10
REACTOME	Signaling by Receptor Tyrosine Kinases	REAC:R-HSA-9006934	0.000843
REACTOME	L1CAM interactions	REAC:R-HSA-373760	0.003406
REACTOME	Synthesis of PIPs at the plasma membrane	REAC:R-HSA-1660499	0.022087

Genes associated with cellular miRs expressed under both TNF-α treatment conditions (5 mM glucose + 10 ng/mL TNF-α, and 25 mM glucose + 10 ng/mL TNF-α)

The biological process GO term clusters demonstrating highest enrichment were 'positive regulation of cellular process', followed by 'anatomical structure development' and 'movement of cell or subcellular component' (Appendix 21). The cellular component GO term cluster showing the highest enrichment was 'plasma membrane region', followed by 'cell projection' and 'cell periphery' (Appendix 22). The molecular function GO term cluster showing highest enrichment was 'enzyme binding', followed by 'regulatory region nucleic acid binding' and 'transcription factor activity, sequence-specific DNA binding' (Appendix 22).

The KEGG term of highest enrichment was 'miR's in cancer', and the REACTOME pathway with the highest enrichment was 'signal transduction' (Table 4).

Table 4: KEGG and REACTOME pathways functionally enriched within the predicted gene list associated with ciGEnC cellular miR expression under both TNF-α treatment conditions (5mM glucose +TNF-α and 25mM glucose + 10 ng/mL TNF-α).

Pathway	Term Name	Term ID	P-Value
KEGG	MiRs in cancer	KEGG:05206	1.06E-06
KEGG	Proteoglycans in cancer	KEGG:05205	0.000251
KEGG	Pathways in cancer	KEGG:05200	0.001676
KEGG	Regulation of actin cytoskeleton	KEGG:04810	0.006861
KEGG	Focal adhesion	KEGG:04510	0.019193
KEGG	Melanogenesis	KEGG:04916	0.039399
REACTOME	Signal Transduction	REAC:R-HSA-162582	9.97E-11
REACTOME	Signaling by Receptor Tyrosine Kinases	REAC:R-HSA-9006934	0.000594
REACTOME	L1CAM interactions	REAC:R-HSA-373760	0.047265

Genes associated with cellular miRs expressed under the 25 mM glucose + 10 ng/mL TNF-α treatment condition

The biological process GO term clusters showing the highest enrichment were 'positive regulation of cellular process', followed by 'anatomical structure development', and 'movement of cell or subcellular component' (Appendix 23). The cellular component GO terms clusters showing the highest enrichment were 'plasma membrane region', followed by 'cell periphery' and 'cell projection' (Appendix 24). The molecular function GO term clusters showing the highest enrichment were 'enzyme binding', followed by 'regulatory region nucleic acid binding' and 'RNA polymerase II transcription factor activity sequence-specific DNA binding' (Appendix 25).

The KEGG and REACTOME pathway terms showing greatest enrichment were ‘MiRs in cancer’ and ‘signal transduction’ respectively (Table 5).

Table 5: KEGG and REACTOME pathways functionally enriched within the predicted gene list associated with ciGEnC cellular miR expression under the 25 mM glucose + 10 ng/mL TNF-α treatment condition.

Pathway	Term Name	Term ID	P-Value
KEGG	MiRs in cancer	KEGG:05206	4.56E-06
KEGG	Pathways in cancer	KEGG:05200	0.00014
KEGG	Regulation of actin cytoskeleton	KEGG:04810	0.021882
KEGG	Focal adhesion	KEGG:04510	0.040359
REACTOME	Signal Transduction	REAC:R-HSA-162582	8.93E-13
REACTOME	Signaling by Receptor Tyrosine Kinases	REAC:R-HSA-9006934	0.002459

Genes associated with cellular miRs expressed under the 25mM glucose treatment condition

The biological process GO term clusters demonstrating greatest enrichment were ‘regulation of cellular component organisation’, followed by ‘anatomical structure development’ and ‘actin filament based process’ (Appendix 27). The cellular component GO term clusters showing highest enrichment were ‘plasma membrane region’, followed by ‘cell periphery’ and ‘cytoplasmic region’ (Appendix 28). The molecular function GO term cluster showing the highest enrichment was ‘transcription regulatory region DNA binding’ followed by ‘cytoskeletal protein binding’ and ‘RNA polymerase II transcription factor activity sequence-specific DNA binding’ (Appendix 29).

The KEGG and REACTOME pathway terms showing greatest enrichment were ‘*PI3K-Akt signaling pathway*’ and ‘signal transduction’ respectively (Table 6).

Table 6: KEGG and REACTOME pathways functionally enriched within the predicted gene list associated with ciGEnC cellular miR expression under the 25mM glucose treatment condition.

Pathway	Term Name	Term ID	P-Value
KEGG	PI3K-Akt signaling pathway	KEGG:04151	0.000114
KEGG	MiRs in cancer	KEGG:05206	0.000323
KEGG	Pathways in cancer	KEGG:05200	0.006913
KEGG	Focal adhesion	KEGG:04510	0.036803
REACTOME	Signal Transduction	REAC:R-HSA-162582	5.49E-08
REACROME	Signaling by Receptor Tyrosine Kinases	REAC:R-HSA-9006934	0.005891
REACTOME	L1CAM interactions	REAC:R-HSA-373760	0.020567

Genes associated with cellular miRs expressed under the 5 mM glucose + 10 ng/mL TNF-α treatment condition

The biological process GO term cluster demonstrating greatest enrichment was ‘positive regulation of cellular process’, which was followed by ‘anatomical structure development’, and ‘dephosphorylation’ (Appendix 30). The cellular component GO term clusters showing highest enrichment were ‘plasma membrane region’, followed by ‘cell periphery’, ‘synapse part’ and ‘cell projection’ (Appendix 31). The molecular function GO term cluster showing highest enrichment was ‘enzyme binding’, followed by ‘regulatory region nucleic acid binding’ and ‘transcription factor activity sequence-specific DNA binding’ (Appendix 32).

The KEGG and REACTOME pathway terms showing greatest enrichment were ‘MiRs in cancer’ and ‘signal transduction’ respectively (Table 7).

Table 7: KEGG and REACTOME pathways functionally enriched within the predicted gene list associated with ciGEnC cellular miR expression under the 5 mM glucose + 10 ng/mL TNF-α treatment condition

Pathway	Term Name	Term ID	P-value
KEGG	MiRs in cancer	KEGG:05206	8.01305E-05
KEGG	Proteoglycans in cancer	KEGG:05205	0.003902512
KEGG	Hippo signaling pathway	KEGG:04390	0.027814775
REACTOME	Signal Transduction	REAC:R-HSA-162582	1.20487E-05
REACTOME	Signaling by Receptor Tyrosine Kinases	REAC:R-HSA-9006934	0.00047111

Functional enrichment of predicted genes, based on differential miR medium abundance

Genes associated with extracellular miRs expressed under all three treatment conditions (25 mM glucose + 10 ng/mL TNF-α, 25mM glucose, 5 mM glucose + 10 ng/mL TNF-α)

The biological process GO term clusters showing the highest enrichment were 'positive regulation of biological process', 'movement of cell or subcellular component', and 'anatomical structure development' (Appendix 33). The cellular component GO term clusters showing the highest enrichment were 'Golgi apparatus', 'glutamatergic synapse', and 'neurone projection' (Appendix 34). The molecular function GO term clusters with the highest enrichment were 'transcription regulatory region DNA binding', 'RNA polymerase II transcription factor activity and sequence-specific DNA binding', followed by 'enzyme binding' (Appendix 35).

The KEGG and REACTOME pathway terms showing greatest enrichment were 'MiRs in cancer' and 'signal transduction' respectively (Table 8).

Table 8: KEGG and REACTOME pathways functionally enriched within the predicted gene list associated with ciGEnC extracellular miR expression under all three treatment conditions (25 mM glucose + 10 ng/mL TNF-α, 25mM glucose, 5 mM glucose + 10 ng/mL TNF-α).

Pathway	Term Name	Term ID	P-Value
KEGG	MiRs in cancer	KEGG:05206	1.69E-11
KEGG	Pathways in cancer	KEGG:05200	9.64E-07
KEGG	Hippo signaling pathway	KEGG:04390	0.000341
KEGG	Proteoglycans in cancer	KEGG:05205	0.000422
KEGG	PI3K-Akt signaling pathway	KEGG:04151	0.001054
KEGG	Wnt signaling pathway	KEGG:04310	0.001989
KEGG	Ras signaling pathway	KEGG:04014	0.002518
KEGG	Signaling pathways regulating pluripotency of stem cells	KEGG:04550	0.003943
KEGG	Axon guidance	KEGG:04360	0.006304
KEGG	ErbB signaling pathway	KEGG:04012	0.011308
KEGG	Regulation of actin cytoskeleton	KEGG:04810	0.037942
REACTOME	Signal Transduction	REAC:R-HSA-162582	4.83E-11
REACTOME	Signaling by Receptor Tyrosine Kinases	REAC:R-HSA-9006934	4.87E-09
REACTOME	Membrane Trafficking	REAC:R-HSA-199991	1.42E-07
REACTOME	Vesicle-mediated transport	REAC:R-HSA-5653656	9.03E-07
REACTOME	Circadian Clock	REAC:R-HSA-400253	0.001086
REACTOME	MAP kinase activation	REAC:R-HSA-450294	0.001297
REACTOME	Diseases of signal transduction	REAC:R-HSA-5663202	0.005546

REACTOME	Signaling by NTRKs	REAC:R-HSA-166520	0.019387
REACTOME	Interleukin-17 signaling	REAC:R-HSA-448424	0.023716
REACTOME	MAPK targets/ Nuclear events mediated by MAP kinases	REAC:R-HSA-450282	0.026634

Genes associated with extracellular miRs expressed under both 25mM glucose conditions (25 mM glucose + 10 ng/mL TNF-α, and 25mM glucose)

The biological process GO term clusters showing the highest enrichment were 'positive regulation of biological process', 'movement of cell or sub cellular component', and 'protein phosphorylation' (Appendix 36). The cellular component GO term clusters demonstrating highest enrichment were 'Golgi apparatus', 'endomembrane system', and 'neurone projection' (Appendix 37). The molecular function GO term clusters of highest enrichment were 'transcription regulatory region DNA binding', 'RNA polymerase II transcription factor activity sequence-specific DNA binding' and 'enzyme binding' (Appendix 38).

The KEGG and REACTOME pathway terms showing greatest enrichment were 'MiRs in cancer' and 'signal transduction' respectively (Table 9).

Table 9: KEGG and REACTOME pathways functionally enriched within the predicted gene list associated with ciGEnC extracellular miR expression under both 25mM glucose treatment conditions (25mM glucose and 25mM glucose + 10 ng/mL TNF-α)

Pathway	Term Name	Term ID	P-Value
KEGG	MiRs in cancer	KEGG:05206	1.71E-09
KEGG	Pathways in cancer	KEGG:05200	1.19E-06
KEGG	Proteoglycans in cancer	KEGG:05205	0.00524
KEGG	Axon guidance	KEGG:04360	0.01138
KEGG	Wnt signaling pathway	KEGG:04310	0.017311
KEGG	Hippo signaling pathway	KEGG:04390	0.019254
KEGG	PI3K-Akt signaling pathway	KEGG:04151	0.019758
KEGG	TGF-β signaling pathway	KEGG:04350	0.046455
REACTOME	Signal Transduction	REAC:R-HSA-162582	9.45E-09
REACTOME	Signaling by Receptor Tyrosine Kinases	REAC:R-HSA-9006934	1.67E-07
REACTOME	MAP kinase activation	REAC:R-HSA-450294	0.000113
REACTOME	Membrane Trafficking	REAC:R-HSA-199991	0.002138
REACTOME	Vesicle-mediated transport	REAC:R-HSA-5653656	0.006941
REACTOME	Interleukin-17 signaling	REAC:R-HSA-448424	0.007518
REACTOME	Diseases of signal transduction	REAC:R-HSA-5663202	0.009667

Genes associated with extracellular miRs expressed under both TNF-α treatment conditions (5 mM glucose + 10 ng/mL TNF-α, and 25 mM glucose + 10 ng/mL TNF-α)

The biological process GO term clusters showing the highest enrichment were 'positive regulation of biological process', 'movement of cell or subcellular components', and 'anatomical structure development' (Appendix 39). The cellular component GO term clusters demonstrating greatest enrichment were 'bounding membrane of organelle', followed by 'endomembrane system' and 'glutamatergic synapse' (Appendix 40). The molecular function GO term clusters showing the highest enrichment were 'transcription regulatory region DNA-binding', 'transcription factor activity sequence-specific DNA binding', and 'enzyme binding' (Appendix 41).

The KEGG and REACTOME pathway terms showing greatest enrichment were 'MiRs in cancer' and 'signal transduction' respectively (Table 10).

Table 10: KEGG and REACTOME pathways functionally enriched within the predicted gene list associated with ciGEnC extracellular miR expression under both TNF-α treatment conditions (5mM glucose +TNF-α and 25mM glucose + 10 ng/mL TNF-α).

Pathway	Term Name	Term ID	P-Value
KEGG	MiRs in cancer	KEGG:05206	1.86E-11
KEGG	Pathways in cancer	KEGG:05200	8.66E-07
KEGG	Proteoglycans in cancer	KEGG:05205	0.000239
KEGG	Hippo signaling pathway	KEGG:04390	0.001468
KEGG	PI3K-Akt signaling pathway	KEGG:04151	0.003683
KEGG	Axon guidance	KEGG:04360	0.007608
KEGG	Wnt signaling pathway	KEGG:04310	0.007678
KEGG	Ras signaling pathway	KEGG:04014	0.013775
KEGG	Signaling pathways regulating pluripotency of stem cells	KEGG:04550	0.015111
KEGG	Regulation of actin cytoskeleton	KEGG:04810	0.027999
KEGG	ErbB signaling pathway	KEGG:04012	0.034971
REACTOME	Signal Transduction	REAC:R-HSA-162582	9.32E-10
REACTOME	Signaling by Receptor Tyrosine Kinases	REAC:R-HSA-9006934	1.89E-08
REACTOME	Membrane Trafficking	REAC:R-HSA-199991	1.96E-07
REACTOME	Vesicle-mediated transport	REAC:R-HSA-5653656	6.71E-07
REACTOME	Signaling by NTRKs	REAC:R-HSA-166520	0.003728
REACTOME	Circadian Clock	REAC:R-HSA-400253	0.00385
REACTOME	MAP kinase activation	REAC:R-HSA-450294	0.004869
REACTOME	Diseases of signal transduction	REAC:R-HSA-5663202	0.012706
REACTOME	Signaling by NTRK1 (TRKA)	REAC:R-HSA-187037	0.034445

Genes associated with extracellular miRs expressed under the 25 mM glucose + 10 ng/mL TNF-α treatment condition

The biological process GO term clusters showing greatest enrichment were 'positive regulation of biological process', followed by 'nervous system development' and 'cell migration' (Appendix 42). The cellular component GO term clusters showing the highest enrichment were 'endomembrane system', 'Golgi apparatus' and 'neuron projection' (Appendix 43). The molecular function GO term clusters demonstrating highest enrichment were 'transcription regulatory region DNA binding', followed by 'transcription factor activity sequence-specific DNA binding' and 'enzyme binding' (Appendix 44).

The KEGG and REACTOME pathway terms showing greatest enrichment were 'MiRs in cancer' and 'signalling by receptor tyrosine kinases' respectively (Table 11).

Table 11: KEGG and REACTOME pathways functionally enriched within the predicted gene list associated with ciGEnC extracellular miR expression under the 25 mM glucose + 10 ng/mL TNF-α treatment condition.

Pathway	Term Name	Term ID	P-Value
KEGG	MiRs in cancer	KEGG:05206	1.04E-07
KEGG	Pathways in cancer	KEGG:05200	0.000118
KEGG	Proteoglycans in cancer	KEGG:05205	0.015513
KEGG	JAK-STAT signaling pathway	KEGG:04630	0.031653
KEGG	Hippo signaling pathway	KEGG:04390	0.037219
KEGG	PI3K-Akt signaling pathway	KEGG:04151	0.047736
REACTOME	Signaling by Receptor Tyrosine Kinases	REAC:R-HSA-9006934	1.12E-06
REACTOME	Signal Transduction	REAC:R-HSA-162582	1.45E-05
REACTOME	Membrane Trafficking	REAC:R-HSA-199991	0.005883
REACTOME	MAP kinase activation	REAC:R-HSA-450294	0.010726
REACTOME	Vesicle-mediated transport	REAC:R-HSA-5653656	0.015297

Genes associated with extracellular miRs expressed under the 25mM glucose treatment condition

The biological process GO term clusters showing greatest enrichment were 'regulation of signalling', 'movement of cell or subcellular component', and 'anatomical structure development' (Appendix 44). The cellular component GO term clusters demonstrating the highest enrichment were 'neuron projection', 'endomembrane system', and 'Golgi apparatus part' (Appendix 45). The molecular function GO term clusters showing the highest enrichment were 'transcription regulatory region DNA binding', 'transcription factor activity sequence-specific DNA binding' and 'enzyme binding' (Appendix 46).

The KEGG and REACTOME pathway terms showing greatest enrichment were ‘MiRs in cancer’ and ‘signalling by receptor tyrosine kinases’ respectively (Table 12).

Table 12: KEGG and REACTOME pathways functionally enriched within the predicted gene list associated with ciGEnC extracellular miR expression under the 25mM glucose treatment condition.

Pathway	Term Name	Term ID	P-Value
KEGG	MiRs in cancer	KEGG:05206	1.28E-07
KEGG	Pathways in cancer	KEGG:05200	3.05E-05
KEGG	Proteoglycans in cancer	KEGG:05205	0.004974
KEGG	PI3K-Akt signaling pathway	KEGG:04151	0.031203
KEGG	Wnt signaling pathway	KEGG:04310	0.046986
REACTOME	Signal Transduction	REAC:R-HSA-162582	4.88E-08
REACTOME	Signaling by Receptor Tyrosine Kinases	REAC:R-HSA-9006934	5.63E-07
REACTOME	MAP kinase activation	REAC:R-HSA-450294	0.001232
REACTOME	Membrane Trafficking	REAC:R-HSA-199991	0.002284
REACTOME	Vesicle-mediated transport	REAC:R-HSA-5653656	0.004957
REACTOME	TRIF(TICAM1)-mediated TLR4 signaling	REAC:R-HSA-937061	0.02246
REACTOME	MyD88-independent TLR4 cascade	REAC:R-HSA-166166	0.02246
REACTOME	Diseases of signal transduction	REAC:R-HSA-5663202	0.042078

Genes associated with extracellular miRs expressed under the 5 mM glucose + 10 ng/mL TNF-α treatment condition

The biological process GO term clusters showing greatest enrichment were ‘positive regulation of cellular process’, ‘anatomical structure development’, and ‘peptidyl-amino acid modification’ (Appendix 48). The cellular component GO term clusters demonstrating greatest enrichment were ‘synapse part’, ‘endomembrane system’ and ‘plasma membrane region’ (Appendix 49). The molecular function GO terms clusters showing the highest enrichment were ‘transcription regulatory region DNA binding’, followed by ‘transcription factor activity sequence-specific DNA binding’, and ‘enzyme binding’ (Appendix 50).

The KEGG and REACTOME pathway terms showing greatest enrichment were ‘MiRs in cancer’ and ‘signalling by receptor tyrosine kinases’ respectively (Table 13).

Table 13: KEGG and REACTOME pathways functionally enriched within the predicted gene list associated with ciGEnC extracellular miR expression under the 5 mM glucose + 10 ng/mL TNF-α treatment condition

Pathway	Term Name	Term ID	P-Value
KEGG	MiRs in cancer	KEGG:05206	1.32E-09
KEGG	Pathways in cancer	KEGG:05200	1.49E-05
KEGG	Hippo signaling pathway	KEGG:04390	0.000811
KEGG	Proteoglycans in cancer	KEGG:05205	0.007498
KEGG	Axon guidance	KEGG:04360	0.008473
KEGG	Wnt signaling pathway	KEGG:04310	0.01917
KEGG	Endocytosis	KEGG:04144	0.025286
KEGG	PI3K-Akt signaling pathway	KEGG:04151	0.029856
KEGG	Regulation of actin cytoskeleton	KEGG:04810	0.031269
REACTOME	Signal Transduction	REAC:R-HSA-162582	9.89E-08
REACTOME	Signaling by Receptor Tyrosine Kinases	REAC:R-HSA-9006934	2.01E-06
REACTOME	Membrane Trafficking	REAC:R-HSA-199991	2.04E-06
REACTOME	Vesicle-mediated transport	REAC:R-HSA-5653656	3.81E-06
REACTOME	Circadian Clock	REAC:R-HSA-400253	0.025742
REACTOME	MAP kinase activation	REAC:R-HSA-450294	0.035259
REACTOME	Signaling by NTRKs	REAC:R-HSA-166520	0.038976

4.3.6 STRING analysis of predicted gene lists

The top 200 genes predicted to be associated with differentially expressed miRs in each treatment group were entered into STRING for the prediction of resultant protein-protein interactions (Appendix 3-14). Figures 52-57 demonstrate theoretical protein-protein interactions predicted from differentially expressed cellular miRs, whilst figures 58-63 demonstrate protein-protein interactions predicted from differentially expressed cellular miRs.

Clusters of proteins were found, having roles previously linked to DKD pathology. These clusters of proteins were highlighted in figures 52 – 63. Also highlighted were any other large clusters of proteins having similar roles.

Protein clusters identified from the analysis of cellular miR targets included proteins associated with the following processes:

- Protein Ubiquitination
- Collagen Production
- Cytoskeletal Arrangement
- Serine/threonine phosphatase activity

Protein clusters identified from the analysis of extracellular miR targets included proteins associated with the following processes:

- Protein Ubiquitination
- Collagen Production
- Cytoskeletal Arrangement
- TGF-β Action
- Activin Receptor Action
- Platelet Derived Growth Factor Action

In addition, the protein Sirtuin-1 (SIRT1) deacetylase was highlighted in analysis of extracellular miR targets. This protein has been found to be of particular interest in DKD, and multiple studies have shown SIRT1 to have a critical role in protecting the kidneys from cellular stress (Zhong et al. 2018). Specifically, SIRT1 is believed to play a protective role in podocytes and renal tubule cells. SIRT1 has been found to be reduced in human kidneys with DKD, and this reduction is more pronounced in the glomerular regions of the kidney (Chuang et al. 2011; Zhong et al. 2018). SIRT1 has also been proposed as a potential drug target in DKD (Chuang et al. 2011; Zhong et al. 2018).

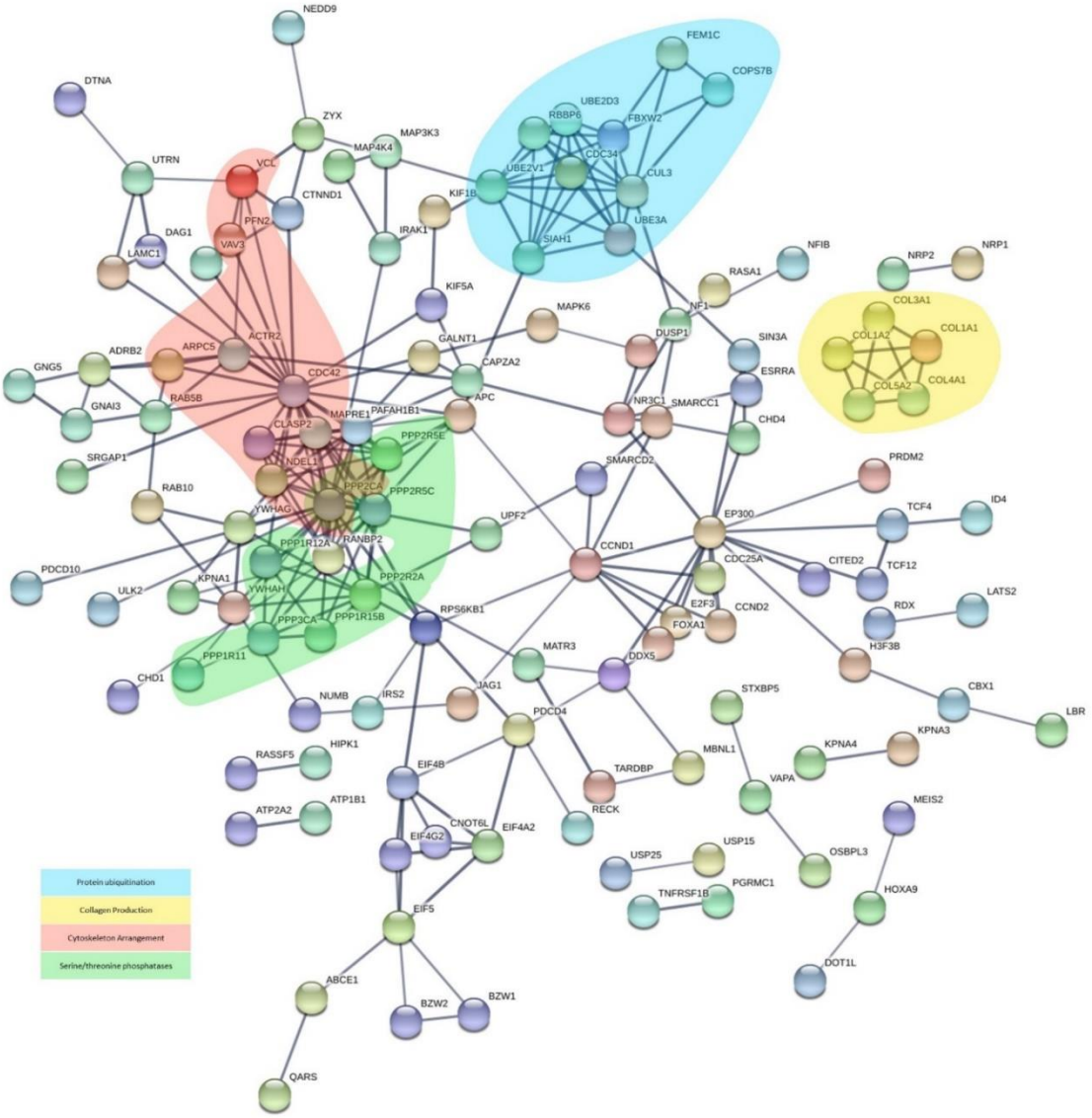

Figure 52: Protein-protein interactions, as predicted by STRING, based on top 200 genes associated with cellular miRs differentially expressed under all three treatment conditions (5mM glucose + 10 ng/mL TNF-α , 25mM glucose, 25mM glucose + 10 ng/mL TNF-α). Line thickness represents confidence of protein-protein interaction prediction.

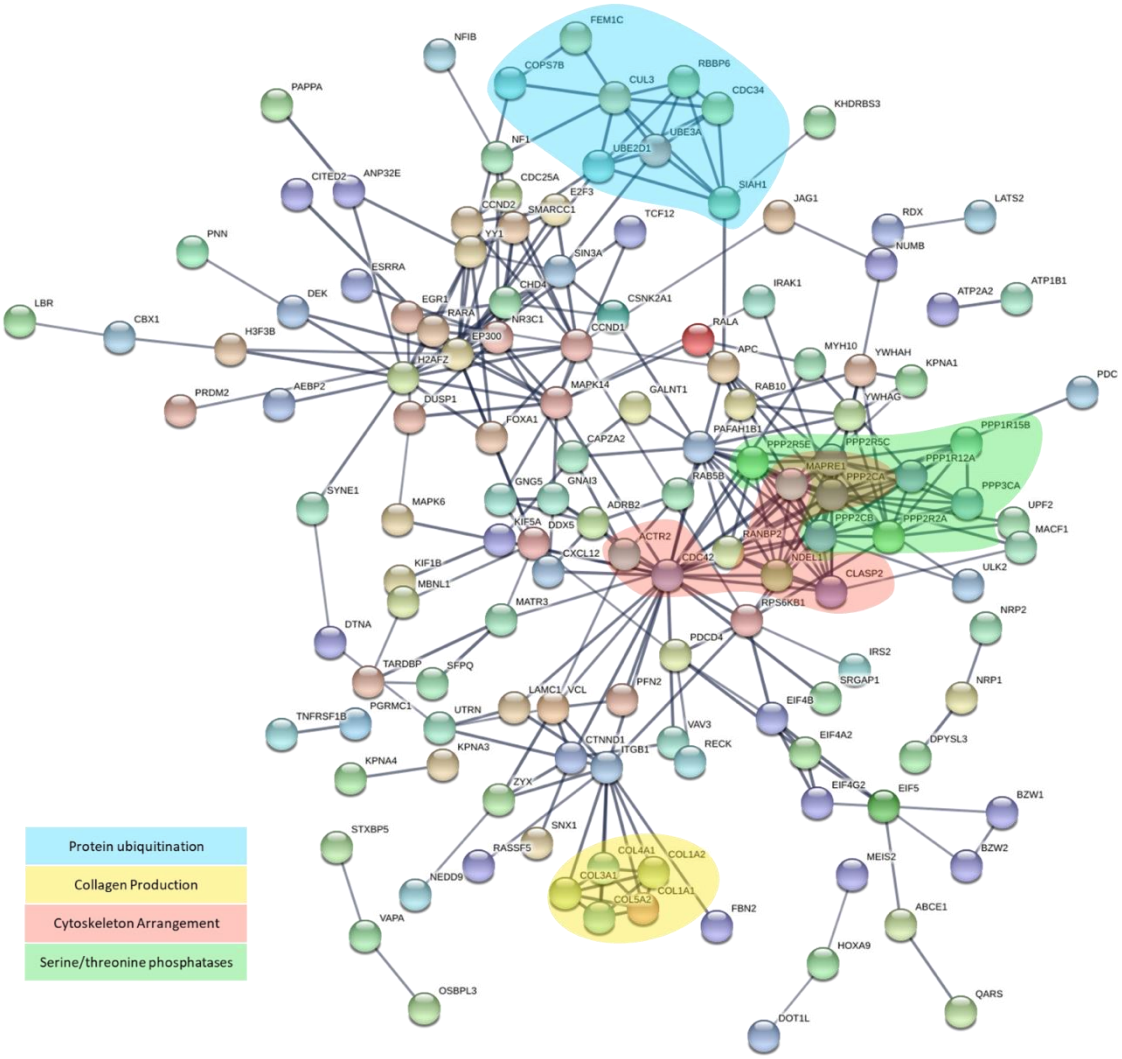

Figure 53: Protein-protein interactions, as predicted by STRING, based on top 200 genes associated with cellular miRs differentially expressed under both high glucose treatment conditions (25mM glucose, 25mM glucose + 10 ng/mL TNF-α). Line thickness represents confidence of protein-protein interaction prediction.

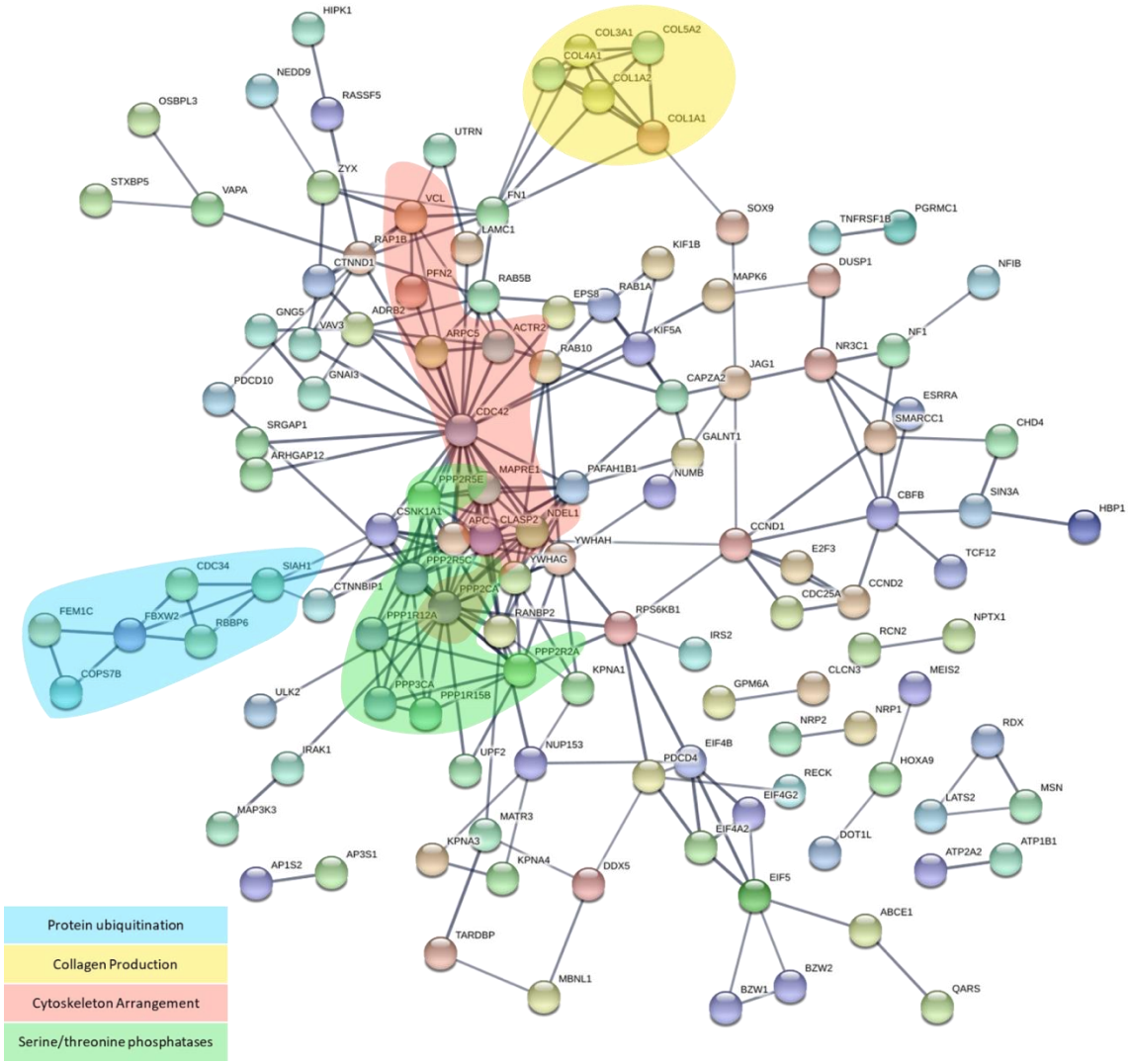

Figure 54: Protein-protein interactions, as predicted by STRING, based on top 200 genes associated with cellular miRs differentially expressed under both TNF-α treatment conditions (5mM glucose + 10 ng/mL TNF-α , 25mM glucose + 10 ng/mL TNF-α). Line thickness represents confidence of protein-protein interaction prediction.

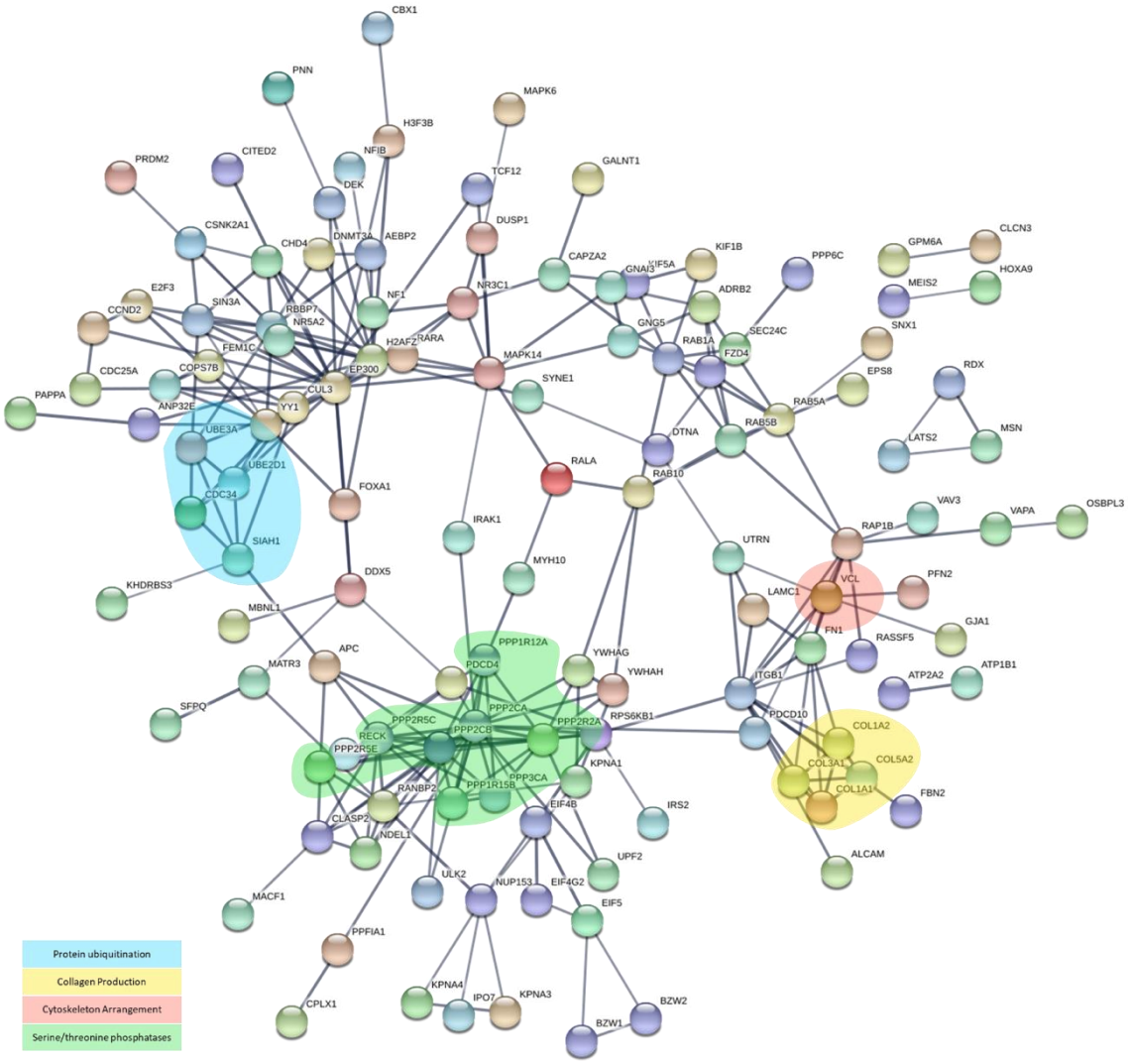

Figure 55: Protein-protein interactions, as predicted by STRING, based on top 200 genes associated with cellular miRs differentially expressed under the 25mM glucose + 10 ng/mL TNF-α treatment condition. Line thickness represents confidence of protein-protein interaction prediction.

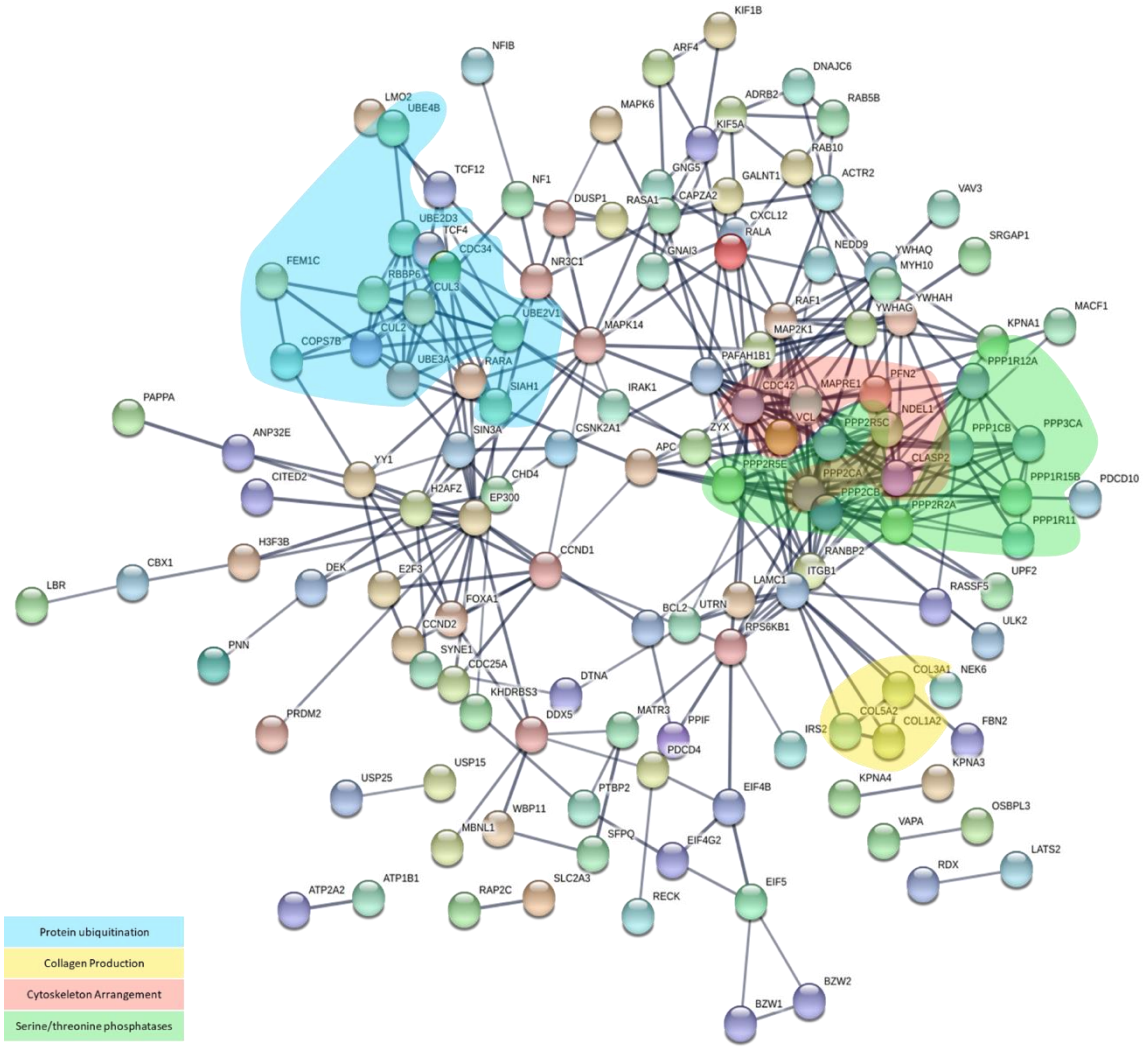

Figure 56: Protein-protein interactions, as predicted by STRING, based on top 200 genes associated with cellular miRs differentially expressed under the 25mM glucose treatment condition. Line thickness represents confidence of protein-protein interaction prediction.

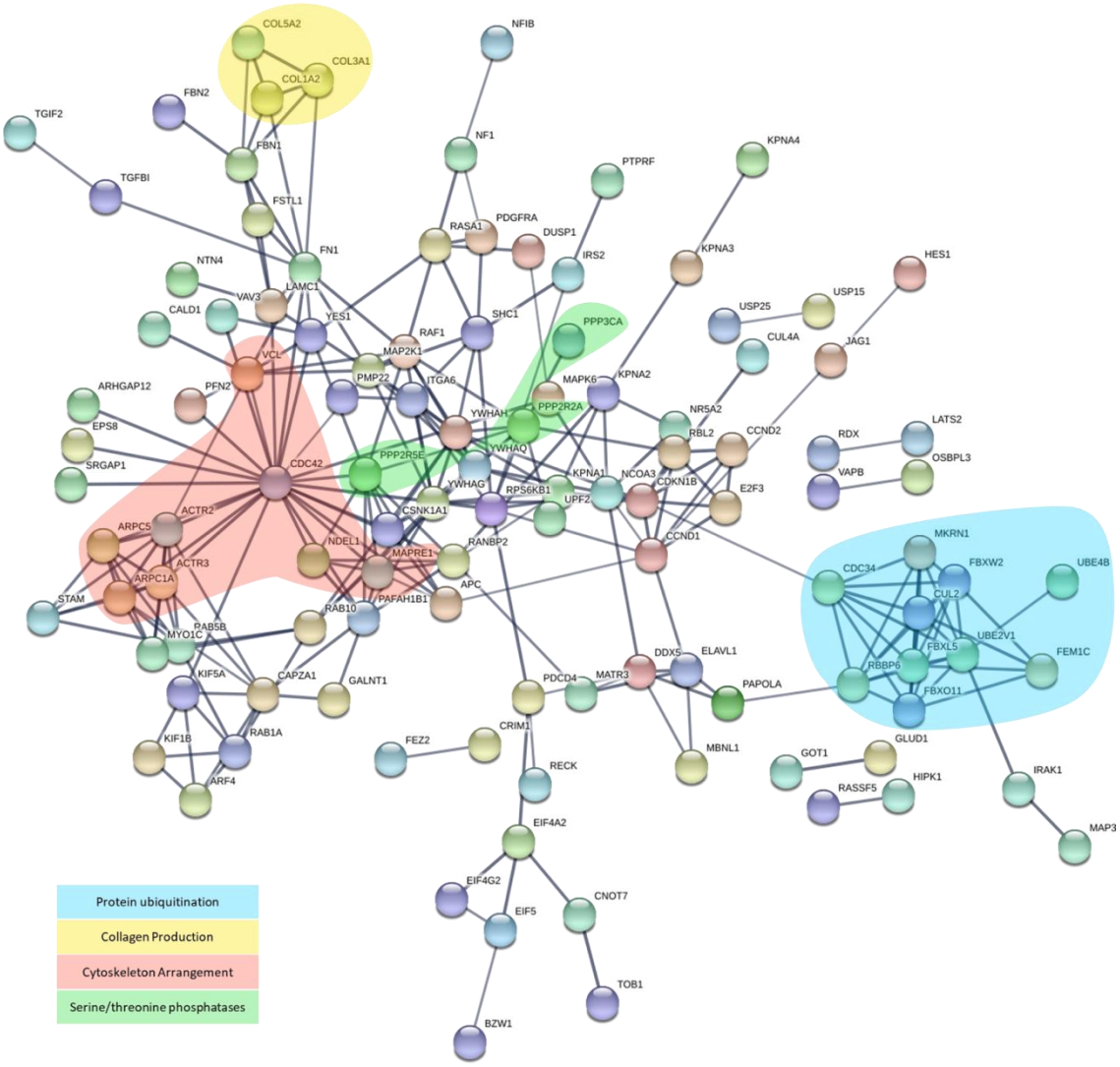

Figure 57: Protein-protein interactions, as predicted by STRING, based on top 200 genes associated with cellular miRs differentially expressed under the 5mM glucose + 10 ng/mL TNF-α treatment condition. Line thickness represents confidence of protein-protein interaction prediction.

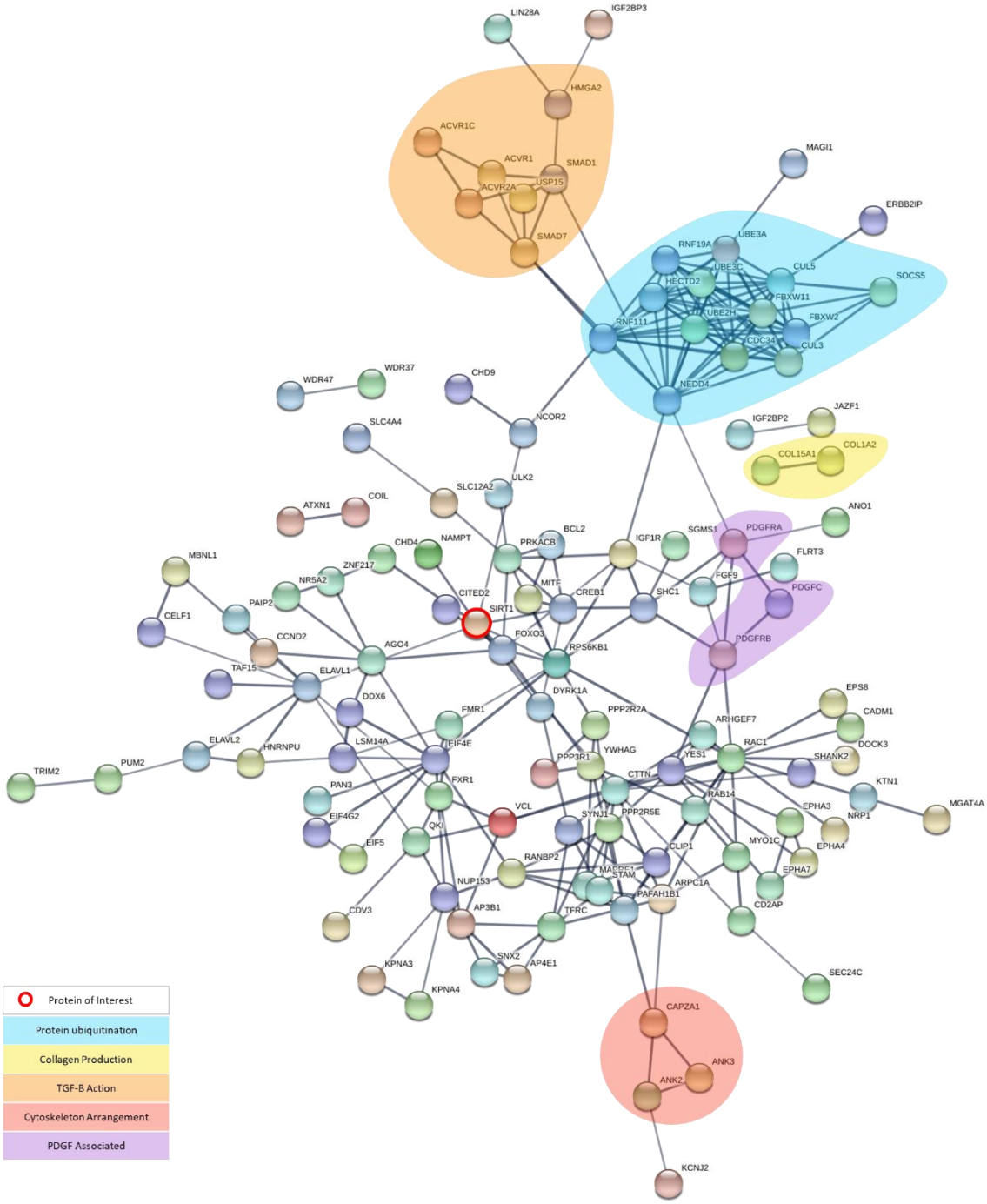

Figure 58: Protein-protein interactions, as predicted by STRING, based on top 200 genes associated with extracellular miRs differentially expressed under all three treatment conditions (5mM glucose + 10 ng/mL TNF-α , 25mM glucose, 25mM glucose + 10 ng/mL TNF-α). Line thickness represents confidence of protein-protein interaction prediction.

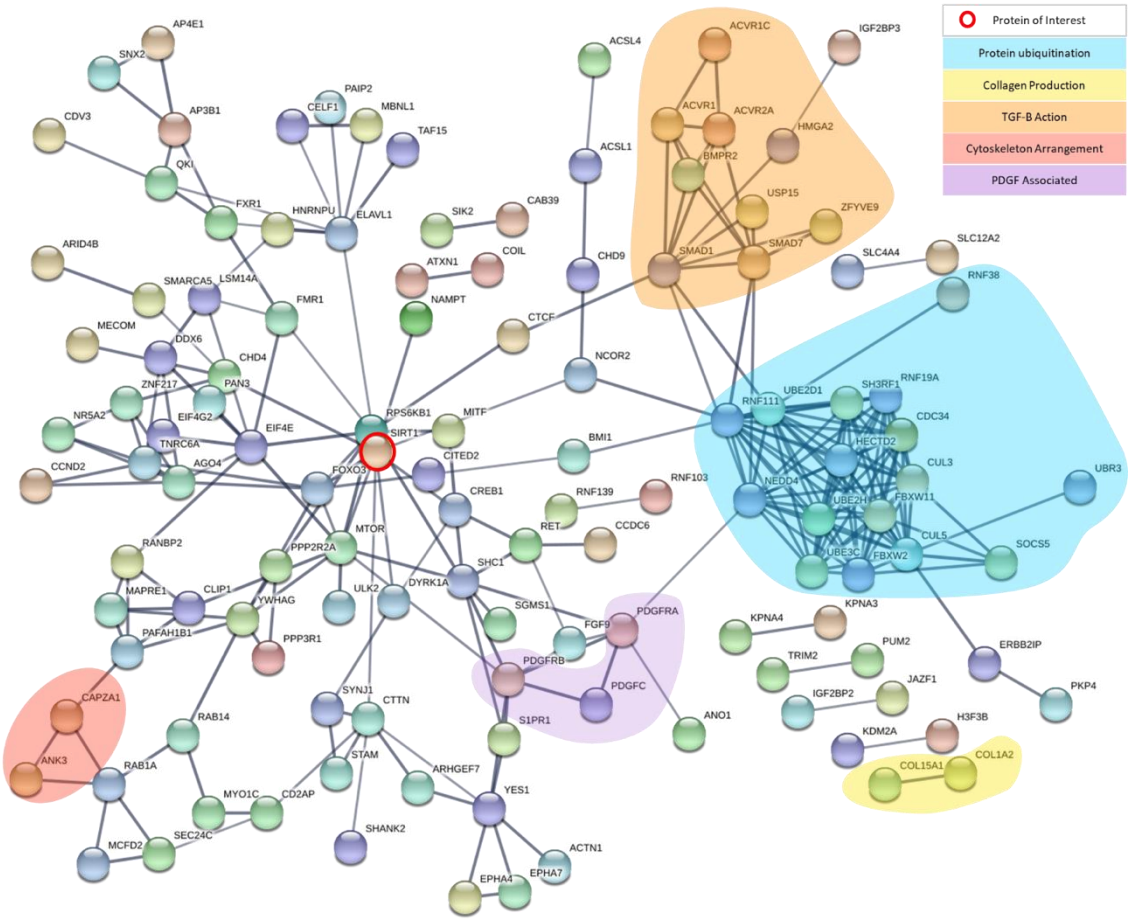

Figure 59: Protein-protein interactions, as predicted by STRING, based on top 200 genes associated with extracellular miRs differentially expressed under both high glucose treatment conditions (25mM glucose, 25mM glucose + 10 ng/mL TNF-α). Line thickness represents confidence of protein-protein interaction prediction.

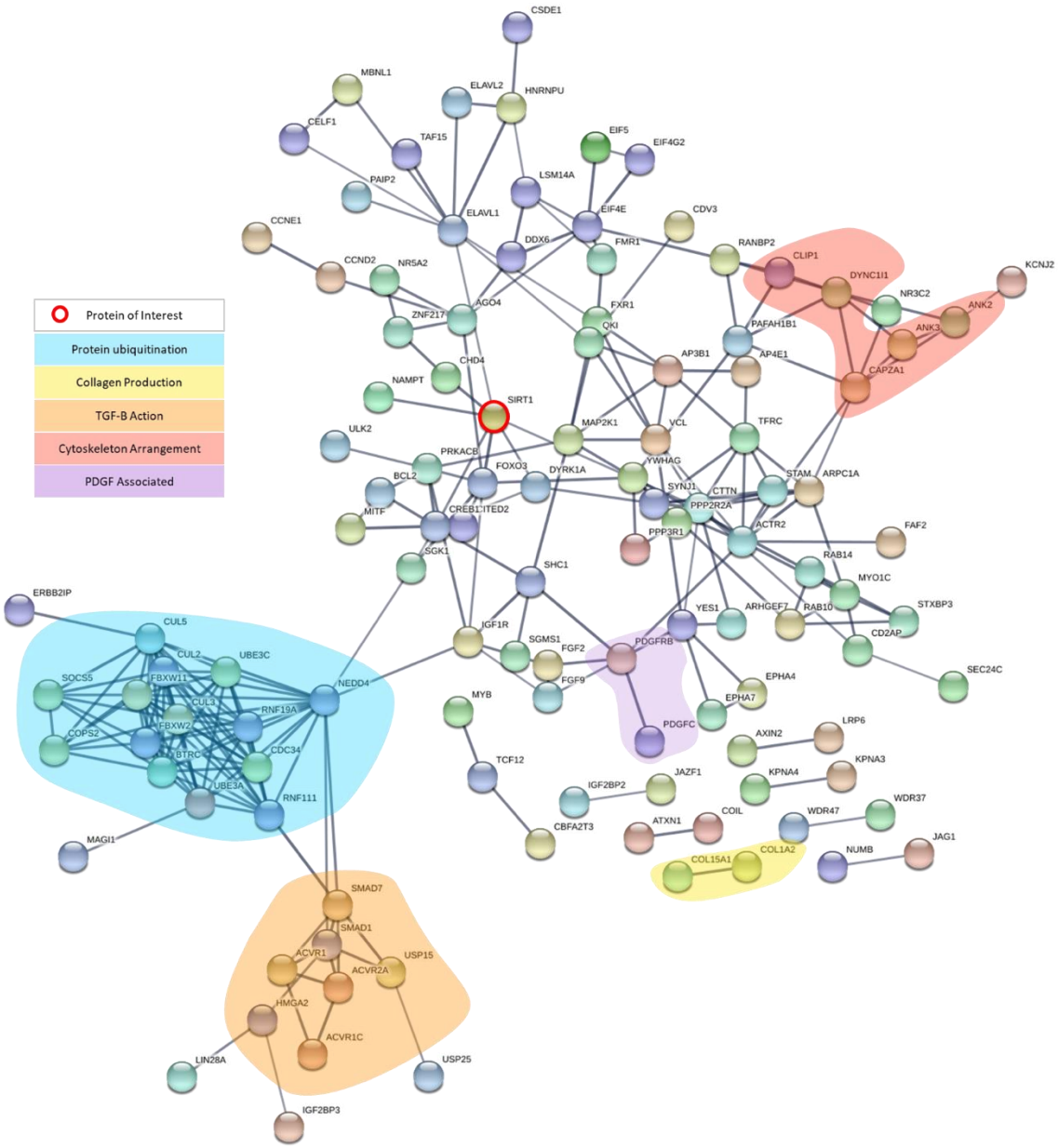

Figure 60: Protein-protein interactions, as predicted by STRING, based on top 200 genes associated with extracellular miRs differentially expressed under both TNF-α treatment conditions (5mM glucose + 10 ng/mL TNF-α , 25mM glucose + 10 ng/mL TNF-α). Line thickness represents confidence of protein-protein interaction prediction.

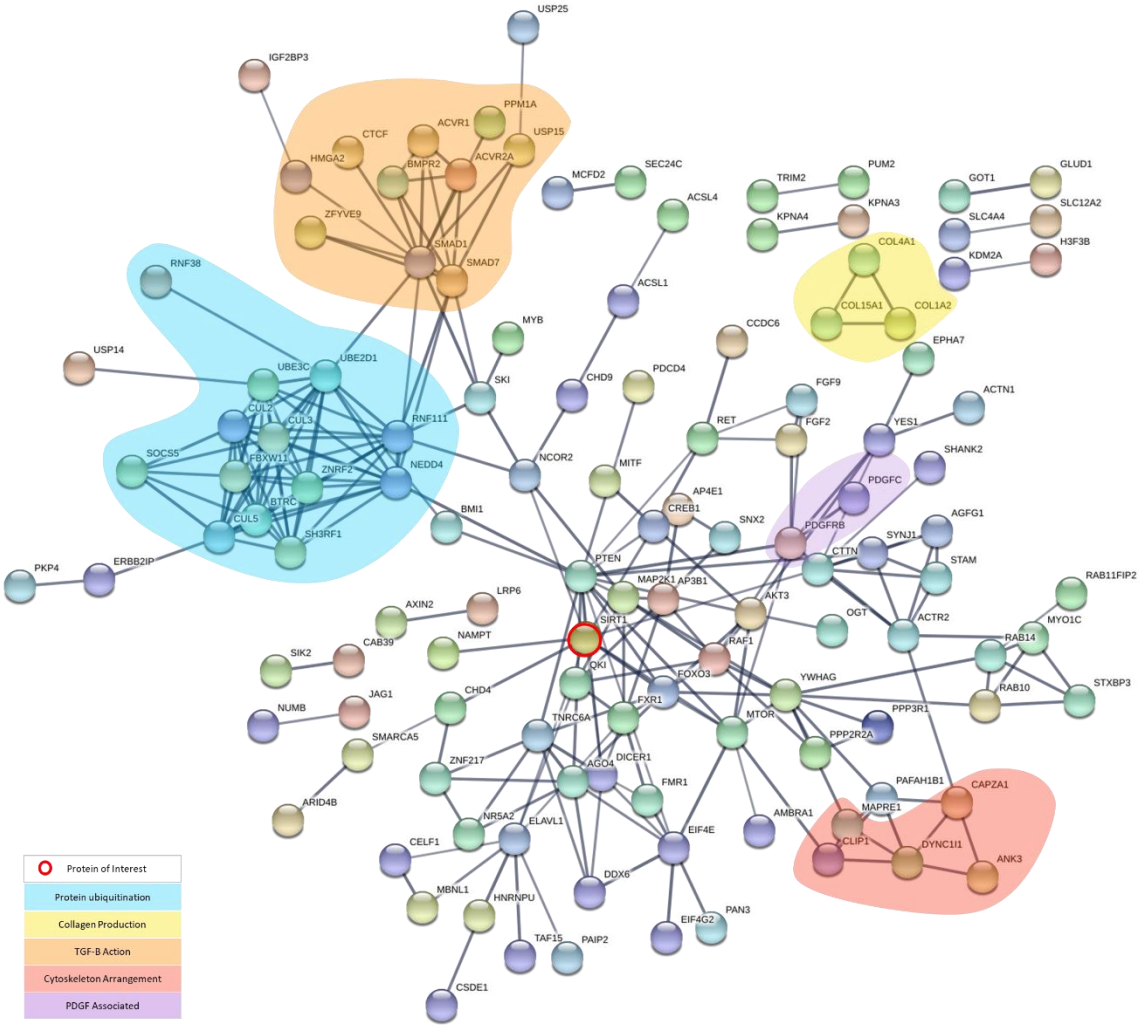

Figure 61: Protein-protein interactions, as predicted by STRING, based on top 200 genes associated with extracellular miRs differentially expressed under the 25mM glucose + 10 ng/mL TNF-α treatment condition. Line thickness represents confidence of protein-protein interaction prediction.

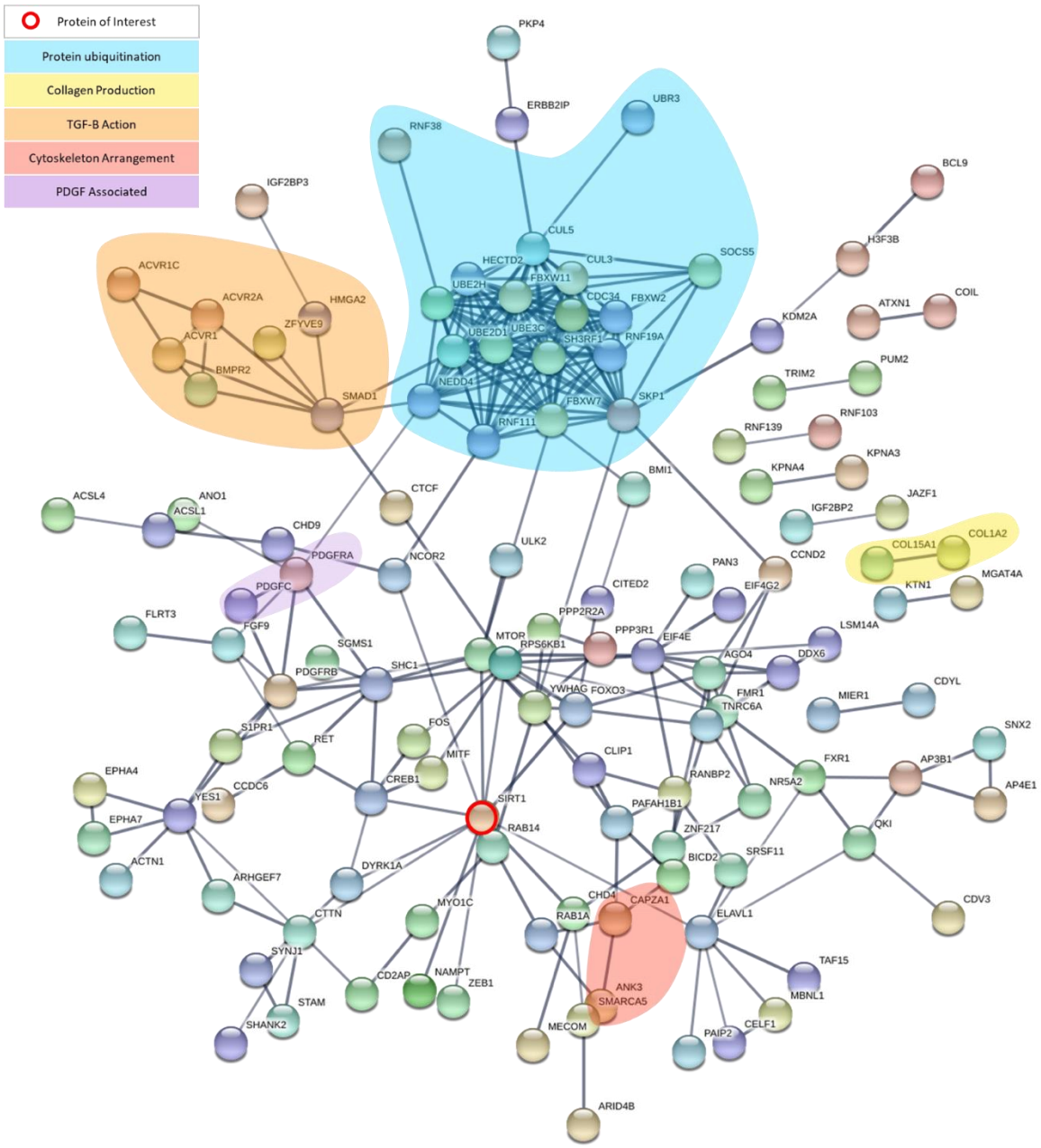

Figure 62: Protein-protein interactions, as predicted by STRING, based on top 200 genes associated with extracellular miRs differentially expressed under the 25mM glucose treatment condition. Line thickness represents confidence of protein-protein interaction prediction.

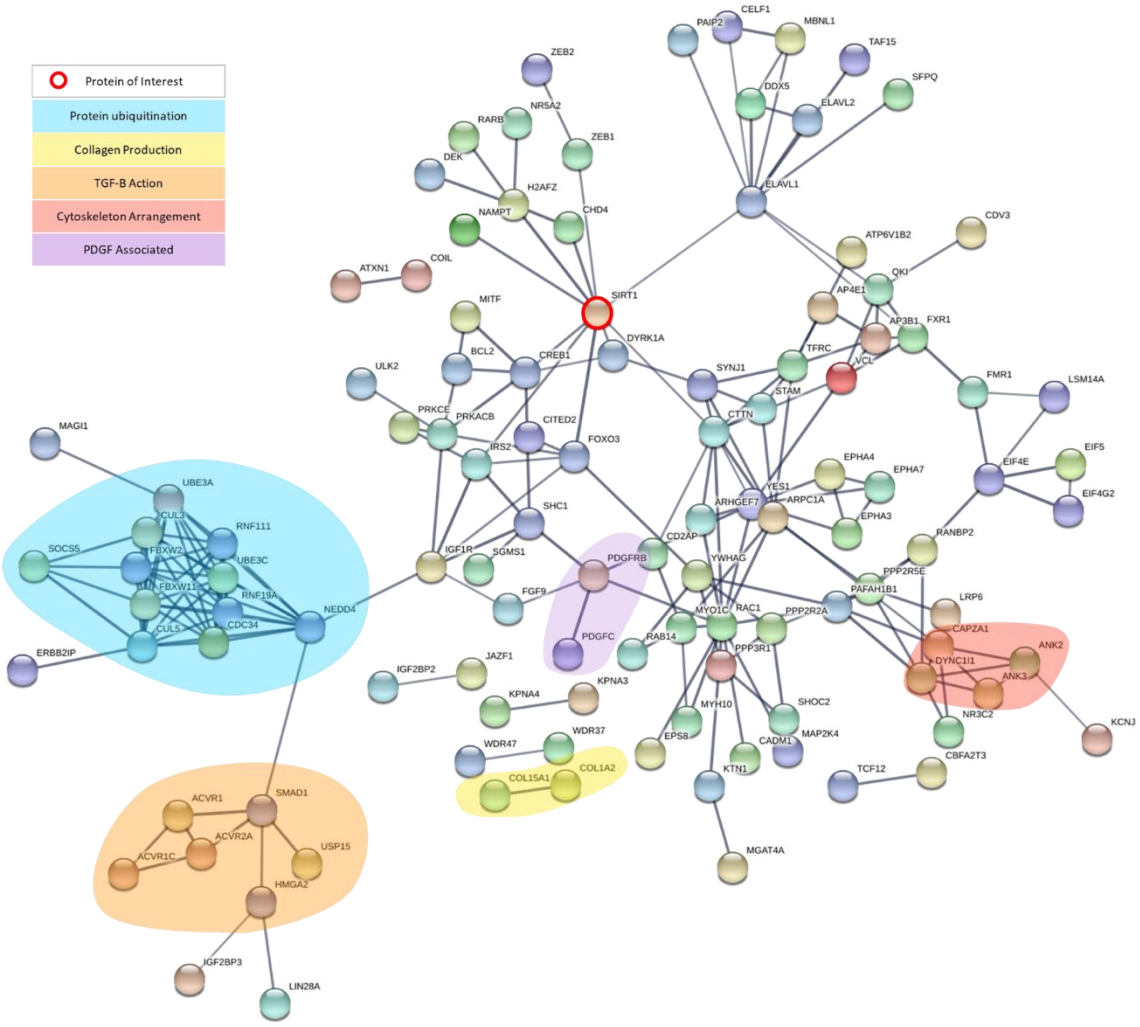

Figure 63: Protein-protein interactions, as predicted by STRING, based on top 200 genes associated with extracellular miRs differentially expressed under the 5mM glucose + 10 ng/mL TNF-α treatment condition. Line thickness represents confidence of protein-protein interaction prediction.

4.4 Discussion

TLDA Assays

This study investigated the effects of hyperglycaemia and/or TNF-α exposure in isolation on the cellular and extracellular miR expression profiles of GEnCs. In TLDA analysis of 377 miRs, differentially expression of numerous transcripts was observed under the various treatment conditions. Data for selected miRs are discussed below.

miR-636

MiR-636 showed increased cellular expression under all three treatment conditions. Salem *et al.* (2018) demonstrated increased expression of miR-636 in the renal tissues of streptozotocin-induced diabetic rats, which increased with the progression of diabetes. These findings support the observations of this study and suggest that the source of increased renal miR-636 could be GEnCs. A study by Eissa (2016) showed a significant increase in miR-636 in the urine of patients with DKD, which correlated with serum

creatinine and urinary protein creatinine ratio. However, analysis of extracellular medium miR-636 did not reveal any significant change in expression following treatment. These intriguing findings therefore appear equivocal on the role of miR-636 in DKD, and future analyses should attempt to identify the biological action of miR-636 in GEnCs.

miR-146

Cellular miR-146a was upregulated under all three treatment conditions, and extracellular miR-146a was upregulated under both 25 mM glucose treatment conditions. Cultured human GEnCs in culture have previously demonstrated increased miR-146a expression in response to high glucose, together with upregulated TNF-α, TGF-β1 and NF-κB expression (Huang *et al.* 2014). Furthermore, Huang et al (2014) found that miR-146a was upregulated in kidney biopsy samples from patients with DKD compared with controls, and that rat models of type I and II diabetes showed increased renal expression of miR-146a over time. Cheng *et al.* (2013) found that inflammatory cytokines, including TNF-α, induced the expression of miR-146a/b in HUVECs, and in contrast with findings by Huang *et al.* (2014), that miR-146a/b negatively regulated inflammation in these cells, through repression of NF-κB and MAP kinase pathways. MiR-146a-mediated repression of the inflammatory response has also been observed in human retinal endothelial cells (Cowan *et al.* 2014). This evidence suggests a protective role for miR-146a, acting against the inflammatory effects of DKD pathogenesis. Further supporting this view, Morishita *et al.* (2015) injected miR-146a via nanoparticles, into mice with induced renal fibrosis. These mice demonstrated reduced expression of α-smooth muscle actin and macrophage infiltration into the fibrotic area of the kidney. The role of miR-146a in GEnC inflammatory processes should therefore be further characterised.

miR-98

Cellular miR-98 expression was downregulated under all three treatment conditions, and extracellular expression was downregulated under the 5 mM + 10 ng/mL TNF-α and 25 mM glucose treatment conditions. A role for miR-98 in regulation of autophagy has been proposed, and reduction in autophagy has been associated with renal damage in diabetes (Matboli *et al.* 2017). In contrast with results of the TLDA however, high glucose concentrations have been shown to induce proliferation in rat aortic endothelial cells, through the upregulation of miR-98 (Li *et al.* 2016). Further work is needed to determine the effects of miR-98 downregulation on GEnCs.

miR-355

Cellular miR-355 was upregulated under both 25 mM glucose treatment conditions. Although miR-355 has not explicitly been linked to DKD, it has been found to target and downregulate multiple genes in the noncanonical TGF-β pathway (Lynch *et al.* 2012; Yan *et al.* 2012), and overactive TGF-β signalling has been implicated as a profibrotic factor in DKD (Zhao *et al.* 2020).

miR-22

Upregulated cellular miR-22 expression was also observed under both 25 mM glucose treatment conditions. A study by Ghai *et al.* (2018) found a significantly higher concentration of miR-22 in the urine of patients with type 1 diabetes and microalbuminuria, compared with type 1 diabetic patients without albuminuria. However, extracellular data did not reveal miR-22 to be differentially expressed in response to treatment, and therefore the data from this study do not suggest GEnCs as the source of increased urinary miR-22. Similarly to miR-355, miR-22 has also been linked to TGF-β regulation, although not specifically in GEnCs (Hong *et al.* 2016; Ghai *et al.* 2018). Further work should therefore aim to elucidate the function of miR-22 in these cells.

miR-138

Cellular miR-138 expression was upregulated under both 25 mM glucose conditions. A study by Liu *et al.* (2020) found that miR-138 expression was upregulated in DKD patient kidney biopsy samples, and that miR-138 could bind to the 3'UTR of sirtuin-1 (SIRT1) and inhibit its function. SIRT1 is a key molecule in energy metabolism, and has been found to be a protective factor against DKD (W. Wang *et al.* 2019a; W. Wang *et al.* 2019b).

miR-486

The second highest upregulation in cellular miR expression was shown for miR-486 under the 25 mM glucose + 10 ng/mL TNF-α treatment condition, and this transcript was also upregulated in 25 mM glucose. Extracellular miR-486 expression was downregulated under all three treatment conditions. By contrast, reduced expression of miR-486 has been reported in the glomeruli and proximal tubules of kidneys from patients with DKD (Baker *et al.* 2017). Also in contrast to the above TLDA data, a longitudinal study by Argyropoulos el al. (2013) found that miR-486 was increased in the urine of patients with albuminuria compared with healthy controls. Future work should validate the expression patterns of miR-486 in a larger sample size.

miR-200b

Cellular miR-200b was upregulated under both TNF-α treatments, being the highest upregulated miR under the 25 mM glucose + 10 ng/mL TNF-α treatment condition, and the second most upregulated miR under the 5 mM glucose + 10 ng/mL TNF-α treatment condition. Extracellular miR-200b was also downregulated under all treatment conditions. Supporting these cellular data, Kato *et al.* (2011) have reported increased miR-200b in the glomeruli of type 1 and type 2 diabetic mouse models. They found that TGF-β levels were upregulated in response to miR-200b in mesangial cells, proposing that this could represent an important cascade leading to a chronic fibrotic state in DKD. Previous research has also reported increased expression of miR-200b in the glomeruli of db/db mice, and in endothelial cells treated with high glucose (Long *et al.* 2011). Our results suggest that GEnCs may be the source of increased miR-200b, and that high glucose conditions induce

this increase. Further work should investigate the expression of TNF-β in GEnCs with increased miR-200b expression.

miR-874a

Cellular miR-874a expression was downregulated under the 5 mM glucose + 10 ng/mL TNF-α treatment condition, and extracellular miR-874a expression was downregulated under all three treatment conditions. A study by Yao *et al.* (2019) also noted decreased miR-874 in a rats with DKD, and in podocytes treated with high glucose. They also demonstrated attenuation of the inflammatory response, including decreased TNF-α, in response to miR-874 overexpression. This suggests a potential protective role for miR-874a. However, miR-874a was not downregulated under the 25mM + 10 ng/mL TNF-α condition. MiR-874a also decreases Toll-like receptor 4 (TLR4) expression in podocytes. TLR4 induces an inflammatory cascade through the release of various cytokines, increasing the expression of TNF-α, interleukin-6, and interleukin-1β (Beutler 2004; Kaur *et al.* 2012). These findings suggests a potential role for extracellular miR-874a in the communication of injury from GEnCs to podocytes and suggests that the above contradictory data should be resolved by further experimentation.

miR-342

Cellular miR-342 was the second most downregulated miR under the 25 mM glucose + 10 ng/mL TNF-α treatment condition. Mir-342 has been linked to the inhibition of TGF-β in endothelial cells, via the suppression of SMAD1/5 phosphorylation (Zhang *et al.* 2017). The downregulation of a TGF-β-suppressing factor could potentially lead to increased expression of TGF-β a known pro-fibrotic factor associated with DKD (Zhao *et al.* 2020). TGF-β has also been reported to induce endothelial-to-mesenchymal transition in GEnCs, contributing to glomerulosclerosis (Li *et al.* 2009).

let-7b

The most downregulated extracellular miR under the 5mM glucose + 10 ng/mL TNF-α treatment condition was let-7b. A study by Wang *et al.* (2014) found that let-7b expression was downregulated in mouse models of diabetic renal fibrosis, and that this transcript downregulated expression of the TGF-β1 receptor and attenuated the profibrotic effects of TGF-β in rat PTECs. These results suggest a protective role for let-7b, and that its downregulation might precipitate TGF-β -driven fibrosis in PTECs.

miR-135b

MiR-135b was the second most upregulated extracellular miR under the 25 mM glucose + 10 ng/mL TNF-α treatment condition. MiR-135b has been associated with podocyte injury, and the ectopic expression of miR-135b (in combination with miR-135a) leads to podocyte injury and disorder of the podocyte cytoskeleton (Yang *et al.* 2015). GEnC-mediated

upregulation of miR-135 in podocytes could represent a potential method of injury progression within the kidney.

miR-362

Under all three treatment conditions miR-362-3p extracellular expression was downregulated. This finding is not supported by Xie *et al*. (2017), who reported an upregulation of miR-362-3p in the urinary exosomes of patients with DKD, compared with patients who had type II diabetes without DKD.

miR-216b and miR-217

Extracellular miR-216b and miR-217 expression were downregulated under all treatment conditions. A study by Li *et al.* (2017) demonstrated that the downregulation of miR-217 in an *in vitro* human podocyte model induced podocyte apoptosis. Future studies might culture podocytes in GEnC conditioned medium to determine if decreased extracellular expression of miR-217 by GEnCs could induce podocyte apoptosis. In contrast, previous research by Fiorentino *et al.* (2013) reported upregulated miR-217 in the kidneys of diabetic mice. Similarly, upregulated miR-217 was found in the serum of patients with DKD (Shao *et al.* 2017).

miR-503

Extracellular miR-503 was downregulated under all three treatment conditions. MiR-503 is involved in endothelial cell dysfunction in diabetes, and overexpression of this transcript causes podocyte injury, whilst its inhibition can reverse injury (Caporali *et al.* 2011; Zha *et al.* 2019). It is therefore possible that reduced miR-503 extracellular expression by GEnCs is a protective measure against podocyte injury.

miR-133

MiR-133a exhibited upregulated extracellular expression under both 25mM glucose treatment conditions. In contrast with these findings, research by Lee *et al.* (2020) reported decreased miR-133a in the urinary exosomes of patients with DKD.

miR-126

Extracellular miR-126 was downregulated under both high glucose treatment conditions. This is in accordance with TaqMan data from Group C ciGEnCs presented in section 3.4.2 (Figure 22c), which also demonstrated a downregulation of extracellular miR-126 in response to 25 mM glucose treatment. By contrast, Beltrami *et al.* (2018) did not report significant changes in extracellular miR-126 in response to increased glucose concentration. Downregulation of miR-126 in high glucose treated mesangial cells has been reported (Barutta *et al.* 2017; Cao *et al.* 2018). Cellular miR-126 was also downregulated in response to the 25 mM glucose + 10 ng/mL TNF-α treatment condition. These data do not concur with the TaqMan results presented in Figure 23c, nor those of Beltrami *et al.* (2018).

miR-130a

Extracellular miR-130a was downregulated under both 25 mM glucose conditions. By contrast, a previous report has described increased detection of miR-130a in the urine of patients with type I diabetes and microalbuminuria, compared with type I diabetic patients without microalbuminuria (Ghai *et al.* 2018). In addition, increased miR-130a detection in urinary exosomes from type I diabetic patients with DKD, compared with type I diabetic patients without DKD has been observed (Barutta *et al.* 2013).

let-7c

Extracellular let-7c was downregulated under both 25 mM glucose treatment conditions. The let-7 family of miRs confers anti-fibrotic effects in lung fibrosis, cardiac fibrosis, and renal fibrosis. Specifically, let-7c targets TGF-βR1, collagen type 1 alpha 1 (COL1A1), and collagen type 1 alpha 2 (COL1A2) (Pandit *et al.* 2010; Y. Wang *et al.* 2019). The upregulation of let-7c in PTECs inhibited the expression of TGF-βR1 and the response to TGF-β1. In addition, TGF-β1 suppressed expression of let-7c (Brennan *et al.* 2013).

miR-218

Extracellular miR-218 expression was downregulated in response to both 25 mM glucose treatment conditions. This downregulation concurs with the study of Li *et al.* (2020) who reported this direction of effect in a rat DKD model and podocyte cultures treated with high glucose *in vitro*. Li *et al.* (2020) also reported that miR-218 overexpression reduced renal injury in their model, and prevented high glucose-induced podocyte apoptosis. Furthermore miR-218 overexpression in podocytes reduced expression of key inflammatory mediators including TNF-α (Li *et al.* 2020). These results suggest a protective role for miR-218, and that downregulation of extracellular GEnC expression could induce podocyte damage.

miR-215

MiR-215 was downregulated under both 25 mM glucose treatment conditions. One study has reported downregulation of miR-215 in TGF-β1-treated rat mesangial cells and PTECs (Wang *et al.* 2010). However, in contrast with these findings, miR-215 was upregulated in mouse mesangial cells treated with TGF-β1 and high glucose, and in glomeruli from type II diabetic mice (Mu *et al.* 2013). The inconsistencies in these data may reflect the influence of different models, and underlines the need for human studies to confirm the applicability of findings to human pathology.

In summary, a number of differentially expressed cellular and extracellular miRs were found in the ciGEnC *in vitro* model, some of which were supported by evidence in the literature. A number of potential mechanisms of action emerged for selected differentially expressed miRs, including regulation of TGF-β signalling (e.g miR-22, miR-200b, miR-342, miR-355, let-7b, and let-7c), and regulation of the inflammatory response (e.g miR-146a and miR-874a)

Biomarker identification by TLDA analysis

The above ciGEnC miRs, identified by differential expression in response to disease conditions *in vitro*, are therefore potential disease biomarkers. Direct analysis of patient samples can also be used to identify disease biomarkers. Beltrami *et al.* (2018) profiled 754 miRs in pooled urine samples from 20 DKD patients. Beltrami *et al.* (2018), found significantly increased expression of 12 miRs, and decreased expression of 35 miRs in the urine of late-stage CKD (stage 3-5) patients with DKD compared with healthy controls. None of the miRs detected in increased abundance in the urine of DKD patients showed upregulated expression in ciGEnC culture medium. However, several miRs downregulated in DKD patient urine samples were also downregulated in this study's analysis of extracellular ciGEnC miRs:

- In all three treatment conditions: miR-200b, miR-362 and miR-618
- In both 25 mM glucose treatment conditions: miR-10a, miR-100 and miR-885
- In 25 mM glucose + 10 ng/mL TNF-α: miR-576.

Identification of significant synergies between the findings of this thesis and those of Beltrami and colleagues (2018) will require further analyses in both patient samples and disease models. Indeed, all of the potentially significant and impactful data generated by this study must be interpreted in the light of the inevitable experimental limitations of this study.

For analysis of TLDA data, miRs with a $\log_2$RQ >1 were defined as upregulated, while those with a $\log_2$RQ < -1 were defined as downregulated. These RQ values were chosen to capture the top 10% and bottom 10% of expression levels, as those of greatest interest. Nevertheless, this could have excluded potentially important miRs.

Due to time constraints, each TLDA analysis was carried out once, therefore statistical significance could not be determined, and $\log_2$RQ values were used to define differential expression thresholds. To mitigate this limitation, triplicate samples were pooled to reduce the probability of significant outlier effects, and this approach has successfully been used to identify candidate urinary miR biomarker data that were replicated in larger, independent patient cohorts (Beltrami *et al.* 2018). Nevertheless, future work would ideally repeat these experiments to reach a sample size capable of determining significance.

Pre-amplification was performed on the miR samples to increase yield, and this is an additional potential confounder. However, variability introduced by pre-amplification has been reported to be smaller than that introduced by the process of reverse transcription (Korenková *et al.* 2015; Okino *et al.* 2016).

Global normalisation was used to normalise miR expression data. Gevaert *et al.* (2018) compared normalisation methods for TLDA data and found that the geNorm normalisation algorithm reduced data dispersion to the greatest extent, although global data normalisation

also performed well. Genovesi *et al.* (2012) conducted TLDA analysis on brain tumour tissue and found that the reference genes present on the TLDA cards were not those with the most stable expression. They also found substantial variability between reference genes between cards A and B. These inconsistencies suggest reference genes on the TLDA cards are not suitable to use for data normalisation. Genovesi *et al.* (2012) also determined that the use of algorithms such as geNorm and NormFinder, and global normalisation, were the best normalisation strategies for TLDA data. NormFinder was used in the work of Beltrami *et al.* (2018), where miR-191 was identified as a suitable TLDA data normaliser for that experimental dataset.

Following global normalisation, further exclusion criteria were assigned to pare down TLDA data, leaving a more manageable number of candidate miR biomarkers. Although these exclusions were necessary in order to identify miRs of greatest interest, their use may have omitted potentially important miRs. Similar to the method used by Gevaert *et al.* (2018), all miRs with a Ct value ≥35 in 2 or more conditions were excluded from further analysis. Ct values ≥35 represent unreliable detection and are therefore considered to be noise as opposed to signal (Van Der Auwera *et al.* 2010; De Ronde *et al.* 2017).

Future work should aim to validate the above TLDA data using individual TaqMan assays for selected miR candidates in DKD patient/control cohorts. Where there is evidence of differential extracellular expression by ciGEnCs, other renal cells such as podocytes and tubular cells could be cocultured with treated GEnCs, or grown in their conditioned medium, to determine whether differentially expressed extracellular miRs confer functional affects. Representative experiments should also be repeated in primary GEnCs to check the reproducibility of miR responses using ciGEnCs.

Analysis in silico

Analysis of cellular and extracellular miR expression revealed numerous gene ontology (GO) term clusters, many of which were similar. GO terms are characterised into those representing biological process (BP), cellular component (CC), and molecular function (MF), selected outputs are discussed below.

GO term analysis of genes associated with differentially expressed cellular ciGEnC miRs

Biological process (BP) GO terms

'Regulation of cellular component organisation' was the BP term of highest enrichment from those genes predicted to be associated with all three treatment conditions, and with the singular 25 mM glucose treatment condition. Child GO terms within this cluster included 'cytoskeleton organisation', 'cellular response to stimulus', and 'actin cytoskeleton organisation' (Appendix 15). These terms suggest that all treatment conditions modulated the cytoskeleton.

‘Anatomical structure development’ was the second most enriched BP GO term cluster under every singular and combined analysis group of treatment conditions. Child GO terms under this cluster included 'cell part morphogenesis', and 'tube development', but also contained irrelevant GO terms such as 'head development' and 'heart development'. 'Cell part morphogenesis' can relate to the morphogenesis of cell projections and mitochondria.

‘Movement of cell or subcellular component' was the third most enriched BP GO term under the subset of genes associated with all three treatment conditions, as well as those associated with both 10 ng/mL TNF-α treatment conditions, and the singular 25 mM glucose + 10 ng/mL TNF- α treatment condition. Child GO terms under this cluster included 'actin filament-based movement' and 'cell motility'.

‘Positive regulation of biological process' was the BP GO term of greatest enrichment in gene lists associated with both 25 mM glucose treatment conditions; both TNF- α treatment conditions; the singular 25 mM glucose + 10 ng/mL TNF- α treatment condition, and the singular 5 mM glucose + TNF-α treatment condition. This GO term encompassed Child GO terms including 'cellular response to stimulus', 'regulation of signalling', and 'regulation of response to stimulus', which were relevant given that treatments were applied to the cells.

'Protein phosphorylation' and ‘dephosphorylation’ were the third most enriched GO terms from genes predicted to be associated with predicted gene lists associated with both 25 mM glucose treatment conditions, and the singular 5 mM glucose + 10 ng/mL treatment condition respectively. Phosphorylation/dephosphorylation is a process involved in multiple cell behaviours, although is notably involved in the modulation of the actin cytoskeleton (Baek *et al.* 2008). This provides further evidence of cytoskeletal modulation in ciGEnCs in response to high glucose and the presence of TNF-α.

‘Cytoskeleton organisation’ and ‘actin filament based process’ were the fourth and third most enriched BP GO terms from genes predicted to be associated with gene lists from the combination of both 25 mM glucose treatment conditions, and the singular 25 mM glucose treatment condition respectively. The findings again support the notion that high glucose treatment modulates the cytoskeleton of ciGEnCs *in vitro*.

Cellular component (CC) GO terms

The CC GO term of greatest enrichment under each analysis condition was 'plasma membrane region', except under the analysis group comprised of both 25 mM glucose treatment conditions, where the greatest enriched GO term was 'plasma membrane part'. Related to these terms was the GO term 'cell periphery', which appeared within the top three enriched terms of all analysis groups except from the combination of all three treatment conditions, and both 25 mM glucose treatment conditions. These findings were

surprising, as there was no evidence of plasma membrane associated activity from the analysis of individual miRs differentially expressed under each treatment condition.

Also surprising was the prevalence of the 'cell projection' CC GO term, which was present in the top three enriched terms of all combined and singular analysis groups aside from the singular 25 mM glucose treatment condition. There is some limited evidence to suggest endothelial cells form projections, although not in response to any of the stimuli used in this study, or in relation to DKD (Fujimoto *et al.* 1975; Carman *et al.* 2003).

'Cytoplasmic region' and the related term 'cytoskeleton' appeared within the top three enriched CC GO terms of analysis groups encompassing genes under all three treatment conditions, under both 25 mM glucose conditions, and under the singular 25 mM glucose treatment condition. These GO terms further support the notion that cytoskeletal modulation is an effect of diabetic/DKD modelling of ciGEnCs.

Molecular function (MF) GO terms

The MF GO term 'Cytoskeletal binding' was within the top three most enriched terms of analysis groups encompassing predicted genes under all three treatment conditions, both 25 mM glucose conditions, and the singular 25 mM glucose treatment condition. These findings again support the idea of cytoskeletal modulation as an effect of the treatment conditions.

The related MF GO terms 'regulatory region nucleic acid binding', 'RNA polymerase II transcription factor activity, 'sequence-specific DNA binding', 'transcription regulatory region DNA binding', and 'transcription factor activity, sequence-specific DNA binding' were present under all combination and singular analysis groups. Nucleic acid binding is associated with a huge range of cellular processes, and therefore was not informative as to the exact effects of treatment on ciGEnCs.

'Enzyme binding' was the MF GO term of greatest enrichment under the analysis group comprised of genes associated with both TNF-α treatment conditions, the singular 25 mM glucose + 10 ng/mL TNF-α treatment condition, and the singular 5 mM glucose + 10 ng/mL TNF-α treatment condition. The 'enzyme binding' cluster was comprised of Child GO terms including 'cytoskeletal protein binding', and 'actin binding'. These provide further evidence of the cytoskeletal involvement in response to the diabetic/DKD treatment conditions.

Overall, cellular expression GO term analysis revealed the enrichment of genes relating to the processes of cytoskeletal modulation, cellular response to stimulus, structure development, regulation of phosphorylation, plasma membrane, and cell projection. Cytoskeletal modulation was the most notable process, which was enriched to some degree under all treatment conditions. This suggests that high glucose and TNF- α treatment cause ciGEnC cytoskeletal change. The cytoskeleton of endothelial cells has been found to be important in maintaining structural integrity and regulation of endothelial repair mechanisms

(Gotlieb *et al.* 1987; Lee and Gotlieb 2003). In addition, cells undergoing endothelial to mesenchymal transition alter their cytoskeletal structure, which is a process known to occur in response to TGF-β which itself is a key molecule driving DKD pathology (Zeisberg *et al.* 2007; Kokudo *et al.* 2008).

GO Term analysis of genes associated with differentially expressed extracellular ciGEnC miRs

Biological process (BP) GO terms

Similarly to GO term analysis of genes associated with differential cellular miR expression, extracellular expression analysis revealed the BP GO term ‘positive regulation of biological process’ as the most enriched term in all combination and singular analysis groups excluding the singular 25 mM glucose treatment condition. Also similar to analysis of cellular expression data, the GO term clusters 'movement of cell or subcellular component’, and ‘anatomical structure development’ featured within the top three enriched GO term clusters under all analysis groups apart from the singular 25 mM glucose + 10 ng/mL TNF-α treatment condition.

Cellular component (CC) GO terms

Compared with cellular results, analysis of CC GO terms associated with extracellular miRs demonstrated substantial differences. The CC GO terms 'Golgi apparatus' and 'neurone projection' were present in all combination and singular analysis groups except the analysis group comprised of both TNF-α containing treatment conditions, and the singualr 5 mM glucose + 10 ng/mL TNF-α treatment condition. Also present in all analysis groups except the group comprised of all three treatment conditions, was the GO term cluster 'endomembrane system'. Both 'Golgi apparatus' and 'endomembrane system' could be linked to the formation of vesicles or exosomes, presenting a possible link with previous research demonstrating the formation of extracellular vesicles (EVs) and exosomes by GEnCs, which can be communicators of injury-inducing stimulus (Thomas *et al.* 2018).

Molecular function (MF) GO terms

Of the MF GO terms, ‘transcription regulatory region DNA binding’ demonstrated the greatest enrichment under all combined and sigular analysis conditions. The similar term ‘transcription factor activity sequence-specific DNA binding’ was also the second most enriched GO term cluster under the analysis group comprised of both TNF-α treatment conditions; the singular 25 mM glucose + 10 ng/mL TNF- α treatment condition; the singular 25mM glucose treatment condition, and the singular 5 mM glucose + 10 ng/mL TNF- α treatment condition. These terms are very general and not informative with respect to a specific biological function.

Enzyme binding was the third most enriched MF GO term cluster under all singular and combination analysis conditions. These results are similar to those from the cellular GO

term analysis. Child GO terms under this cluster included 'cytoskeletal protein binding' and 'actin binding', again suggesting an association with cytoskeletal modulation.

In summary, extracellular expression GO term analysis found a strong enrichment of cytoskeletal-associated GO terms under all treatment conditions, as did the cellular data analysis. Also highly enriched were terms relating to anatomical structure development, the Golgi, and the endomembrane system. The enrichment of cytoskeletal modulators in extracellular miR gene targets is of interest since podocyte injury is a key pathogenic factor in DKD pathology and results in cytoskeletal rearrangement (Wang *et al.* 2020). The release of cytoskeletal-modifying miRs by GEnCs might represent an important mediator of diabetic injury.

KEGG and REACTOME pathways

Supporting findings of the GO term analysis, the KEGG pathway 'regulation of the actin cytoskeleton' was enriched under all combination and singular cellular analysis groups except the singular 25 mM glucose condition, and the singular 5 mM glucose + 10 ng/mL TNF-α treatment condition. This result provides further support of ciGEnC cytoskeleton modulation in response to experimental diabetes/DKD model treatments. Several KEGG terms related to cancer such as 'miRs in cancer' and 'pathways in cancer' were enriched under all cellular analysis groups. While these do not appear to bear direct relevance to the pathogenesis of DKD, considerable overlap between cancer and fibrosis pathways is now widely acknowledged. The KEGG pathway 'PI3K-Akt signalling pathway' was also enriched under several analysis conditions, including the analysis groups encompassing genes differentially regulated under all three treatment conditions, and both 25 mM glucose treatment conditions. This might suggest a mechanism by which some miRs mediate pathological changes in ciGEnCs.

REACTOME pathways enriched under all combined and singular cellular analysis groups included 'signal transduction' and 'signalling by receptor tyrosine kinases'. These results again may provide evidence of the mechanisms by which some the pathological changes in ciGENCs occur in response to the treatment conditions.

'Regulation of the actin cytoskeleton' was also the KEGG pathway enriched under many of the extracellular analysis groups, including the analysis group comprised of genes associated with all three treatment conditions, with both TNF-α containing treatment conditions, and the singular 5 mM glucose + 10 ng/mL TNF-α treatment condition. These results also support extracellular GO term results, providing further evidence suggesting that miRs released by ciGEnCs in response to diabetic/DKD stimuli have influence cytoskeletal changes. Numerous signalling pathways were enriched under all analysis conditions, including 'hippo signalling pathway', 'PI3K-Akt signalling pathway', 'Wnt signalling pathway', 'Ras signalling pathway', and 'TGF-β signalling pathway'. The 'TGF-β signalling pathway' was enriched under the analysis group comprised of genes associated

with both 25 mM glucose treatment conditions, and is of particular interest due to the association of TGF-β with DKD pathology. It also supports previous findings of miR-355, miR-22, miR-200b, miR-342, let-7b, and let-7c involvement in TGF-β signalling.

Analysis of the extracellular GEnC miR data revealed the REACTOME pathways 'signal transduction' and 'signalling by receptor tyrosine kinases' were enriched under all combined and singular analysis groups. In addition, the related terms ' membrane trafficking' and 'vesicle-mediated transport' appeared in all analysis groups, supporting GO term results from extracellular data, suggesting the enrichment of genes associated with the endomembrane system.

STRING analysis

The STRING analysis of cellular data revealed a network of proteins associated with protein ubiquitination in all analysis groups. Protein ubiquitination is a reversible process of enzymatic post-translational protein modification whereby a ubiquitin protein is attached. The process of ubiquitination is involved in a wide range of cellular processes, notably protein degradation via the ubiquitin-proteasome pathway, transcription, translation, regulation of membrane trafficking and autophagy (Sun and Chen 2004; Xu and Jaffrey 2011).

Several proteins involved in protein ubiquitination were highlighted by STRING analysis, including E2 ubiquitin-conjugating enzymes (such as UBE2H), and E3 ubiquitin protein ligases (such as RNF111, NEDD4, UBE3C). A mutation in genes encoding enzymes related to the ubiquitin-proteasome system (UPS) is known to cause renal disease through a number of mechanisms, although none yet directly linked to glomerular endothelial cells (Meyer-Schwesinger 2019). High glucose has been shown to increase the level of ubiquitin-conjugated proteins in retinal endothelial cells and pericytes, which was hypothesised to be protective against cellular stress and damage caused by high glucose conditions (Yadranji Aghdam *et al.* 2013). Additional evidence suggests impaired protesome activity in the kidneys of rats with streptozotocin-induced diabetes, although this has been suggested to reflect saturation of the UPS by the high levels of proteins damaged by diabetic stimulus (Portero-Otín *et al.* 1999; Meyer-Schwesinger 2019). It has been also suggested that urinary free ubiquitin could itself be used as a DKD biomarker (Xu and Jaffrey 2011). The E3 ubiquitin protein ligase RNF111 is of particular interest, as it promotes the ubiquitination, and therefore degradation, of negative regulators of the TGF-β signalling pathway, providing a link to an already well established mediator of renal injury in diabetes (Liu *et al.* 2008; Sharma *et al.* 2011).

Overall, there appears to be some evidence of protein ubiquitination dysregulation in DKD. It is possible that GEnCs protein ubiquitination is dysregulated in response to diabetic/DKD stimuli, and that these cells release miRs which could effect the protein ubiquitination processes of neighbouring renal cells. Further research is required to investigate GEnC

ubiquitination, and to determine if GEnC conditioned medium elicits functional effects on the UPS of podocytes and PTECs.

Numerous collagens were highlighted in STRING analysis: COL15A1, COL1A2 and COL4A1 in the extracellular data; COL3A1, COL1A1, COL4A1, COL5A2 and COL1A2 in the cellular data. The collagen IV family are the major class of collagens within the glomerular basement membrane, which is mostly comprised of α3, α4, and α5 subunits forming a triple helix structure (Miner 2012). A genome wide association study of DKD analysed almost 20,000 individuals with type 1 diabetes across a range of renal functions, and identified the loci of strongest association with DKD was a mutation in the collagen type IV α3 chain (COL4A3) gene. Furthermore, homozygous mutations in COL4A3 or COL4A4 (encoding the α3 and α4 respectively) are known to cause Alport syndrome, a basement membrane condition which leads to end stage renal failure.

Neither COL4A3 nor COL4A4 appeared in STRING analyses of the top 200 predicted gene-targets, although both appeared as cellular miR-targets under all three treatment conditions within the miR-DIP analysis. The COL4A1 protein, encoding the collagen type IV α1 subunit, appeared in the STRING analysis of genes associated with differentially expressed miRs in cells under all three treatment conditions, both 25 mM glucose treatment conditions, and both 10 ng/mL TNF-α treatment conditions. COL4A1 also appeared in the extracellular STRING analysis under the 25 mM glucose + 10 ng/mL TNF-α treatment condition. COL4A1 mutations have been shown to cause kidney disease, and mice mutant for COL4A1 have shown glomerular basement membrane defects (Van Agtmael *et al.* 2005; Gould *et al.* 2006; Plaisier *et al.* 2007). A study by Woroniecka *et al.* (2011) identified 1700 differentially expressed genes in human kidney samples from patients with DKD compared with controls. COL1A2 was among those genes demonstrating the greatest increase in expression in glomeruli and tubular DKD samples, whist COL3A1 was also highly upregulated in tubular samples. COL1A2 appeared in STRING analysis results of cellular and extracellular data, under all analysis conditions. COL3A1 appeared in the extracellular STRING analysis results under all analysis conditions. Our results support research suggesting the dysregulation of collagens in DKD, by demonstrating that miRs differentially regulated in ciGEnCs have predicted targets related to collagen regulation. Further work should aim to better characterise the effect of miRs on collagen production in ciGEnCs and determine whether extracellular miRs can affect the collagen regulation of podocytes and tubular cells.

Another cluster of related proteins identified under in both the cellular and extracellular STRING analyses were related to the process of cytoskeletal rearrangement. These findings support the findings of the GO term analysis, and KEGG pathway analysis. There are no studies reporting modification of the GEnC cytoskeleton as being a factor associated with diabetic stimulus, or as a pathological factor occurring in DKD. There is however strong

evidence for the modification of the podocyte cytoskeleton as a pathogenic factor (Maezawa and Yokote 2019; Wang *et al.* 2020). Our results suggest that cytoskeletal modification occurs in GEnCs in response to high glucose and TNF-α treatment. Further work should aim to test this hypothesis. The suggesting of cytoskeletal modifiers being released extracellularly by GEnCs in response to diabetic conditions has already been partially supported in the literature. A study by Wu *et al.* (2017) found that exosomes from GEnCs treated with high glucose were able to induce cytoskeletal disorganisation in podocytes, which lead to foot process effacement. Our results suggest that TNF-α treatment would lead to the same effect, and future work should aim to determine whether that is indeed the case.

A cluster of proteins involved in serine-threonine phosphatase activity were present in the STRING analysis of cellular data under all analysis conditions, but not in extracellular data. The serine-threonine pathway regulates a wide range of signalling pathways in eukaryotic cells. Specific proteins appearing in the STRING analysis included several protein phosphatase 2A subunits. The major function of protein phosphatase 2A is believed to be the negative control of cellular growth and division. Protein phosphatase 2A has been shown to be activated in endothelial cells undergoing an endothelial to mesenchymal transition, and the inhibition of protein phosphatase activity was able to prevent the transition. This has important implications in DKD, as endothelial to mesenchymal transition plays an important role in renal fibrosis (Deng *et al.* 2016). It is important to note however that these studies were conducted in HUVECs, and as demonstrated by our previous results, cannot be assumed to replicate the response of GEnCs. Future work should investigate whether the same process occurs in ciGEnCs.

Several proteins related to TGF-β activation were evident from STRING analysis of extracellular data. TGF-β is a widely accepted molecular mediator of injury in DKD. The TGF-β signalling pathway is activated in DKD, promoting inflammation, and renal fibrosis through ECM dysregulation, promoting the cross-linking of collagen and elastin fibres, and the promotion of proximal tubular and GEnC de-differentiation. The inhibition of TGF-β1 has been shown to attenuate the development of fibrosis in animal models of diabetes (Meng 2019). The release of miRs mediating TGF-β signalling, as evidenced by this analysis, would have a range of effects on neighbouring renal cells. TGF-β is known to induce the de-differentiation of proximal tubular cells, contirubting to renal fibrosis, and induce autophagy of podocytes, and podocyte detachment (Fujimoto *et al.* 2003; Zeisberg *et al.* 2003; Lin and Susztak 2016). Furthermore, in mesangial cells TGF-β induces the accumulation of ECM components (Fujimoto *et al.* 2003).

Small clusters of PDGF-associated proteins appeared in the extracellular STRING analysis, including two PDGF receptors (PDGFRA and PDGFRB), and one of the four PDGF isoforms (PDGF-C). There is some evidence of PDGF activity contributing to renal fibrosis in DKD, namely through the recruitment of mesenchymal cells into glomerular and

tubulointerstitial regions of the kidney, and through promotion of ECM accumulation and inflammation (Ostendorf *et al.* 2014). Our results suggest that high glucose and TNF-α treatment conditions induce the release of PDGF associated miRs by ciGEnCs. Further work should aim to determine whether these miRs are able to influence other renal cells such as podocytes, mesangial cells, and tubular cells.

Sirtuin-1 (SIRT1) was a protein which appeared in the STRING analysis of all singular and combination treatment group analyses of extracellular data.

Several studies have demonstrated a role for Sirtuin-1 (SIRT1) in DKD. SIRT1 is believed to play a protective role in podocytes and renal tubule cells, and has been proposed as a potential drug target in DKD. SIRT1 has been found to be reduced in human kidneys with DKD, and this reduction is more pronounced in the glomerular regions of the kidney (Chuang *et al.* 2011; Zhong *et al.* 2018). A study by Zhong *et al.* (2018) found that SIRT1 overexpression in podocytes attenuated proteinuria and kidney injury in a type 1 diabetic mouse model. Furthermore, podocyte-specific deletion of SIRT1 in a diabetic mouse model lead to worse proteinuria and kidney injury, compared with diabetic mouse models without SIRT1 podocyte deletion (Liu *et al.* 2014). The exact protective mechanisms of SIRT1 are unknown, although are believed to be related to the regulation of autophagy and response to oxidative stress. (Kume *et al.* 2012; Yacoub *et al.* 2014; Lo *et al.* 2017; Zhong *et al.* 2018). These data suggest that high glucose and TNF-α treatment conditions induce the release of miRs regulating SIRT1 by ciGEnCs. Further work will be required to determine if these miRs infer a protective effect on other renal cells.

Consideration of the limitations of in silico analysis

miRDIP v4.1 was the computational tool used to predict miR targets (Tokar *et al.* 2018). Each miR-target prediction tool has its own limitations. To mitigate these limitations, data outputs from several algorithms are frequently combined, but performed manually this process is time-consuming, limiting the number of algorithms used for comparison (Lopez-Anton *et al.* 2017). MiRDIP v4.1 faciltates the integration of 30 different miR-target prediction databases, including miRbase, TargetScan, MirTar, PicTar, and DIANA (Tokar *et al.* 2018).

miRDIP assigns gene prediction results one of four confidence categories: ‘very high’, ‘high’, ‘medium’ and ‘low’ confidence. Only results of ‘very high’ confidence were taken forward in this analysis, which corresponded to the top 1% of data. A common problem with miR-target prediction tools is a bias towards certain biological processes and pathways, with the integration of multiple tools often leading to bias accumulation. Tokar *et al.* (2018) demonstrates that mirDIP algorithms do not cumulate prediction bias towards a particular biological process or pathway.

These advanced computational tools generate predictions that provide a logical starting point for functional experimental analysis. However, the prediction of mRNA targets of miRs is challenging since mRNA-miR interactions are complex, with one miR often regulating multiple mRNAs, and there is also a lack of experimentally validated miR-mRNA interactions (Roberts and Borchert 2017). The results of all miR-target prediction software should therefore be treated with the above caveats in mind.

G:Profiler is a web server for characterising gene lists. The g:GOSt tool within G:Profiler was used to perform statistical enrichment analysis, generating Gene Ontology (GO) terms, KEGG pathways, and REACTOME pathways, to interpret the gene lists provided. The g:GOSt tool finds over-representation of terms/pathways in the gene list, in comparison with an appropriate background gene list. In this study this background list was a comprehensive inventory of genes expressed in GEnCs, compiled by Sengoelge *et al.* (2014), chosen to control for normal GEnC expression patterns. Ideally, this background gene list would have been generated from ciGEnCs under control treatment conditions, but such data were not available. The background gene list for extracellular expression was a complete list of genes expressed in the nephron. The ideal background gene list for the extracellular expression analysis would have been the complete basal expression profile of the medium under the control treatment condition, however this data was not available. Although the background lists used were not ideal, they offered the closest alternative available, and were likely to give more accurate results than the use of the default option of the complete human Ensembl database.

Gene ontology (GO) terms were entered into REVIGO, which runs an algorithm clustering similar GO terms, allowing for the removal of redundant GO terms and therefore simpler interpretation. REVIGO was chosen over other summarisation methods such as 'GO Slim' terms, as they limit the resulting GO term list to only high level terms, from which it is difficult to extrapolate biological meaning (Supek *et al.* 2011).

Chapter 5 – Discussion

5.1 Summary

The work described in this thesis was based on the hypothesis that cellular and extracellular ciGEnC miR expression changes in response to diabetic kidney disease (DKD)-specific stimuli can mediate renal injury and, by profiling these changes in an appropriate model, disease biomarkers might be identified by their functional effects. Using ciGEnCs from Dr Simon Satchell's laboratory, the project aims were to: i) culture and extract RNA from ciGEnC *in vitro* models of diabetes mellitus (hyperglycaemia) and DKD (hyperglycaemia and TNF-α) and ii) profile and analyse ciGEnC cellular and extracellular miR expression in these models.

At the beginning of this project, the maintenance of viable ciGEnC cells in culture proved challenging and required. Consequently, a lengthy initial set-up phase was required to ensure that cells of appropriate phenotype were used for the miR expression profiling assays on which all downstream data analyses were based. Inclusion of VEGF in the ciGEnC culture medium, and cell passage number, impacted significantly on ciGEnC miR expression.

Experimental evidence suggested that HUVECs were not a suitable model for ciGEnC miR response to high glucose and TNF-α, and thus could not be used as an alternative to ciGEnCs in this analysis. This finding suggests that microvascular and macrovascular endothelial cells do not respond in the same way to diabetic stimulus.

Differential cellular and extracellular ciGEnC miR expression was observed in response to high glucose and/or TNF-α. Analysis *in silico* suggested that these miRs shared a substantial number of gene targets. Further *in silico* examination suggested enrichment of biochemical pathways related to TGF-α signaling, cytoskeletal modulation, protein ubiquitination, and collagen regulation. However, none of the above biological processes has been explicitly described in GEnCs, and the results of these *in silico* studies must be interpreted with appropriate caution. It is hoped that the results of this study will lead to future work validating the relevance of its findings.

5.2 Future Work

This study identified a number of differentially regulated cellular and extracellular miRs in ciGEnCs under high glucose and TNF-α treatment conditions. Future work should investigate these findings further through the replication of TLDA analysis with increased sample size ($n \geq 3$) to facilitate statistical analysis of expression data. Ideally, these experiments should be repeated in ciGEnCs of lower passage number, or primary GEnCs, as the data presented in this thesis show the influence passage number can have on miR response.

The isolation of sufficient exosomes from HUVECs for labelling and subsequent uptake experiments was not possible due to time constraints, and HUVECs were shown to be an unsuitable model for GEnC miR expression. These experiments should be repeated in low passage ciGEnCs, or ideally primary GEnCs. Labelled exosomes could then be added to PTEC culture medium to investigate uptake and the functional effects of that uptake, thereby providing evidence of GEnC-to-PTEC communication.

CiGEnCs are a useful cell model and respond to various stimuli in a similar manner to primary GEnCs (Satchell *et al.* 2006). However, the exact miR response of primary GEnCs has not been well studied and therefore it is not known how the miR response of ciGEnCs compares. Representative experiments should be replicated in primary GEnCs.

GEnCs could be co-cultured with podocytes in a vessel allowing continuous medium flow. As previously discussed, podocytes release factors, including VEGF, which influence GEnC development and maintenance *in vivo*. GEnCs *in vivo* experience continuous blood flow of blood over their surface, which influences their behavior in comparison with standard culture conditions (Levesque *et al.* 1990; Estrada *et al.* 2011a; Estrada *et al.* 2011b).

Several potential miR DKD biomarkers were highlighted by the TLDA analysis that previous studies have suggested are associated with DKD. These associations should be investigated further using bespoke miR RT-qPCR assays. Certain differentially expressed extracellular miRs might potentially influence other renal cells such as podocytes, mesangial cells and PTECs. Future experiments could test this by treating ciGEnCs in co-culture with other renal cells, and investigating the effect of this on co-cultured renal cell gene expression. Alternatively, conditioned medium from treated ciGEnCs could be added to cultures of other renal cell types.

Differentially expressed cellular miRs were predicted to influence the gene expression of ciGEnCs. This could be tested by monitoring the mRNA and miR expression of treated cells in culture, and by investigating the effect manipulating expression of specific miRs on gene expression.

Analysis *in silico* of genes associated with differentially regulated miRs revealed a number of potential effects on key cellular biological processes. The relevance of these pathways should be investigated in further studies, to investigate their involvement in ciGEnC responses to high glucose and TNF-α treatment conditions, and to determine if they can impact neighboring renal cells in culture and *in vivo*.

Finally, experiments in this study conducted in culture cannot be assumed to reflect the precise response of cells *in vivo*. MiRs identified in these analyses should be studied in animal models and investigated in human tissue samples to determine their clinical relevance.

5.3 Conclusion

To conclude, this study has demonstrated that ciGEnCs treated with high glucose and/or TNF-α exhibit differential cellular and extracellular miR expression. There was a large overlap between miRs differentially expressed under different treatment conditions, and in the genes predicted to be targeted by those miRs. In silico analysis of differentially expressed cellular and extracellular miRs revealed enrichment of pathways related to TGF-β signalling, cytoskeletal modulation, protein ubiquitination, and collagen regulation. Analysis of extracellular miR data highlighted enrichment of processes related to the formation of vesicles and PDGFs. Further work will be required to determine the relevance of these findings to the responses of ciGEnCs to diabetic/DKD stimuli in vivo, and the potential utility of these miRs as disease biomarkers.

References

Abbasi, M.A. hme., Chertow, G.M. and Hall, Y.N. (2010). End-stage renal disease. *BMJ clinical evidence* **2010**.

Van Agtmael, T., Schlötzer-Schrehardt, U., McKie, L., Brownstein, D.G., Lee, A.W., Cross, S.H., … Jackson, I.J. (2005). Dominant mutations of Col4a1 result in basement membrane defects which lead to anterior segment dysgenesis and glomerulopathy. *Human Molecular Genetics*. doi: https://doi.org/10.1093/hmg/ddi348.

Alicic, R.Z., Rooney, M.T. and Tuttle, K.R. (2017). Diabetic kidney disease: Challenges, progress, and possibilities. *Clinical Journal of the American Society of Nephrology* **12**(12):2032–2045. doi: https://doi.org/10.2215/CJN.11491116.

Allali, J., Chauve, C., Denise, A., Drevet, C., Ferraro, P., Gautheret, D., … Thermes, C. (2012). BRASERO: A resource for benchmarking RNA secondary structure comparison algorithms. *Advances in Bioinformatics* **2012**(893048):5. doi: https://doi.org/10.1155/2012.

Alpers, C.E. and Hudkins, K.L. (2011). Mouse models of diabetic nephropathy. *Current Opinion in Nephrology and Hypertension* **20**(3):278–284.

Alphonsus, C.S. and Rodseth, R.N. (2014). The endothelial glycocalyx: a review of the vascular barrier. *Anaesthesia* **69**(7):777–784. doi: https://doi.org/10.1111/anae.12661.

Anders, H.J., Huber, T.B., Isermann, B. and Schiffer, M. (2018). CKD in diabetes: Diabetic kidney disease versus nondiabetic kidney disease. *Nature Reviews Nephrology* **14**(6):361–377.

Ang, G.Y. (2018). Reversibility of diabetes mellitus: Narrative review of the evidence. *World journal of diabetes* **9**(7):127–131. doi: https://doi.org/10.4239/wjd.v9.i7.127.

Araki, S.I., Haneda, M., Sugimoto, T., Isono, M., Isshiki, K., Kashiwagi, A. and Koya, D. (2005). Factors associated with frequent remission of microalbuminuria in patients with type 2 diabetes. *Diabetes* **54**(10):2983–2987. doi: https://doi.org/10.2337/diabetes.54.10.2983.

Argyropoulos, C., Wang, K., Bernardo, J., Ellis, D., Orchard, T., Galas, D. and Johnson, J. (2015). Urinary MicroRNA Profiling Predicts the Development of Microalbuminuria in Patients with Type 1 Diabetes. *Journal of Clinical Medicine* **4**(7):1498–1517. doi: https://doi.org/10.3390/jcm4071498.

Argyropoulos, C., Wang, K., Mcclarty, S., Huang, D., Bernardo, J., Ellis, D., … Johnson, J. (2013). Urinary MicroRNA Profiling in the Nephropathy of Type 1 Diabetes. doi: https://doi.org/10.1371/journal.pone.0054662.

Arif, E. and Nihalani, D. (2013). Glomerular Filtration Barrier Assembly: An insight.

Postdoc journal : a journal of postdoctoral research and postdoctoral affairs **1**(4):33.

Aronoff, S.L., Berkowitz, K., Shreiner, B. and Want, L. (2004). Glucose Metabolism and Regulation: Beyond Insulin and Glucagon. *Diabetes Spectrum* **17**(3):183–190. doi: https://doi.org/10.2337/diaspect.17.3.183.

Van Der Auwera, I., Limame, R., Van Dam, P., Vermeulen, P.B., Dirix, L.Y. and Van Laere, S.J. (2010). Integrated miRNA and mRNA expression profiling of the inflammatory breast cancer subtype. *British Journal of Cancer* **103**(4):532–541. doi: https://doi.org/10.1038/sj.bjc.6605787.

Badal, S.S. and Danesh, F.R. (2014). New Insights Into Molecular Mechanisms of Diabetic Kidney Disease. *American Journal of Kidney Diseases* **63**(2):S63–S83. doi: https://doi.org/10.1053/j.ajkd.2013.10.047.

Baek, K., Liu, X., Ferron, F., Shu, S., Korn, E.D. and Dominguez, R. (2008). Modulation of actin structure and function by phosphorylation of Tyr-53 and profilin binding. *Proceedings of the National Academy of Sciences of the United States of America* **105**(33):11748–11753. doi: https://doi.org/10.1073/pnas.0805852105.

Baker, M.A., Davis, S.J., Liu, P., Pan, X., Williams, A.M., Iczkowski, K.A., … Liang, M. (2017). Tissue-Specific MicroRNA Expression Patterns in Four Types of Kidney Disease. *Journal of the American Society of Nephrology* **28**(10):2985–2992. doi: https://doi.org/10.1681/ASN.2016121280.

Bakris, G.L., Weir, M.R., Shanifar, S., Zhang, Z., Douglas, J., Van Dijk, D.J. and Brenner, B.M. (2003). Effects of blood pressure level on progression of diabetic nephropathy: Results from the RENAAL study. *Archives of Internal Medicine* **163**(13):1555–1565. doi: https://doi.org/10.1001/archinte.163.13.1555.

Ballermann, B.J. and Obeidat, M. (2014). Tipping the balance from angiogenesis to fibrosis in CKD. *Kidney International Supplements* **4**(1):45–52. doi: https://doi.org/10.1038/kisup.2014.9.

Barrera-Chimal, J. and Jaisser, F. (2020). Pathophysiologic mechanisms in diabetic kidney disease: A focus on current and future therapeutic targets. *Diabetes, Obesity and Metabolism* **22**(S1):16–31. doi: https://doi.org/10.1111/dom.13969.

Barutta, F., Bellini, S., Mastrocola, R., Bruno, G. and Gruden, G. (2018). MicroRNA and Microvascular Complications of Diabetes. *International Journal of Endocrinology* **2018**:1–20. doi: https://doi.org/10.1155/2018/6890501.

Barutta, F., Bruno, G., Matullo, G., Chaturvedi, N., Grimaldi, S., Schalkwijk, C., … Gruden, G. (2017). MicroRNA-126 and micro-/macrovascular complications of type 1 diabetes in the EURODIAB Prospective Complications Study. *Acta Diabetologica* **54**(2):133–139. doi:

https://doi.org/10.1007/s00592-016-0915-4.

Barutta, F., Tricarico, M., Corbelli, A., Annaratone, L., Pinach, S., Grimaldi, S., … Gruden, G. (2013). Urinary exosomal microRNAs in incipient diabetic nephropathy. Martelli, F. (ed.). *PloS one* **8**(11):e73798. doi: https://doi.org/10.1371/journal.pone.0073798.

Baud, L. and Ardaillou, R. (1995). Tumor necrosis factor in renal injury. *Mineral and electrolyte metabolism* **21**(4–5):336–41.

Baud, L., Fouqueray, B. and Philippe, C. (1994). Involvement of tumor necrosis factor-α in glomerular injury. *Springer Seminars in Immunopathology* **16**(1):53–61. doi: https://doi.org/10.1007/BF00196713.

Baudin, B., Bruneel, A., Bosselut, N. and Vaubourdolle, M. (2007). A protocol for isolation and culture of human umbilical vein endothelial cells Cardiovascular diseases among Tunisian population, molecular and metabolic approaches View project Bikunin proteoglycans: Convenient serum biomarkers of alterations in the proteoglycan biosynthesis and Golgi homeostasis View project A protocol for isolation and culture of human umbilical vein endothelial cells. doi: https://doi.org/10.1038/nprot.2007.54.

BC Faculty *Opentextbc.Ca*. Available at: opentextbc.ca [Accessed: 1 April 2020].

Beltrami, C. (2014). *The Identification of MiRNA Biomarkers of Chronic Kidney Disease and Development of Minimally-Invasive Methods of Molecular Detection*.

Beltrami, C., Clayton, A., Newbury, L., Corish, P., Jenkins, R., Phillips, A., … Bowen, T. (2015). Stabilization of Urinary MicroRNAs by Association with Exosomes and Argonaute 2 Protein. *Non-Coding RNA* **1**(2):151–166. doi: https://doi.org/10.3390/ncrna1020151.

Beltrami, C., Simpson, K., Jesky, M., Wonnacott, A., Carrington, C., Holmans, P., … Bowen, T. (2018). Association of Elevated Urinary miR-126, miR-155, and miR-29b with Diabetic Kidney Disease. *The American Journal of Pathology* **188**(9):1982–1992. doi: https://doi.org/10.1016/j.ajpath.2018.06.006.

Bendtsen, T.F. and Nyengaard, J.R. (1992). The number of glomeruli in Type 1 (insulin-dependent) and Type 2 (non-insulin-dependent) diabetic patients. *Diabetologia* **35**(9):844–850. doi: https://doi.org/10.1007/BF00399930.

Berg, T.J., Bangstad, H.J., Torjesen, P.A., Østerby, R., Bucala, R. and Hanssen, K.F. (1997). Advanced glycation end products in serum predict changes in the kidney morphology of patients with insulin-dependent diabetes mellitus. *Metabolism: Clinical and Experimental* **46**(6):661–665. doi: https://doi.org/10.1016/S0026-0495(97)90010-X.

Bergsmedh, A., Szeles, A., Henriksson, M., Bratt, A., Folkman, M.J., Spetz, A.-L. and Holmgren, L. (2001). Horizontal transfer of oncogenes by uptake of apoptotic bodies. *Proceedings of the National Academy of Sciences* **98**(11):6407–6411. doi:

https://doi.org/10.1073/pnas.101129998.

Bertani, T., Abbate, M., Zoja, C., Corna, D., Perico, N., Ghezzi, P. and Remuzzi, G. (1989). Tumor necrosis factor induces glomerular damage in the rabbit. *American Journal of Pathology* **134**(2):419–430.

Bertuccio, C., Veron, D., Aggarwal, P.K., Holzman, L. and Tufro, A. (2011). Vascular Endothelial Growth Factor Receptor 2 Direct Interaction with Nephrin Links VEGF-A Signals to Actin in Kidney Podocytes. *Journal of Biological Chemistry* **286**(46):39933–39944. doi: https://doi.org/10.1074/jbc.M111.241620.

Beutler, B. (2004). Inferences, questions and possibilities in Toll-like receptor signalling. *Nature* **430**(6996):257–263.

Bilous, R.W., Mauer, S.M., Sutherland, E.R. and Steffes, M.W. (1989). Mean glomerular volume and rate of development of diabetic nephropathy. *Diabetes* **38**(9):1142–1147. doi: https://doi.org/10.2337/diab.38.9.1142.

Bjarnegard, M., Enge, M., Norlin, J., Gustafsdottir, S., Fredriksson, S., Abramsson, A., … Betsholtz, C. (2004). Endothelium-specific ablation of PDGFB leads to pericyte loss and glomerular, cardiac and placental abnormalities. *Development* **131**(8):1847–1857. doi: https://doi.org/10.1242/dev.01080.

Bohrer, M.P., Baylis, C., Humes, H.D., Glassock, R.J., Robertson, C.R. and Brenner, B.M. (1978). Permselectivity of the Glomerular Capillary Wall. *Journal of Clinical Investigation* **61**(1):72–78. doi: https://doi.org/10.1172/JCI108927.

Boor, P., Van Roeyen, C.R.C., Kunter, U., Villa, L., Bücher, E., Hohenstein, B., … Ostendorf, T. (2010). PDGF-C mediates glomerular capillary repair. *American Journal of Pathology* **177**(1):58–69. doi: https://doi.org/10.2353/ajpath.2010.091008.

Brennan, E.P., Nolan, K.A., Börgeson, E., Gough, O.S., McEvoy, C.M., Docherty, N.G., … Godson, C. (2013). Lipoxins attenuate renal fibrosis by inducing let-7c and suppressing TGFβR1. *Journal of the American Society of Nephrology* **24**(4):627–637. doi: https://doi.org/10.1681/ASN.2012060550.

Brownlee, M. (2001). Biochemistry and molecular cell biology of diabetic complications. *Nature* **414**(6865):813–820. doi: https://doi.org/10.1038/414813a.

Brunton, S. (2016). Pathophysiology of Type 2 Diabetes: The Evolution of Our Understanding. *The Journal of family practice* **65**(4).

Byron, A., Randles, M.J., Humphries, J.D., Mironov, A., Hamidi, H., Harris, S., … Lennon, R. (2014). Glomerular cell cross-talk influences composition and assembly of extracellular matrix. *Journal of the American Society of Nephrology* **25**(5):953–966. doi: https://doi.org/10.1681/ASN.2013070795.

Cameron, J.S. (2006). The discovery of diabetic nephropathy: From small print to centre stage. *Journal of Nephrology* **19**(SUPPL. 10).

Cantaluppi, V., Gatti, S., Medica, D., Figliolini, F., Bruno, S., Deregibus, M.C., … Camussi, G. (2012). Microvesicles derived from endothelial progenitor cells protect the kidney from ischemia-reperfusion injury by microRNA-dependent reprogramming of resident renal cells. *Kidney International* **82**(4):412–427. doi: https://doi.org/10.1038/ki.2012.105.

Cao, D. wei, Jiang, C. ming, Wan, C., Zhang, M., Zhang, Q. yan, Zhao, M., … Han, X. (2018). Upregulation of MiR-126 Delays the Senescence of Human Glomerular Mesangial Cells Induced by High Glucose via Telomere-p53-p21-Rb Signaling Pathway. *Current Medical Science* **38**(5):758–764. doi: https://doi.org/10.1007/s11596-018-1942-x.

Cao, Q., Chen, X., Huang, C. and Pollock, C.A. (2019). MicroRNA as novel biomarkers and therapeutic targets in diabetic kidney disease: An update. *FASEB BioAdvances* **1**(6):fba.2018-00064. doi: https://doi.org/10.1096/fba.2018-00064.

Caporali, A., Meloni, M., Völlenkle, C., Bonci, D., Sala-Newby, G.B., Addis, R., … Emanueli, C. (2011). Deregulation of microRNA-503 contributes to diabetes mellitus-induced impairment of endothelial function and reparative angiogenesis after Limb Ischemia. *Circulation* **123**(3):282–291. doi: https://doi.org/10.1161/CIRCULATIONAHA.110.952325.

Caramori, M.L., Parks, A. and Mauer, M. (2013). Renal lesions predict progression of diabetic nephropathy in type 1 diabetes. *Journal of the American Society of Nephrology* **24**(7):1175–1181. doi: https://doi.org/10.1681/ASN.2012070739.

Carman, C. V., Jun, C.-D., Salas, A. and Springer, T.A. (2003). Endothelial Cells Proactively Form Microvilli-Like Membrane Projections upon Intercellular Adhesion Molecule 1 Engagement of Leukocyte LFA-1. *The Journal of Immunology* **171**(11):6135–6144. doi: https://doi.org/10.4049/jimmunol.171.11.6135.

Chen, S, Cohen, M.P., Lautenslager, G.T., Shearman, C.W. and Ziyadeh, F.N. (2001). Glycated albumin stimulates TGF-β 1 production and protein kinase C activity in glomerular endothelial cells. *Kidney international* **59**(2):673–81. doi: https://doi.org/10.1046/j.1523-1755.2001.059002673.x.

Chen, Sheldon, Cohen, M.P., Lautenslager, G.T., Shearman, C.W. and Ziyadeh, F.N. (2001). Glycated albumin stimulates TGF-β1 production and protein kinase C activity in glomerular endothelial cells. *Kidney International* **59**(2):673–681. doi: https://doi.org/10.1046/j.1523-1755.2001.059002673.x.

Chen, S., Kasama, Y., Lee, J.S., Jim, B., Marin, M. and Ziyadeh, F.N. (2004). Podocyte-Derived Vascular Endothelial Growth Factor Mediates the Stimulation of 3(IV) Collagen Production by Transforming Growth Factor- 1 in Mouse Podocytes. *Diabetes*

53(11):2939–2949. doi: https://doi.org/10.2337/diabetes.53.11.2939.

Cheng, H.S., Sivachandran, N., Lau, A., Boudreau, E., Zhao, J.L., Baltimore, D., … Fish, J.E. (2013). MicroRNA-146 represses endothelial activation by inhibiting pro-inflammatory pathways. *EMBO Molecular Medicine* **5**(7):949–966. doi: https://doi.org/10.1002/emmm.201202318.

Chmielewski, C. (2003). Renal anatomy and overview of nephron function. *Nephrology nursing journal : journal of the American Nephrology Nurses' Association* **30**(2):185–90; quiz 191–2.

Chuang, P.Y., Dai, Y., Liu, R., He, H., Kretzler, M., Jim, B., … He, J.C. (2011). Alteration of forkhead box o (foxo4) acetylation mediates apoptosis of podocytes in diabetes mellitus. *PLoS ONE* **6**(8). doi: https://doi.org/10.1371/journal.pone.0023566.

Cogswell, J.P., Ward, J., Taylor, I.A., Waters, M., Shi, Y., Cannon, B., … Richards, C.A. (2008). Identification of miRNA changes in Alzheimer's disease brain and CSF yields putative biomarkers and insights into disease pathways. *Journal of Alzheimer's Disease* **14**(1):27–41. doi: https://doi.org/10.3233/JAD-2008-14103.

Conserva, F., Pontrelli, P., Accetturo, M. and Gesualdo, L. (2013). The pathogenesis of diabetic nephropathy: Focus on microRNAs and proteomics. *Journal of Nephrology* **26**(5):811–820.

Cowan, C., Muraleedharan, C.K., O'Donnell, J.J., Singh, P.K., Lum, H., Kumar, A. and Xu, S. (2014). MicroRNA-146 inhibits thrombin-induced NF-κB activation and subsequent inflammatory responses in human retinal endothelial cells. *Investigative Ophthalmology and Visual Science* **55**(8):4944–4951. doi: https://doi.org/10.1167/iovs.13-13631.

Curthoys, N.P. and Moe, O.W. (2014). Proximal Tubule Function and Response to Acidosis. *Clinical Journal of the American Society of Nephrology* **9**(9):1627–1638. doi: https://doi.org/10.2215/CJN.10391012.

Deen, W.M., Lazzara, M.J. and Myers, B.D. (2001). Structural determinants of glomerular permeability. *American Journal of Physiology-Renal Physiology* **281**(4):F579–F596. doi: https://doi.org/10.1152/ajprenal.2001.281.4.F579.

Deng, Y., Guo, Y., Liu, P., Zeng, R., Ning, Y., Pei, G., … Xu, G. (2016). Blocking protein phosphatase 2A signaling prevents endothelial-to-mesenchymal transition and renal fibrosis: A peptide-based drug therapy. *Scientific Reports* **6**. doi: https://doi.org/10.1038/srep19821.

Dhaun, N., Webb, D.J. and Kluth, D.C. (2012). Endothelin-1 and the kidney--beyond BP. *British journal of pharmacology* **167**(4):720–31. doi: https://doi.org/10.1111/j.1476-5381.2012.02070.x.

Dieter, B.P., Alicic, R.Z., Meek, R.L., Anderberg, R.J., Cooney, S.K. and Tuttle, K.R. (2015). Novel therapies for diabetic kidney disease: Storied past and forward paths. *Diabetes Spectrum* **28**(3):167–174. doi: https://doi.org/10.2337/diaspect.28.3.167.

Drummond, K.N., Kramer, M.S., Suissa, S., Lévy-Marchal, C., Dell'Aniello, S., Sinaiko, A. and Mauer, M. (2003). Effects of duration and age at onset of type 1 diabetes on preclinical manifestations of nephropathy. *Diabetes* **52**(7):1818–1824. doi: https://doi.org/10.2337/diabetes.52.7.1818.

Du, B., Yu, M. and Zheng, J. (2018). Transport and interactions of nanoparticles in the kidneys. *Nature Reviews Materials* **3**(10):358–374. doi: https://doi.org/10.1038/s41578-018-0038-3.

Eissa, S., Matboli, M. and Bekhet, M.M. (2016). Clinical verification of a novel urinary microRNA panal: 133b, -342 and -30 as biomarkers for diabetic nephropathy identified by bioinformatics analysis. *Biomedicine & Pharmacotherapy* **83**:92–99. doi: https://doi.org/10.1016/j.biopha.2016.06.018.

Eremina, V., Cui, S., Gerber, H., Ferrara, N., Haigh, J., Nagy, A., … Quaggin, S.E. (2006). Vascular Endothelial Growth Factor A Signaling in the Podocyte-Endothelial Compartment Is Required for Mesangial Cell Migration and Survival. *Journal of the American Society of Nephrology* **17**(3):724–735. doi: https://doi.org/10.1681/ASN.2005080810.

Eremina, V., Jefferson, J.A., Kowalewska, J., Hochster, H., Haas, M., Weisstuch, J., … Quaggin, S.E. (2008). VEGF inhibition and renal thrombotic microangiopathy. *New England Journal of Medicine* **358**(11):1129–1136. doi: https://doi.org/10.1056/NEJMoa0707330.

Estrada, R., Giridharan, G.A., Nguyen, M.D., Prabhu, S.D. and Sethu, P. (2011). Microfluidic endothelial cell culture model to replicate disturbed flow conditions seen in atherosclerosis susceptible regions. *Biomicrofluidics* **5**(3). doi: https://doi.org/10.1063/1.3608137.

Estrada, R., Giridharan, G.A., Nguyen, M.D., Roussel, T.J., Shakeri, M., Parichehreh, V., … Sethu, P. (2011). Endothelial cell culture model for replication of physiological profiles of pressure, flow, stretch, and shear stress *in vitro*. *Analytical Chemistry* **83**(8):3170–3177. doi: https://doi.org/10.1021/ac2002998.

Farquhar, M.G. (2006). The glomerular basement membrane: not gone, just forgotten. *The Journal of Clinical Investigation* **116**(8):2090–2093. doi: https://doi.org/10.1172/JCI29488.

Ferreira, R., Santos, T., Amar, A., Gong, A., Chen, T.C., Tahara, S.M., … Hofman, F.M. (2014). Argonaute-2 promotes miR-18a entry in human brain endothelial cells. *Journal of the American Heart Association* **3**(3). doi: https://doi.org/10.1161/JAHA.114.000968.

Fiorentino, L., Cavalera, M., Mavilio, M., Conserva, F., Menghini, R., Gesualdo, L. and Federici, M. (2013). Regulation of TIMP3 in diabetic nephropathy: A role for microRNAs. *Acta Diabetologica* **50**(6):965–969. doi: https://doi.org/10.1007/s00592-013-0492-8.

Forbes, J.M. and Cooper, M.E. (2013). Mechanisms of diabetic complications. *Physiological Reviews* **93**(1):137–188.

Fu, J., Lee, K., Chuang, P.Y., Liu, Z. and He, J.C. (2015). Glomerular endothelial cell injury and cross talk in diabetic kidney disease. *American journal of physiology. Renal physiology* **308**(4):F287-97. doi: https://doi.org/10.1152/ajprenal.00533.2014.

Fujimoto, M., Maezawa, Y., Yokote, K., Joh, K., Kobayashi, K., Kawamura, H., … Mori, S. (2003). Mice lacking Smad3 are protected against streptozotocin-induced diabetic glomerulopathy. *Biochemical and Biophysical Research Communications* **305**(4):1002–1007. doi: https://doi.org/10.1016/S0006-291X(03)00885-4.

Fujimoto, S., Yamamoto, K. and Takeshige, Y. (1975). Electron microscopy of endothelial microvilli of large arteries. *The Anatomical Record* **183**(2):259–265. doi: https://doi.org/10.1002/ar.1091830204.

Gale, N.W. and Yancopoulos, G.D. (1999). Growth factors acting via endothelial cell-specific receptor tyrosine kinases: VEGFs, Angiopoietins, and ephrins in vascular development. *Genes & Development* **13**(9):1055–1066. doi: https://doi.org/10.1101/gad.13.9.1055.

Gallo, A., Tandon, M., Alevizos, I. and Illei, G.G. (2012). The majority of microRNAs detectable in serum and saliva is concentrated in exosomes. *PLoS ONE* **7**(3):e30679. doi: https://doi.org/10.1371/journal.pone.0030679.

Genovesi, L.A., Anderson, D., Carter, K.W., Giles, K.M. and Dallas, P.B. (2012). Identification of suitable endogenous control genes for microRNA expression profiling of childhood medulloblastoma and human neural stem cells. *BMC Research Notes* **5**(1):1–12. doi: https://doi.org/10.1186/1756-0500-5-507.

Gevaert, A.B., Witvrouwen, I., Vrints, C.J., Heidbuchel, H., Van Craenenbroeck, E.M., Van Laere, S.J. and Van Craenenbroeck, A.H. (2018). MicroRNA profiling in plasma samples using qPCR arrays: Recommendations for correct analysis and interpretation Dettman, R. W. (ed.). *PLOS ONE* **13**(2):e0193173. doi: https://doi.org/10.1371/journal.pone.0193173.

Ghai, V., Wu, X., Bheda-Malge, A., Argyropoulos, C.P., Bernardo, J.F., Orchard, T., … Wang, K. (2018). Genome-wide Profiling of Urinary Extracellular Vesicle microRNAs Associated With Diabetic Nephropathy in Type 1 Diabetes. *Kidney International Reports* **3**(3):555–572. doi: https://doi.org/10.1016/j.ekir.2017.11.019.

Gharib, S.A., Pippin, J.W., Ohse, T., Pickering, S.G., Krofft, R.D. and Shankland, S.J.

(2014). Transcriptional Landscape of Glomerular Parietal Epithelial Cells James, L. R. (ed.). *PLoS ONE* **9**(8):e105289. doi: https://doi.org/10.1371/journal.pone.0105289.

Gómez-Chiarri, M., Hamilton, T.A., Egido, J. and Emancipator, S.N. (1993). Expression of IP-10, a lipopolysaccharide- and interferon-gamma-inducible protein, in murine mesangial cells in culture. *The American journal of pathology* **142**(2):433–9.

Gonzales, P.A., Pisitkun, T., Hoffert, J.D., Tchapyjnikov, D., Star, R.A., Kleta, R., … Knepper, M.A. (2009). Large-Scale Proteomics and Phosphoproteomics of Urinary Exosomes. *Journal of the American Society of Nephrology* **20**(2):363–379. doi: https://doi.org/10.1681/ASN.2008040406.

Gotlieb, A.I., Wong, M.K., Boden, P. and Fone, A.C. (1987). The role of the cytoskeleton in endothelial repair. *Scanning microscopy* **1**(4):1715–26.

Gould, D.B., Phalan, F.C., Van Mil, S.E., Sundberg, J.P., Vahedi, K., Massin, P., … John, S.W.M. (2006). Role of COL4A1 in small-vessel disease and hemorrhagic stroke. *New England Journal of Medicine* **354**(14):1489–1496. doi: https://doi.org/10.1056/NEJMoa053727.

Gracia, T., Wang, X., Su, Y., Norgett, E.E., Williams, T.L., Moreno, P., … Karet Frankl, F.E. (2017). Urinary Exosomes Contain MicroRNAs Capable of Paracrine Modulation of Tubular Transporters in Kidney. *Scientific Reports* **7**(1):40601. doi: https://doi.org/10.1038/srep40601.

Griffiths-Jones, S., Saini, H.K., Van Dongen, S. and Enright, A.J. (2008). miRBase: Tools for microRNA genomics. *Nucleic Acids Research* **36**(SUPPL. 1). doi: https://doi.org/10.1093/nar/gkm952.

Guan, F., Villegas, G., Teichman, J., Mundel, P. and Tufro, A. (2006). Autocrine VEGF-A system in podocytes regulates podocin and its interaction with CD2AP. *American Journal of Physiology-Renal Physiology* **291**(2):F422–F428. doi: https://doi.org/10.1152/ajprenal.00448.2005.

Ha, M. and Kim, V.N. (2014). Regulation of microRNA biogenesis. *Nature Reviews Molecular Cell Biology* **15**(8):509–524. doi: https://doi.org/10.1038/nrm3838.

Haas, M. (2009). Alport syndrome and thin glomerular basement membrane nephropathy: a practical approach to diagnosis. *Archives of pathology & laboratory medicine* **133**(2):224–32. doi: https://doi.org/10.1043/1543-2165-133.2.224.

Hamer, R., Molostvov, G., Lowe, D., Satchell, S., Mathieson, P., Ilyas, R., … Zehnder, D. (2012). Human leukocyte antigen-specific antibodies and gamma-interferon stimulate human microvascular and glomerular endothelial cells to produce complement factor C4. *Transplantation* **93**(9):867–873. doi: https://doi.org/10.1097/TP.0b013e31824b3762.

Hanke, M., Hoefig, K., Merz, H., Feller, A.C., Kausch, I., Jocham, D., … Sczakiel, G. (2010). A robust methodology to study urine microRNA as tumor marker: MicroRNA-126 and microRNA-182 are related to urinary bladder cancer. *Urologic Oncology: Seminars and Original Investigations* **28**(6):655–661. doi: https://doi.org/10.1016/j.urolonc.2009.01.027.

Haraldsson, B., Nyström, J. and Deen, W.M. (2008). Properties of the Glomerular Barrier and Mechanisms of Proteinuria. *Physiological Reviews* **88**(2):451–487. doi: https://doi.org/10.1152/physrev.00055.2006.

Hill, N., Michell, D.L., Ramirez-Solano, M., Sheng, Q., Pusey, C., Vickers, K.C. and Woollard, K.J. (2020). Glomerular endothelial derived vesicles mediate podocyte dysfunction: A potential role for miRNA Dussaule, J.-C. (ed.). *PLOS ONE* **15**(3):e0224852. doi: https://doi.org/10.1371/journal.pone.0224852.

Hong, Y., Cao, H., Wang, Q., Ye, J., Sui, L., Feng, J., … Chen, X. (2016). MiR-22 may Suppress Fibrogenesis by Targeting TGFβR i in Cardiac Fibroblasts. *Cellular Physiology and Biochemistry* **40**(6):1345–1353. doi: https://doi.org/10.1159/000453187.

Huang, W. (2017). MicroRNAs: Biomarkers, Diagnostics, and Therapeutics. *Methods in Molecular Biology*. Humana Press Inc., pp. 57–67.

Huang, Y., Liu, Y., Li, L., Su, B., Yang, L., Fan, W., … Liu, F. (2014). Involvement of inflammation-related miR-155 and miR-146a in diabetic nephropathy: implications for glomerular endothelial injury. *BMC nephrology* **15**(1):142. doi: https://doi.org/10.1186/1471-2369-15-142.

Jarad, G., Cunningham, J., Shaw, A.S. and Miner, J.H. (2006). Proteinuria precedes podocyte abnormalities inLamb2-/- mice, implicating the glomerular basement membrane as an albumin barrier. *Journal of Clinical Investigation* **116**(8):2272–2279. doi: https://doi.org/10.1172/JCI28414.

Jeansson, M. and Haraldsson, B. (2006). Morphological and functional evidence for an important role of the endothelial cell glycocalyx in the glomerular barrier. *American Journal of Physiology-Renal Physiology* **290**(1):F111–F116. doi: https://doi.org/10.1152/ajprenal.00173.2005.

Jha, V., Garcia-Garcia, G., Iseki, K., Li, Z., Naicker, S., Plattner, B., … Yang, C.-W. (2013). Chronic kidney disease: global dimension and perspectives. *The Lancet* **382**(9888):260–272. doi: https://doi.org/10.1016/S0140-6736(13)60687-X.

Jia, Y., Guan, M., Zheng, Z., Zhang, Q., Tang, C., Xu, W., … Xue, Y. (2016). miRNAs in Urine Extracellular Vesicles as Predictors of Early-Stage Diabetic Nephropathy. *Journal of Diabetes Research* **2016**:1–10. doi: https://doi.org/10.1155/2016/7932765.

Jing, J. and Gao, Y. (2018). Urine biomarkers in the early stages of diseases: Current status and perspective. *Discovery Medicine* **25**(136):57–65.

Kato, M., Arce, L., Wang, M., Putta, S., Lanting, L. and Natarajan, R. (2011). A microRNA circuit mediates transforming growth factor-β1 autoregulation in renal glomerular mesangial cells. *Kidney International* **80**(4):358–368. doi: https://doi.org/10.1038/ki.2011.43.

Kaur, H., Chien, A. and Jialal, I. (2012). Hyperglycemia induces toll like receptor 4 expression and activity in mouse mesangial cells: Relevance to diabetic nephropathy. *American Journal of Physiology - Renal Physiology* **303**(8). doi: https://doi.org/10.1152/ajprenal.00319.2012.

Keller, S., Rupp, C., Stoeck, A., Runz, S., Fogel, M., Lugert, S., … Altevogt, P. (2007). CD24 is a marker of exosomes secreted into urine and amniotic fluid. *Kidney International* **72**(9):1095–1102. doi: https://doi.org/10.1038/sj.ki.5002486.

Kitching, A.R. and Hutton, H.L. (2016). The Players: Cells Involved in Glomerular Disease. *Clinical Journal of the American Society of Nephrology : CJASN* **11**(9):1664. doi: https://doi.org/10.2215/CJN.13791215.

Klein, J.D., Blount, M.A. and Sands, J.M. (2011). Urea Transport in the Kidney. *Comprehensive Physiology*. Hoboken, NJ, USA: John Wiley & Sons, Inc., pp. 699–729.

Knepper, M.A. and Pisitkun, T. (2007). Exosomes in urine: Who would have thought…? *Kidney International* **72**(9):1043–1045. doi: https://doi.org/10.1038/sj.ki.5002510.

Kobrin, S.M. (1998). Diabetic nephropathy. *Disease-a-month : DM* **44**(5):214–34.

Kokudo, T., Suzuki, Y., Yoshimatsu, Y., Yamazaki, T., Watabe, T. and Miyazono, K. (2008). Snail is required for TGFβ-induced endothelial-mesenchymal transition of embryonic stem cell-derived endothelial cells. *Journal of Cell Science* **121**(20):3317–3324. doi: https://doi.org/10.1242/jcs.028282.

Korenková, V., Scott, J., Novosadová, V., Jindrichová, M., Langerová, L., Švec, D., … Sjöback, R. (2015). Pre-amplification in the context of high-throughput qPCR gene expression experiment. *BMC Molecular Biology* **16**(1):5. doi: https://doi.org/10.1186/s12867-015-0033-9.

Kosaka, N., Izumi, H., Sekine, K. and Ochiya, T. (2010). MicroRNA as a new immune-regulatory agent in breast milk. *Silence* **1**(1):7. doi: https://doi.org/10.1186/1758-907X-1-7.

Kume, S., Thomas, M.C. and Koya, D. (2012). Nutrient sensing, autophagy, and diabetic nephropathy. *Diabetes* **61**(1):23–29.

Kuppe, C., Leuchtle, K., Wagner, A., Kabgani, N., Saritas, T., Puelles, V.G., … Moeller,

M.J. (2019). Novel parietal epithelial cell subpopulations contribute to focal segmental glomerulosclerosis and glomerular tip lesions. *Kidney International* **96**(1):80–93. doi: https://doi.org/10.1016/J.KINT.2019.01.037.

Kuravi, S.J., McGettrick, H.M., Satchell, S.C., Saleem, M.A., Harper, L., Williams, J.M., … Savage, C.O.S. (2014). Podocytes Regulate Neutrophil Recruitment by Glomerular Endothelial Cells via IL-6–Mediated Crosstalk. *The Journal of Immunology* **193**(1):234–243. doi: https://doi.org/10.4049/jimmunol.1300229.

Kurihara, H. and Sakai, T. (2017). Cell biology of mesangial cells: the third cell that maintains the glomerular capillary. *Anatomical Science International* **92**(2):173–186. doi: https://doi.org/10.1007/s12565-016-0334-1.

Kusner, D.J., Luebbers, E.L., Nowinski, R.J., Konieczkowski, M., King, C.H. and Sedor, J.R. (1991). Cytokine- and LPS-induced synthesis of interleukin-8 from human mesangial cells. *Kidney International* **39**(6):1240–1248. doi: https://doi.org/10.1038/ki.1991.157.

Lagos-Quintana, M., Rauhut, R., Meyer, J., Borkhardt, A. and Tuschl, T. (2003). New microRNAs from mouse and human. *RNA* **9**(2):175–179. doi: https://doi.org/10.1261/rna.2146903.

Lai, F.M.M., Szeto, C.C., Choi, P.C.L., Ho, K.K.L., Tang, N.L.S., Chow, K.M., … To, K.F. (2004). Isolate diffuse thickening of glomerular capillary basement membrane: A renal lesion in prediabetes? *Modern Pathology* **17**(12):1506–1512. doi: https://doi.org/10.1038/modpathol.3800219.

Lapuz, M.H. (1997). Diabetic nephropathy. *The Medical clinics of North America* **81**(3):679–88. doi: https://doi.org/10.1016/s0025-7125(05)70539-3.

Lawrie, C.H. (2013). *MicroRNAs in Medicine*. Lawrie, C. H. (ed.). Hoboken, NJ, USA: John Wiley & Sons, Inc.

Lee, K.M., Choi, K.H. and Ouellette, M.M. (2004). Use of exogenous hTERT to immortalize primary human cells. *Cytotechnology* **45**(1–2):33. doi: https://doi.org/10.1007/10.1007/S10616-004-5123-3.

Lee, R.C. and Ambros, V. (2001). An extensive class of small RNAs in Caenorhabditis elegans. *Science* **294**(5543):862–864. doi: https://doi.org/10.1126/science.1065329.

Lee, R.C., Feinbaum, R.L. and Ambros, V. (1993). The C. elegans heterochronic gene lin-4 encodes small RNAs with antisense complementarity to lin-14. *Cell* **75**(5):843–854. doi: https://doi.org/10.1016/0092-8674(93)90529-Y.

Lee, T.-Y.J. and Gotlieb, A.I. (2003). Microfilaments and microtubules maintain endothelial integrity. *Microscopy research and technique* **60**(1):115–27. doi: https://doi.org/10.1002/jemt.10250.

Lee, W.-C., Li, L.-C., Ng, H.-Y., Lin, P.-T., Chiou, T.T.-Y., Kuo, W.-H. and Lee, C.-T. (2020). Urinary Exosomal MicroRNA Signatures in Nephrotic, Biopsy-Proven Diabetic Nephropathy. *Journal of Clinical Medicine* **9**(4):1220. doi: https://doi.org/10.3390/jcm9041220.

Levesque, M.J., Nerem, R.M. and Sprague, E.A. (1990). Vascular endottielial cell proliferation in culture and the influence of flow. *Biomaterials* **11**(9):702–707. doi: https://doi.org/10.1016/0142-9612(90)90031-K.

Li, J., Liu, B., Xue, H., Zhou, Q.Q. and Peng, L. (2017). MiR-217 Is a useful diagnostic biomarker and regulates human podocyte cells apoptosis via targeting tnfsf11 in membranous nephropathy. *BioMed Research International*. doi: https://doi.org/10.1155/2017/2168767.

Li, J., Qu, X. and Bertram, J.F. (2009). Endothelial-myofibroblast transition contributes to the early development of diabetic renal interstitial fibrosis in streptozotocin-induced diabetic mice. *American Journal of Pathology* **175**(4):1380–1388. doi: https://doi.org/10.2353/ajpath.2009.090096.

Li, M., Guo, Q., Cai, H., Wang, H., Ma, Z. and Zhang, X. (2020). miR-218 regulates diabetic nephropathy via targeting IKK-β and modulating NK-κB-mediated inflammation. *Journal of Cellular Physiology* **235**(4):3362–3371. doi: https://doi.org/10.1002/jcp.29224.

Li, X.X., Liu, Y.M., Li, Y.J., Xie, N., Yan, Y.F., Chi, Y.L., … Wang, P.Y. (2016). High glucose concentration induces endothelial cell proliferation by regulating cyclin-D2-related miR-98. *Journal of Cellular and Molecular Medicine* **20**(6):1159–1169. doi: https://doi.org/10.1111/jcmm.12765.

Liew, H., Roberts, M.A., MacGinley, R. and McMahon, L.P. (2017). Endothelial glycocalyx in health and kidney disease: Rising star or false Dawn? *Nephrology* **22**(12):940–946. doi: https://doi.org/10.1111/nep.13161.

Lin, J.S. and Susztak, K. (2016). Podocytes: the Weakest Link in Diabetic Kidney Disease? *Current Diabetes Reports* **16**(5):45–45.

Lin, Y.C., Chang, Y.H., Yang, S.Y., Wu, K.D. and Chu, T.S. (2018). Update of pathophysiology and management of diabetic kidney disease. *Journal of the Formosan Medical Association* **117**(8):662–675.

Liu, F., Guo, J., Qiao, Y., Pan, S., Duan, J., Liu, D. and Liu, Z. (2020). *Mir-138 Plays an Important Role in Diabetic Nephropathy through SIRT1-P38-TTP Regulatory Axis Authors' Information*.

Liu, F.Y., Li, X.Z., Peng, Y.M., Liu, H. and Liu, Y.H. (2008). Arkadia regulates TGF-β signaling during renal tubular epithelial to mesenchymal cell transition. *Kidney*

International **73**(5):588–594. doi: https://doi.org/10.1038/sj.ki.5002713.

Liu, R., Zhong, Y., Li, X., Chen, H., Jim, B., Zhou, M.M., … He, J.C. (2014). Role of transcription factor acetylation in diabetic kidney disease. *Diabetes* **63**(7):2440–2453. doi: https://doi.org/10.2337/db13-1810.

Lo, C.S., Shi, Y., Chenier, I., Ghosh, A., Wu, C.H., Cailhier, J.F., … Chan, J.S.D. (2017). Heterogeneous nuclear ribonucleoprotein F stimulates sirtuin-1 gene expression and attenuates nephropathy progression in diabetic mice. *Diabetes*. American Diabetes Association Inc., pp. 1964–1978.

Long, J., Wang, Y., Wang, W., Chang, B.H.J. and Danesh, F.R. (2011). MicroRNA-29c is a signature microRNA under high glucose conditions that targets Sprouty homolog 1, and its *in vivo* knockdown prevents progression of diabetic nephropathy. *Journal of Biological Chemistry* **286**(13):11837–11848. doi: https://doi.org/10.1074/jbc.M110.194969.

Lu, L., Li, J., Moussaoui, M. and Boix, E. (2018). Immune Modulation by Human Secreted RNases at the Extracellular Space. *Frontiers in Immunology* **9**:1012. doi: https://doi.org/10.3389/fimmu.2018.01012.

Lynch, J., Fay, J., Meehan, M., Bryan, K., Watters, K.M., Murphy, D.M. and Stallings, R.L. (2012). MiRNA-335 suppresses neuroblastoma cell invasiveness by direct targeting of multiple genes from the non-canonical TGF-β signalling pathway. *Carcinogenesis*. doi: https://doi.org/10.1093/carcin/bgs114.

MacFarlane, L.-A. and R. Murphy, P. (2010). MicroRNA: Biogenesis, Function and Role in Cancer. *Current Genomics* **11**(7):537–561. doi: https://doi.org/10.2174/138920210793175895.

MacIsaac, R.J. and Jerums, G. (2011). Diabetic kidney disease with and without albuminuria. *Current Opinion in Nephrology and Hypertension* **20**(3):246–257.

Maezawa, Y., Takemoto, M. and Yokote, K. (2015). Cell biology of diabetic nephropathy: Roles of endothelial cells, tubulointerstitial cells and podocytes. *Journal of Diabetes Investigation* **6**(1):3–15. doi: https://doi.org/10.1111/jdi.12255.

Maezawa, Y. and Yokote, K. (2019). Human glomerular transcriptome of diabetic kidneys: Can the podocyte cytoskeleton be a therapeutic target? *Journal of Diabetes Investigation* **10**(2):224–226.

Makarova, J.A., Shkurnikov, M.U., Wicklein, D., Lange, T., Samatov, T.R., Turchinovich, A.A. and Tonevitsky, A.G. (2016). Intracellular and extracellular microRNA: An update on localization and biological role. *Progress in Histochemistry and Cytochemistry* **51**(3–4):33–49.

Marsden, P.A., Dorfman, D.M., Collins, T., Brenner, B.M., Orkin, S.H. and Ballermann,

B.J. (1991). Regulated expression of endothelin 1 in glomerular capillary endothelial cells. *The American journal of physiology* **261**(1 Pt 2):F117-25. doi: https://doi.org/10.1152/ajprenal.1991.261.1.F117.

Marshall, C.B. (2016). Rethinking glomerular basement membrane thickening in diabetic nephropathy: adaptive or pathogenic? *American journal of physiology. Renal physiology* **311**(5):F831–F843. doi: https://doi.org/10.1152/ajprenal.00313.2016.

Mason, R.M. and Wahab, N.A. (2003). Extracellular matrix metabolism in diabetic nephropathy. *Journal of the American Society of Nephrology* **14**(5):1358–1373.

Matboli, M., Eissa, S., Ibrahim, D., Hegazy, M.G.A., Imam, S.S. and Habib, E.K. (2017). Caffeic Acid Attenuates Diabetic Kidney Disease via Modulation of Autophagy in a High-Fat Diet/Streptozotocin- Induced Diabetic Rat. *Scientific Reports* **7**(1). doi: https://doi.org/10.1038/s41598-017-02320-z.

Mauer, M., Zinman, B., Gardiner, R., Suissa, S., Sinaiko, A., Strand, T., … Klein, R. (2009). Renal and retinal effects of enalapril and losartan in type 1 diabetes. *New England Journal of Medicine* **361**(1):40–51. doi: https://doi.org/10.1056/NEJMoa0808400.

Mauer, S.M., Steffes, M.W., Ellis, E.N., Sutherland, D.E., Brown, D.M. and Goetz, F.C. (1984). Structural-functional relationships in diabetic nephropathy. *Journal of Clinical Investigation* **74**(4):1143–1155. doi: https://doi.org/10.1172/JCI111523.

Mauer, S.M., Sutherland, D.E.R. and Steffes, M.W. (1992). Relationship of systemic blood pressure to nephropathology in insulin-dependent diabetes mellitus. *Kidney International* **41**(4):736–740. doi: https://doi.org/10.1038/ki.1992.115.

Mccarthy, E.T., Sharma, R., Sharma, M., Li, J.Z., Ge, X.L., Dileepan, K.N. and Savin, V.J. (1998). TNF-α increases albumin permeability of isolated rat glomeruli through the generation of superoxide. *Journal of the American Society of Nephrology* **9**(3):433–438.

McCormick, J.A. and Ellison, D.H. (2014). Distal Convoluted Tubule. *Comprehensive Physiology*. Hoboken, NJ, USA: John Wiley & Sons, Inc., pp. 45–98.

Meng, X.M. (2019). Inflammatory Mediators and Renal Fibrosis. *Advances in Experimental Medicine and Biology*. Springer New York LLC, pp. 381–406.

Meyer-Schwesinger, C. (2019). The ubiquitin–proteasome system in kidney physiology and disease. *Nature Reviews Nephrology* **15**(7):393–411.

Miesen, L., Steenbergen, E. and Smeets, B. (2017). Parietal cells-new perspectives in glomerular disease. *Cell and tissue research* **369**(1):237–244. doi: https://doi.org/10.1007/s00441-017-2600-5.

Miner, J.H. (2012). The glomerular basement membrane. *Experimental Cell Research*

318(9):973–978. doi: https://doi.org/10.1016/j.yexcr.2012.02.031.

Mitchell, P.S., Parkin, R.K., Kroh, E.M., Fritz, B.R., Wyman, S.K., Pogosova-Agadjanyan, E.L., … Tewari, M. (2008). Circulating microRNAs as stable blood-based markers for cancer detection. *Proceedings of the National Academy of Sciences of the United States of America* **105**(30):10513–10518. doi: https://doi.org/10.1073/pnas.0804549105.

Mlcochova, H., Hezova, R., Meli, A.C. and Slaby, O. (2015). Urinary microRNAs as a new class of noninvasive biomarkers in oncology, nephrology, and cardiology. *Methods in molecular biology (Clifton, N.J.)* **1218**:439–463.

Montecalvo, A., Larregina, A.T., Shufesky, W.J., Beer Stolz, D., Sullivan, M.L.G., Karlsson, J.M., … Morelli, A.E. (2012). Mechanism of transfer of functional microRNAs between mouse dendritic cells via exosomes. *Blood* **119**(3):756–766. doi: https://doi.org/10.1182/blood-2011-02-338004.

Monteys, A.M., Spengler, R.M., Wan, J., Tecedor, L., Lennox, K.A., Xing, Y. and Davidson, B.L. (2010). Structure and activity of putative intronic miRNA promoters. *RNA* **16**(3):495–505. doi: https://doi.org/10.1261/rna.1731910.

Moran, Y., Agron, M., Praher, D. and Technau, U. (2017). The evolutionary origin of plant and animal microRNAs. *Nature Ecology and Evolution* **1**(3):27.

Morishita, Y., Imai, T., Yoshizawa, H., Watanabe, M., Ishibashi, K., Muto, S. and Nagata, D. (2015). Delivery of microRNA-146a with polyethylenimine nanoparticles inhibits renal fibrosis *in vivo*. *International Journal of Nanomedicine* **10**:3475–3488. doi: https://doi.org/10.2147/IJN.S82587.

Mu, J., Pang, Q., Guo, Y.H., Chen, J.G., Zeng, W., Huang, Y.J., … Feng, B. (2013). Functional Implications of MicroRNA-215 in TGF-β1-Induced Phenotypic Transition of Mesangial Cells by Targeting CTNNBIP1. *PLoS ONE* **8**(3). doi: https://doi.org/10.1371/journal.pone.0058622.

Mulcahy, L.A., Pink, R.C. and Carter, D.R.F. (2014). Routes and mechanisms of extracellular vesicle uptake. *Journal of Extracellular Vesicles* **3**(1):24641. doi: https://doi.org/10.3402/jev.v3.24641.

Najafian, B., Alpers, C.E. and Fogo, A.B. (2011). Pathology of human diabetic nephropathy. *Contributions to Nephrology* **170**:36–47. doi: https://doi.org/10.1159/000324942.

Najafian, B. and Mauer, M. (2009). Progression of diabetic nephropathy in type 1 diabetic patients. *Diabetes Research and Clinical Practice* **83**(1):1–8.

Nascimento, L.R. do and Domingueti, C.P. (2019). MicroRNAs: new biomarkers and promising therapeutic targets for diabetic kidney disease. *Jornal brasileiro de nefrologia :*

'orgao oficial de Sociedades Brasileira e Latino-Americana de Nefrologia **41**(3):412–422.

Nathan, D.M., Bayless, M., Cleary, P., Genuth, S., Gubitosi-Klug, R., Lachin, J.M., … Zinman, B. (2013). Diabetes control and complications trial/epidemiology of diabetes interventions and complications study at 30 years: Advances and contributions. *Diabetes* **62**(12):3976–3986.

Nosadini, R., Velussi, M., Brocco, E., Bruseghin, M., Abaterusso, C., Saller, A., … Fioretto, P. (2000). Course of renal function in type 2 diabetic patients with abnormalities of albumin excretion rate. *Diabetes* **49**(3):476–484. doi: https://doi.org/10.2337/diabetes.49.3.476.

O'Brien, J., Hayder, H., Zayed, Y. and Peng, C. (2018). Overview of microRNA biogenesis, mechanisms of actions, and circulation. *Frontiers in Endocrinology* **9**(AUG).

O'Hare, M.J., Bond, J., Clarke, C., Takeuchi, Y., Atherton, A.J., Berry, C., … Jat, P.S. (2001). Conditional immortalization of freshly isolated human mammary fibroblasts and endothelial cells. *Proceedings of the National Academy of Sciences of the United States of America* **98**(2):646–651. doi: https://doi.org/10.1073/pnas.98.2.646.

Odden, M.C., Shlipak, M.G. and Tager, I.B. (2009). Serum creatinine and functional limitation in elderly persons. *Journals of Gerontology - Series A Biological Sciences and Medical Sciences*. doi: https://doi.org/10.1093/gerona/gln037.

Ohse, T., Pippin, J.W., Chang, A.M., Krofft, R.D., Miner, J.H., Vaughan, M.R. and Shankland, S.J. (2009). The enigmatic parietal epithelial cell is finally getting noticed: a review. *Kidney international* **76**(12):1225–38. doi: https://doi.org/10.1038/ki.2009.386.

Okino, S.T., Kong, M., Sarras, H. and Wang, Y. (2016). Evaluation of bias associated with high-multiplex, target-specific pre-amplification. *Biomolecular Detection and Quantification* **6**:13–21. doi: https://doi.org/10.1016/j.bdq.2015.12.001.

Ostendorf, T., Boor, P., Van Roeyen, C.R.C. and Floege, J. (2014). Platelet-derived growth factors (PDGFs) in glomerular and tubulointerstitial fibrosis. *Kidney International Supplements* **4**(1):65–69.

Osterby, R. (1974). Early phases in the development of diabetic glomerulopathy. *Acta medica Scandinavica*.

Pagtalunan, M.E., Miller, P.L., Jumping-Eagle, S., Nelson, R.G., Myers, B.D., Rennke, H.G., … Meyer, T.W. (1997). Podocyte loss and progressive glomerular injury in type II diabetes. *The Journal of clinical investigation* **99**(2):342–8. doi: https://doi.org/10.1172/JCI119163.

Pandit, K. V., Corcoran, D., Yousef, H., Yarlagadda, M., Tzouvelekis, A., Gibson, K.F., … Kaminski, N. (2010). Inhibition and role of let-7d in idiopathic pulmonary fibrosis. *American*

Journal of Respiratory and Critical Care Medicine **182**(2):220–229. doi: https://doi.org/10.1164/rccm.200911-1698OC.

Pavenstädt, H., Kriz, W. and Kretzler, M. (2003). Cell Biology of the Glomerular Podocyte. *Physiological Reviews* **83**(1):253–307. doi: https://doi.org/10.1152/physrev.00020.2002.

Pisitkun, T., Shen, R.-F. and Knepper, M.A. (2004). Identification and proteomic profiling of exosomes in human urine. *Proceedings of the National Academy of Sciences* **101**(36):13368–13373. doi: https://doi.org/10.1073/pnas.0403453101.

Plaisier, E., Gribouval, O., Alamowitch, S., Mougenot, B., Prost, C., Verpont, M.C., … Ronco, P. (2007). COL4A1 mutations and hereditary angiopathy, nephropathy, aneurysms, and muscle cramps. *New England Journal of Medicine* **357**(26):2687–2695. doi: https://doi.org/10.1056/NEJMoa071906.

Pollak, M.R., Quaggin, S.E., Hoenig, M.P. and Dworkin, L.D. (2014). The glomerulus: the sphere of influence. *Clinical journal of the American Society of Nephrology : CJASN* **9**(8):1461–9. doi: https://doi.org/10.2215/CJN.09400913.

Polonsky, K.S. (2012). The Past 200 Years in Diabetes. *New England Journal of Medicine* **367**(14):1332–1340. doi: https://doi.org/10.1056/NEJMra1110560.

Pomatto, M.A.C., Gai, C., Bussolati, B. and Camussi, G. (2017). Extracellular vesicles in renal pathophysiology. *Frontiers in Molecular Biosciences* **4**(JUN).

Portero-Otín, M., Pamplona, R., Ruiz, M.C., Cabiscol, E., Prat, J. and Bellmunt, M.J. (1999). Diabetes induces an impairment in the proteolytic activity against oxidized proteins and a heterogeneous effect in nonenzymatic protein modifications in the cytosol of rat liver and kidney. *Diabetes* **48**(11):2215–2220. doi: https://doi.org/10.2337/diabetes.48.11.2215.

Pourghasem, M., Shafi, H. and Babazadeh, Z. (2015). Histological changes of kidney in diabetic nephropath. *Caspian Journal of Internal Medicine* **6**(3):120–127.

Pries, A.R., Secomb, T.W. and Gaehtgens, P. (2000). The endothelial surface layer. *Pflügers Archiv - European Journal of Physiology* **440**(5):653–666. doi: https://doi.org/10.1007/s004240000307.

Prud'homme, G.J., Glinka, Y., Lichner, Z. and Yousef, G.M. (2016). Neuropilin-1 is a receptor for extracellular miRNA and AGO2/miRNA complexes and mediates the internalization of miRNAs that modulate cell function. *Oncotarget* **7**(42):68057–68071. doi: https://doi.org/10.18632/ONCOTARGET.10929.

Ramnath, R., Foster, R.R., Qiu, Y., Cope, G., Butler, M.J., Salmon, A.H., … Satchell, S.C. (2014). Matrix metalloproteinase 9-mediated shedding of syndecan 4 in response to tumor necrosis factor α: A contributor to endothelial cell glycocalyx dysfunction. *FASEB Journal* **28**(11):4686–4699. doi: https://doi.org/10.1096/fj.14-252221.

Raudvere, U., Kolberg, L., Kuzmin, I., Arak, T., Adler, P., Peterson, H. and Vilo, J. (2019). G:Profiler: A web server for functional enrichment analysis and conversions of gene lists (2019 update). *Nucleic Acids Research* **47**(W1):W191–W198. doi: https://doi.org/10.1093/nar/gkz369.

Reeves, W.B., Winters, C.J. and Andreoli, T.E. (2001). Chloride Channels in the Loop of Henle. *Annual Review of Physiology* **63**(1):631–645. doi: https://doi.org/10.1146/annurev.physiol.63.1.631.

Reidy, K., Kang, H.M., Hostetter, T. and Susztak, K. (2014). Molecular mechanisms of Diabetic kidney disease. *Journal of Clinical Investigation* **124**(6):2333–2340.

Reine, T.M., Lanzalaco, F., Kristiansen, O., Enget, A.R., Satchell, S., Jenssen, T.G. and Kolset, S.O. (2019). Matrix metalloproteinase-9 mediated shedding of syndecan-4 in glomerular endothelial cells. *Microcirculation* **26**(4). doi: https://doi.org/10.1111/micc.12534.

Reitsma, S., Slaaf, D.W., Vink, H., van Zandvoort, M.A.M.J. and oude Egbrink, M.G.A. (2007). The endothelial glycocalyx: composition, functions, and visualization. *Pflugers Archiv : European journal of physiology* **454**(3):345–59. doi: https://doi.org/10.1007/s00424-007-0212-8.

Rice, W.L., Van Hoek, A.N., Păunescu, T.G., Huynh, C., Goetze, B., Singh, B., … Brown, D. (2013). High Resolution Helium Ion Scanning Microscopy of the Rat Kidney Sands, J. M. (ed.). *PLoS ONE* **8**(3):e57051. doi: https://doi.org/10.1371/journal.pone.0057051.

Roberts, J.T. and Borchert, G.M. (2017). Computational prediction of microRNA target genes, target prediction databases, and web resources. *Methods in Molecular Biology* **1617**:109–122. doi: https://doi.org/10.1007/978-1-4939-7046-9_8.

Rodriguez, A., Griffiths-Jones, S., Ashurst, J.L. and Bradley, A. (2004). Identification of mammalian microRNA host genes and transcription units. *Genome Research* **14**(10 A):1902–1910. doi: https://doi.org/10.1101/gr.2722704.

Rodriguez, J.A., Orbe, J., De Lizarrondo, S.M., Calvayrac, O., Rodriguez, C., Martinez-Gonzalez, J. and Paramo, J.A. (2008). Metalloproteinases and atherothrombosis: MMP-10 mediates vascular remodeling promoted by inflammatory stimuli. *Frontiers in Bioscience* **13**(8):2916–2921.

De Ronde, M.W.J., Ruijter, J.M., Lanfear, D., Bayes-Genis, A., Kok, M.G.M., Creemers, E.E., … Pinto-Sietsma, S.J. (2017). Practical data handling pipeline improves performance of qPCR-based circulating miRNA measurements. *RNA* **23**(5):811–821. doi: https://doi.org/10.1261/rna.059063.116.

Ryan, M.J., Johnson, G., Kirk, J., Fuerstenberg, S.M., Zager, R.A. and Torok-Storb, B.

(1994). HK-2: An immortalized proximal tubule epithelial cell line from normal adult human kidney. *Kidney International* **45**(1):48–57. doi: https://doi.org/10.1038/ki.1994.6.

Saleem, M.A. (2015). One hundred ways to kill a podocyte: FIGURE 1: *Nephrology Dialysis Transplantation* **30**(8):1266–1271. doi: https://doi.org/10.1093/ndt/gfu363.

Saleem, M.A., O'Hare, M.J., Reiser, J., Coward, R.J., Inward, C.D., Farren, T., … Mundel, P. (2002). A conditionally immortalized human podocyte cell line demonstrating nephrin and podocin expression. *Journal of the American Society of Nephrology* **13**(3):630–638.

Salem, A.M., Ragheb, A.S., Hegazy, M.G.A., Matboli, M. and Eissa, S. (2018). Caffeic Acid Modulates miR-636 Expression in Diabetic Nephropathy Rats. *Indian Journal of Clinical Biochemistry*:1–8. doi: https://doi.org/10.1007/s12291-018-0743-0.

Salih, V., Knowles, J.C., O'Hare, M.J. and Olsen, I. (2001). Retroviral transduction of alveolar bone cells with a temperature-sensitive SV40 large T antigen. *Cell and Tissue Research* **304**(3):371–376. doi: https://doi.org/10.1007/s004410100391.

Sampaio, F.J. (2000). Renal anatomy. Endourologic considerations. *The Urologic clinics of North America* **27**(4):585–607, vii.

Sanz-Rubio, D., Martin-Burriel, I., Gil, A., Cubero, P., Forner, M., Khalyfa, A. and Marin, J.M. (2018). Stability of Circulating Exosomal miRNAs in Healthy Subjects article. *Scientific Reports* **8**(1). doi: https://doi.org/10.1038/s41598-018-28748-5.

Satchell, S.C. and Braet, F. (2009). Glomerular endothelial cell fenestrations: an integral component of the glomerular filtration barrier. *American journal of physiology. Renal physiology* **296**(5):F947-56. doi: https://doi.org/10.1152/ajprenal.90601.2008.

Satchell, S.C., Tasman, C.H., Singh, A., Ni, L., Geelen, J., Von Ruhland, C.J., … Mathieson, P.W. (2006). Conditionally immortalized human glomerular endothelial cells expressing fenestrations in response to VEGF. *Kidney International* **69**(9):1633–1640. doi: https://doi.org/10.1038/sj.ki.5000277.

Scherbaum, W.A. (2009). The role of amylin in the physiology of glycemic control. *Experimental and Clinical Endocrinology & Diabetes* **106**(02):97–102. doi: https://doi.org/10.1055/s-0029-1211958.

Schrijvers, B.F., De Vriese, A.S. and Flyvbjerg, A. (2004). From hyperglycemia to diabetic kidney disease: The role of metabolic, hemodynamic, intracellular factors and growth factors/cytokines. *Endocrine Reviews* **25**(6):971–1010.

Sengoelge, G., Luo, W., Fine, D., Perschl, A.M., Fierlbeck, W., Haririan, A., … Ballermann, B.J. (2005). A SAGE-based comparison between glomerular and aortic endothelial cells. *American Journal of Physiology-Renal Physiology* **288**(6):F1290–F1300. doi: https://doi.org/10.1152/ajprenal.00076.2004.

Sengoelge, G., Winnicki, W., Kupczok, A., von Haeseler, A., Schuster, M., Pfaller, W., … Sunder-Plassmann, G. (2014). A SAGE based approach to human glomerular endothelium: Defining the transcriptome, finding a novel molecule and highlighting endothelial diversity. *BMC Genomics* **15**(1):725. doi: https://doi.org/10.1186/1471-2164-15-725.

Shao, Y., Ren, H., Lv, C., Ma, X., Wu, C. and Wang, Q. (2017). Changes of serum Mir-217 and the correlation with the severity in type 2 diabetes patients with different stages of diabetic kidney disease. *Endocrine* **55**(1):130–138. doi: https://doi.org/10.1007/s12020-016-1069-4.

Sharma, V., Antonacopoulou, A.G., Tanaka, S., Panoutsopoulos, A.A., Bravou, V., Kalofonos, H.P. and Episkopou, V. (2011). Enhancement of TGF-β signaling responses by the E3 ubiquitin ligase Arkadia provides tumor suppression in colorectal cancer. *Cancer Research* **71**(20):6438–6449. doi: https://doi.org/10.1158/0008-5472.CAN-11-1645.

Singh, A., Fridén, V., Dasgupta, I., Foster, R.R., Welsh, G.I., Tooke, J.E., … Satchell, S.C. (2011). High glucose causes dysfunction of the human glomerular endothelial glycocalyx. *American journal of physiology. Renal physiology* **300**(1):F40-8. doi: https://doi.org/10.1152/ajprenal.00103.2010.

Singh, L., Singh, G. and Dinda, A.K. (2015). Understanding podocytopathy and its relevance to clinical nephrology. *Indian journal of nephrology* **25**(1):1–7. doi: https://doi.org/10.4103/0971-4065.134531.

Singh, P. and Thomson, S.C. (2010). Renal homeostasis and tubuloglomerular feedback. *Current Opinion in Nephrology and Hypertension* **19**(1):59–64. doi: https://doi.org/10.1097/MNH.0b013e3283331ffd.

Singhal, P.C., Scharschmidt, L.A., Gibbons, N. and Hays, R.M. (1986). Contraction and relaxation of cultured mesangial cells on a silicone rubber surface. *Kidney International* **30**(6):862–873. doi: https://doi.org/10.1038/KI.1986.266.

Sison, K., Eremina, V., Baelde, H., Min, W., Hirashima, M., Fantus, I.G. and Quaggin, S.E. (2010). Glomerular Structure and Function Require Paracrine, Not Autocrine, VEGF–VEGFR-2 Signaling. *Journal of the American Society of Nephrology* **21**(10):1691–1701. doi: https://doi.org/10.1681/ASN.2010030295.

Sochett, E.B., Cherney, D.Z.I., Curtis, J.R., Dekker, M.G., Scholey, J.W. and Miller, J.A. (2006). Impact of renin angiotensin system modulation on the hyperfiltration state in type 1 diabetes. *Journal of the American Society of Nephrology* **17**(6):1703–1709. doi: https://doi.org/10.1681/ASN.2005080872.

Soler, A.P., Mullin, J.M., Knudsen, K.A. and Marano, C.W. (1996). Tissue remodeling

during tumor necrosis factor-induced apoptosis in LLC-PK1 renal epithelial cells. *American Journal of Physiology* **270**(5 PART 2). doi: https://doi.org/10.1152/ajprenal.1996.270.5.f869.

Soulis, T., Thallas, V., Youssef, S., Gilbert, R.E., McWilliam, B.G., Murray-McIntosh, R.P. and Cooper, M.E. (1997). Advanced glycation end products and their receptors co-localise in rat organs susceptible to diabetic microvascular injury. *Diabetologia* **40**(6):619–628. doi: https://doi.org/10.1007/s001250050725.

Striker, L.J. and Striker, G.E. (1996). Administration of AGEs *in vivo* induces extracellular matrix gene expression. *Nephrology, dialysis, transplantation : official publication of the European Dialysis and Transplant Association - European Renal Association* **11 Suppl 5**:62–5. doi: https://doi.org/10.1093/ndt/11.supp5.62.

Su, W., Cao, R., He, Y.C., Guan, Y.F. and Ruan, X.Z. (2017). Crosstalk of Hyperglycemia and Dyslipidemia in Diabetic Kidney Disease. *Kidney Diseases* **3**(4):171–180. doi: https://doi.org/10.1159/000479874.

Subramanya, A.R. and Ellison, D.H. (2014). Distal convoluted tubule. *Clinical journal of the American Society of Nephrology : CJASN* **9**(12):2147–63. doi: https://doi.org/10.2215/CJN.05920613.

Sun, L. and Chen, Z.J. (2004). The novel functions of ubiquitination in signaling. *Current Opinion in Cell Biology* **16**(2):119–126.

Supek, F., Bošnjak, M., Škunca, N. and Šmuc, T. (2011). REVIGO summarizes and visualizes long lists of gene ontology terms. *PLoS ONE* **6**(7). doi: https://doi.org/10.1371/journal.pone.0021800.

Szklarczyk, D., Gable, A.L., Lyon, D., Junge, A., Wyder, S., Huerta-Cepas, J., … Von Mering, C. (2019). STRING v11: Protein-protein association networks with increased coverage, supporting functional discovery in genome-wide experimental datasets. *Nucleic Acids Research*. doi: https://doi.org/10.1093/nar/gky1131.

Tati, R., Kristoffersson, A.-C., Ståhl, A., Mörgelin, M., Motto, D., Satchell, S., … Karpman, D. (2011). Phenotypic Expression of ADAMTS13 in Glomerular Endothelial Cells Câmara, N. O. S. (ed.). *PLoS ONE* **6**(6):e21587. doi: https://doi.org/10.1371/journal.pone.0021587.

Tervaert, T.W.C., Mooyaart, A.L., Amann, K., Cohen, A.H., TerenceCook, H., Drachenberg, C.B., … Bruijn, J.A. (2010). Pathologic classification of diabetic nephropathy. *Journal of the American Society of Nephrology* **21**(4):556–563.

The Human Protein Atlas *Downloadable Data - The Human Protein Atlas*. Available at: https://www.proteinatlas.org/about/download [Accessed: 8 March 2020].

The UK Prospective Diabetes Study (1998). Intensive blood-glucose control with

sulphonylureas or insulin compared with conventional treatment and risk of complications in patients with type 2 diabetes (UKPDS 33). UK Prospective Diabetes Study (UKPDS) Group. *Lancet* **352**(9131):837–853. doi: https://doi.org/10.1249/MSS.0b013e3181801d40.

Thomas, M., Fraser, D. and Bowen, T. (2018). Biogenesis, Stabilization, and Transport of microRNAs in Kidney Health and Disease. *Non-Coding RNA* **4**(4):30. doi: https://doi.org/10.3390/ncrna4040030.

Thul, P.J. and Lindskog, C. (2018). The human protein atlas: A spatial map of the human proteome. *Protein Science* **27**(1):233–244. doi: https://doi.org/10.1002/pro.3307.

Thurston, G., Rudge, J.S., Ioffe, E., Zhou, H., Ross, L., Croll, S.D., … Yancopoulos, G.D. (2000). Angiopoietin-1 protects the adult vasculature against plasma leakage. *Nature Medicine* **6**(4):460–463. doi: https://doi.org/10.1038/74725.

Tokar, T., Pastrello, C., Rossos, A.E.M., Abovsky, M., Hauschild, A.C., Tsay, M., … Jurisica, I. (2018). MirDIP 4.1 - Integrative database of human microRNA target predictions. *Nucleic Acids Research* **46**(D1):D360–D370. doi: https://doi.org/10.1093/nar/gkx1144.

Tonneijck, L., Muskiet, M.H.A., Smits, M.M., Van Bommel, E.J., Heerspink, H.J.L., Van Raalte, D.H. and Joles, J.A. (2017). Glomerular hyperfiltration in diabetes: Mechanisms, clinical significance, and treatment. *Journal of the American Society of Nephrology* **28**(4):1023–1039.

Topley, N., Floege, J., Wessel, K., Hass, R., Radeke, H.H., Kaever, V. and Resch, K. (1989). Prostaglandin E2 production is synergistically increased in cultured human glomerular mesangial cells by combinations of IL-1 and tumor necrosis factor-alpha 1. *The Journal of Immunology* **143**(6):1989–1995.

Tossidou, I., Starker, G., Krüger, J., Meier, M., Leitges, M., Haller, H. and Schiffer, M. (2009). PKC-alpha modulates TGF-β signaling and impairs podocyte survival. *Cellular Physiology and Biochemistry* **24**(5–6):627–634. doi: https://doi.org/10.1159/000257518.

Toyoda, M., Najafian, B., Kim, Y., Caramori, M.L. and Mauer, M. (2007). Podocyte detachment and reduced glomerular capillary endothelial fenestration in human type 1 diabetic nephropathy. *Diabetes* **56**(8):2155–2160. doi: https://doi.org/10.2337/db07-0019.

Trionfini, P., Benigni, A. and Remuzzi, G. (2015). MicroRNAs in kidney physiology and disease. *Nature Reviews Nephrology* **11**(1):23–33. doi: https://doi.org/10.1038/nrneph.2014.202.

Trushin, S.A., Pennington, K.N., Carmona, E.M., Asin, S., Savoy, D.N., Billadeau, D.D. and Paya, C. V. (2003). Protein Kinase Cα (PKCα) Acts Upstream of PKCθ To Activate IκB Kinase and NF-κB in T Lymphocytes. *Molecular and Cellular Biology* **23**(19):7068–

7081. doi: https://doi.org/10.1128/mcb.23.19.7068-7081.2003.

Turchinovich, A., Tonevitsky, A.G. and Burwinkel, B. (2016). Extracellular miRNA: A Collision of Two Paradigms. *Trends in Biochemical Sciences* **41**(10):883–892. doi: https://doi.org/10.1016/j.tibs.2016.08.004.

Tuttle, K.R. (2017). Back to the future: Glomerular hyperfiltration and the diabetic kidney. *Diabetes* **66**(1):14–16.

Valadi, H., Ekström, K., Bossios, A., Sjöstrand, M., Lee, J.J. and Lötvall, J.O. (2007). Exosome-mediated transfer of mRNAs and microRNAs is a novel mechanism of genetic exchange between cells. *Nature Cell Biology* **9**(6):654–659. doi: https://doi.org/10.1038/ncb1596.

Vandesompele, J., De Preter, K., Pattyn, F., Poppe, B., Van Roy, N., De Paepe, A., … Anderson, D.G. (2008). Examination of real-time polymerase chain reaction methods for the detection and quantification of modified siRNA. *Analytical biochemistry* **3**(6):e4. doi: https://doi.org/10.1016/j.molcel.2011.02.008.

Vasudevan, S. (2012). Posttranscriptional Upregulation by MicroRNAs. *Wiley Interdisciplinary Reviews: RNA* **3**(3):311–330.

Velez, J.C.Q. (2009). The importance of the intrarenal renin-angiotensin system. *Nature Clinical Practice Nephrology* **5**(2):89–100.

Veron, D., Reidy, K.J., Bertuccio, C., Teichman, J., Villegas, G., Jimenez, J., … Tufro, A. (2010). Overexpression of VEGF-A in podocytes of adult mice causes glomerular disease. *Kidney International* **77**(11):989–999. doi: https://doi.org/10.1038/ki.2010.64.

Vickers, K.C., Palmisano, B.T., Shoucri, B.M., Shamburek, R.D. and Remaley, A.T. (2011). MicroRNAs are transported in plasma and delivered to recipient cells by high-density lipoproteins. *Nature Cell Biology* **13**(4):423–435. doi: https://doi.org/10.1038/ncb2210.

Vlassara, H., Fuh, H., Makita, Z., Krungkrai, S., Cerami, A. and Bucala, R. (1992). Exogenous advanced glycosylation end products induce complex vascular dysfunction in normal animals: A model for diabetic and aging complications. *Proceedings of the National Academy of Sciences of the United States of America* **89**(24):12043–12047. doi: https://doi.org/10.1073/pnas.89.24.12043.

Wagner, J., Riwanto, M., Besler, C., Knau, A., Fichtlscherer, S., Röxe, T., … Dimmeler, S. (2013). Characterization of levels and cellular transfer of circulating lipoprotein-bound microRNAs. *Arteriosclerosis, Thrombosis, and Vascular Biology* **33**(6):1392–1400. doi: https://doi.org/10.1161/ATVBAHA.112.300741.

Wang, B., Herman-Edelstein, M., Koh, P., Burns, W., Jandeleit-Dahm, K., Watson, A., …

Cooper, M.E. (2010). E-cadherin expression is regulated by miR-192/215 by a mechanism that is independent of the profibrotic effects of transforming growth factor-β. *Diabetes* **59**(7):1794–1802.

Wang, B., Jha, J.C., Hagiwara, S., Mcclelland, A.D., Jandeleit-Dahm, K., Thomas, M.C., … Kantharidis, P. (2014). Transforming growth factor-β1-mediated renal fibrosis is dependent on the regulation of transforming growth factor receptor 1 expression by let-7b. *Kidney International* **85**(2):352–361. doi: https://doi.org/10.1038/ki.2013.372.

Wang, C., Yang, Cuihua, Chen, X., Yao, B., Yang, Chen, Zhu, C., … Zhang, C. (2011). Altered profile of seminal plasma microRNAs in the molecular diagnosis of male infertility. *Clinical Chemistry* **57**(12):1722–1731. doi: https://doi.org/10.1373/clinchem.2011.169714.

Wang, D. and Sun, W. (2014). Urinary extracellular microvesicles: Isolation methods and prospects for urinary proteome. *Proteomics* **14**(16):1922–1932.

Wang, J., Chen, J. and Sen, S. (2016). MicroRNA as Biomarkers and Diagnostics. *Journal of Cellular Physiology* **231**(1):25–30.

Wang, J., Zhong, J., Yang, H.-C. and Fogo, A.B. (2018). Cross Talk from Tubules to Glomeruli. *Toxicologic Pathology* **46**(8):944–948. doi: https://doi.org/10.1177/0192623318796784.

Wang, Q., Tian, X., Wang, Yuyang, Wang, Yan, Li, J., Zhao, T. and Li, P. (2020). Role of Transient Receptor Potential Canonical Channel 6 (TRPC6) in Diabetic Kidney Disease by Regulating Podocyte Actin Cytoskeleton Rearrangement. *Journal of Diabetes Research*.

Wang, W., Sun, W., Cheng, Y., Xu, Z. and Cai, L. (2019a). Role of sirtuin-1 in diabetic nephropathy. *Journal of Molecular Medicine* **97**(3):291–309.

Wang, W., Sun, W., Cheng, Y., Xu, Z. and Cai, L. (2019b). Management of diabetic nephropathy: The role of sirtuin-1. *Future Medicinal Chemistry* **11**(17):2241–2245.

Wang, Y., Pang, L., Zhang, Y., Lin, J. and Zhou, H. (2019). Fenofibrate Improved Interstitial Fibrosis of Renal Allograft through Inhibited Epithelial-Mesenchymal Transition Induced by Oxidative Stress. *Oxidative Medicine and Cellular Longevity*. doi: https://doi.org/10.1155/2019/8936856.

Webber, J. and Clayton, A. (2013). How pure are your vesicles? *Journal of Extracellular Vesicles* **2**(1). doi: https://doi.org/10.3402/jev.v2i0.19861.

Weiner, D.E. (2009). Public health consequences of chronic kidney disease. *Clinical Pharmacology and Therapeutics* **86**(5):566–569.

Wightman, B., Ha, I. and Ruvkun, G. (1993). Posttranscriptional regulation of the

heterochronic gene lin-14 by lin-4 mediates temporal pattern formation in C. elegans. *Cell* **75**(5):855–862. doi: https://doi.org/10.1016/0092-8674(93)90530-4.

Woroniecka, K.I., Park, A.S.D., Mohtat, D., Thomas, D.B., Pullman, J.M. and Susztak, K. (2011). Transcriptome analysis of human diabetic kidney disease. *Diabetes* **60**(9):2354–2369. doi: https://doi.org/10.2337/db10-1181.

Wu, X., Gao, Y., Xu, L., Dang, W., Yan, H., Zou, D., … Han, Z. (2017). Exosomes from high glucose-treated glomerular endothelial cells trigger the epithelial-mesenchymal transition and dysfunction of podocytes. *Scientific Reports* **7**(1):1–12. doi: https://doi.org/10.1038/s41598-017-09907-6.

Xie, Y., Jia, Y., Cuihua, X., Hu, F., Xue, M. and Xue, Y. (2017). Urinary Exosomal MicroRNA Profiling in Incipient Type 2 Diabetic Kidney Disease. *Journal of Diabetes Research*. doi: https://doi.org/10.1155/2017/6978984.

Xu, G. and Jaffrey, S.R. (2011). The new landscape of protein ubiquitination. *Nature Biotechnology* **29**(12):1098–1100. doi: https://doi.org/10.1038/nbt.2061.

Yacoub, R., Lee, K. and He, J.C. (2014). The role of SIRT1 in diabetic kidney disease. *Frontiers in Endocrinology* **5**(OCT).

Yadranji Aghdam, S., Gurel, Z., Ghaffarieh, A., Sorenson, C.M. and Sheibani, N. (2013). High glucose and diabetes modulate cellular proteasome function: Implications in the pathogenesis of diabetes complications. *Biochemical and Biophysical Research Communications* **432**(2):339–344. doi: https://doi.org/10.1016/j.bbrc.2013.01.101.

Yan, Z., Xiong, Y., Xu, W., Gao, J., Cheng, Y., Wang, Z., … Zheng, G. (2012). Identification of hsa-miR-335 as a prognostic signature in gastric cancer. *PLoS ONE* **7**(7). doi: https://doi.org/10.1371/journal.pone.0040037.

Yang, X., Wang, X., Nie, F., Liu, T., Yu, X., Wang, H., … Li, G. (2015). MiR-135 family members mediate podocyte injury through the activation of Wnt/β-catenin signaling. *International Journal of Molecular Medicine* **36**(3):669–677. doi: https://doi.org/10.3892/ijmm.2015.2259.

Yao, T., Zha, D., Gao, P., Shui, H. and Wu, X. (2019). MiR-874 alleviates renal injury and inflammatory response in diabetic nephropathy through targeting toll-like receptor-4. *Journal of Cellular Physiology* **234**(1):871–879. doi: https://doi.org/10.1002/jcp.26908.

Ying, S.Y., Chang, C.P. and Lin, S.L. (2010). Intron-mediated RNA interference, intronic microRNAs, and applications. *Methods in molecular biology (Clifton, N.J.)* **629**:205–237. doi: https://doi.org/10.1007/978-1-60761-657-3_14.

Yip, J., Mattock, M.B., Morocutti, A., Sethi, M., Trevisan, R. and Viberti, G. (1993). Insulin resistance in insulin-dependent diabetic patients with microalbuminuria. *The Lancet*

342(8876):883–887. doi: https://doi.org/10.1016/0140-6736(93)91943-G.

Zang, J., Maxwell, A.P., Simpson, D.A. and McKay, G.J. (2019). Differential Expression of Urinary Exosomal MicroRNAs miR-21-5p and miR-30b-5p in Individuals with Diabetic Kidney Disease. *Scientific Reports* **9**(1). doi: https://doi.org/10.1038/s41598-019-47504-x.

Zeisberg, E.M., Tarnavski, O., Zeisberg, M., Dorfman, A.L., McMullen, J.R., Gustafsson, E., … Kalluri, R. (2007). Endothelial-to-mesenchymal transition contributes to cardiac fibrosis. *Nature Medicine* **13**(8):952–961. doi: https://doi.org/10.1038/nm1613.

Zeisberg, M., Hanai, J.I., Sugimoto, H., Mammoto, T., Charytan, D., Strutz, F. and Kalluri, R. (2003). BMP-7 counteracts TGF-β1-induced epithelial-to-mesenchymal transition and reverses chronic renal injury. *Nature Medicine* **9**(7):964–968. doi: https://doi.org/10.1038/nm888.

Zernecke, A., Bidzhekov, K., Noels, H., Shagdarsuren, E., Gan, L., Denecke, B., … Weber, C. (2009). Delivery of MicroRNA-126 by Apoptotic Bodies Induces CXCL12-Dependent Vascular Protection. *Science Signaling* **2**(100):ra81–ra81. doi: https://doi.org/10.1126/scisignal.2000610.

Zha, F., Bai, L., Tang, B., Li, J., Wang, Y., Zheng, P.X., … Bai, S. (2019). MicroRNA-503 contributes to podocyte injury via targeting E2F3 in diabetic nephropathy. *Journal of Cellular Biochemistry* **120**(8):12574–12581. doi: https://doi.org/10.1002/jcb.28524.

Zhang, Y., Liu, D., Chen, X., Li, J., Li, L., Bian, Z., … Zhang, C.-Y. (2010). Secreted Monocytic miR-150 Enhances Targeted Endothelial Cell Migration. *Molecular Cell* **39**(1):133–144. doi: https://doi.org/10.1016/j.molcel.2010.06.010.

Zhang, Y., Sun, X., Icli, B. and Feinberg, M.W. (2017). Emerging roles for microRNAs in diabetic microvascular disease: Novel targets for therapy. *Endocrine Reviews* **38**(2):145–168.

Zhang, Z., Peng, H., Chen, J., Chen, X., Han, F., Xu, X., … Yan, N. (2009). MicroRNA-21 protects from mesangial cell proliferation induced by diabetic nephropathy in db/db mice. *FEBS Letters* **583**(12):2009–2014. doi: https://doi.org/10.1016/j.febslet.2009.05.021.

Zhao, L., Zou, Y. and Liu, F. (2020). Transforming Growth Factor-B1 in Diabetic Kidney Disease. *Frontiers in Cell and Developmental Biology* **8**.

Zhong, Y., Lee, K. and He, J.C. (2018). SIRT1 is a potential drug target for treatment of diabetic kidney disease. *Frontiers in Endocrinology* **9**(OCT).

Zhou, B., Lu, Y., Hajifathalian, K., Bentham, J., Di Cesare, M., Danaei, G., … Zuñiga Cisneros, J. (2016). Worldwide trends in diabetes since 1980: a pooled analysis of 751 population-based studies with 4·4 million participants. *The Lancet* **387**(10027):1513–1530. doi: https://doi.org/10.1016/S0140-6736(16)00618-8.

Ziyadeh, F.N., Han, D.C., Cohen, J.A., Guo, J. and Cohen, M.P. (1998). Glycated albumin stimulates fibronectin gene expression in glomerular mesangial cells: Involvement of the transforming growth factor-β system. *Kidney International* **53**(3):631–638. doi: https://doi.org/10.1046/j.1523-1755.1998.00815.x.

Appendix:

Appendix 1: Ct values corresponding to extracellular and cellular miR-126, miR-155, and 29b individual Taqman assay results

Extracellular miR-126			
GROUP A		Ct Value	Mean Ct Value
	Sample 1	28.68229	
5mM Glucose	Sample 2	28.94079	28.81000519
	Sample 3	28.80694	
	Sample 1	28.99502	
5mM Glucose + TNF-α	Sample 2	28.44943	28.54443169
	Sample 3	28.18884	
	Sample 1	27.89421	
25mM Glucose	Sample 2	28.0696	27.9819177
	Sample 3	27.98194	
	Sample 1	27.9322	
25mM Glucose + TNF-α	Sample 2	27.79572	27.77563794
	Sample 3	27.599	
GROUP B			
	Sample 1	27.489	
5mM Glucose	Sample 2	26.818	26.81834412
	Sample 3	26.148	
	Sample 1	27.414	
5mM Glucose + TNF-α	Sample 2	27.137	27.13118935
	Sample 3	26.842	
	Sample 1	27.220	
25mM Glucose	Sample 2	27.076	25.93625768
	Sample 3	23.512	
	Sample 1	26.920	
25mM Glucose + TNF-α	Sample 2	27.019	26.96967379
	Sample 3	26.971	
GROUP C			
	Sample 1	21.899	
5mM Glucose	Sample 2	21.376	21.68294017
	Sample 3	21.774	
	Sample 1	21.214	
5mM Glucose + TNF-α	Sample 2	21.136	21.11035156
	Sample 3	20.981	
	Sample 1	24.258	
25mM Glucose	Sample 2	23.880	23.96368599
	Sample 3	23.753	
	Sample 1	23.388	
25mM Glucose + TNF-α	Sample 2	23.061	22.98947398
	Sample 3	22.520	
Extracellular miR-29b			
GROUP A			
5mM Glucose	Sample 1	32.24968	32.2829895
	Sample 2	31.77917	

	Sample 3	32.82012	
	Sample 1	32.02837	
5mM Glucose + TNF-α	Sample 2	32.09571	31.90814336
	Sample 3	31.60035	
	Sample 1	32.06431	
25mM Glucose	Sample 2	31.60791	31.78767459
	Sample 3	31.69081	
	Sample 1	32.06482	
25mM Glucose + TNF-α	Sample 2	31.69484	31.67385228
	Sample 3	31.2619	
GROUP B			
	Sample 1	33.623	
5mM Glucose	Sample 2	34.808	34.24194972
	Sample 3	34.294	
	Sample 1	33.361	
5mM Glucose + TNF-α	Sample 2	34.936	34.37987137
	Sample 3	34.842	
	Sample 1	35.800	
25mM Glucose	Sample 2	35.511	34.43206596
	Sample 3	31.985	
	Sample 1	34.755	
25mM Glucose + TNF-α	Sample 2	34.210	34.60475286
	Sample 3	34.849	
Extracellular miR-155			
GROUP A			
	Sample 1	30.92513	
5mM Glucose	Sample 2	30.16678	30.66739972
	Sample 3	30.91029	
	Sample 1	30.97306	
5mM Glucose + TNF-α	Sample 2	30.53473	30.54130872
	Sample 3	30.11613	
	Sample 1	30.09659	
25mM Glucose	Sample 2	30.1763	30.15210915
	Sample 3	30.18344	
	Sample 1	30.22087	
25mM Glucose + TNF-α	Sample 2	30.13599	30.09941165
	Sample 3	29.94138	
GROUP B			
	Sample 1	30.877	
5mM Glucose	Sample 2	30.565	30.82926305
	Sample 3	31.045	
	Sample 1	30.936	
5mM Glucose + TNF-α	Sample 2	30.970	31.06596057
	Sample 3	31.292	
	Sample 1	30.781	
25mM Glucose	Sample 2	30.913	30.13146019
	Sample 3	28.700	
	Sample 1	30.297	
25mM Glucose + TNF-α	Sample 2	31.078	30.81671143
	Sample 3	31.075	

Cellular miR-126			
GROUP A			
	Sample 1	26.802	
5mM Glucose	Sample 2	26.528	26.164
	Sample 3	25.162	
	Sample 1	25.958	
5mM Glucose + TNF-α	Sample 2	26.977	27.29667
	Sample 3	28.955	
	Sample 1	26.581	
25mM Glucose	Sample 2	29.323	27.78933
	Sample 3	27.464	
	Sample 1	28.335	
25mM Glucose + TNF-α	Sample 2	26.607	27.30333
	Sample 3	26.968	
GROUP B			
	Sample 1	23.81771	
5mM Glucose	Sample 2	24.14086	23.88382
	Sample 3	23.69289	
	Sample 1	24.06245	
5mM Glucose + TNF-α	Sample 2	24.1271	24.09413
	Sample 3	24.09283	
	Sample 1	23.99491	
25mM Glucose	Sample 2	24.0175	24.03004
	Sample 3	24.0777	
	Sample 1	24.37784	
25mM Glucose + TNF-α	Sample 2	24.23145	24.13316
	Sample 3	23.79019	
GROUP C			
	Sample 1	23.033	
5mM Glucose	Sample 2	22.592	22.93333
	Sample 3	23.175	
	Sample 1	23.115	
5mM Glucose + TNF-α	Sample 2	23.367	23.23433
	Sample 3	23.221	
	Sample 1	22.663	
25mM Glucose	Sample 2	23.433	23.29
	Sample 3	23.774	
	Sample 1	24.421	
25mM Glucose + TNF-α	Sample 2	24.332	24.15967
	Sample 3	23.726	
Cellular miR-155			
GROUP A			
	Sample 1	29.26584	
5mM Glucose	Sample 2	29.23726	28.77285
	Sample 3	27.81546	
	Sample 1	28.07174	
5mM Glucose + TNF-α	Sample 2	29.00009	29.47651
	Sample 3	31.35772	
	Sample 1	29.11551	
25mM Glucose	Sample 2	31.82255	30.34042
	Sample 3	30.08322	
25mM Glucose + TNF-α	Sample 1	30.78617	29.87579

	Sample 2	29.26085	
	Sample 3	29.58035	
GROUP B			
	Sample 1	29.1237	
5mM Glucose	Sample 2	29.00516	28.97722
	Sample 3	28.8028	
	Sample 1	28.94044	
5mM Glucose + TNF-α	Sample 2	28.48238	28.73812
	Sample 3	28.79156	
	Sample 1	28.88445	
25mM Glucose	Sample 2	28.92252	28.89241
	Sample 3	28.87025	
	Sample 1	28.88256	
25mM Glucose + TNF-α	Sample 2	28.80045	28.6572
	Sample 3	28.28859	
Cellular miR-29b			
GROUP A			
	Sample 1	30.82082	
5mM Glucose	Sample 2	30.32301	30.25016
	Sample 3	29.60664	
	Sample 1	29.89407	
5mM Glucose + TNF-α	Sample 2	29.81632	30.49316
	Sample 3	31.76909	
	Sample 1	30.15116	
25mM Glucose	Sample 2	32.7331	31.36341
	Sample 3	31.20596	
	Sample 1	31.54541	
25mM Glucose + TNF-α	Sample 2	30.11139	30.85465
	Sample 3	30.90714	
GROUP B			
	Sample 1	28.34113	
5mM Glucose	Sample 2	29.21901	28.72307
	Sample 3	28.60907	
	Sample 1	28.25917	
5mM Glucose + TNF-α	Sample 2	28.60271	28.50295
	Sample 3	28.64697	
	Sample 1	28.75021	
25mM Glucose	Sample 2	28.97276	28.9358
	Sample 3	29.08444	
	Sample 1	28.94203	
25mM Glucose + TNF-α	Sample 2	28.516	28.8838
	Sample 3	29.19336	

Appendix 2: Thermofisher Assay Names and Corresponding miRBaseIDs

ThermoFisher Assay Name	miRBase ID
hsa-let-7b-002619	hsa-let-7b-5p
hsa-let-7c-000379	hsa-let-7c-5p
hsa-let-7e-002406	hsa-let-7e-5p
hsa-miR-100-000437	hsa-miR-100-5p
hsa-miR-101-002253	hsa-miR-101-3p
hsa-miR-107-000443	hsa-miR-107
hsa-miR-10a-000387	hsa-miR-10a-5p
hsa-miR-10b-002218	hsa-miR-10b-5p
hsa-miR-126-002228	hsa-miR-126-3p
hsa-miR-130a-000454	hsa-miR-130a-3p
hsa-miR-130b-000456	hsa-miR-130b-3p
hsa-miR-133a-002246	hsa-miR-133a-3p
hsa-miR-135b-002261	hsa-miR-135b-5p
hsa-miR-138-002284	hsa-miR-138-5p
hsa-miR-146a-000468	hsa-miR-146a-5p
hsa-miR-146b-001097	hsa-miR-146b-5p
hsa-miR-15a-000389	hsa-miR-15a-5p
hsa-miR-15b-000390	hsa-miR-15b-5p
hsa-miR-181a-000480	hsa-miR-181a-5p
hsa-miR-181c-000482	hsa-miR-181c-5p
hsa-miR-182-002334	hsa-miR-182-5p
hsa-miR-183-002269	hsa-miR-183-5p
hsa-miR-18a-002422	hsa-miR-18a-5p
hsa-miR-18b-002217	hsa-miR-18b-5p
hsa-miR-192-000491	hsa-miR-192-5p
hsa-miR-194-000493	hsa-miR-194-5p
hsa-miR-198-002273	hsa-miR-198
hsa-miR-200a-000502	hsa-miR-200a-3p
hsa-miR-200b-002251	hsa-miR-200b-3p
hsa-miR-203-000507	hsa-miR-203a-3p
hsa-miR-210-000512	hsa-miR-210-3p
hsa-miR-21-000397	hsa-miR-21-5p
hsa-miR-214-002306	hsa-miR-214-3p
hsa-miR-215-000518	hsa-miR-215-5p
hsa-miR-216a-002220	hsa-miR-216a-5p
hsa-miR-216b-002326	hsa-miR-216b-5p
hsa-miR-217-002337	hsa-miR-217
hsa-miR-218-000521	hsa-miR-218-5p
hsa-miR-22-000398	hsa-miR-22-3p
hsa-miR-23a-000399	hsa-miR-23a-3p
hsa-miR-23b-000400	hsa-miR-23b-3p
hsa-miR-296-000527	hsa-miR-296-5p
hsa-miR-29b-000413	hsa-miR-29b-3p
hsa-miR-301b-002392	hsa-miR-301b-3p

hsa-miR-328-000543	hsa-miR-328-3p
hsa-miR-331-000545	hsa-miR-331-3p
hsa-miR-331-5p-002233	hsa-miR-331-5p
hsa-miR-335-000546	hsa-miR-335-5p
hsa-miR-337-5p-002156	hsa-miR-337-5p
hsa-miR-339-5p-002257	hsa-miR-339-5p
hsa-miR-342-5p-002147	hsa-miR-342-5p
hsa-miR-361-000554	hsa-miR-361-5p
hsa-miR-362-3p-002117	hsa-miR-362-3p
hsa-miR-365-001020	hsa-miR-365a-3p
hsa-miR-375-000564	hsa-miR-375
hsa-miR-376c-002122	hsa-miR-376c-3p
hsa-miR-382-000572	hsa-miR-382-5p
hsa-miR-409-5p-002331	hsa-miR-409-5p
hsa-miR-411-001610	hsa-miR-411-5p
hsa-miR-422a-002297	hsa-miR-422a
hsa-miR-423-5p-002340	hsa-miR-423-5p
hsa-miR-431-001979	hsa-miR-431-5p
hsa-miR-433-001028	hsa-miR-433-3p
hsa-miR-449-001030	hsa-miR-449a
hsa-miR-455-001280	hsa-miR-455-5p
hsa-miR-455-3p-002244	hsa-miR-455-3p
hsa-miR-483-5p-002338	hsa-miR-483-5p
hsa-miR-485-3p-001277	hsa-miR-485-3p
hsa-miR-486-3p-002093	hsa-miR-486-3p
hsa-miR-487a-001279	hsa-miR-487a-3p
hsa-miR-493-002364	hsa-miR-493-5p
hsa-miR-501-001047	hsa-miR-501-5p
hsa-miR-502-001109	hsa-miR-502-5p
hsa-miR-502-3p-002083	hsa-miR-502-3p
hsa-miR-503-001048	hsa-miR-503-5p
hsa-miR-505-002089	hsa-miR-505-3p
hsa-miR-517a-002402	hsa-miR-517a
hsa-miR-518d-001159	hsa-miR-518d-3p
hsa-miR-519a-002415	hsa-miR-519a-3p
hsa-miR-532-3p-002355	hsa-miR-532-3p
hsa-miR-542-3p-001284	hsa-miR-542-3p
hsa-miR-548a-001538	hsa-miR-548a-3p
hsa-miR-548d-5p-002237	hsa-miR-548d-5p
hsa-miR-561-001528	hsa-miR-561-3p
hsa-miR-576-3p-002351	hsa-miR-576-3p
hsa-miR-589-002409	hsa-miR-589-3p
hsa-miR-618-001593	hsa-miR-618
hsa-miR-636-002088	hsa-miR-636
hsa-miR-652-002352	hsa-miR-652-3p
hsa-miR-654-001611	hsa-miR-654-5p
hsa-miR-655-001612	hsa-miR-655-3p
hsa-miR-660-001515	hsa-miR-660-5p

hsa-miR-708-002341	hsa-miR-708-5p
hsa-miR-758-001990	hsa-miR-758-3p
hsa-miR-874-002268	hsa-miR-874-3p
hsa-miR-885-5p-002296	hsa-miR-885-5p
hsa-miR-886-3p-002194	hsa-miR-886-3p
hsa-miR-886-5p-002193	hsa-miR-886-5p
hsa-miR-888-002212	hsa-miR-888-5p
hsa-miR-889-002202	hsa-miR-889-3p
hsa-miR-891a-002191	hsa-miR-891a-5p
hsa-miR-9-000583	hsa-miR-9-5p
hsa-miR-98-000577	hsa-miR-98-5p
hsa-miR-99a-000435	hsa-miR-99a-5p
hsa-miR-99b-000436	hsa-miR-99b-5p

Appendix 3: Integrative scores for top 200 predicted MiRDIP gene targets of cellular miRs expressed in ciGEnCs under the 25 mM glucose concentration treatment condition, used for STRING analysis

Gene Name	Integrative Score
H3F3B	0.986407
BZW1	0.9823
MYH10	0.972689
HMGA2	0.970436
PPP6C	0.965989
COL1A2	0.965909
PAPPA	0.963751
DR1	0.958225
KPNA4	0.954686
PAFAH1B1	0.954247
GALNT1	0.952344
RAF1	0.950849
KIF1B	0.950075
SNRK	0.949257
USP15	0.94925
CUL3	0.947329
SIN3A	0.946991
TLK1	0.945177
DUSP1	0.943424
ZFYVE26	0.943024
E2F3	0.942689
SLC4A4	0.940823
RDX	0.940107
CHD4	0.93985
PTP4A1	0.937658
LMO2	0.935674
N4BP1	0.935051
DYRK1A	0.934944
PRDM2	0.933977
RPS6KB1	0.93287
FBXO8	0.932795
KPNA3	0.932763
USP25	0.931467
HIC2	0.930854
YWHAH	0.930687
EIF4G2	0.93033
CCND2	0.929144
GLUD1	0.929056
RAP2C	0.928846
MTMR4	0.928434
PDCD4	0.927942
SP3	0.927936
COL3A1	0.927861
SFPQ	0.927746
ATP2B1	0.927182
ATP1B1	0.926344
UBE3A	0.926206
TAGLN	0.926113
RAB10	0.926111
TCF12	0.925501
CDC34	0.925157
IRAK1	0.925093
MBNL1	0.924626
PPM1A	0.924416
ULK2	0.924052
H2AFZ	0.923771
YWHAG	0.923298
ZFPM2	0.922762
CUL2	0.922514
C1orf21	0.921645
RBM6	0.921415
LYPLA1	0.921258
ACTR2	0.920978
CCND1	0.92084
CRIM1	0.920741
PFN2	0.920682
PGRMC2	0.919971
RASSF5	0.919494
TGFBR3	0.918804
BNIP3L	0.918607
BCL2L2	0.917814
RASA1	0.917602
MAP2K1	0.917597
CBX1	0.917171
NLGN1	0.91603
PPP2R2A	0.915916
CXCL12	0.915549
BRD3	0.915404
MACF1	0.915282
EIF5	0.915281
NDST2	0.914595
NR3C1	0.913945
ITGB1	0.913665
NEDD9	0.91291
KIF5A	0.912755
UPF2	0.912639
CLCN3	0.911526
NF1	0.911402
CDC42	0.910913
CITED2	0.910704
IRS2	0.910191
AUH	0.909851
MAPK14	0.909789
NDEL1	0.909205
NFIB	0.908498
OSBPL3	0.908229
ATP6V1B2	0.90797
PPIF	0.906733
PDE7B	0.906353
DEK	0.906189
TGIF2	0.906122
PPP2CA	0.906039
PTPRG	0.905517
DDX5	0.905441
VCL	0.90523
PKP4	0.904889
TMEM2	0.904697
PKIA	0.904605
NAP1L1	0.904307
EP300	0.904225
UBE4B	0.904157
RANBP2	0.903597
STK39	0.903176
MAPK6	0.90276
PTBP2	0.902034
OSBPL11	0.901893
YWHAQ	0.901804
RECK	0.901391
PCMT1	0.901139
LAMC1	0.89969
DTNA	0.899
PPP2CB	0.898611
LATS2	0.898574
LBR	0.898383
BCL2	0.898321
STRBP	0.898214
RBBP6	0.898099
COL5A2	0.897551
MAPRE1	0.897269
GNG5	0.896844
ERCC6	0.896738
MBNL2	0.896199

FIGN	0.895975
RBM15	0.895845
FLOT2	0.895828
SYNE1	0.894994
BTBD3	0.89498
KHDRBS3	0.894869
ZFP36L2	0.894857
UBE2V1	0.894855
TAF12	0.893657
APC	0.893481
SIAH1	0.893082
USP3	0.893053
YY1	0.892234
CSNK2A1	0.892003
MEIS2	0.891983
RARA	0.891706
KPNA1	0.891691
UBE2D3	0.89152
PPP1R11	0.890923
BTG1	0.890422
ZYX	0.890345
PNN	0.88945
DPYSL3	0.889065
WBP11	0.888631
FBN2	0.888
EIF4B	0.887381
CAPZA2	0.88736
FOXA1	0.887223
SRGAP1	0.887214
ANP32E	0.886531
INPP5A	0.886495
CELSR2	0.885635
RAB5B	0.885446
PRDM4	0.885375
SLC2A3	0.88526
SEC14L1	0.885154
PPP1CB	0.885144
ADRB2	0.885066
PPP1R15B	0.884724
CD164	0.884258
GNAI3	0.884002
ARF4	0.88378
PPP2R5C	0.883638
PCDHA6	0.883588
RALA	0.883503
PPP2R5E	0.883202
OSMR	0.883037
ATP2A2	0.882858

NEK6	0.882708
SLC2A1	0.881486
NRP2	0.880984
FEM1C	0.880605
PDCD10	0.879941
PPP1R12A	0.879498
SOX4	0.87917
VAPA	0.878822
IPO7	0.878794
BZW2	0.878274
DNAJC6	0.878194
PPP3CA	0.877141
UTRN	0.876759
COPS7B	0.876666
DYRK2	0.876143
CLASP2	0.875855
TCF4	0.875814
CDC25A	0.875445
VAV3	0.875261
MATR3	0.875211

Appendix 4: Integrative scores for top 200 MiRDIP predicted gene targets of cellular miRs expressed in ciGEnCs under the 5 mM glucose + TNF- α treatment condition, used for STRING analysis

Gene Name	Integrative Score
ADD3	0.972397
HMGA2	0.970436
PPP6C	0.965989
COL1A2	0.965909
PAPPA	0.963751
TGFBI	0.957755
ARF4	0.956927
DUSP1	0.956894
PAFAH1B1	0.954247
FBN1	0.954157
PDCD4	0.953635
CAPZA1	0.952918
GALNT1	0.952344
NR5A2	0.951482
RAF1	0.950849
KIF1B	0.950075
ELAVL1	0.949795
TOX	0.949258
SNRK	0.949257
USP15	0.94925
JAG1	0.947855
RBL2	0.946083
CDKN1B	0.945568
CSNK1A1	0.945431
TLK1	0.945177
FBXL5	0.944521
FBN2	0.94444
FEZ2	0.943238
ZFYVE26	0.943024
TCF12	0.941257
SLC4A4	0.940823
ARHGAP12	0.940699
CUL4A	0.940368
RDX	0.940107
CHD4	0.93985
FSTL1	0.938826
ATP1B1	0.937391
MYO1C	0.93735
NEDD9	0.937145
EIF4A2	0.936719
STAM	0.936467
PPP3CA	0.936209
N4BP1	0.935051
DYRK1A	0.934944
PRDM2	0.933977
AKAP12	0.933651
MKRN1	0.933332
ACTR3	0.932365
HBP1	0.932307
VAV3	0.93211
PTP4A1	0.932063
PFN2	0.931937
VAPB	0.931863
USP25	0.931467
RAB1A	0.931085
HIC2	0.930854
YWHAH	0.930687
EIF4G2	0.93033
NFIB	0.930178
SRGAP1	0.929937
SACS	0.929876
CCND2	0.929144
GLUD1	0.929056
RAP2C	0.928846
CRIM1	0.928534
MTMR4	0.928434
HIVEP2	0.92816
COL3A1	0.927861
MTHFD2	0.927666
TOB1	0.927111
HIPK1	0.926848
GOT1	0.926533
PPP2R2A	0.926355
PRRG1	0.926118
RAB10	0.926111
CDC34	0.925157
IRAK1	0.925093
NDUFA4	0.924886
MBNL1	0.924626
PPM1A	0.924416
ULK2	0.924052
ID4	0.923772
TRIP11	0.923424
ZFPM2	0.922762
CUL2	0.922514
FBXW2	0.921713
RBM6	0.921415
ACTR2	0.920978
CCND1	0.92084
MTMR2	0.919543
RASSF5	0.919494
TGFBR3	0.918804
YES1	0.9185
BCL2L2	0.917814
RNF128	0.917781
PLEKHA1	0.917617
SHC1	0.9176
MAP2K1	0.917597
NPAS2	0.916984
PHF2	0.91693
C1orf21	0.916708
NLGN1	0.91603
NCOA3	0.915771
MAP3K3	0.915728
HOXB7	0.915645
EIF5	0.915281
KPNA3	0.915161
ARPC1A	0.915099
NDST2	0.914595
VCL	0.914523
INSIG1	0.91429
ERG	0.913881
AUH	0.913279
PCMT1	0.913164
KIF5A	0.912755
UPF2	0.912639
FBXO11	0.912212
PPP2R5E	0.912111
KPNA4	0.912057
ZFP91	0.91192
NF1	0.911402
CALD1	0.911365
CDC42	0.910913
CITED2	0.910704
PCDHA6	0.91028
CNOT7	0.910247
NDEL1	0.909205
USP3	0.909084
RANBP2	0.90908
SRPK1	0.90899
EPS8	0.908984
SP3	0.908934

OSBPL3	0.908229
SERP1	0.908
PMP22	0.907536
ELK3	0.907227
PDGFRA	0.906686
TGIF2	0.906122
DDX5	0.906035
MMP16	0.905976
HES1	0.905422
TMEM2	0.904697
ARPC5	0.904614
MAPRE1	0.904595
NAP1L1	0.904307
UBE4B	0.904157
RAB5B	0.904084
FN1	0.903623
E2F3	0.903448
GNPNAT1	0.903359
SS18L1	0.903097
RPS6KB1	0.902931
MAPK6	0.90276
ZNF148	0.902627
PHTF2	0.902573
KPNA1	0.902413
MMD	0.902261
PDCD10	0.902251
YWHAQ	0.901804
RECK	0.901391
NRP1	0.901054
CD164	0.900405
AP3S1	0.900213
PAPOLA	0.899774
LAMC1	0.89969
DDHD1	0.899414
LATS2	0.898574
IRS2	0.898376
BCL2	0.898321
PTPRF	0.898275
STRBP	0.898214
LAPTM4A	0.898109
RBBP6	0.898099
SSX2IP	0.898014
STC1	0.897996
CDCA4	0.897637
COL5A2	0.897551
ITGA6	0.897234
GNG5	0.896844
ERCC6	0.896738
MBNL2	0.896199
PKIA	0.896073
FIGN	0.895975
RCN2	0.895834
FLOT2	0.895828
MATR3	0.89521
YWHAG	0.89506
SPTLC2	0.895028
BTBD3	0.89498
UBE2V1	0.894855
NTN4	0.894409
KPNA2	0.894381
RASA1	0.894182
VANGL1	0.894067
DHX40	0.893957
SLC25A22	0.893681
APC	0.893481
ENPP5	0.893425
FEM1C	0.892044

Appendix 5: Integrative scores for top 200 MiRDIP predicted gene targets of cellular miRs expressed in ciGEnCs under the 25 mM glucose + TNF- α treatment condition, used for STRING analysis

Gene Name	Integrative Score
BZW1	0.9823
COL1A2	0.976781
MYH10	0.972689
DUSP1	0.971767
HMGA2	0.970436
PPP6C	0.965989
DR1	0.958225
STC1	0.95524
KPNA4	0.953209
FBN2	0.953107
GALNT1	0.952344
SNRK	0.949257
CUL3	0.947329
PPFIA1	0.947323
SIN3A	0.946991
RAP1B	0.944855
ZFYVE26	0.943024
E2F3	0.942689
KIF1B	0.942636
SLC4A4	0.940823
RDX	0.940107
CHD4	0.93985
PTP4A1	0.937658
UBE2D1	0.936784
EMP1	0.936466
RAB1A	0.93642
EIF4G2	0.936311
N4BP1	0.935051
DYRK1A	0.934944
PRDM2	0.933977
PAPPA	0.933617
CDYL	0.933362
KPNA3	0.932763
TLK1	0.93236
HIC2	0.930854
YWHAH	0.930687
CCND2	0.929144
GLUD1	0.929056
PKP4	0.92894
RAP2C	0.928846
MTMR4	0.928434
COL3A1	0.927861
SFPQ	0.927746
AEBP2	0.926472
UBE3A	0.926206
TAGLN	0.926113
RAB10	0.926111
TCF12	0.925501
CDC34	0.925157
IRAK1	0.925093
MBNL1	0.924626
PDCD4	0.924268
ULK2	0.924052
H2AFZ	0.923771
YWHAG	0.923298
ZFPM2	0.922762
FEZ2	0.922543
C1orf21	0.921645
RANBP2	0.92136
LYPLA1	0.921258
PFN2	0.920682
PGRMC2	0.919971
RASSF5	0.919494
TGFBR3	0.918804
BNIP3L	0.918607
CBX1	0.917171
PPP2R2A	0.915916
BRD3	0.915404
MACF1	0.915282
EIF5	0.915281
NDST2	0.914595
TOB1	0.91395
NR3C1	0.913945
ITGB1	0.913665
NDFIP1	0.913411
NEDD9	0.91291
KIF5A	0.912755
UPF2	0.912639
AP3S1	0.911614
CLCN3	0.911526
NF1	0.911402
RAB5A	0.91108
CITED2	0.910704
IRS2	0.910191
MAPK14	0.909789
NDEL1	0.909205
SP3	0.908934
EPS8	0.908798
OSBPL3	0.908229
ATP6V1B2	0.90797
PDE7B	0.906353
DEK	0.906189
PPP2CA	0.906039
PTPRG	0.905517
DDX5	0.905441
VCL	0.90523
ZNF207	0.904937
TMEM2	0.904697
NAP1L1	0.904307
EP300	0.904225
STK39	0.903176
FN1	0.903139
MAPK6	0.90276
RANBP9	0.902759
RPS6KB1	0.902478
OSBPL11	0.901893
MMD	0.901644
NR5A2	0.900748
SEL1L	0.89951
DTNA	0.899
GJA1	0.8987
PPP2CB	0.898611
LATS2	0.898574
STRBP	0.898214
FZD4	0.897808
COL5A2	0.897551
GNG5	0.896844
ERCC6	0.896738
TGIF2	0.896621
DNMT3A	0.896606
MBNL2	0.896199
FIGN	0.895975
RBM15	0.895845
FLOT2	0.895828
LAMC1	0.895359
PPP2R5E	0.895047
SYNE1	0.894994
BTBD3	0.89498
KHDRBS3	0.894869
ZFP36L2	0.894857
MATR3	0.894504
TAF12	0.893657

APC	0.893481
SIAH1	0.893082
USP3	0.893053
YY1	0.892234
CSNK2A1	0.892003
MEIS2	0.891983
GNAI3	0.891804
RARA	0.891706
KPNA1	0.891691
BTG1	0.890422
PNN	0.88945
DPYSL3	0.889065
PPM1F	0.888939
EIF4B	0.887381
CAPZA2	0.88736
GPM6A	0.887318
BCL2L2	0.887304
FOXA1	0.887223
SRGAP1	0.887214
RBBP7	0.887168
ANP32E	0.886531
INPP5A	0.886495
RECK	0.88577

CELSR2	0.885635
RAB5B	0.885446
SEC14L1	0.885154
ADRB2	0.885066
NUP153	0.884962
ATP1B1	0.884796
PPP1R15B	0.884724
NFIB	0.884166
ADD3	0.88369
PPP2R5C	0.883638
RALA	0.883503
MYEF2	0.883045
OSMR	0.883037
ATP2A2	0.882858
FLRT2	0.882312
DLG5	0.881699
SLC2A1	0.881486
SEC24C	0.881411
TNFRSF1B	0.881092
ALCAM	0.881063
NRP2	0.880984
CPLX1	0.880972
CNN3	0.880617

FEM1C	0.880605
PDCD10	0.879941
COL1A1	0.879505
PPP1R12A	0.879498
SOX4	0.87917
VAPA	0.878822
IPO7	0.878794
NACA	0.878392
BZW2	0.878274
MSN	0.87783
PKIA	0.877152
PPP3CA	0.877141
UTRN	0.876759
COPS7B	0.876666
DYRK2	0.876143
CLASP2	0.875855
CDC25A	0.875445
VAV3	0.875261
HOXA9	0.874865
SNX1	0.874798
QARS	0.874726

Appendix 6: Combined integrative scores for top 200 MiRDIP predicted gene targets of cellular miRs expressed in ciGEnCs under all three treatment conditions (25 mM glucose, 10 ng/µl TNF-α, 25 mM glucose + 10 ng/µl TNF-α), used for STRING analysis

Gene Name	Integrative score in each condition			Combined integrative score
	25mM	5mM + TNF-α	25mM + TNF-α	
BZW1	0.9823	0.9823	0.9823	2.946899589
HMGA2	0.970436	0.970436	0.970436	2.911308838
COL1A2	0.965909	0.965909	0.976781	2.908597967
PPP6C	0.965989	0.965989	0.965989	2.897966761
DUSP1	0.943424	0.956894	0.971767	2.872084722
PAPPA	0.963751	0.963751	0.933617	2.861119243
GALNT1	0.952344	0.952344	0.952344	2.857032733
SNRK	0.949257	0.949257	0.949257	2.847771445
KIF1B	0.950075	0.950075	0.942636	2.84278603
ZFYVE26	0.943024	0.943024	0.943024	2.829073474
TLK1	0.945177	0.945177	0.93236	2.822713695
SLC4A4	0.940823	0.940823	0.940823	2.822470273
RDX	0.940107	0.940107	0.940107	2.820320735
KPNA4	0.954686	0.912057	0.953209	2.819952184
CHD4	0.93985	0.93985	0.93985	2.819549687
PTP4A1	0.937658	0.932063	0.937658	2.807379345
PDCD4	0.927942	0.953635	0.924268	2.805845047

N4BP1	0.935051	0.935051	0.935051	2.805153896
DYRK1A	0.934944	0.934944	0.934944	2.804830872
DR1	0.958225	0.885653	0.958225	2.802102964
PRDM2	0.933977	0.933977	0.933977	2.801929817
EIF4G2	0.93033	0.93033	0.936311	2.79697027
HIC2	0.930854	0.930854	0.930854	2.792563343
TCF12	0.925501	0.941257	0.925501	2.792258806
YWHAH	0.930687	0.930687	0.930687	2.79206034
E2F3	0.942689	0.903448	0.942689	2.788825206
CCND2	0.929144	0.929144	0.929144	2.787432698
GLUD1	0.929056	0.929056	0.929056	2.787168646
RAP2C	0.928846	0.928846	0.928846	2.786538842
FBN2	0.888	0.94444	0.953107	2.785546236
MTMR4	0.928434	0.928434	0.928434	2.785303273
COL3A1	0.927861	0.927861	0.927861	2.78358152
KPNA3	0.932763	0.915161	0.932763	2.780687027
RAB10	0.926111	0.926111	0.926111	2.778333397
PAFAH1B1	0.954247	0.954247	0.869169	2.777663342
CDC34	0.925157	0.925157	0.925157	2.775470268
IRAK1	0.925093	0.925093	0.925093	2.775278248
MBNL1	0.924626	0.924626	0.924626	2.77387825
PFN2	0.920682	0.931937	0.920682	2.773300393
ULK2	0.924052	0.924052	0.924052	2.772156164
ZFPM2	0.922762	0.922762	0.922762	2.768286318
USP15	0.94925	0.94925	0.867962	2.766461257
NEDD9	0.91291	0.937145	0.91291	2.762965072
C1orf21	0.921645	0.916708	0.921645	2.759996808
RASSF5	0.919494	0.919494	0.919494	2.758481955
PPP2R2A	0.915916	0.926355	0.915916	2.758187677
TGFBR3	0.918804	0.918804	0.918804	2.756412551
ATP1B1	0.926344	0.937391	0.884796	2.748530656
EIF5	0.915281	0.915281	0.915281	2.745842257
SP3	0.927936	0.908934	0.908934	2.745803802
NDST2	0.914595	0.914595	0.914595	2.743784279
YWHAG	0.923298	0.89506	0.923298	2.741656851
RPS6KB1	0.93287	0.902931	0.902478	2.738279055
KIF5A	0.912755	0.912755	0.912755	2.73826421
UPF2	0.912639	0.912639	0.912639	2.737915557
NF1	0.911402	0.911402	0.911402	2.734205802
RANBP2	0.903597	0.90908	0.92136	2.734036652
CITED2	0.910704	0.910704	0.910704	2.732112125
NDEL1	0.909205	0.909205	0.909205	2.727616303
VCL	0.90523	0.914523	0.90523	2.724984323
OSBPL3	0.908229	0.908229	0.908229	2.724685934
BCL2L2	0.917814	0.917814	0.887304	2.7229327
NFIB	0.908498	0.930178	0.884166	2.722841139
SIN3A	0.946991	0.828185	0.946991	2.722167361
STC1	0.866479	0.897996	0.95524	2.719714543

IRS2	0.910191	0.898376	0.910191	2.718758524
DDX5	0.905441	0.906035	0.905441	2.716916385
ACTR2	0.920978	0.920978	0.872637	2.714592211
TMEM2	0.904697	0.904697	0.904697	2.71408959
NAP1L1	0.904307	0.904307	0.904307	2.712922157
TGIF2	0.906122	0.906122	0.896621	2.708865513
MAPK6	0.90276	0.90276	0.90276	2.708280783
SRGAP1	0.887214	0.929937	0.887214	2.704363672
H3F3B	0.986407	0.729765	0.986407	2.702579374
BRD3	0.915404	0.865738	0.915404	2.69654678
LATS2	0.898574	0.898574	0.898574	2.695721174
USP3	0.893053	0.909084	0.893053	2.69519023
LAMC1	0.89969	0.89969	0.895359	2.694738891
STRBP	0.898214	0.898214	0.898214	2.694640971
COL5A2	0.897551	0.897551	0.897551	2.692654285
CCND1	0.92084	0.92084	0.850945	2.692624263
JAG1	0.871823	0.947855	0.871823	2.691500566
GNG5	0.896844	0.896844	0.896844	2.690532981
PPP3CA	0.877141	0.936209	0.877141	2.690490464
PPP2R5E	0.883202	0.912111	0.895047	2.690359441
ERCC6	0.896738	0.896738	0.896738	2.690213663
MBNL2	0.896199	0.896199	0.896199	2.688598117
RECK	0.901391	0.901391	0.88577	2.688551179
FIGN	0.895975	0.895975	0.895975	2.687925762
FLOT2	0.895828	0.895828	0.895828	2.687483369
KPNA1	0.891691	0.902413	0.891691	2.685794358
BTBD3	0.89498	0.89498	0.89498	2.684939673
VAV3	0.875261	0.93211	0.875261	2.682632159
APC	0.893481	0.893481	0.893481	2.680442766
PKIA	0.904605	0.896073	0.877152	2.677829473
EIF4A2	0.870345	0.936719	0.870345	2.677408338
NR3C1	0.913945	0.848779	0.913945	2.676667867
MEIS2	0.891983	0.891983	0.891983	2.675950353
CDC42	0.910913	0.910913	0.853701	2.675527388
RAB5B	0.885446	0.904084	0.885446	2.674976569
CBX1	0.917171	0.839389	0.917171	2.673730273
PGRMC2	0.919971	0.832826	0.919971	2.672768183
PNN	0.88945	0.88945	0.88945	2.668351103
ID4	0.872212	0.923772	0.872212	2.668195743
GNAI3	0.884002	0.891804	0.891804	2.667610688
MATR3	0.875211	0.89521	0.894504	2.66492433
RBBP6	0.898099	0.898099	0.868606	2.664803698
EIF4B	0.887381	0.887381	0.887381	2.662143041
PDCD10	0.879941	0.902251	0.879941	2.662133078
CAPZA2	0.88736	0.88736	0.88736	2.662079981
PLEKHA1	0.871909	0.917617	0.871909	2.661434823
INPP5A	0.886495	0.886495	0.886495	2.659483841
SIAH1	0.893082	0.871865	0.893082	2.658029836

PPP2CA	0.906039	0.845162	0.906039	2.657241165
CELSR2	0.885635	0.885635	0.885635	2.656904849
SEC14L1	0.885154	0.885154	0.885154	2.655461651
ADRB2	0.885066	0.885066	0.885066	2.65519752
PPP1R15B	0.884724	0.884724	0.884724	2.65417183
FEM1C	0.880605	0.892044	0.880605	2.653253633
MAPRE1	0.897269	0.904595	0.850396	2.652261019
OSBPL11	0.901893	0.846656	0.901893	2.65044244
OSMR	0.883037	0.883037	0.883037	2.649112272
PPM1A	0.924416	0.924416	0.799085	2.647917425
ATP2A2	0.882858	0.879878	0.882858	2.645595437
NRP1	0.871287	0.901054	0.871287	2.643627452
ZYX	0.890345	0.890345	0.862801	2.643491728
NRP2	0.880984	0.880984	0.880984	2.642952431
CLCN3	0.911526	0.818318	0.911526	2.641369722
ATP2B1	0.927182	0.856928	0.856928	2.64103868
INSIG1	0.862319	0.91429	0.862319	2.638927662
PPP1R12A	0.879498	0.879498	0.879498	2.638492958
VAPA	0.878822	0.878822	0.878822	2.63646511
BZW2	0.878274	0.878274	0.878274	2.634822236
SOX4	0.87917	0.874712	0.87917	2.63305237
CRIM1	0.920741	0.928534	0.78373	2.633004697
USP25	0.931467	0.931467	0.769689	2.63262309
UTRN	0.876759	0.876759	0.876759	2.63027768
CDYL	0.817087	0.879565	0.933362	2.630013915
COPS7B	0.876666	0.876666	0.876666	2.629998437
CLASP2	0.875855	0.877263	0.875855	2.628973513
PPP2R5C	0.883638	0.86142	0.883638	2.628695736
EP300	0.904225	0.820111	0.904225	2.628561439
DYRK2	0.876143	0.876143	0.876143	2.628428212
BNIP3L	0.918607	0.790453	0.918607	2.627666958
PDE7B	0.906353	0.81448	0.906353	2.627186325
COL1A1	0.873656	0.873656	0.879505	2.626816637
CDC25A	0.875445	0.875445	0.875445	2.626333699
HOXA9	0.874865	0.874865	0.874865	2.624596083
QARS	0.874726	0.874726	0.874726	2.624176662
AEBP2	0.810345	0.887332	0.926472	2.624149285
LBR	0.898383	0.860604	0.860604	2.6195911
NLGN1	0.91603	0.91603	0.78738	2.61944109
TNFRSF1B	0.86847	0.86847	0.881092	2.618031665
RCN2	0.867632	0.895834	0.85449	2.617955871
ARPC5	0.856283	0.904614	0.856283	2.617178811
CUL3	0.947329	0.71988	0.947329	2.614538432
FOXA1	0.887223	0.838307	0.887223	2.612753555
SMARCC1	0.870782	0.870782	0.870782	2.612346791
CTNND1	0.870664	0.870664	0.870664	2.611993237
RASA1	0.917602	0.894182	0.799981	2.611764542
PTPRG	0.905517	0.800465	0.905517	2.611498453

MYEF2	0.84503	0.883045	0.883045	2.611120113
UBE2V1	0.894855	0.894855	0.819422	2.609131567
DTNA	0.899	0.810452	0.899	2.608452217
COL4A1	0.869312	0.869312	0.869312	2.607936943
MAP3K3	0.845868	0.915728	0.845868	2.607463166
POGZ	0.858499	0.889649	0.858499	2.606647232
ATP6V1B2	0.90797	0.786847	0.90797	2.602787335
HIPK1	0.837823	0.926848	0.837823	2.602493791
UBE2D3	0.89152	0.886736	0.822483	2.600738846
NUMB	0.866521	0.866521	0.866521	2.599563934
MMD	0.794372	0.902261	0.901644	2.598277022
STXBP5	0.866035	0.866035	0.866035	2.598104007
PDAP1	0.865552	0.865552	0.865552	2.596656043
TARDBP	0.865489	0.865489	0.865489	2.596465884
TCF4	0.875814	0.878535	0.840167	2.59451642
DOT1L	0.864375	0.864375	0.864375	2.593125514
ABCE1	0.864264	0.864264	0.864264	2.592791876
PGRMC1	0.864228	0.864228	0.864228	2.592683491
TRAM1	0.871966	0.871966	0.847048	2.590979281
NME4	0.863123	0.863123	0.863123	2.5893681
ESRRA	0.863089	0.863089	0.863089	2.58926838
PPP1R11	0.890923	0.890923	0.806631	2.588476535
DAG1	0.870717	0.870717	0.845564	2.586997549
ADD3	0.730817	0.972397	0.88369	2.586904351
FARP1	0.86228	0.86228	0.86228	2.586838557
UBE3A	0.926206	0.729689	0.926206	2.582100031
BLMH	0.859602	0.859602	0.859602	2.578805662
SACS	0.82403	0.929876	0.82403	2.577935634
FBXW2	0.827482	0.921713	0.827482	2.576676846
SEC23IP	0.866948	0.842643	0.866948	2.576538103
ALCAM	0.808178	0.885018	0.881063	2.574258927
CD164	0.884258	0.900405	0.789004	2.573667004
SMARCD2	0.846989	0.891997	0.83334	2.572326413
MAP4K4	0.855711	0.860193	0.855711	2.57161584
CHD1	0.857008	0.857008	0.857008	2.571024393
DLG5	0.843867	0.843867	0.881699	2.569432406
RAI14	0.855959	0.855959	0.855959	2.567875557
CLDN12	0.851158	0.86512	0.851158	2.567435892
CNOT6L	0.84126	0.884521	0.840599	2.566380017

Appendix 7: Combined integrative scores for top 200 MiRDIP predicted gene targets of cellular miRs expressed in ciGEnCs under both high glucose treatment conditions(25 mM glucose, 25 mM glucose + 10 ng/µl TNF-α), used for STRING analysis

Gene Name	Integrative score in each condition		Combined integrative score
	5mM	25mM	
H3F3B	0.986407	0.986407	1.972814651
BZW1	0.9823	0.9823	1.964599726
MYH10	0.972689	0.972689	1.945378653
COL1A2	0.965909	0.976781	1.942689382
HMGA2	0.970436	0.970436	1.940872559
PPP6C	0.965989	0.965989	1.931977841
DR1	0.958225	0.958225	1.916449988
DUSP1	0.943424	0.971767	1.915190956
KPNA4	0.954686	0.953209	1.907895222
GALNT1	0.952344	0.952344	1.904688488
SNRK	0.949257	0.949257	1.898514297
PAPPA	0.963751	0.933617	1.897368116
CUL3	0.947329	0.947329	1.894658057
SIN3A	0.946991	0.946991	1.893982354
KIF1B	0.950075	0.942636	1.892710772
ZFYVE26	0.943024	0.943024	1.886048982
E2F3	0.942689	0.942689	1.885377378
SLC4A4	0.940823	0.940823	1.881646849
RDX	0.940107	0.940107	1.880213823
CHD4	0.93985	0.93985	1.879699791
TLK1	0.945177	0.93236	1.877536876
PTP4A1	0.937658	0.937658	1.875316563
N4BP1	0.935051	0.935051	1.870102597
DYRK1A	0.934944	0.934944	1.869887248
PRDM2	0.933977	0.933977	1.867953211
EIF4G2	0.93033	0.936311	1.866640419
KPNA3	0.932763	0.932763	1.865526384
HIC2	0.930854	0.930854	1.861708895
YWHAH	0.930687	0.930687	1.86137356
CCND2	0.929144	0.929144	1.858288465
GLUD1	0.929056	0.929056	1.858112431
RAP2C	0.928846	0.928846	1.857692562
MTMR4	0.928434	0.928434	1.856868848
COL3A1	0.927861	0.927861	1.855721013
SFPQ	0.927746	0.927746	1.855491611
UBE3A	0.926206	0.926206	1.852411216
TAGLN	0.926113	0.926113	1.852226133
RAB10	0.926111	0.926111	1.852222265
PDCD4	0.927942	0.924268	1.852209579
TCF12	0.925501	0.925501	1.851001477
CDC34	0.925157	0.925157	1.850313512

IRAK1	0.925093	0.925093	1.850185498
MBNL1	0.924626	0.924626	1.849252167
ULK2	0.924052	0.924052	1.848104109
H2AFZ	0.923771	0.923771	1.847541754
YWHAG	0.923298	0.923298	1.846596511
ZFPM2	0.922762	0.922762	1.845524212
C1orf21	0.921645	0.921645	1.843289025
LYPLA1	0.921258	0.921258	1.842515863
PFN2	0.920682	0.920682	1.841363498
FBN2	0.888	0.953107	1.841106275
PGRMC2	0.919971	0.919971	1.839942078
RASSF5	0.919494	0.919494	1.83898797
TGFBR3	0.918804	0.918804	1.837608367
BNIP3L	0.918607	0.918607	1.837213844
SP3	0.927936	0.908934	1.836870033
RPS6KB1	0.93287	0.902478	1.835348129
CBX1	0.917171	0.917171	1.834341522
PKP4	0.904889	0.92894	1.833828183
PPP2R2A	0.915916	0.915916	1.831832351
BRD3	0.915404	0.915404	1.830808871
MACF1	0.915282	0.915282	1.83056304
EIF5	0.915281	0.915281	1.830561505
NDST2	0.914595	0.914595	1.82918952
NR3C1	0.913945	0.913945	1.827889241
ITGB1	0.913665	0.913665	1.827329336
NEDD9	0.91291	0.91291	1.825819984
KIF5A	0.912755	0.912755	1.825509474
UPF2	0.912639	0.912639	1.825277038
RANBP2	0.903597	0.92136	1.824956978
PAFAH1B1	0.954247	0.869169	1.823416185
CLCN3	0.911526	0.911526	1.823051512
NF1	0.911402	0.911402	1.822803868
STC1	0.866479	0.95524	1.821718586
CITED2	0.910704	0.910704	1.821408083
IRS2	0.910191	0.910191	1.820382296
MAPK14	0.909789	0.909789	1.819577819
NDEL1	0.909205	0.909205	1.818410869
USP15	0.94925	0.867962	1.817211477
OSBPL3	0.908229	0.908229	1.816457289
ATP6V1B2	0.90797	0.90797	1.815940117
PDE7B	0.906353	0.906353	1.812706306
DEK	0.906189	0.906189	1.812377878
PPP2CA	0.906039	0.906039	1.812078715
ATP1B1	0.926344	0.884796	1.811139974
PTPRG	0.905517	0.905517	1.81103358
DDX5	0.905441	0.905441	1.810881804
VCL	0.90523	0.90523	1.810460886
TMEM2	0.904697	0.904697	1.80939306

NAP1L1	0.904307	0.904307	1.808614771
EP300	0.904225	0.904225	1.808450766
STK39	0.903176	0.903176	1.806351819
MAPK6	0.90276	0.90276	1.805520522
BCL2L2	0.917814	0.887304	1.80511858
OSBPL11	0.901893	0.901893	1.803786312
TGIF2	0.906122	0.896621	1.802743292
DTNA	0.899	0.899	1.798000397
PPP2CB	0.898611	0.898611	1.797221401
LATS2	0.898574	0.898574	1.79714745
STRBP	0.898214	0.898214	1.796427314
COL5A2	0.897551	0.897551	1.795102857
LAMC1	0.89969	0.895359	1.795049038
GNG5	0.896844	0.896844	1.793688654
ACTR2	0.920978	0.872637	1.79361458
ERCC6	0.896738	0.896738	1.793475775
NFIB	0.908498	0.884166	1.792663139
MBNL2	0.896199	0.896199	1.792398744
FIGN	0.895975	0.895975	1.791950508
RBM15	0.895845	0.895845	1.791690343
FLOT2	0.895828	0.895828	1.791655579
SYNE1	0.894994	0.894994	1.789987909
BTBD3	0.89498	0.89498	1.789959782
KHDRBS3	0.894869	0.894869	1.789737277
ZFP36L2	0.894857	0.894857	1.789713908
TAF12	0.893657	0.893657	1.78731492
RECK	0.901391	0.88577	1.787160592
APC	0.893481	0.893481	1.786961844
SIAH1	0.893082	0.893082	1.786164527
USP3	0.893053	0.893053	1.786106663
YY1	0.892234	0.892234	1.784467192
ATP2B1	0.927182	0.856928	1.784110543
CSNK2A1	0.892003	0.892003	1.784006392
MEIS2	0.891983	0.891983	1.783966902
RARA	0.891706	0.891706	1.783412439
KPNA1	0.891691	0.891691	1.783381664
PKIA	0.904605	0.877152	1.781756711
BTG1	0.890422	0.890422	1.780844122
PNN	0.88945	0.88945	1.778900735
PPP2R5E	0.883202	0.895047	1.778248479
DPYSL3	0.889065	0.889065	1.778129145
GNAI3	0.884002	0.891804	1.775806534
EIF4B	0.887381	0.887381	1.774762027
CAPZA2	0.88736	0.88736	1.774719988
FOXA1	0.887223	0.887223	1.774446464
SRGAP1	0.887214	0.887214	1.774427023
ANP32E	0.886531	0.886531	1.773062874
INPP5A	0.886495	0.886495	1.772989227

CCND1	0.92084	0.850945	1.771784626
CELSR2	0.885635	0.885635	1.7712699
RAB5B	0.885446	0.885446	1.770892072
SEC14L1	0.885154	0.885154	1.770307767
ADRB2	0.885066	0.885066	1.77013168
MATR3	0.875211	0.894504	1.76971449
PPP1R15B	0.884724	0.884724	1.769447886
UBE2D1	0.831512	0.936784	1.768296734
PPP2R5C	0.883638	0.883638	1.767276154
RALA	0.883503	0.883503	1.767005259
RBBP6	0.898099	0.868606	1.766704611
OSMR	0.883037	0.883037	1.766074848
ATP2A2	0.882858	0.882858	1.765716968
CDC42	0.910913	0.853701	1.76461439
SLC2A1	0.881486	0.881486	1.762972464
NRP2	0.880984	0.880984	1.761968287
FEM1C	0.880605	0.880605	1.761209763
PDCD10	0.879941	0.879941	1.75988234
PPP1R12A	0.879498	0.879498	1.758995306
LBR	0.898383	0.860604	1.758986932
SOX4	0.87917	0.87917	1.758340521
VAPA	0.878822	0.878822	1.757643407
IPO7	0.878794	0.878794	1.75758833
BZW2	0.878274	0.878274	1.756548157
CXCL12	0.915549	0.839038	1.754587049
PPP3CA	0.877141	0.877141	1.754281157
UTRN	0.876759	0.876759	1.753518453
COPS7B	0.876666	0.876666	1.753332292
COL1A1	0.873656	0.879505	1.753160606
ZYX	0.890345	0.862801	1.753146408
DYRK2	0.876143	0.876143	1.752285475
CLASP2	0.875855	0.875855	1.751710028
CDC25A	0.875445	0.875445	1.750889132
VAV3	0.875261	0.875261	1.750522555
CDYL	0.817087	0.933362	1.750448508
HOXA9	0.874865	0.874865	1.749730722
SNX1	0.874798	0.874798	1.749595363
TNFRSF1B	0.86847	0.881092	1.749561709
QARS	0.874726	0.874726	1.749451108
MAPRE1	0.897269	0.850396	1.747665587
ID4	0.872212	0.872212	1.74442386
PLEKHA1	0.871909	0.871909	1.743817589
JAG1	0.871823	0.871823	1.743645616
NRP1	0.871287	0.871287	1.742573115
SMARCC1	0.870782	0.870782	1.741564527
CTNND1	0.870664	0.870664	1.741328824
EIF4A2	0.870345	0.870345	1.740689727
COL4A1	0.869312	0.869312	1.738624629

AEBP2	0.810345	0.926472	1.736817531
SEC23IP	0.866948	0.866948	1.733895316
NUMB	0.866521	0.866521	1.733042623
STXBP5	0.866035	0.866035	1.732069338
TYRO3	0.865757	0.865757	1.731514606
PDAP1	0.865552	0.865552	1.731104029
TARDBP	0.865489	0.865489	1.730977256
DOT1L	0.864375	0.864375	1.728750343
ABCE1	0.864264	0.864264	1.728527917
PGRMC1	0.864228	0.864228	1.72845566
MYEF2	0.84503	0.883045	1.728074937
EGR1	0.863954	0.863954	1.727907247
NME4	0.863123	0.863123	1.7262454
ESRRA	0.863089	0.863089	1.72617892
DLG5	0.843867	0.881699	1.725565865
EPHA2	0.862675	0.862675	1.725349132
INSIG1	0.862319	0.862319	1.724637742
FARP1	0.86228	0.86228	1.724559038
PPM1A	0.924416	0.799085	1.723501064
CLK3	0.861102	0.861102	1.722204017
RCN2	0.867632	0.85449	1.722122191
MTMR6	0.860438	0.860438	1.720876456
BLMH	0.859602	0.859602	1.719203775
TRAM1	0.871966	0.847048	1.719013439
TCERG1	0.859314	0.859314	1.718627326
USP10	0.859059	0.859059	1.718118412
RASA1	0.917602	0.799981	1.717582414
POGZ	0.858499	0.858499	1.716998199
DAG1	0.870717	0.845564	1.71628079
ZNF292	0.874114	0.842	1.716114591
TCF4	0.875814	0.840167	1.715981659
RNF11	0.857949	0.857949	1.715898297
UBE2V1	0.894855	0.819422	1.714276831
WRNIP1	0.857116	0.857116	1.714231721
CHD1	0.857008	0.857008	1.714016262
UBE2D3	0.89152	0.822483	1.71400287
ARPC5	0.856283	0.856283	1.712565096
RAI14	0.855959	0.855959	1.711917038
MAP4K4	0.855711	0.855711	1.711422503
DOCK4	0.855259	0.855259	1.710518705
EDN1	0.855166	0.855166	1.710331125
RYBP	0.855121	0.855121	1.710241416
UBE2G1	0.853889	0.853889	1.707777546
CLNS1A	0.853517	0.853517	1.707033851
CD47	0.853492	0.853492	1.706983179
EML4	0.852319	0.852319	1.704638449
CRIM1	0.920741	0.78373	1.704471037
ADRB3	0.851857	0.851857	1.703713315

FOXC1	0.851842	0.851842	1.703684552
BTG2	0.85904	0.84455	1.703589386
NLGN1	0.91603	0.78738	1.703410768
AHR	0.851581	0.851581	1.703161653
SPAG9	0.851197	0.851197	1.702394316
CLDN12	0.851158	0.851158	1.702315598
COL4A2	0.850956	0.850956	1.701911433
MAT2A	0.850862	0.850862	1.701723469
USP25	0.931467	0.769689	1.701156269
HMGA1	0.850365	0.850365	1.700730412
CLIC4	0.850002	0.850002	1.70000397
LRRN3	0.849776	0.849776	1.699551252
RGS2	0.849379	0.849379	1.698757397
PPP1R11	0.890923	0.806631	1.697553824
MAPK9	0.848624	0.848624	1.697247211
DLST	0.848444	0.848444	1.696887788
SPRED1	0.834278	0.862542	1.696819547

Appendix 8: Combined integrative scores for top 200 MiRDIP predicted gene targets of cellular miRs expressed in ciGEnCs under both TNF- α treatment conditions (10 ng/µl TNF-α, 25 mM glucose + 10 ng/µl TNF-α), used for STRING analysis

Gene Name	Integrative score in each condition		Combined integrative score
	5mM + TNF-α	25mM + TNF-α	
BZW1	0.982299863	0.982299863	1.964599726
COL1A2	0.965908585	0.976780797	1.942689382
HMGA2	0.970436279	0.970436279	1.940872559
PPP6C	0.96598892	0.96598892	1.931977841
DUSP1	0.956893766	0.9717672	1.928660966
GALNT1	0.952344244	0.952344244	1.904688488
SNRK	0.949257148	0.949257148	1.898514297
FBN2	0.944439961	0.953106616	1.897546577
PAPPA	0.963751128	0.933616988	1.897368116
KIF1B	0.950075257	0.942635515	1.892710772
ZFYVE26	0.943024491	0.943024491	1.886048982
SLC4A4	0.940823424	0.940823424	1.881646849
RDX	0.940106912	0.940106912	1.880213823
CHD4	0.939849896	0.939849896	1.879699791
PDCD4	0.953635468	0.924267911	1.877903379
TLK1	0.945176819	0.932360056	1.877536876
N4BP1	0.935051299	0.935051299	1.870102597
DYRK1A	0.934943624	0.934943624	1.869887248
PTP4A1	0.932062781	0.937658282	1.869721063
PRDM2	0.933976606	0.933976606	1.867953211
RAB1A	0.931085422	0.936419871	1.867505292
TCF12	0.941257328	0.925500739	1.866758067
EIF4G2	0.930329851	0.936310568	1.866640419
FEZ2	0.94323777	0.922543228	1.865780998
KPNA4	0.912056962	0.953209485	1.865266447
HIC2	0.930854448	0.930854448	1.861708895
YWHAH	0.93068678	0.93068678	1.86137356
CCND2	0.929144233	0.929144233	1.858288465
GLUD1	0.929056215	0.929056215	1.858112431
RAP2C	0.928846281	0.928846281	1.857692562
MTMR4	0.928434424	0.928434424	1.856868848
ADD3	0.972397316	0.883689779	1.856087095
COL3A1	0.927860507	0.927860507	1.855721013
STC1	0.897995957	0.955240016	1.853235973
PFN2	0.931936896	0.920681749	1.852618644
NR5A2	0.951482257	0.900747898	1.852230156
RAB10	0.926111132	0.926111132	1.852222265
CDC34	0.925156756	0.925156756	1.850313512
IRAK1	0.925092749	0.925092749	1.850185498
NEDD9	0.937145089	0.912909992	1.850055081
MBNL1	0.924626083	0.924626083	1.849252167

ULK2	0.924052055	0.924052055	1.848104109
KPNA3	0.915160643	0.932763192	1.847923835
E2F3	0.903447828	0.942688689	1.846136517
ZFPM2	0.922762106	0.922762106	1.845524212
DR1	0.885652976	0.958224994	1.84387797
PPP2R2A	0.926355326	0.915916175	1.842271502
TOB1	0.927110616	0.913950293	1.841060909
RASSF5	0.919493985	0.919493985	1.83898797
C1orf21	0.916707784	0.921644512	1.838352296
TGFBR3	0.918804184	0.918804184	1.837608367
EIF5	0.915280752	0.915280752	1.830561505
RANBP2	0.909079675	0.921360189	1.830439864
RAP1B	0.885061889	0.944854853	1.829916742
NDST2	0.91459476	0.91459476	1.82918952
KIF5A	0.912754737	0.912754737	1.825509474
UPF2	0.912638519	0.912638519	1.825277038
PAFAH1B1	0.954247158	0.869169027	1.823416185
NF1	0.911401934	0.911401934	1.822803868
ATP1B1	0.937390683	0.8847962	1.822186883
CITED2	0.910704042	0.910704042	1.821408083
VCL	0.914523437	0.905230443	1.81975388
JAG1	0.94785495	0.871822808	1.819677758
NDEL1	0.909205434	0.909205434	1.818410869
YWHAG	0.89506034	0.923298256	1.818358595
SP3	0.908933769	0.908933769	1.817867538
EPS8	0.908983805	0.908798003	1.817781808
USP15	0.94924978	0.867961697	1.817211477
SRGAP1	0.929936649	0.887213512	1.817150161
OSBPL3	0.908228645	0.908228645	1.816457289
NFIB	0.930178	0.884165565	1.814343565
AEBP2	0.887331754	0.926472493	1.813804247
PPP3CA	0.936209307	0.877140579	1.813349886
CDYL	0.879565407	0.933361841	1.812927248
AP3S1	0.900213376	0.911614315	1.811827691
DDX5	0.906034581	0.905440902	1.811475483
TMEM2	0.90469653	0.90469653	1.80939306
NAP1L1	0.904307386	0.904307386	1.808614771
IRS2	0.898376229	0.910191148	1.808567376
VAV3	0.932109604	0.875261278	1.807370881
PPP2R5E	0.912110961	0.895046591	1.807157552
EIF4A2	0.936718611	0.870344863	1.807063474
FN1	0.903623427	0.903138504	1.80676193
MAPK6	0.902760261	0.902760261	1.805520522
RPS6KB1	0.902930926	0.902477716	1.805408642
BCL2L2	0.91781412	0.887304459	1.80511858
MMD	0.902261177	0.901643678	1.803904854
TGIF2	0.906122221	0.896621071	1.802743292
USP3	0.909083567	0.893053331	1.802136898

HBP1	0.932306752	0.869363868	1.80167062
LATS2	0.898573725	0.898573725	1.79714745
STRBP	0.898213657	0.898213657	1.796427314
ID4	0.923771883	0.87221193	1.795983813
COL5A2	0.897551428	0.897551428	1.795102857
LAMC1	0.899689853	0.895359186	1.795049038
KPNA1	0.902412695	0.891690832	1.794103527
GNG5	0.896844327	0.896844327	1.793688654
ACTR2	0.920977631	0.872636949	1.79361458
ERCC6	0.896737888	0.896737888	1.793475775
MBNL2	0.896199372	0.896199372	1.792398744
FIGN	0.895975254	0.895975254	1.791950508
FLOT2	0.89582779	0.89582779	1.791655579
BTBD3	0.894979891	0.894979891	1.789959782
MATR3	0.895209841	0.894503837	1.789713678
RAB5B	0.904084497	0.885446036	1.789530533
PLEKHA1	0.917617234	0.871908795	1.789526029
RECK	0.901390587	0.885770006	1.787160592
APC	0.893480922	0.893480922	1.786961844
MEIS2	0.891983451	0.891983451	1.783966902
ARHGAP12	0.940699262	0.842937025	1.783636286
GNAI3	0.891804154	0.891804154	1.783608309
PDCD10	0.902250738	0.87994117	1.782191908
BRD3	0.865737909	0.915404435	1.781142345
PNN	0.889450368	0.889450368	1.778900735
PPM1F	0.888939339	0.888939339	1.777878678
INSIG1	0.91428992	0.862318871	1.776608791
GPM6A	0.888148965	0.887318196	1.775467161
SIN3A	0.828185007	0.946991177	1.775176184
EIF4B	0.887381014	0.887381014	1.774762027
CAPZA2	0.887359994	0.887359994	1.774719988
PKIA	0.896072762	0.877152026	1.773224787
INPP5A	0.886494614	0.886494614	1.772989227
FEM1C	0.892043871	0.880604881	1.772648752
NRP1	0.901054337	0.871286558	1.772340894
CCND1	0.920839637	0.850944989	1.771784626
CELSR2	0.88563495	0.88563495	1.7712699
MTMR2	0.919542529	0.851227794	1.770770323
SEC14L1	0.885153884	0.885153884	1.770307767
ADRB2	0.88506584	0.88506584	1.77013168
NUP153	0.884961535	0.884961535	1.769923069
PPP1R15B	0.884723943	0.884723943	1.769447886
RBBP6	0.898099087	0.868605524	1.766704611
MYEF2	0.883045176	0.883045176	1.766090352
ALCAM	0.885017664	0.881062821	1.766080485
OSMR	0.883037424	0.883037424	1.766074848
SIAH1	0.871865309	0.893082264	1.764947572
HIPK1	0.926847796	0.837822998	1.764670793

CDC42	0.910912998	0.853701392	1.76461439
ATP2A2	0.879878469	0.882858484	1.762736953
NR3C1	0.848778626	0.913944621	1.762723246
NRP2	0.880984144	0.880984144	1.761968287
CPLX1	0.880971543	0.880971543	1.761943087
MAP3K3	0.915728155	0.845867506	1.761595661
CNN3	0.880617302	0.880617302	1.761234603
ARPC5	0.904613715	0.856282548	1.760896263
ELK3	0.907227106	0.852540423	1.759767529
PPP1R12A	0.879497653	0.879497653	1.758995306
VAPA	0.878821703	0.878821703	1.757643407
RANBP9	0.854853881	0.902758542	1.757612423
CBX1	0.839388751	0.917170761	1.756559512
BZW2	0.878274079	0.878274079	1.756548157
MSN	0.877830292	0.877830292	1.755660585
MAPRE1	0.904595433	0.850396299	1.754991731
SACS	0.929875716	0.824029959	1.753905675
SOX4	0.874711849	0.879170261	1.75388211
UTRN	0.876759227	0.876759227	1.753518453
COPS7B	0.876666146	0.876666146	1.753332292
COL1A1	0.87365603	0.879504576	1.753160606
ZYX	0.89034532	0.862801089	1.753146408
CLASP2	0.877263485	0.875855014	1.753118499
PGRMC2	0.832826105	0.919971039	1.752797144
DYRK2	0.876142737	0.876142737	1.752285475
PPP2CA	0.84516245	0.906039358	1.751201808
CDC25A	0.875444566	0.875444566	1.750889132
RCN2	0.895833679	0.854490289	1.750323969
HOXA9	0.874865361	0.874865361	1.749730722
TNFRSF1B	0.868469956	0.881091753	1.749561709
QARS	0.874725554	0.874725554	1.749451108
FBXW2	0.921712538	0.827482154	1.749194692
OSBPL11	0.846656128	0.901893156	1.748549284
POGZ	0.889649033	0.858499099	1.748148133
AP1S2	0.885228966	0.862005658	1.747234624
PPP2R5C	0.861419582	0.883638077	1.745057659
SMARCC1	0.870782264	0.870782264	1.741564527
CTNND1	0.870664412	0.870664412	1.741328824
WAC	0.869787343	0.869787343	1.739574685
CTNNBIP1	0.876111293	0.862774631	1.738885924
PHTF2	0.902572681	0.836103544	1.738676225
COL4A1	0.869312314	0.869312314	1.738624629
SOX9	0.887842964	0.850750119	1.738593083
HIVEP2	0.928159597	0.809754938	1.737914534
MTHFD2	0.927666353	0.809280999	1.736947352
CBFB	0.87558774	0.86040729	1.73599503
NDFIP1	0.821657726	0.913410841	1.735068567
SRF	0.870359829	0.863382731	1.733742561

NPTX1	0.890607027	0.842543265	1.733150292
NUMB	0.866521311	0.866521311	1.733042623
STXBP5	0.866034669	0.866034669	1.732069338
PDAP1	0.865552014	0.865552014	1.731104029
TARDBP	0.865488628	0.865488628	1.730977256
CLCN3	0.81831821	0.911525756	1.729843966
MARCKS	0.869816581	0.859276816	1.729093397
DOT1L	0.864375171	0.864375171	1.728750343
ABCE1	0.864263959	0.864263959	1.728527917
PGRMC1	0.86422783	0.86422783	1.72845566
NOG	0.864116039	0.864116039	1.728232078
ZNF148	0.902626826	0.825387661	1.728014486
CSNK1A1	0.945430953	0.782581193	1.728012146
NME4	0.8631227	0.8631227	1.7262454
ESRRA	0.86308946	0.86308946	1.72617892
DLG5	0.843866541	0.881699324	1.725565865
FOXA1	0.838307091	0.887223232	1.725530323
SMARCD2	0.89199718	0.833339818	1.725336997
CNOT6L	0.884521288	0.840599006	1.725120294
FARP1	0.862279519	0.862279519	1.724559038
EP300	0.820110674	0.904225383	1.724336056
BAZ2B	0.870800866	0.853223918	1.724024784
PKD1	0.86725582	0.856317031	1.723572851
PPM1A	0.92441636	0.799084704	1.723501064
LBR	0.860604168	0.860604168	1.721208337
PDE7B	0.814480019	0.906353153	1.720833172
CNOT7	0.91024713	0.810508315	1.720755444
RBBP7	0.83249138	0.887167761	1.719659141
BLMH	0.859601887	0.859601887	1.719203775
TRAM1	0.871965843	0.847047596	1.719013439
TCF4	0.878534761	0.840167364	1.718702125
SPRED1	0.85430153	0.862542001	1.716843531
AKAP12	0.933651182	0.782710644	1.716361826
DAG1	0.870716759	0.845564031	1.71628079
CLDN12	0.865120294	0.851157799	1.716278093
H3F3B	0.729764723	0.986407325	1.716172048
MAP4K4	0.860193337	0.855711252	1.715904589
CDR2	0.857917397	0.857917397	1.715834793
UBE2V1	0.894854736	0.819422095	1.714276831
CHD1	0.857008131	0.857008131	1.714016262
ATP2B1	0.856928137	0.856928137	1.713856273
DNMT3A	0.817030748	0.896606045	1.713636793
DPYSL2	0.882214187	0.830457378	1.712671566
CRIM1	0.928533661	0.783730403	1.712264064
RAI14	0.855958519	0.855958519	1.711917038
EDN1	0.855165562	0.855165562	1.710331125
NPAS2	0.916984224	0.793273007	1.710257231
RYBP	0.855120708	0.855120708	1.710241416

PSIP1	0.855323033	0.854829225	1.710152257
SMOC2	0.890513151	0.819322437	1.709835587
SEC23IP	0.842642787	0.866947658	1.709590445
DTNA	0.81045182	0.899000199	1.709452019
UBE2D3	0.886735976	0.822483103	1.709219079
BNIP3L	0.790453114	0.918606922	1.709060036
ASF1A	0.853954453	0.853954453	1.707908905
PTPRG	0.800464873	0.90551679	1.705981663
FAM8A1	0.852582947	0.852582947	1.705165894
HIF1A	0.857670189	0.846615829	1.704286018
ADRB3	0.851856657	0.851856657	1.703713315
BTG2	0.859039624	0.844549762	1.703589386
NLGN1	0.916030322	0.787380446	1.703410768
CPD	0.874582639	0.82858145	1.70316409
AHR	0.851580827	0.851580827	1.703161653
RUNX1	0.855401327	0.847748188	1.703149515
ETS1	0.867043186	0.834914297	1.701957482

Appendix 9: Integrative scores for top 200 MiRDIP predicted gene targets of miRs detected in the medium of ciGEnCs under the 25 mM glucose concentration treatment condition, used for STRING analysis

Gene Name	Integrative Score
COL1A2	0.9767808
HMGA2	0.97043628
ARID3B	0.96244326
MIER1	0.96216139
CACNB2	0.96133696
FBXW11	0.96059451
MAP4K3	0.95972466
PBX3	0.95771519
ONECUT1	0.95692517
FAM3C	0.95635408
ADD3	0.9562834
FMR1	0.95579937
FXR1	0.95538986
KPNA4	0.95468574
COL15A1	0.9541353
ACTN1	0.95397201
NEDD4	0.95338173
CLIP1	0.95312455
CAPZA1	0.9529181
EIF4E	0.95260876
RNF103	0.95175707
NR5A2	0.95148226
QKI	0.95120429
ANK3	0.95036695
ACVR1	0.95022086
ELAVL1	0.94979532
KPNA3	0.9495237
ATXN1	0.94939196
NCOR2	0.94900567
AKAP1	0.94833857
LRIG3	0.94803503
RALBP1	0.94766879
TBPL1	0.94715716
SNX2	0.94631875
KDM2A	0.94630514
TNRC6A	0.94628011
TSC22D2	0.94617575
RNF38	0.94616175
RAB14	0.94583432
YBX3	0.94541548
ARID1A	0.94533156
FGF9	0.9452976
TOB1	0.94527134
AGO4	0.94478163
PPP3R1	0.94471419
S1PR1	0.94420805
SMARCAD1	0.94405909
SMARCA5	0.94393431
EIF4G2	0.94365119
GALNT3	0.9433774
NAMPT	0.94317673
FOXO3	0.94317345
SOCS5	0.94228805
IGF2BP3	0.94194381
AP3B1	0.94165958
CAMSAP2	0.94139262
VGLL4	0.94124393
MTSS1	0.94109962
SLC4A4	0.94082342
SHANK2	0.94076198
YES1	0.9406225
RDX	0.94010691
NUMB	0.93998746
CHD4	0.93996161
ZFPM2	0.93958366
ACSL1	0.93941712
SYNJ1	0.93887406
MPHOSPH9	0.93870792
H3F3B	0.93812075
TLK1	0.93790921
SP3	0.93789721
SMAD1	0.93773901
ATP1B1	0.93739068
MYO1C	0.93734972
PUM2	0.93723356
FOXP1	0.93712523
ABRAXAS2	0.93711523
ZNF217	0.93709608
ZFC3H1	0.93701464
UBE2D1	0.93678428
MITF	0.93677974
RET	0.93673983
STAM	0.93646736
KTN1	0.93644038
RAB1A	0.93641987
SEMA5A	0.93623246
LMO2	0.93567414
CTTN	0.93554427
DYRK1A	0.93494362
UBE3C	0.93488072
FBXW7	0.9346033
CCNJ	0.9345131
MBNL1	0.93443004
FNDC3A	0.93431786
ARL8B	0.93418151
BMI1	0.9340911
PRDM2	0.93397661
DDX19B	0.93396827
NAA15	0.9334624
FOXN3	0.93336458
CDYL	0.93336184
PPP2R2A	0.93323993
RPS6KB1	0.93287041
ANO1	0.93285755
ACVR2A	0.9327814
DR1	0.93260572
PAIP2	0.93243789
MTOR	0.93232794
RNF219	0.93187004
DCBLD2	0.93156288
CREB1	0.93113974
INTS6	0.93093335
ACSL4	0.93081618
KCNJ2	0.93054905
CTCF	0.93034226
CUL5	0.93023823
PDGFRB	0.93005533
ARID4B	0.92998871
SIK2	0.92986791
ACVR1C	0.92944217
EPHA7	0.92942251
ELK3	0.92934546
CCND2	0.92914423
SIRT1	0.92909107
NPTN	0.92906484
PKP4	0.92893962
CHD9	0.92887132
CCDC6	0.92873043
YWHAG	0.92862288
CRIM1	0.92853366
PEX5L	0.9284787
COIL	0.92822111
PDGFC	0.9278362
MTHFD2	0.92766635
CDV3	0.92749741
ATP2B1	0.92718241
EPHA4	0.92714837
BMPR2	0.9269145
HIPK1	0.9268478
TAF15	0.92670784
DDX6	0.9266681
GOT1	0.92653281
CELF1	0.9260306

IGF2BP2	0.92587966
TRIM2	0.92572265
PAN3	0.92556122
PIEZO2	0.92552335
SNX16	0.92533949
CDC34	0.92515676
IRAK1	0.92509275
HBP1	0.92497804
SH3RF1	0.92471094
AP4E1	0.92449813
SGMS1	0.92412614
RNF111	0.9240895
BICD2	0.92405457
ULK2	0.92405205
FOS	0.92390196
CDK17	0.92381996
HECTD2	0.92363494
CITED2	0.92354759
PDGFRA	0.92330465
ST8SIA4	0.92316893
UBE2H	0.92291215
LSM14A	0.92275557
MECOM	0.9227503
KLF5	0.92273627
HIVEP1	0.92272877
ZFYVE9	0.92264493
NMT2	0.92238038
CBFA2T3	0.9223712
ARHGAP12	0.92199645
RNF139	0.92193356
DOCK3	0.92192103
FBXW2	0.92171254
RANBP2	0.92136019
SULF1	0.92135149
ERBIN	0.92133258
USP48	0.92112708
JAZF1	0.92106731
CD2AP	0.92084422
ZDHHC17	0.92051381
WDR47	0.92019178
NAV3	0.91994895
CUL3	0.91983409
PAFAH1B1	0.91973034
SKP1	0.9194376
SRSF11	0.9194226
BCL9	0.91922381
MGAT4A	0.91913165
ARHGEF7	0.91882637
FLRT3	0.91850997
UBR3	0.91846983
CMPK1	0.91843959
C16orf70	0.91815617
RNF19A	0.91783925
ZEB1	0.91774624
SHC1	0.91760016
BACH2	0.9174413
TCF20	0.91723164

Appendix 10: Integrative scores for top 200 MiRDIP predicted gene targets of miRs detected in the medium of ciGEnCs under the 5 mM glucose + TNF- α treatment condition, used for STRING analysis

Gene Name	Integrative Score
COL1A2	0.9767808
MYH10	0.97268933
HMGA2	0.97043628
ARID3B	0.96244326
MAP2K4	0.96193621
FBXW11	0.96059451
MAP4K3	0.95972466
ZEB2	0.95925504
DR1	0.95822499
PBX3	0.95771519
ONECUT1	0.95692517
ADD3	0.9562834
FMR1	0.95579937
FXR1	0.95538986
COL15A1	0.9541353
NEDD4	0.95338173
KPNA4	0.95320948
CAPZA1	0.9529181
EIF4E	0.95260876
NR5A2	0.95148226
ANK3	0.95036695
ELAVL1	0.94979532
KPNA3	0.9495237
LRIG3	0.94803503
ATXN1	0.94785036
CUL3	0.94732903
TBPL1	0.94715716
TSC22D2	0.94617575
KLF12	0.94585298
RAB14	0.94583432
YBX3	0.94541548
TFRC	0.9454147
QKI	0.94539444
FGF9	0.9452976
PPP3R1	0.94471419
SMARCAD1	0.94405909
GALNT3	0.9433774
NAMPT	0.94317673
FOXO3	0.94317345
SOCS5	0.94228805
IGF2BP3	0.94194381
AP3B1	0.94165958
CAMSAP2	0.94139262
ELAVL2	0.94113153
MTSS1	0.94109962
SLC4A4	0.94082342
YES1	0.9406225
RDX	0.94010691
NUMB	0.93998746
CHD4	0.9398499
TSHZ3	0.9396003
VGLL4	0.93845014
TLK1	0.93790921
SP3	0.93789721
SMAD1	0.93773901
ATP1B1	0.93739068
MYO1C	0.93734972
FOXP1	0.93712523
ZFC3H1	0.93701464
MITF	0.93677974
STAM	0.93646736
KTN1	0.93644038
EIF4G2	0.93631057
SEMA5A	0.93623246
CTTN	0.93554427
DYRK1A	0.93494362
UBE3C	0.93488072
CCNJ	0.9345131
FNDC3A	0.93431786
PRDM2	0.93397661
DDX19B	0.93396827
NAA15	0.9334624
FOXN3	0.93336458
ANO1	0.93285755
TOB1	0.93244505
PAIP2	0.93243789
ARID1A	0.93206823
CREB1	0.93113974
INTS6	0.93093335
KCNJ2	0.93054905
CUL5	0.93023823
PDGFRB	0.93005533
ACVR1C	0.92944217
EPHA7	0.92942251
LRP6	0.92928585
CCND2	0.92914423
SIRT1	0.92909107
YWHAG	0.92862288
CRIM1	0.92853366
COIL	0.92822111
PDGFC	0.9278362
SFPQ	0.92774581
MTHFD2	0.92766635
CDV3	0.92749741
EPHA4	0.92714837
HIPK1	0.9268478
TAF15	0.92670784
GOT1	0.92653281
UBE3A	0.92620561
DNAJC13	0.92612197
CELF1	0.9260306
IGF2BP2	0.92587966
TRIM2	0.92572265
TCF12	0.92550074
SNX16	0.92533949
CDC34	0.92515676
AP4E1	0.92449813
SGMS1	0.92412614
RNF111	0.9240895
ULK2	0.92405205
H2AFZ	0.92377088
CITED2	0.92354759
USP15	0.92315588
LSM14A	0.92275557
KLF5	0.92273627
CBFA2T3	0.9223712
FBXW2	0.92171254
RANBP2	0.92136019
ERBIN	0.92133258
JAZF1	0.92106731
ST8SIA4	0.92099245
CD2AP	0.92084422
SYNJ1	0.92047662
WDR47	0.92019178
PGRMC2	0.91997104
PAFAH1B1	0.91973034
MGAT4A	0.91913165
ARHGEF7	0.91882637
CDK17	0.91861678
RNF19A	0.91783925
ZEB1	0.91774624
SHC1	0.91760016
BACH2	0.9174413
CBX1	0.91717076
FAF2	0.91695351
EPHA3	0.91682992
BCL2	0.91678017
ANK2	0.91628342
PPP2R2A	0.91591618
MBNL1	0.915815
BRD3	0.91540444
MAP7	0.91533867
DYNC1I1	0.91531402

ARPC1A	0.91509945
TRPM7	0.9148895
ACVR1	0.91465499
NDST2	0.91459476
VCL	0.91452344
EIF5	0.91442615
ZNF532	0.91409676
KATNBL1	0.91403426
ERG	0.91388097
FAM91A1	0.91348383
RARB	0.91330127
AUH	0.91327889
PCMT1	0.91316369
SLC10A3	0.91290258
LIN28A	0.91284967
PHLDB2	0.91253546
STK38L	0.91246808
JMJD1C	0.91239909
PPP2R5E	0.91211096
PRKCE	0.91188939
IGF1R	0.91123894
ISL1	0.91087461
PID1	0.91078698
ZC3H15	0.91048333
PRKACB	0.91028242
MAGI1	0.9102254
IRS2	0.91019115
ACVR2A	0.91011153
SLC20A2	0.91008796
RUFY3	0.90985758
WDR37	0.90972988
SRPK1	0.90898982
EPS8	0.9089838
NR3C2	0.90882714
GOLT1B	0.90825915
OSBPL3	0.90822864
ATP6V1B2	0.90797006
SLC35D2	0.90796738
FAM13C	0.90785813
FRAS1	0.90719466
PPM1D	0.90688059
YPEL5	0.90684146
CADM1	0.90676793
SEMA6A	0.90675832
ARL3	0.90652646
KIAA1217	0.90641993
CCSER2	0.90630752
DEK	0.90618894
SHOC2	0.90611635
YAF2	0.90566278
CAB39	0.90560001
CHD9	0.90552518
DDX5	0.9054409
RAC1	0.90522439
PCDH18	0.90516381
GNPTAB	0.90512875
LPGAT1	0.90470498

Appendix 11: Integrative scores for top 200 MiRDIP predicted gene targets of miRs detected in the medium of ciGEnCs under the 25 mM glucose + TNF- α treatment condition, used for STRING analysis

Gene Name	Integrative Score
COL1A2	0.9767808
KPNA4	0.97327382
FGF2	0.97279405
ATP1B1	0.96635547
HMGA2	0.96478458
MIER1	0.96420801
SMAD7	0.96175949
PAFAH1B1	0.96060931
FBXW11	0.96059451
ZNRF2	0.95976358
RUNX1T1	0.958989
CUL3	0.95854765
CCNE1	0.95836378
AGO4	0.95760876
ARID3B	0.9572873
ACVR2A	0.95692968
ONECUT1	0.95692517
FAM3C	0.95635408
ADD3	0.9562834
BTRC	0.9562754
RAF1	0.9562253
USP15	0.9560337
FMR1	0.95579937
FXR1	0.95538986
GPR63	0.95527076
TRIB2	0.95448632
OGT	0.95435354
COL15A1	0.9541353
ACTN1	0.95397201
ACVR1	0.95372471
PDCD4	0.95363547
NEDD4	0.95338173
STXBP3	0.95325846
CLIP1	0.95312455
CAPZA1	0.9529181
EIF4E	0.95260876
KIF1B	0.95251816
RNF103	0.95175707
NR5A2	0.95148226
MCFD2	0.95104448
AXIN2	0.95098964
KCNJ2	0.95057721
ARMC1	0.95050301
ANK3	0.95036695
ELAVL1	0.94979532
KPNA3	0.9495237
SEC24C	0.94947654
TLK1	0.94941166
NCOR2	0.94900567
OSBPL3	0.94885738
ATP13A3	0.94884055
NACC2	0.94880966
PID1	0.94856524
AKAP1	0.94833857
JAG1	0.94785495
LRP6	0.94777552
RALBP1	0.94766879
MAP4K3	0.94742106
TBPL1	0.94715716
HNRNPU	0.94714696
SLC12A2	0.94679722
MAPRE1	0.9467581
SNX2	0.94647962
ATXN1	0.94636678
KDM2A	0.94630514
TSC22D2	0.94617575
RNF38	0.94616175
SKI	0.94614354
RAB14	0.94583432
CUL2	0.94558689
YBX3	0.94541548
QKI	0.94539444
FGF9	0.9452976
TOB1	0.94527134
PPP3R1	0.94471419
PPM1D	0.94415987
BACH2	0.94412347
SMARCA5	0.94393431
GALNT3	0.9433774
NAMPT	0.94317673
FOXO3	0.94317345
EIF4G2	0.94306974
CAB39	0.94269244
SOCS5	0.94228805
AP3B1	0.94165958
DYNC1I1	0.94155739
CLCN3	0.94145853
CAMSAP2	0.94139262
VGLL4	0.94124393
MTSS1	0.94109962
SHANK2	0.94076198
YES1	0.9406225
MOB4	0.94023662
MYB	0.94013507
NUMB	0.93998746
CHD4	0.93996161
AGFG1	0.93975754
ZFPM2	0.93958366
ACSL1	0.93941712
AKT3	0.93919228
DDX6	0.93907419
ACTR2	0.93894273
NEK6	0.93874569
MPHOSPH9	0.93870792
TNRC6A	0.93838535
H3F3B	0.93812075
N4BP1	0.93792442
SP3	0.93789721
LRIG3	0.93780145
SMAD1	0.93773901
MAP7	0.93769538
MPP5	0.93759971
USP25	0.93737085
SMARCAD1	0.93736285
MYO1C	0.93734972
CTCF	0.93726765
PUM2	0.93723356
FOXP1	0.93712523
ABRAXAS2	0.93711523
ZNF217	0.93709608
ZFC3H1	0.93701464
MITF	0.93677974
RET	0.93673983
STAM	0.93646736
KTN1	0.93644038
CTTN	0.93554427
BMPR2	0.93523874
PBX3	0.93501223
UBE3C	0.93488072
MBNL1	0.93443004
BMI1	0.9340911
ARHGAP12	0.93381812
NAA15	0.9334624
FOXN3	0.93336458
PPP2R2A	0.93323993
ANO1	0.93285755
PAIP2	0.93243789
MTOR	0.93232794
ARID1A	0.93206823
RNF219	0.93187004
CREB1	0.93113974

RBM6	0.93098869
INTS6	0.93093335
ACSL4	0.93081618
ZFYVE9	0.93050483
CUL5	0.93023823
NFIB	0.930178
PDGFRB	0.93005533
ARID4B	0.92998871
SIK2	0.92986791
AMBRA1	0.92944922
EPHA7	0.92942251
ELK3	0.92934546
PPM1A	0.92923221
COL4A1	0.92919965
SIRT1	0.92909107
GLUD1	0.92905622
BCL2L2	0.9289655
PKP4	0.92893962
CHD9	0.92887132
NPTN	0.92881093
CCDC6	0.92873043
SLC4A4	0.92866276
YWHAG	0.92862288
CRIM1	0.92853366
PEX5L	0.9284787
RAB11FIP2	0.92844614
MAP2K1	0.92816116
CSDE1	0.92801994
PDGFC	0.9278362
MTHFD2	0.92766635
DICER1	0.92759208
RDX	0.92744504
SYNJ1	0.92705998
PTEN	0.92684848
HIPK1	0.9268478
TAF15	0.92670784
UBE2D1	0.92665631
GOT1	0.92653281
AUH	0.92625861
RAB10	0.92611113
CELF1	0.9260306
TRIM2	0.92572265
HBP1	0.92564339
CMPK1	0.92563744
PAN3	0.92556122
KCNK10	0.92555535
PIEZO2	0.92552335
SNX16	0.92533949

IRAK1	0.92509275
IGF2BP3	0.92473992
FBXO33	0.92473524
SH3RF1	0.92471094
TCERG1	0.92461219
ERBIN	0.92456334
AP4E1	0.92449813
USP14	0.92439694
SGMS1	0.92412614
RNF111	0.9240895
DDX19B	0.92399446

Appendix 12: Combined integrative scores for top 200 MiRDIP predicted gene targets of miRs detected in the medium of ciGEnCs under all three treatment conditions (25 mM glucose, 10 ng/µl TNF-α, 25 mM glucose + 10 ng/µl TNF-α), used for STRING analysis

Gene Name	Integrative score in each condition			Combined integrative score
	25mM	5mM + TNF-α	25mM + TNF-α	
COL1A2	0.9767808	0.9767808	0.9767808	2.93034239
HMGA2	0.97043628	0.97043628	0.96478458	2.905657143
ARID3B	0.96244326	0.96244326	0.9572873	2.882173813
FBXW11	0.96059451	0.96059451	0.96059451	2.881783519
KPNA4	0.95468574	0.95320948	0.97327382	2.881169038
ONECUT1	0.95692517	0.95692517	0.95692517	2.870775505
ADD3	0.9562834	0.9562834	0.9562834	2.868850207
FMR1	0.95579937	0.95579937	0.95579937	2.867398122
MAP4K3	0.95972466	0.95972466	0.94742106	2.866870377
FXR1	0.95538986	0.95538986	0.95538986	2.866169595
COL15A1	0.9541353	0.9541353	0.9541353	2.862405914
NEDD4	0.95338173	0.95338173	0.95338173	2.860145178
CAPZA1	0.9529181	0.9529181	0.9529181	2.858754299
EIF4E	0.95260876	0.95260876	0.95260876	2.857826272
NR5A2	0.95148226	0.95148226	0.95148226	2.854446772
ANK3	0.95036695	0.95036695	0.95036695	2.851100836
PBX3	0.95771519	0.95771519	0.93501223	2.850442599
ELAVL1	0.94979532	0.94979532	0.94979532	2.849385966
KPNA3	0.9495237	0.9495237	0.9495237	2.848571113
ATXN1	0.94939196	0.94785036	0.94636678	2.843609104
QKI	0.95120429	0.94539444	0.94539444	2.841993169
TBPL1	0.94715716	0.94715716	0.94715716	2.841471469
ATP1B1	0.93739068	0.93739068	0.96635547	2.841136835
TSC22D2	0.94617575	0.94617575	0.94617575	2.838527257
RAB14	0.94583432	0.94583432	0.94583432	2.837502974
YBX3	0.94541548	0.94541548	0.94541548	2.83624645
FGF9	0.9452976	0.9452976	0.9452976	2.835892805
PPP3R1	0.94471419	0.94471419	0.94471419	2.834142558
LRIG3	0.94803503	0.94803503	0.93780145	2.833871508
GALNT3	0.9433774	0.9433774	0.9433774	2.830132209
NAMPT	0.94317673	0.94317673	0.94317673	2.829530181
FOXO3	0.94317345	0.94317345	0.94317345	2.829520351
SOCS5	0.94228805	0.94228805	0.94228805	2.826864164
CUL3	0.91983409	0.94732903	0.95854765	2.825710772
SMARCAD1	0.94405909	0.94405909	0.93736285	2.825481037
TLK1	0.93790921	0.93790921	0.94941166	2.825230076
AP3B1	0.94165958	0.94165958	0.94165958	2.824978725
CAMSAP2	0.94139262	0.94139262	0.94139262	2.824177866
MTSS1	0.94109962	0.94109962	0.94109962	2.823298869
EIF4G2	0.94365119	0.93631057	0.94306974	2.823031493
TOB1	0.94527134	0.93244505	0.94527134	2.822987727

YES1	0.9406225	0.9406225	0.9406225	2.821867509
VGLL4	0.94124393	0.93845014	0.94124393	2.820937989
NUMB	0.93998746	0.93998746	0.93998746	2.819962367
CHD4	0.93996161	0.9398499	0.93996161	2.819773121
ACVR1	0.95022086	0.91465499	0.95372471	2.81860056
SP3	0.93789721	0.93789721	0.93789721	2.813691635
MIER1	0.96216139	0.88717127	0.96420801	2.813540668
SMAD1	0.93773901	0.93773901	0.93773901	2.813217034
MYO1C	0.93734972	0.93734972	0.93734972	2.81204917
KCNJ2	0.93054905	0.93054905	0.95057721	2.811675309
FOXP1	0.93712523	0.93712523	0.93712523	2.811375686
ZFC3H1	0.93701464	0.93701464	0.93701464	2.811043923
MITF	0.93677974	0.93677974	0.93677974	2.810339209
SLC4A4	0.94082342	0.94082342	0.92866276	2.810309608
ARID1A	0.94533156	0.93206823	0.93206823	2.809468033
STAM	0.93646736	0.93646736	0.93646736	2.809402083
KTN1	0.93644038	0.93644038	0.93644038	2.809321153
IGF2BP3	0.94194381	0.94194381	0.92473992	2.808627538
RDX	0.94010691	0.94010691	0.92744504	2.807658859
CTTN	0.93554427	0.93554427	0.93554427	2.806632823
UBE3C	0.93488072	0.93488072	0.93488072	2.804642175
NAA15	0.9334624	0.9334624	0.9334624	2.800387194
FOXN3	0.93336458	0.93336458	0.93336458	2.800093751
PAFAH1B1	0.91973034	0.91973034	0.96060931	2.800069979
ACVR2A	0.9327814	0.91011153	0.95692968	2.799822606
ANO1	0.93285755	0.93285755	0.93285755	2.798572663
PAIP2	0.93243789	0.93243789	0.93243789	2.797313656
CREB1	0.93113974	0.93113974	0.93113974	2.793419213
INTS6	0.93093335	0.93093335	0.93093335	2.792800044
DDX19B	0.93396827	0.93396827	0.92399446	2.791930995
ZEB2	0.91588498	0.95925504	0.91588498	2.791024994
CUL5	0.93023823	0.93023823	0.93023823	2.790714684
PDGFRB	0.93005533	0.93005533	0.93005533	2.790165995
DYRK1A	0.93494362	0.93494362	0.91929719	2.789184438
EPHA7	0.92942251	0.92942251	0.92942251	2.788267528
SIRT1	0.92909107	0.92909107	0.92909107	2.787273222
FNDC3A	0.93431786	0.93431786	0.91835886	2.786994582
SYNJ1	0.93887406	0.92047662	0.92705998	2.786410661
YWHAG	0.92862288	0.92862288	0.92862288	2.785868639
CRIM1	0.92853366	0.92853366	0.92853366	2.785600982
CLIP1	0.95312455	0.87928559	0.95312455	2.785534688
MBNL1	0.93443004	0.915815	0.93443004	2.784675081
AGO4	0.94478163	0.88219383	0.95760876	2.78458421
PRDM2	0.93397661	0.93397661	0.91607122	2.784024431
PDGFC	0.9278362	0.9278362	0.9278362	2.783508608
CCNJ	0.9345131	0.9345131	0.91415073	2.783176931
MTHFD2	0.92766635	0.92766635	0.92766635	2.78299906

PPP2R2A	0.93323993	0.91591618	0.93323993	2.782396026
ACVR1C	0.92944217	0.92944217	0.92307295	2.781957289
HIPK1	0.9268478	0.9268478	0.9268478	2.780543387
TAF15	0.92670784	0.92670784	0.92670784	2.780123511
USP15	0.90091932	0.92315588	0.9560337	2.780108891
GOT1	0.92653281	0.92653281	0.92653281	2.779598416
ZFPM2	0.93958366	0.90033583	0.93958366	2.779503141
CCND2	0.92914423	0.92914423	0.92103991	2.779328373
DR1	0.93260572	0.95822499	0.88824868	2.77907939
BACH2	0.9174413	0.9174413	0.94412347	2.779006058
CELF1	0.9260306	0.9260306	0.9260306	2.778091808
TRIM2	0.92572265	0.92572265	0.92572265	2.777167939
RNF38	0.94616175	0.8840958	0.94616175	2.776419293
SNX16	0.92533949	0.92533949	0.92533949	2.776018461
AP4E1	0.92449813	0.92449813	0.92449813	2.77349438
EPHA4	0.92714837	0.92714837	0.91843976	2.772736494
SGMS1	0.92412614	0.92412614	0.92412614	2.772378413
RNF111	0.9240895	0.9240895	0.9240895	2.772268497
COIL	0.92822111	0.92822111	0.91545051	2.771892725
CDC34	0.92515676	0.92515676	0.92093111	2.771244626
CITED2	0.92354759	0.92354759	0.92354759	2.770642755
MAP7	0.91533867	0.91533867	0.93769538	2.768372727
LSM14A	0.92275557	0.92275557	0.92275557	2.768266698
KLF5	0.92273627	0.92273627	0.92273627	2.7682088
CDV3	0.92749741	0.92749741	0.91254894	2.767543754
ULK2	0.92405205	0.92405205	0.91943294	2.767537054
ST8SIA4	0.92316893	0.92099245	0.92316893	2.767330298
ERBIN	0.92133258	0.92133258	0.92456334	2.767228501
CBFA2T3	0.9223712	0.9223712	0.9223712	2.767113603
IGF2BP2	0.92587966	0.92587966	0.91425935	2.766018671
CDK17	0.92381996	0.91861678	0.92350361	2.765940344
OSBPL3	0.90822864	0.90822864	0.94885738	2.765314667
FBXW2	0.92171254	0.92171254	0.92171254	2.765137614
RANBP2	0.92136019	0.92136019	0.92136019	2.764080568
CHD9	0.92887132	0.90552518	0.92887132	2.763267823
JAZF1	0.92106731	0.92106731	0.92106731	2.763201927
CD2AP	0.92084422	0.92084422	0.92084422	2.762532655
CCDC6	0.92873043	0.90412649	0.92873043	2.761587349
WDR47	0.92019178	0.92019178	0.92019178	2.760575339
ZNF217	0.93709608	0.883322	0.93709608	2.757514158
ARHGEF7	0.91882637	0.91882637	0.91882637	2.756479107
CAB39	0.90560001	0.90560001	0.94269244	2.75389247
RNF19A	0.91783925	0.91783925	0.91783925	2.75351774
SNX2	0.94631875	0.86051175	0.94647962	2.753310115
AUH	0.91327889	0.91327889	0.92625861	2.752816391
SHC1	0.91760016	0.91760016	0.91760016	2.752800472
SMAD7	0.89525944	0.89525944	0.96175949	2.752278364

DDX6	0.9266681	0.88545389	0.93907419	2.751196174
FAF2	0.91695351	0.91695351	0.91695351	2.750860531
BCL2	0.91678017	0.91678017	0.91678017	2.75034051
ANK2	0.91628342	0.91628342	0.91628342	2.748850266
HNRNPU	0.89986293	0.89986293	0.94714696	2.74687282
ARPC1A	0.91509945	0.91509945	0.91509945	2.745298358
TRPM7	0.9148895	0.9148895	0.9148895	2.744668505
EIF5	0.91442615	0.91442615	0.91528075	2.744133042
ARMC1	0.89653602	0.89653602	0.95050301	2.743575043
VCL	0.91452344	0.91452344	0.91452344	2.74357031
ERG	0.91388097	0.91388097	0.91388097	2.741642899
SLC10A3	0.91290258	0.91290258	0.91290258	2.73870773
LIN28A	0.91284967	0.91284967	0.91284967	2.738549003
RPS6KB1	0.93287041	0.90293093	0.90247772	2.738279055
KDM2A	0.94630514	0.84547354	0.94630514	2.738083813
PHLDB2	0.91253546	0.91253546	0.91253546	2.737606374
STK38L	0.91246808	0.91246808	0.91246808	2.73740423
JMJD1C	0.91239909	0.91239909	0.91239909	2.737197281
PCMT1	0.90952729	0.91316369	0.91108889	2.733779877
IGF1R	0.91123894	0.91123894	0.91123894	2.733716833
ZBTB5	0.91598624	0.90098668	0.91598624	2.732959158
SLC20A2	0.91008796	0.91008796	0.91275246	2.732928382
DNAJC13	0.9033877	0.92612197	0.9033877	2.732897378
ISL1	0.91087461	0.91087461	0.91087461	2.732623839
ZC3H15	0.91048333	0.91048333	0.91048333	2.731449999
TFRC	0.89288426	0.9454147	0.89288426	2.731183218
PRKACB	0.91028242	0.91028242	0.91028242	2.730847263
PDGFRA	0.92330465	0.88421177	0.92330465	2.730821075
MAGI1	0.9102254	0.9102254	0.9102254	2.73067619
SHANK2	0.94076198	0.84838653	0.94076198	2.729910486
PAN3	0.92556122	0.87776254	0.92556122	2.728884988
MGAT4A	0.91913165	0.91913165	0.89016491	2.7284282
NDST2	0.91459476	0.91459476	0.89792439	2.727113914
SRPK1	0.90898982	0.90898982	0.90898982	2.726969446
EPS8	0.9089838	0.9089838	0.908798	2.726765612
NCOR2	0.94900567	0.82704081	0.94900567	2.725052156
UBE3A	0.89940139	0.92620561	0.89940139	2.725008387
MOB4	0.89920985	0.88539844	0.94023662	2.724844902
SEC24C	0.89389157	0.88141067	0.94947654	2.72477878
FAM13C	0.90785813	0.90785813	0.90785813	2.72357438
PUM2	0.93723356	0.84842674	0.93723356	2.722893863
NFIB	0.90849757	0.88416557	0.930178	2.722841139
ELAVL2	0.8909092	0.94113153	0.88989771	2.721938436
WDR37	0.90972988	0.90972988	0.90196891	2.721428674
ACSL4	0.93081618	0.85922341	0.93081618	2.720855772
SLC12A2	0.91619878	0.85781792	0.94679722	2.720813919
CADM1	0.90676793	0.90676793	0.90676793	2.720303801

PPP2R5E	0.91211096	0.91211096	0.89605893	2.720280849
HBP1	0.92497804	0.86936387	0.92564339	2.7199853
KIAA1217	0.90641993	0.90641993	0.90641993	2.719259805
CCSER2	0.90630752	0.90630752	0.90630752	2.718922567
HECTD2	0.92363494	0.87119216	0.92363494	2.718462036
EPHA3	0.91682992	0.91682992	0.88463937	2.71829921
FLRT3	0.91850997	0.88976812	0.90916839	2.717446484
NRP1	0.91519592	0.90105434	0.90105434	2.71730459
UBE2H	0.92291215	0.87005024	0.92291215	2.715874538
NUP153	0.91541993	0.88496153	0.91541993	2.7158014
RAC1	0.90522439	0.90522439	0.90522439	2.715673169
SLC35D2	0.90796738	0.90796738	0.89971777	2.715652523
PCDH18	0.90516381	0.90516381	0.90516381	2.715491441
ZNF532	0.91409676	0.91409676	0.88648769	2.714681213
MAPRE1	0.91607912	0.8503963	0.9467581	2.713233519
GNPTAB	0.90512875	0.90512875	0.90274984	2.713007333
PALLD	0.90419777	0.90419777	0.90419777	2.712593308
DOCK3	0.92192103	0.86750137	0.92212769	2.711550093

Appendix 13: Combined integrative scores for top 200 MiRDIP predicted gene targets of miRs detected in the medium of ciGEnCs under both high glucose treatment conditions (25 mM glucose, 25 mM glucose + 10 ng/µl TNF-α), used for STRING analysis

Gene Name	Integrative score in each condition		Combined Integrative Score
	25mM	25mM + TNF- α	
COL1A2	0.9767808	0.976780797	1.953561594
HMGA2	0.97043628	0.964784584	1.935220863
KPNA4	0.95468574	0.973273816	1.927959553
MIER1	0.96216139	0.964208012	1.926369401
FBXW11	0.96059451	0.960594506	1.921189012
ARID3B	0.96244326	0.957287298	1.919730556
ONECUT1	0.95692517	0.956925168	1.913850337
FAM3C	0.95635408	0.956354082	1.912708164
ADD3	0.9562834	0.956283402	1.912566804
FMR1	0.95579937	0.955799374	1.911598748
FXR1	0.95538986	0.955389865	1.91077973
COL15A1	0.9541353	0.954135305	1.90827061
ACTN1	0.95397201	0.953972005	1.90794401
MAP4K3	0.95972466	0.947421063	1.90714572
NEDD4	0.95338173	0.953381726	1.906763452
CLIP1	0.95312455	0.95312455	1.9062491
CAPZA1	0.9529181	0.9529181	1.9058362
EIF4E	0.95260876	0.952608757	1.905217515
ACVR1	0.95022086	0.953724709	1.90394557
ATP1B1	0.93739068	0.966355469	1.903746152
RNF103	0.95175707	0.951757067	1.903514134
NR5A2	0.95148226	0.951482257	1.902964515
AGO4	0.94478163	0.957608758	1.902390384
ANK3	0.95036695	0.950366945	1.900733891
ELAVL1	0.94979532	0.949795322	1.899590644
KPNA3	0.9495237	0.949523704	1.899047408
NCOR2	0.94900567	0.949005673	1.898011346
AKAP1	0.94833857	0.948338565	1.896677131
QKI	0.95120429	0.94539444	1.896598729
ATXN1	0.94939196	0.946366782	1.895758746
RALBP1	0.94766879	0.947668792	1.895337583
TBPL1	0.94715716	0.947157156	1.894314313
SNX2	0.94631875	0.94647962	1.892798369
PBX3	0.95771519	0.935012229	1.892727414
KDM2A	0.94630514	0.946305137	1.892610274
TSC22D2	0.94617575	0.946175752	1.892351504
RNF38	0.94616175	0.946161746	1.892323493
RAB14	0.94583432	0.945834325	1.891668649
YBX3	0.94541548	0.945415483	1.890830967
FGF9	0.9452976	0.945297602	1.890595203

TOB1	0.94527134	0.945271336	1.890542672
ACVR2A	0.9327814	0.956929676	1.889711072
PPP3R1	0.94471419	0.944714186	1.889428372
SMARCA5	0.94393431	0.943934309	1.887868618
TLK1	0.93790921	0.949411658	1.887320867
GALNT3	0.9433774	0.943377403	1.886754806
EIF4G2	0.94365119	0.943069737	1.886720926
NAMPT	0.94317673	0.943176727	1.886353454
FOXO3	0.94317345	0.94317345	1.886346901
LRIG3	0.94803503	0.937801449	1.885836479
TNRC6A	0.94628011	0.938385352	1.88466546
SOCS5	0.94228805	0.942288055	1.884576109
AP3B1	0.94165958	0.941659575	1.88331915
CAMSAP2	0.94139262	0.941392622	1.882785244
VGLL4	0.94124393	0.941243926	1.882487853
MTSS1	0.94109962	0.941099623	1.882199246
SHANK2	0.94076198	0.940761976	1.881523951
SMARCAD1	0.94405909	0.937362848	1.881421943
YES1	0.9406225	0.940622503	1.881245006
KCNJ2	0.93054905	0.950577206	1.881126258
PAFAH1B1	0.91973034	0.960609305	1.880339642
NUMB	0.93998746	0.939987456	1.879974911
CHD4	0.93996161	0.939961613	1.879923225
ZFPM2	0.93958366	0.939583657	1.879167314
ACSL1	0.93941712	0.939417117	1.878834234
CUL3	0.91983409	0.958547651	1.878381743
MPHOSPH9	0.93870792	0.938707923	1.877415845
ARID1A	0.94533156	0.932068234	1.877399799
H3F3B	0.93812075	0.938120748	1.876241496
SP3	0.93789721	0.937897212	1.875794423
SMAD1	0.93773901	0.937739011	1.875478022
MYO1C	0.93734972	0.937349723	1.874699447
PUM2	0.93723356	0.937233561	1.874467122
FOXP1	0.93712523	0.937125229	1.874250457
ABRAXAS2	0.93711523	0.937115228	1.874230456
ZNF217	0.93709608	0.937096079	1.874192158
ZFC3H1	0.93701464	0.937014641	1.874029282
MITF	0.93677974	0.936779736	1.873559472
RET	0.93673983	0.936739826	1.873479651
STAM	0.93646736	0.936467361	1.872934722
KTN1	0.93644038	0.936440384	1.872880769
CTTN	0.93554427	0.935544274	1.871088549
UBE3C	0.93488072	0.934880725	1.86976145
SLC4A4	0.94082342	0.928662759	1.869486183
MBNL1	0.93443004	0.93443004	1.86886008
BMI1	0.9340911	0.934091099	1.868182199
CTCF	0.93034226	0.937267648	1.867609908

RDX	0.94010691	0.927445036	1.867551947
NAA15	0.9334624	0.933462398	1.866924796
FOXN3	0.93336458	0.933364584	1.866729168
IGF2BP3	0.94194381	0.924739924	1.866683731
PPP2R2A	0.93323993	0.933239926	1.866479851
SYNJ1	0.93887406	0.92705998	1.865934039
DDX6	0.9266681	0.93907419	1.865742286
ANO1	0.93285755	0.932857554	1.865715109
PAIP2	0.93243789	0.932437885	1.864875771
MTOR	0.93232794	0.932327936	1.864655872
RNF219	0.93187004	0.931870039	1.863740078
UBE2D1	0.93678428	0.926656312	1.863440591
SLC12A2	0.91619878	0.946797219	1.862996
MAPRE1	0.91607912	0.9467581	1.86283722
CREB1	0.93113974	0.931139738	1.862279476
BMPR2	0.9269145	0.935238737	1.862153242
INTS6	0.93093335	0.930933348	1.861866696
ACSL4	0.93081618	0.930816181	1.861632363
BACH2	0.9174413	0.944123466	1.861564762
CUL5	0.93023823	0.930238228	1.860476456
PDGFRB	0.93005533	0.930055332	1.860110663
ARID4B	0.92998871	0.929988706	1.859977411
SIK2	0.92986791	0.929867908	1.859735816
EPHA7	0.92942251	0.929422509	1.858845019
ELK3	0.92934546	0.929345458	1.858690915
SIRT1	0.92909107	0.929091074	1.858182148
DDX19B	0.93396827	0.923994455	1.857962725
PKP4	0.92893962	0.928939623	1.857879246
NPTN	0.92906484	0.928810927	1.857875765
CHD9	0.92887132	0.928871323	1.857742645
CCDC6	0.92873043	0.928730428	1.857460857
YWHAG	0.92862288	0.92862288	1.85724576
OSBPL3	0.90822864	0.948857377	1.857086022
CRIM1	0.92853366	0.928533661	1.857067322
SMAD7	0.89525944	0.96175949	1.857018927
PEX5L	0.9284787	0.928478702	1.856957404
USP15	0.90091932	0.956033698	1.856953013
ARHGAP12	0.92199645	0.933818118	1.855814572
PDGFC	0.9278362	0.927836203	1.855672406
MTHFD2	0.92766635	0.927666353	1.855332707
DYRK1A	0.93494362	0.91929719	1.854240814
HIPK1	0.9268478	0.926847796	1.853695591
TAF15	0.92670784	0.926707837	1.853415674
ZFYVE9	0.92264493	0.930504832	1.85314976
GOT1	0.92653281	0.926532805	1.853065611
MAP7	0.91533867	0.937695378	1.853034052
NACC2	0.90408174	0.948809664	1.852891401

FNDC3A	0.93431786	0.918358858	1.85267672
ACVR1C	0.92944217	0.923072947	1.852515118
CELF1	0.9260306	0.926030603	1.852061205
S1PR1	0.94420805	0.907479333	1.851687388
TRIM2	0.92572265	0.925722646	1.851445293
PAN3	0.92556122	0.925561223	1.851122446
PIEZO2	0.92552335	0.925523351	1.851046703
SNX16	0.92533949	0.925339487	1.850678974
HBP1	0.92497804	0.925643389	1.850621432
IRAK1	0.92509275	0.925092749	1.850185498
CCND2	0.92914423	0.921039908	1.850184141
PRDM2	0.93397661	0.91607122	1.850047826
SH3RF1	0.92471094	0.924710943	1.849421886
AP4E1	0.92449813	0.924498127	1.848996254
CCNJ	0.9345131	0.914150731	1.848663831
CAB39	0.90560001	0.942692444	1.848292457
SGMS1	0.92412614	0.924126138	1.848252275
RNF111	0.9240895	0.924089499	1.848178998
CDK17	0.92381996	0.923503607	1.847323568
HECTD2	0.92363494	0.92363494	1.847269879
CITED2	0.92354759	0.923547585	1.84709517
ARMC1	0.89653602	0.950503011	1.847039027
HNRNPU	0.89986293	0.947146955	1.847009888
PDGFRA	0.92330465	0.923304651	1.846609303
MCFD2	0.89546539	0.951044483	1.846509876
ST8SIA4	0.92316893	0.923168926	1.846337852
CDC34	0.92515676	0.920931114	1.84608787
ERBIN	0.92133258	0.92456334	1.84589592
UBE2H	0.92291215	0.922912151	1.845824302
EPHA4	0.92714837	0.918439755	1.845588125
LSM14A	0.92275557	0.922755566	1.845511132
MECOM	0.9227503	0.922750297	1.845500594
KLF5	0.92273627	0.922736267	1.845472533
HIVEP1	0.92272877	0.92272877	1.84545754
NMT2	0.92238038	0.92238038	1.844760759
CBFA2T3	0.9223712	0.922371201	1.844742402
CMPK1	0.91843959	0.925637442	1.844077031
DOCK3	0.92192103	0.922127695	1.844048722
RNF139	0.92193356	0.921933561	1.843867122
USP48	0.92112708	0.922667133	1.843794211
COIL	0.92822111	0.915450511	1.843671618
ULK2	0.92405205	0.919432944	1.843484999
FBXW2	0.92171254	0.921712538	1.843425076
SEC24C	0.89389157	0.949476537	1.843368105
RANBP2	0.92136019	0.921360189	1.842720379
SULF1	0.92135149	0.921351492	1.842702983
JAZF1	0.92106731	0.921067309	1.842134618

CD2AP	0.92084422	0.920844218	1.841688436
CLCN3	0.89992351	0.941458531	1.841382037
WDR47	0.92019178	0.92019178	1.84038356
IGF2BP2	0.92587966	0.914259349	1.84013901
CDV3	0.92749741	0.912548944	1.840046349
NAV3	0.91994895	0.919948951	1.839897901
AUH	0.91327889	0.926258606	1.839537498
MOB4	0.89920985	0.940236617	1.839446462
ATP2B1	0.92718241	0.911944493	1.8391269
NFIB	0.90849757	0.930178	1.838675573
OGT	0.883944	0.954353539	1.83829754
ARHGEF7	0.91882637	0.918826369	1.837652738
RAB1A	0.93641987	0.900522704	1.836942575
UBR3	0.91846983	0.918469829	1.836939657
C16orf70	0.91815617	0.918156172	1.836312343
RNF19A	0.91783925	0.917839247	1.835678493
RPS6KB1	0.93287041	0.902477716	1.835348129
SHC1	0.91760016	0.917600157	1.835200315
TCF20	0.91723164	0.917231642	1.834463284

Appendix 14: Combined integrative scores for top 200 MiRDIP predicted gene targets of miRs detected in the medium of ciGEnCs under both TNF- α treatment conditions (10 ng/µl TNF-α, 25 mM glucose + 10 ng/µl TNF-α), used for STRING analysis

Gene Name	Integrative score in each condition		Combined Integrative Score
	5mM + TNF- α	25mM + TNF- α	
COL1A2	0.9767808	0.9767808	1.953561594
HMGA2	0.97043628	0.96478458	1.935220863
KPNA4	0.95320948	0.97327382	1.926483301
FBXW11	0.96059451	0.96059451	1.921189012
ARID3B	0.96244326	0.9572873	1.919730556
ONECUT1	0.95692517	0.95692517	1.913850337
ADD3	0.9562834	0.9562834	1.912566804
FMR1	0.95579937	0.95579937	1.911598748
FXR1	0.95538986	0.95538986	1.91077973
COL15A1	0.9541353	0.9541353	1.90827061
MAP4K3	0.95972466	0.94742106	1.90714572
NEDD4	0.95338173	0.95338173	1.906763452
CUL3	0.94732903	0.95854765	1.905876679
CAPZA1	0.9529181	0.9529181	1.9058362
EIF4E	0.95260876	0.95260876	1.905217515
ATP1B1	0.93739068	0.96635547	1.903746152
NR5A2	0.95148226	0.95148226	1.902964515
ANK3	0.95036695	0.95036695	1.900733891
ELAVL1	0.94979532	0.94979532	1.899590644
KPNA3	0.9495237	0.9495237	1.899047408
TBPL1	0.94715716	0.94715716	1.894314313
ATXN1	0.94785036	0.94636678	1.894217141
PBX3	0.95771519	0.93501223	1.892727414
TSC22D2	0.94617575	0.94617575	1.892351504
RAB14	0.94583432	0.94583432	1.891668649
YBX3	0.94541548	0.94541548	1.890830967
QKI	0.94539444	0.94539444	1.89078888
FGF9	0.9452976	0.9452976	1.890595203
PPP3R1	0.94471419	0.94471419	1.889428372
TLK1	0.93790921	0.94941166	1.887320867
GALNT3	0.9433774	0.9433774	1.886754806
NAMPT	0.94317673	0.94317673	1.886353454
FOXO3	0.94317345	0.94317345	1.886346901
LRIG3	0.94803503	0.93780145	1.885836479
SOCS5	0.94228805	0.94228805	1.884576109
AP3B1	0.94165958	0.94165958	1.88331915
CAMSAP2	0.94139262	0.94139262	1.882785244
MTSS1	0.94109962	0.94109962	1.882199246
SMARCAD1	0.94405909	0.93736285	1.881421943
YES1	0.9406225	0.9406225	1.881245006
KCNJ2	0.93054905	0.95057721	1.881126258

PAFAH1B1	0.91973034	0.96060931	1.880339642
NUMB	0.93998746	0.93998746	1.879974911
CHD4	0.9398499	0.93996161	1.879811508
VGLL4	0.93845014	0.94124393	1.879694063
EIF4G2	0.93631057	0.94306974	1.879380305
USP15	0.92315588	0.9560337	1.879189576
TOB1	0.93244505	0.94527134	1.877716391
LRP6	0.92928585	0.94777552	1.877061373
SP3	0.93789721	0.93789721	1.875794423
SMAD1	0.93773901	0.93773901	1.875478022
ZEB2	0.95925504	0.91588498	1.875140018
MYO1C	0.93734972	0.93734972	1.874699447
FOXP1	0.93712523	0.93712523	1.874250457
ZFC3H1	0.93701464	0.93701464	1.874029282
MITF	0.93677974	0.93677974	1.873559472
STAM	0.93646736	0.93646736	1.872934722
KTN1	0.93644038	0.93644038	1.872880769
CTTN	0.93554427	0.93554427	1.871088549
UBE3C	0.93488072	0.93488072	1.86976145
SLC4A4	0.94082342	0.92866276	1.869486183
ACVR1	0.91465499	0.95372471	1.868379699
RDX	0.94010691	0.92744504	1.867551947
ACVR2A	0.91011153	0.95692968	1.86704121
NAA15	0.9334624	0.9334624	1.866924796
FOXN3	0.93336458	0.93336458	1.866729168
IGF2BP3	0.94194381	0.92473992	1.866683731
ANO1	0.93285755	0.93285755	1.865715109
PAIP2	0.93243789	0.93243789	1.864875771
ARID1A	0.93206823	0.93206823	1.864136469
CREB1	0.93113974	0.93113974	1.862279476
INTS6	0.93093335	0.93093335	1.861866696
BACH2	0.9174413	0.94412347	1.861564762
CUL5	0.93023823	0.93023823	1.860476456
PDGFRB	0.93005533	0.93005533	1.860110663
PID1	0.91078698	0.94856524	1.859352221
EPHA7	0.92942251	0.92942251	1.858845019
BTRC	0.90247708	0.9562754	1.858752483
SIRT1	0.92909107	0.92909107	1.858182148
DDX19B	0.93396827	0.92399446	1.857962725
YWHAG	0.92862288	0.92862288	1.85724576
OSBPL3	0.90822864	0.94885738	1.857086022
CRIM1	0.92853366	0.92853366	1.857067322
SMAD7	0.89525944	0.96175949	1.857018927
DYNC1I1	0.91531402	0.94155739	1.856871413
PDGFC	0.9278362	0.9278362	1.855672406
MTHFD2	0.92766635	0.92766635	1.855332707
DYRK1A	0.93494362	0.91929719	1.854240814

HIPK1	0.9268478	0.9268478	1.853695591
TAF15	0.92670784	0.92670784	1.853415674
GOT1	0.92653281	0.92653281	1.853065611
MAP7	0.91533867	0.93769538	1.853034052
FNDC3A	0.93431786	0.91835886	1.85267672
ACVR1C	0.92944217	0.92307295	1.852515118
FGF2	0.87963848	0.97279405	1.852432528
CELF1	0.9260306	0.9260306	1.852061205
STXBP3	0.8984876	0.95325846	1.851746056
TRIM2	0.92572265	0.92572265	1.851445293
MIER1	0.88717127	0.96420801	1.85137928
PPM1D	0.90688059	0.94415987	1.851040451
SNX16	0.92533949	0.92533949	1.850678974
MBNL1	0.915815	0.93443004	1.850245041
CCND2	0.92914423	0.92103991	1.850184141
PRDM2	0.93397661	0.91607122	1.850047826
PDCD4	0.89602885	0.95363547	1.849664322
PPP2R2A	0.91591618	0.93323993	1.849156101
AP4E1	0.92449813	0.92449813	1.848996254
CCNJ	0.9345131	0.91415073	1.848663831
CAB39	0.90560001	0.94269244	1.848292457
SGMS1	0.92412614	0.92412614	1.848252275
RNF111	0.9240895	0.9240895	1.848178998
SYNJ1	0.92047662	0.92705998	1.847536601
CITED2	0.92354759	0.92354759	1.84709517
ARMC1	0.89653602	0.95050301	1.847039027
HNRNPU	0.89986293	0.94714696	1.847009888
DR1	0.95822499	0.88824868	1.846473673
CDC34	0.92515676	0.92093111	1.84608787
ERBIN	0.92133258	0.92456334	1.84589592
KIF1B	0.8932721	0.95251816	1.845790267
EPHA4	0.92714837	0.91843976	1.845588125
LSM14A	0.92275557	0.92275557	1.845511132
KLF5	0.92273627	0.92273627	1.845472533
CBFA2T3	0.9223712	0.9223712	1.844742402
ST8SIA4	0.92099245	0.92316893	1.844161372
COIL	0.92822111	0.91545051	1.843671618
ULK2	0.92405205	0.91943294	1.843484999
FBXW2	0.92171254	0.92171254	1.843425076
RANBP2	0.92136019	0.92136019	1.842720379
JAZF1	0.92106731	0.92106731	1.842134618
CDK17	0.91861678	0.92350361	1.842120383
CD2AP	0.92084422	0.92084422	1.841688436
WDR47	0.92019178	0.92019178	1.84038356
IGF2BP2	0.92587966	0.91425935	1.84013901
CDV3	0.92749741	0.91254894	1.840046349
ZFPM2	0.90033583	0.93958366	1.839919484

AGO4	0.88219383	0.95760876	1.839802584
AXIN2	0.88879031	0.95098964	1.839779947
AUH	0.91327889	0.92625861	1.839537498
TFRC	0.9454147	0.89288426	1.838298961
ARHGEF7	0.91882637	0.91882637	1.837652738
RARB	0.91330127	0.9233698	1.836671075
RNF19A	0.91783925	0.91783925	1.835678493
SHC1	0.91760016	0.91760016	1.835200315
CHD9	0.90552518	0.92887132	1.834396501
FAF2	0.91695351	0.91695351	1.833907021
BCL2	0.91678017	0.91678017	1.83356034
CCDC6	0.90412649	0.92873043	1.832856921
N4BP1	0.89465012	0.93792442	1.832574534
ANK2	0.91628342	0.91628342	1.832566844
CLIP1	0.87928559	0.95312455	1.832410138
CSDE1	0.90404689	0.92801994	1.832066822
ELAVL2	0.94113153	0.88989771	1.83102924
SEC24C	0.88141067	0.94947654	1.830887212
RNF38	0.8840958	0.94616175	1.830257547
ARPC1A	0.91509945	0.91509945	1.830198905
TRPM7	0.9148895	0.9148895	1.829779003
EIF5	0.91442615	0.91528075	1.829706897
DNAJC13	0.92612197	0.9033877	1.829509676
GPR63	0.8739314	0.95527076	1.82920216
USP25	0.89177407	0.93737085	1.829144924
CCNE1	0.87076626	0.95836378	1.829130044
VCL	0.91452344	0.91452344	1.829046873
TRIB2	0.87439471	0.95448632	1.828881029
CUL2	0.88245059	0.94558689	1.82803748
ERG	0.91388097	0.91388097	1.827761932
SLC10A3	0.91290258	0.91290258	1.825805153
LIN28A	0.91284967	0.91284967	1.825699335
MOB4	0.88539844	0.94023662	1.825635056
UBE3A	0.92620561	0.89940139	1.825606997
PHLDB2	0.91253546	0.91253546	1.825070916
STK38L	0.91246808	0.91246808	1.824936153
MYB	0.88466775	0.94013507	1.824802818
JMJD1C	0.91239909	0.91239909	1.824798187
DDX6	0.88545389	0.93907419	1.824528078
PCMT1	0.91316369	0.91108889	1.824252588
ACTR2	0.8848548	0.93894273	1.823797527
SLC20A2	0.91008796	0.91275246	1.822840423
IGF1R	0.91123894	0.91123894	1.822477889
ISL1	0.91087461	0.91087461	1.821749226
ZC3H15	0.91048333	0.91048333	1.820966666
PRKACB	0.91028242	0.91028242	1.820564842
MAGI1	0.9102254	0.9102254	1.820450793

ZNF217	0.883322	0.93709608	1.820418079
JAG1	0.87182281	0.94785495	1.819677758
SGK1	0.89636502	0.9226721	1.819037118
MAP2K1	0.89086523	0.92816116	1.819026393
SRPK1	0.90898982	0.90898982	1.817979631
EPS8	0.9089838	0.908798	1.817781808
NR3C2	0.90882714	0.90882714	1.817654287
ZBTB5	0.90098668	0.91598624	1.816972918
FAM13C	0.90785813	0.90785813	1.815716253
TCF12	0.92550074	0.88939994	1.814900683
RAB10	0.8885846	0.92611113	1.814695737
NFIB	0.88416557	0.930178	1.814343565
CADM1	0.90676793	0.90676793	1.813535867
KIAA1217	0.90641993	0.90641993	1.81283987
COPS2	0.89192517	0.92078691	1.812712076
CCSER2	0.90630752	0.90630752	1.812615045
NDST2	0.91459476	0.89792439	1.812519154
WDR37	0.90972988	0.90196891	1.81169879

Appendix 15: Tree map of biological process GO terms functionally enriched within the predicted gene list associated with differentially expressed cellular miRs in ciGEnCs under all three treatment conditions (25mM glucose, 5mM glucose + 10 ng/mL TNF-α, and 25mM glucose + 10 ng/mL TNF-α).

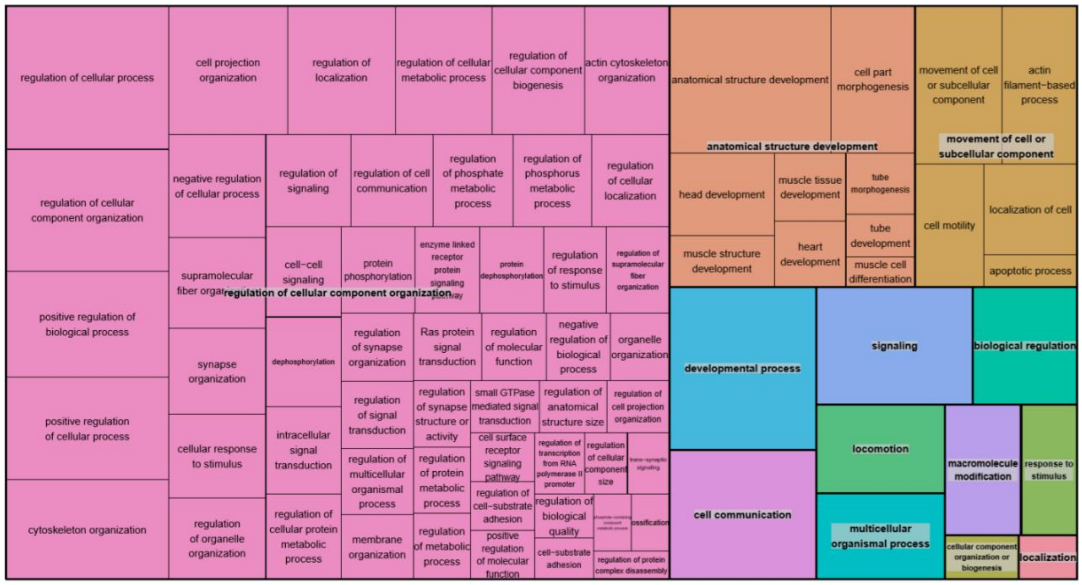

Appendix 16: Tree map of cellular component GO terms functionally enriched within the predicted gene list associated with differentially expressed cellular miRs in ciGEnCs under all three treatment conditions (25mM glucose, 5mM glucose + 10 ng/mL TNF-α, and 25mM glucose + 10 ng/mL TNF-α).

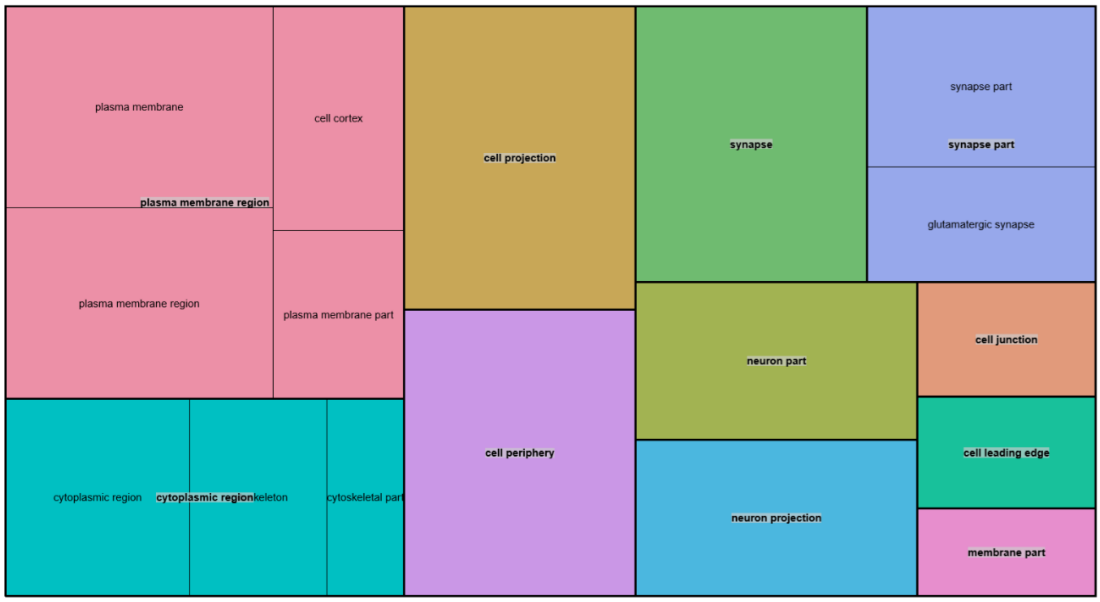

Appendix 17: Tree map of molecular function GO terms functionally enriched within the predicted gene list associated with differentially expressed cellular miRs in ciGEnCs under all three treatment conditions (25mM glucose, 5mM glucose + 10 ng/mL TNF-α, and 25mM glucose + 10 ng/mL TNF-α).

Appendix 18: Tree map of biological process GO terms functionally enriched within the predicted gene list associated with differentially expressed cellular miRs in ciGEnCs under both the 25mM glucose, and 25mM glucose + 10 ng/mL TNF-α treatment conditions.

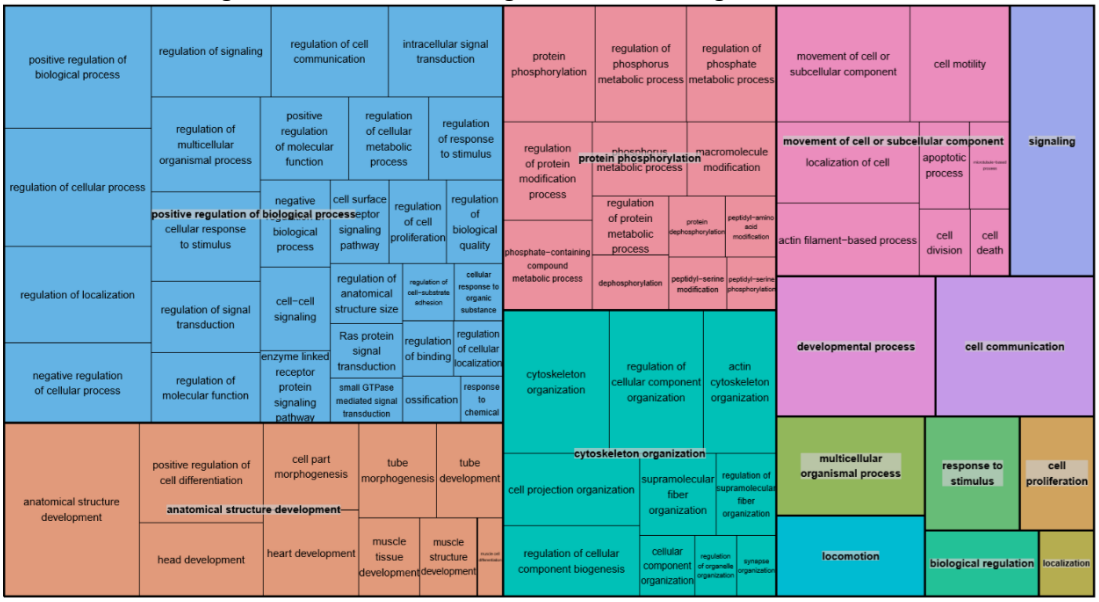

Appendix 19: Tree map of cellular component GO terms functionally enriched within the predicted gene list associated with differentially expressed cellular miRs in ciGEnCs under both the 25mM glucose, and 25mM glucose + 10 ng/mL TNF-α treatment conditions.

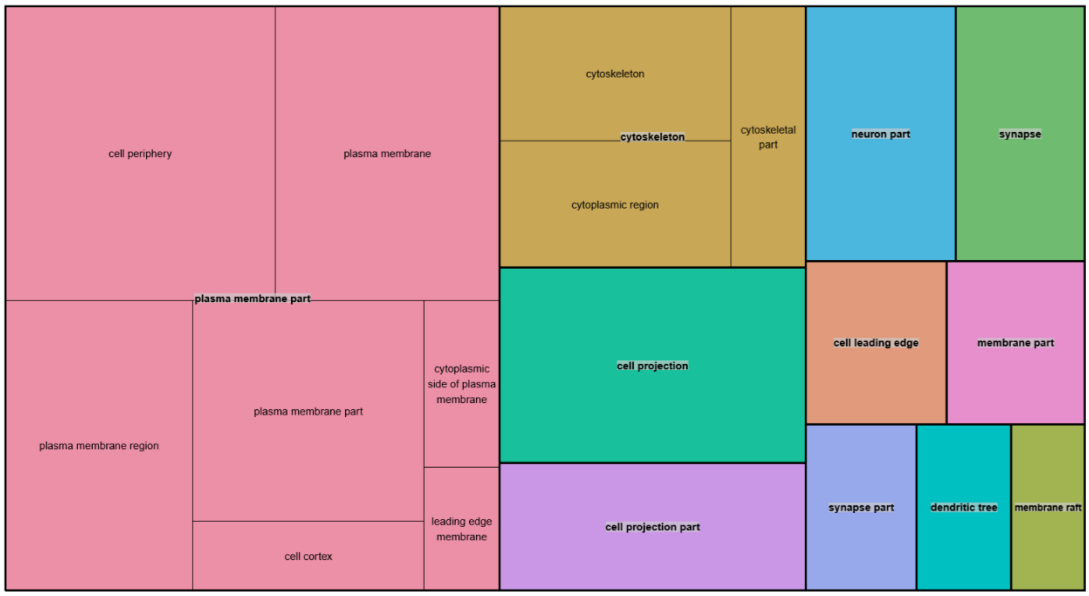

Appendix 20: Tree map of molecular function GO terms functionally enriched within the predicted gene list associated with differentially expressed cellular miRs in ciGEnCs under both the 25mM glucose, and 25mM glucose + 10 ng/mL TNF-α treatment conditions.

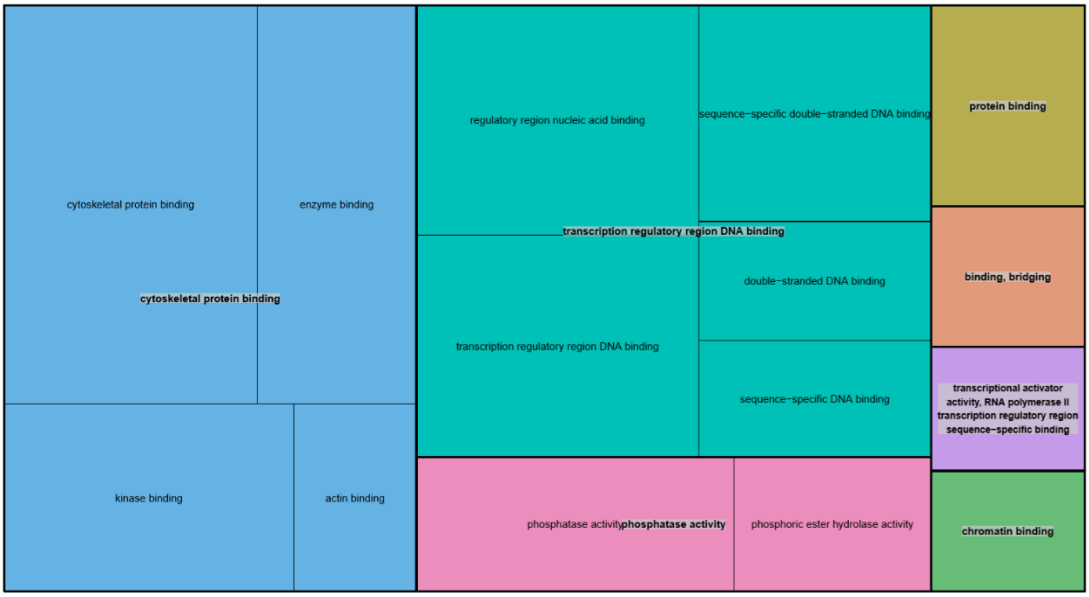

Appendix 21: Tree map of biological process GO terms functionally enriched within the predicted gene list associated with differentially expressed cellular miRs in ciGEnCs under both the 5mM glucose + 10 ng/mL TNF-α, and 25mM glucose + 10 ng/mL TNF-α treatment conditions.

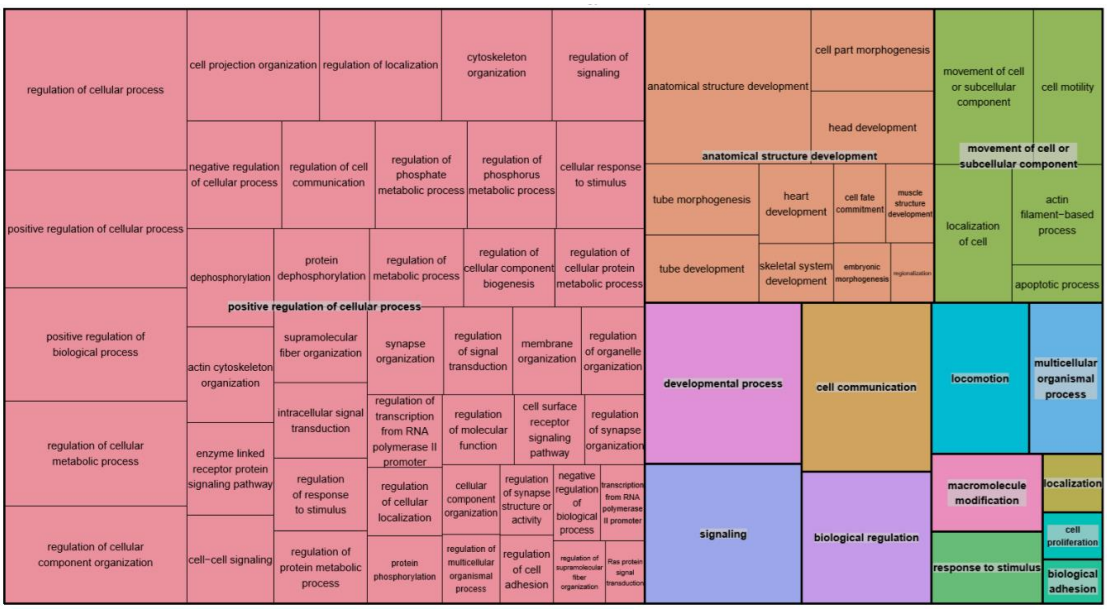

Appendix 22: Tree map of cellular component GO terms functionally enriched within the predicted gene list associated with differentially expressed cellular miRs in ciGEnCs under both the 5mM glucose + 10 ng/mL TNF-α, and 25mM glucose + 10 ng/mL TNF-α treatment conditions.

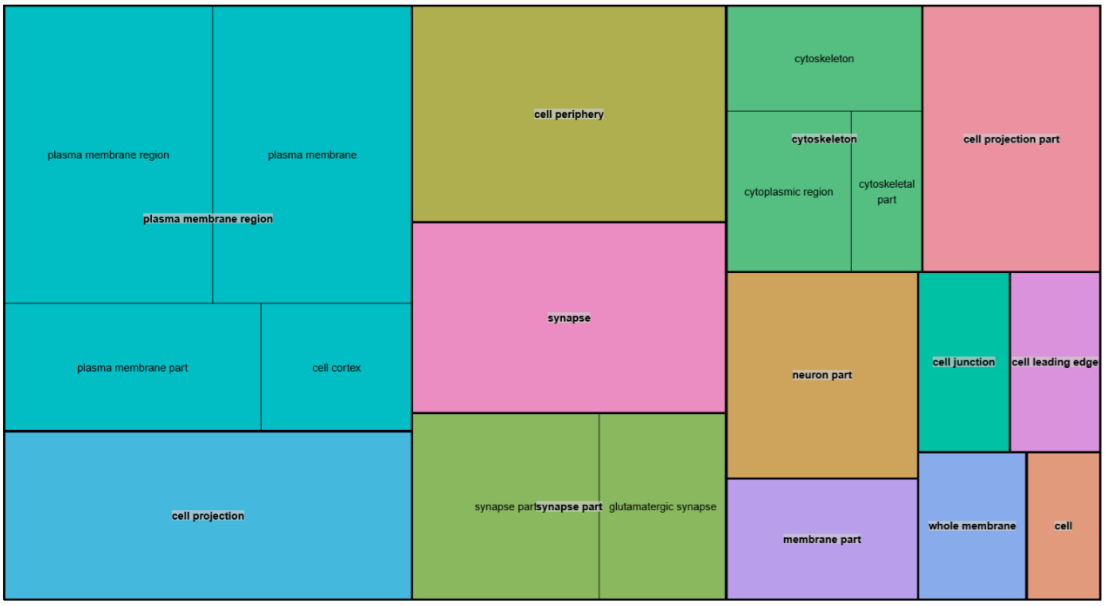

Appendix 23: Tree map of molecular function GO terms functionally enriched within the predicted gene list associated with differentially expressed cellular miRs in ciGEnCs under both the 5mM glucose + 10 ng/mL TNF-α, and 25mM glucose + 10 ng/mL TNF-α treatment conditions.

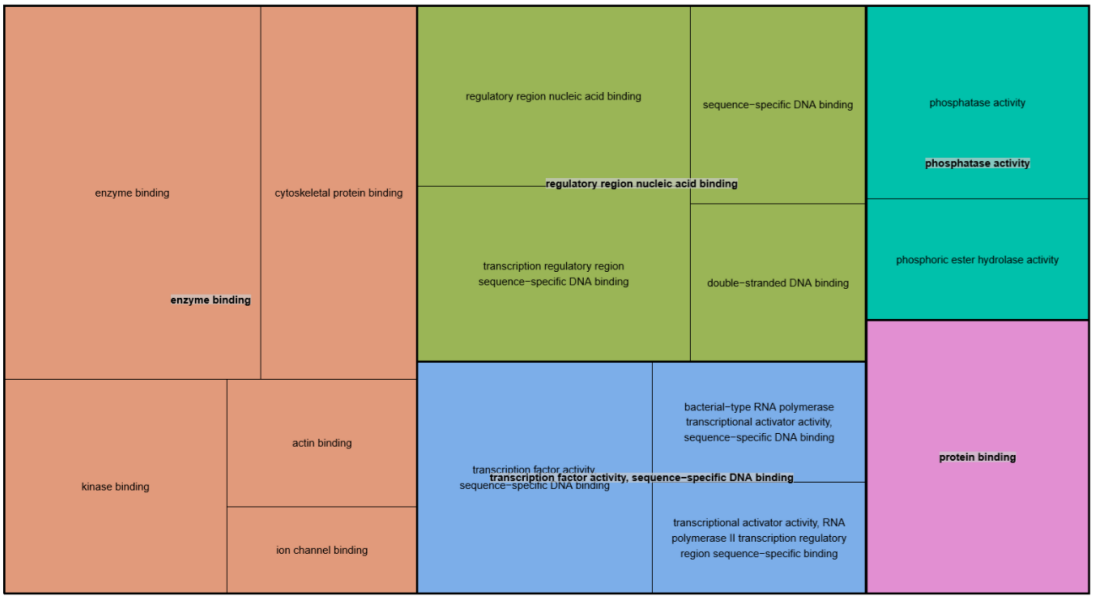

Appendix 24: Tree map of biological process GO terms functionally enriched within the predicted gene list associated with differentially expressed cellular miRs in ciGEnCs under the 25mM glucose + 10 ng/mL TNF-α treatment condition.

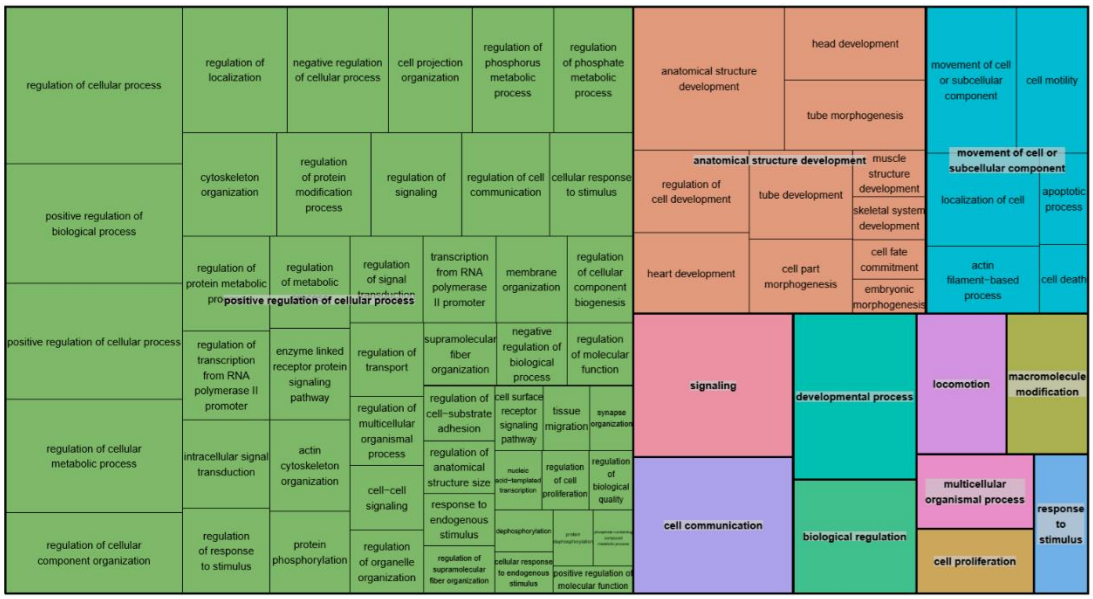

Appendix 25: Tree map of cellular component GO terms functionally enriched within the predicted gene list associated with differentially expressed cellular miRs in ciGEnCs under the 25mM glucose + 10 ng/mL TNF-α treatment condition

Appendix 26: Tree map of molecular function GO terms functionally enriched within the predicted gene list associated with differentially expressed cellular miRs in ciGEnCs under the 25mM glucose + 10 ng/mL TNF-α treatment condition.

Appendix 27: Tree map of biological process GO terms functionally enriched within the predicted gene list associated with differentially expressed cellular miRs in ciGEnCs under the 25mM glucose treatment condition.

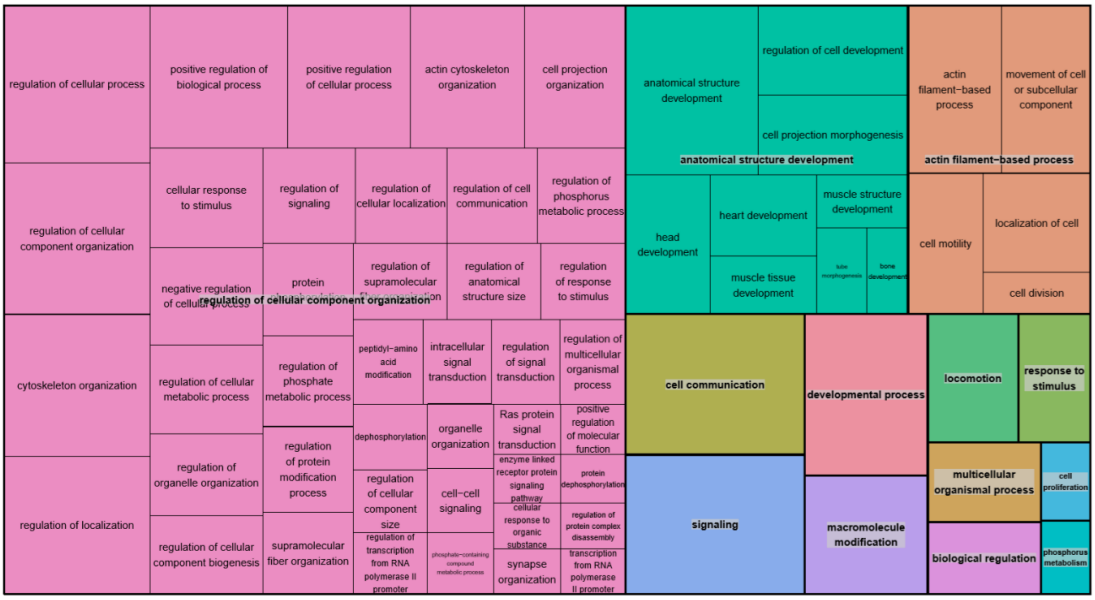

Appendix 28: Tree map of cellular component GO terms functionally enriched within the predicted gene list associated with differentially expressed cellular miRs in ciGEnCs under the 25mM glucose treatment condition.

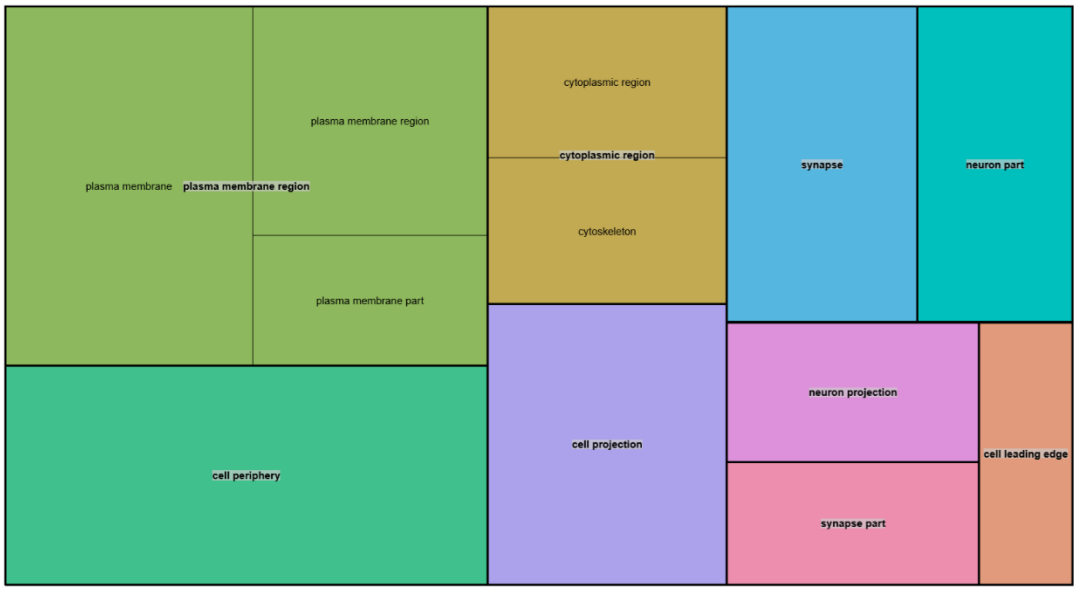

Appendix 29: Tree map of molecular function GO terms functionally enriched within the predicted gene list associated with differentially expressed cellular miRs in ciGEnCs under the 25mM glucose treatment condition.

Appendix 30: Tree map of biological process GO terms functionally enriched within the predicted gene list associated with differentially expressed cellular miRs in ciGEnCs under the 5mM glucose + 10 ng/mL TNF-α treatment condition.

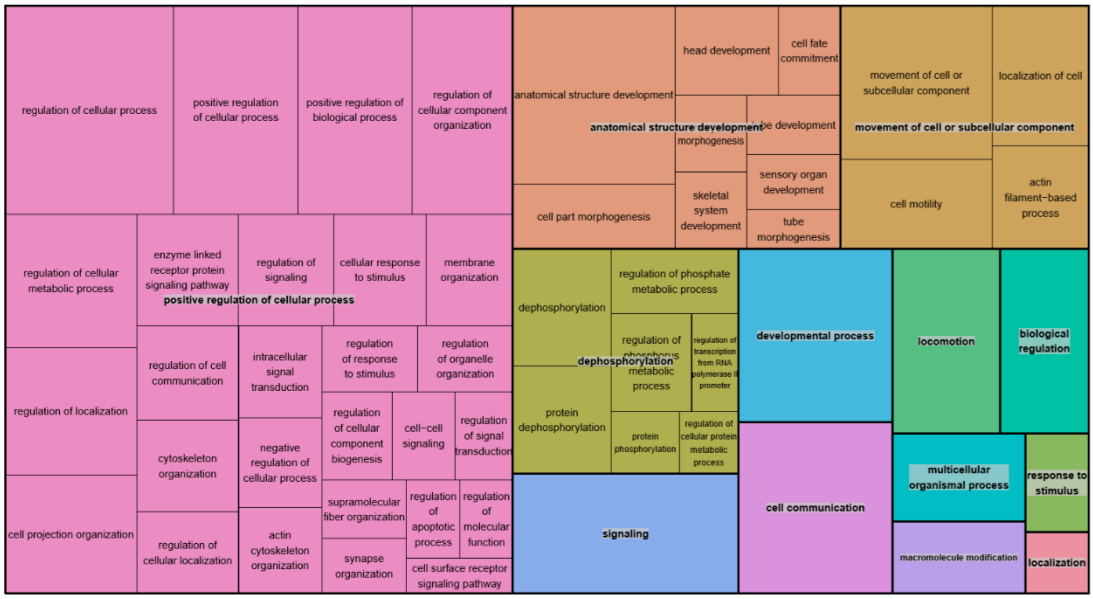

Appendix 31: Tree map of cellular component GO terms functionally enriched within the predicted gene list associated with differentially expressed cellular miRs in ciGEnCs under the 5mM glucose + 10 ng/mL TNF-α treatment condition.

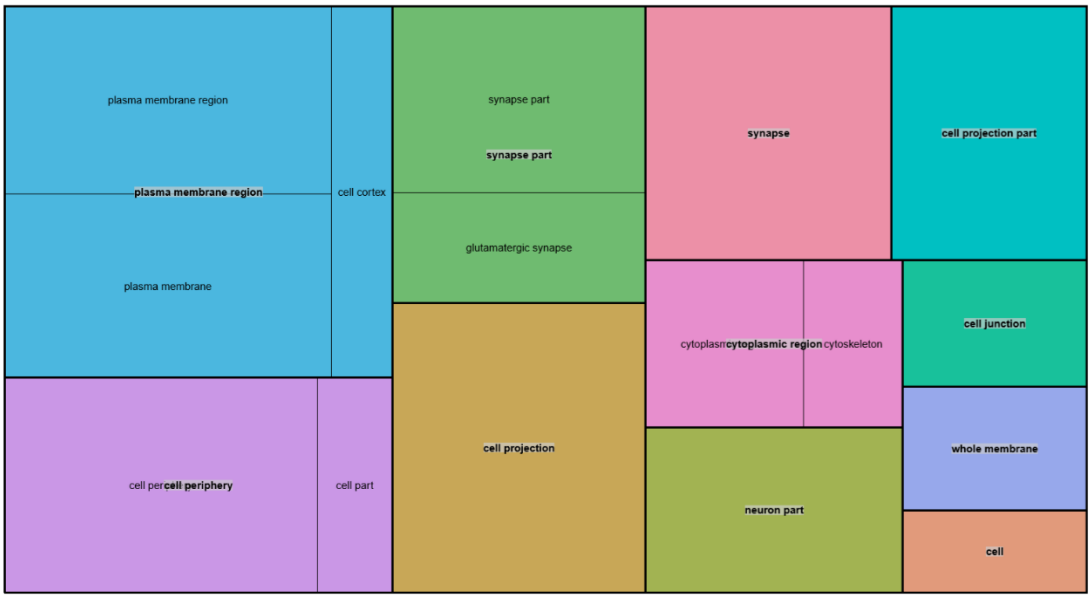

Appendix 32: Tree map of molecular function GO terms functionally enriched within the predicted gene list associated with differentially expressed cellular miRs in ciGEnCs under the 5mM glucose + 10 ng/mL TNF-α treatment condition.

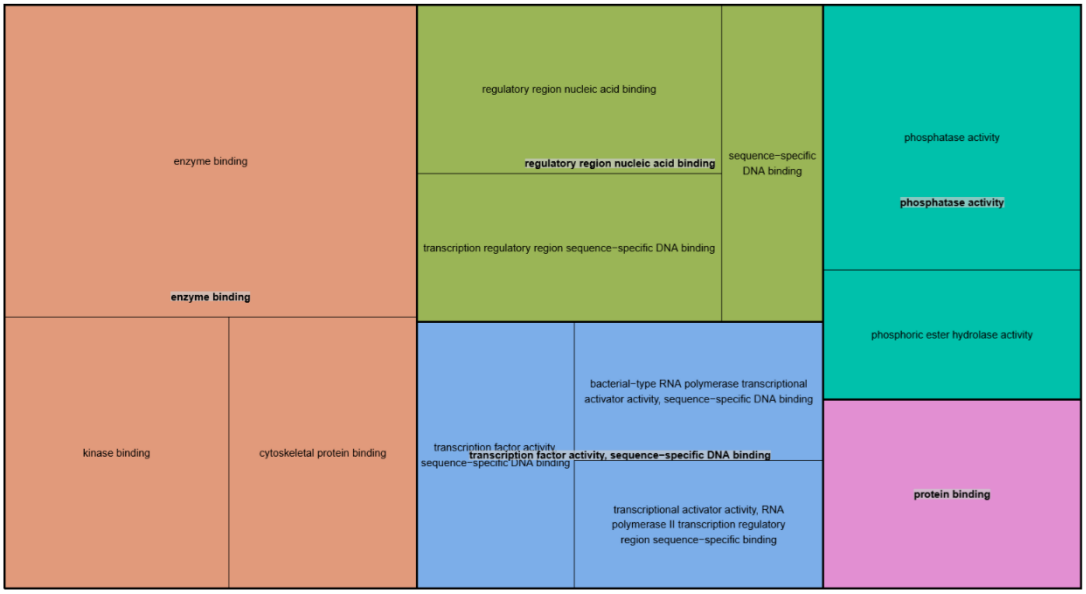

Appendix 33: Tree map of biological process GO terms functionally enriched within the predicted gene list associated with differentially expressed extracellular miRs in ciGEnC medium under all three treatment conditions (25mM glucose, 5mM glucose + 10 ng/mL TNF-α, and 25mM glucose + 10 ng/mL TNF-α).

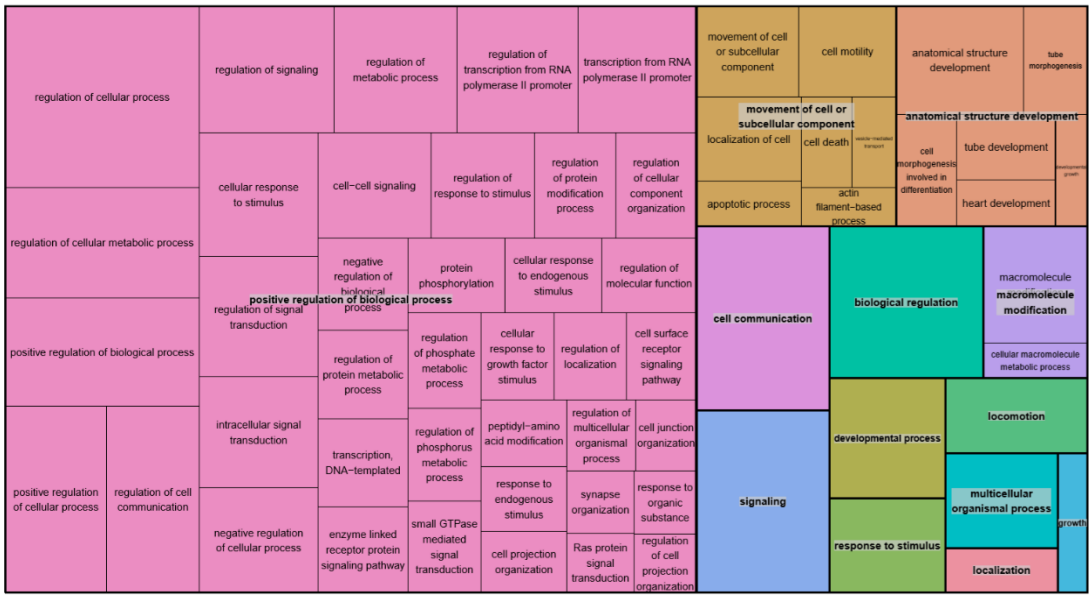

Appendix 34: Tree map of cellular component GO terms functionally enriched within the predicted gene list associated with differentially expressed extracellular miRs in ciGEnC medium under all three treatment conditions (25mM glucose, 5mM glucose + 10 ng/mL TNF-α, and 25mM glucose + 10 ng/mL TNF-α).

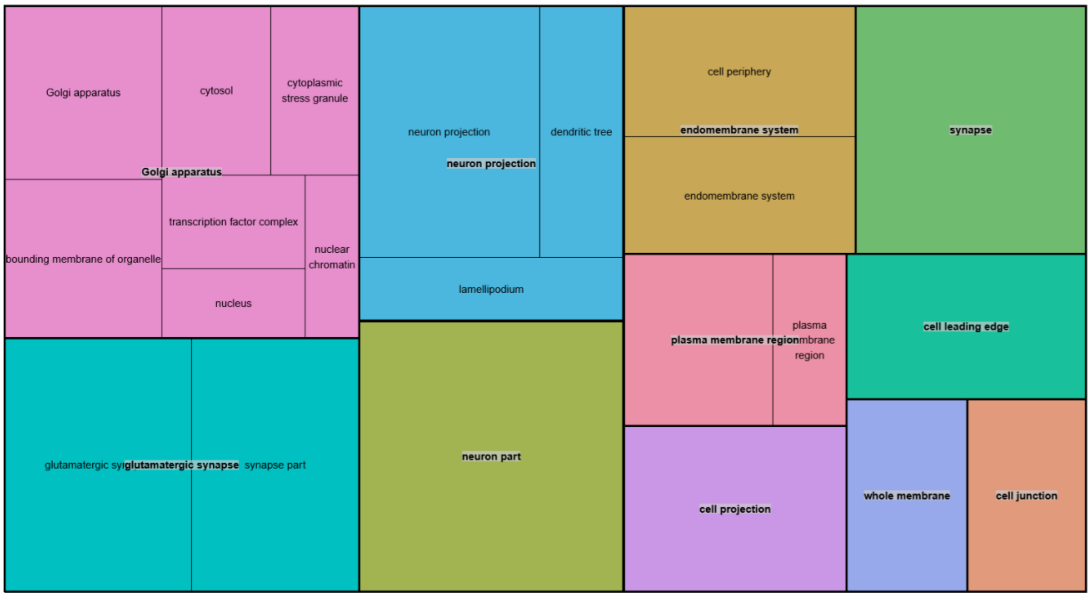

Appendix 35: Tree map of molecular function GO terms functionally enriched within the predicted gene list associated with differentially expressed extracellular miRs in ciGEnC medium under all three treatment conditions (25mM glucose, 5mM glucose + 10 ng/mL TNF-α, and 25mM glucose + 10 ng/mL TNF-α).

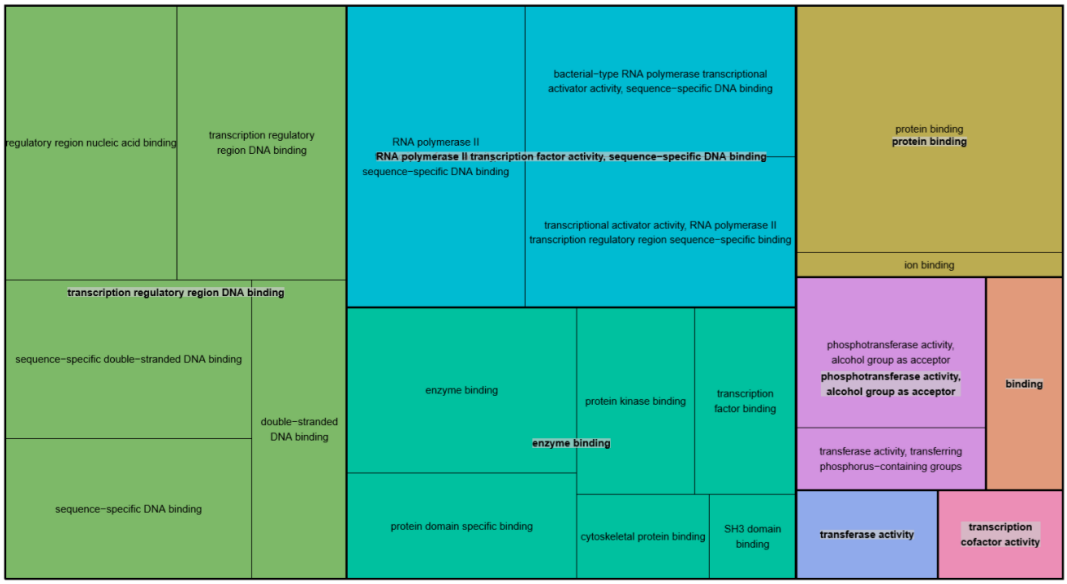

Appendix 36: Tree map of biological process GO terms functionally enriched within the predicted gene list associated with differentially expressed extracellular miRs in ciGEnC medium under both the 25mM glucose, and 25mM glucose + 10 ng/mL TNF-α treatment conditions.

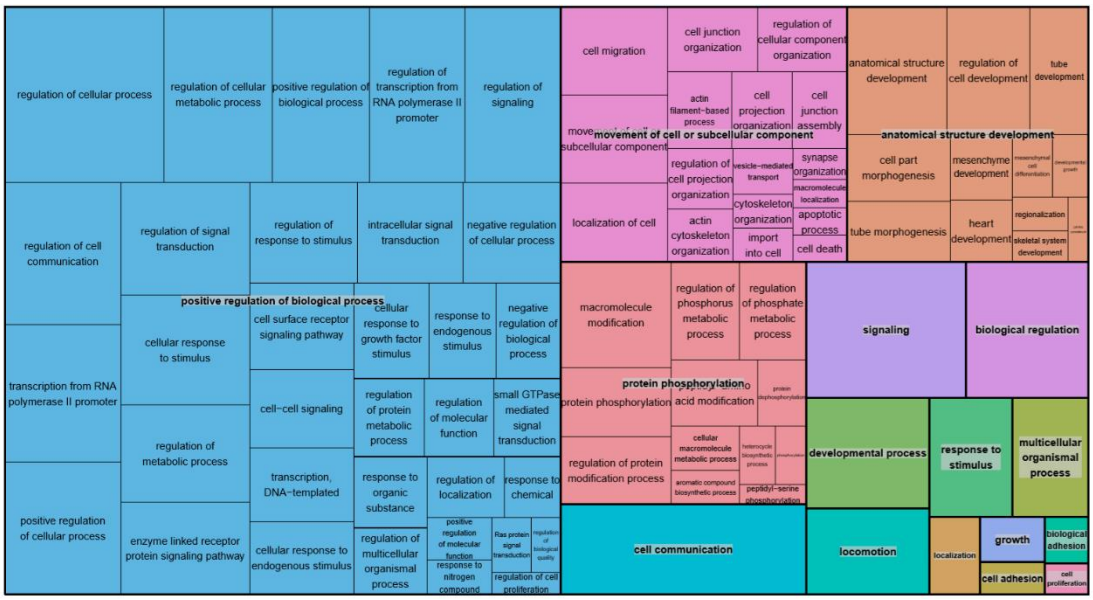

Appendix 37: Tree map of cellular component GO terms functionally enriched within the predicted gene list associated with differentially expressed extracellular miRs in ciGEnC medium under both the 25mM glucose, and 25mM glucose + 10 ng/mL TNF-α treatment conditions.

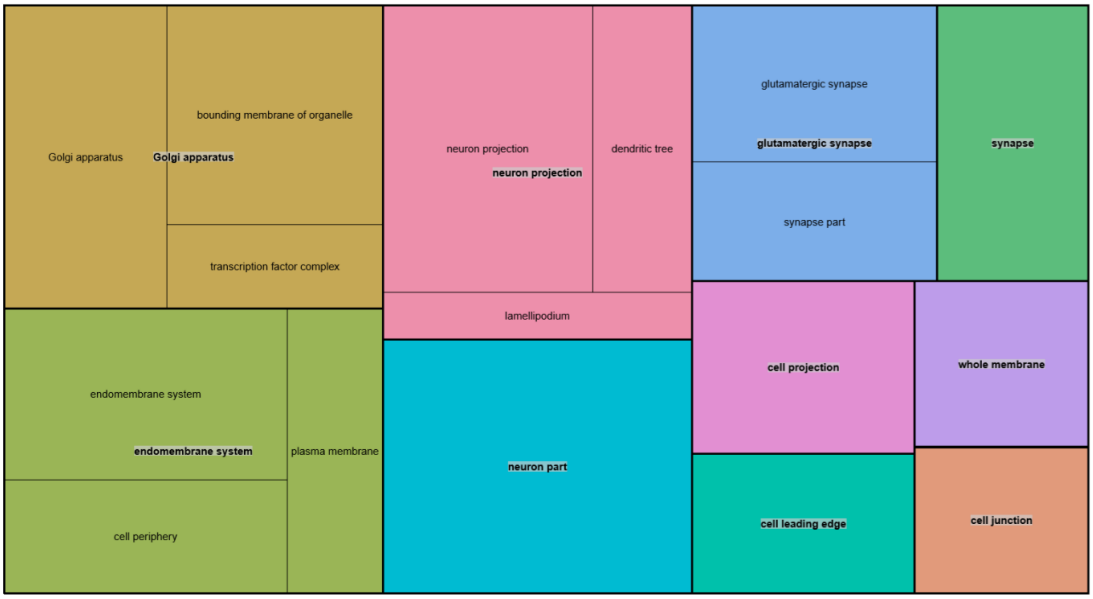

Appendix 38: Tree map of molecular function GO terms functionally enriched within the predicted gene list associated with differentially expressed extracellular miRs in ciGEnC medium under both the 25mM glucose, and 25mM glucose + 10 ng/mL TNF-α treatment conditions.

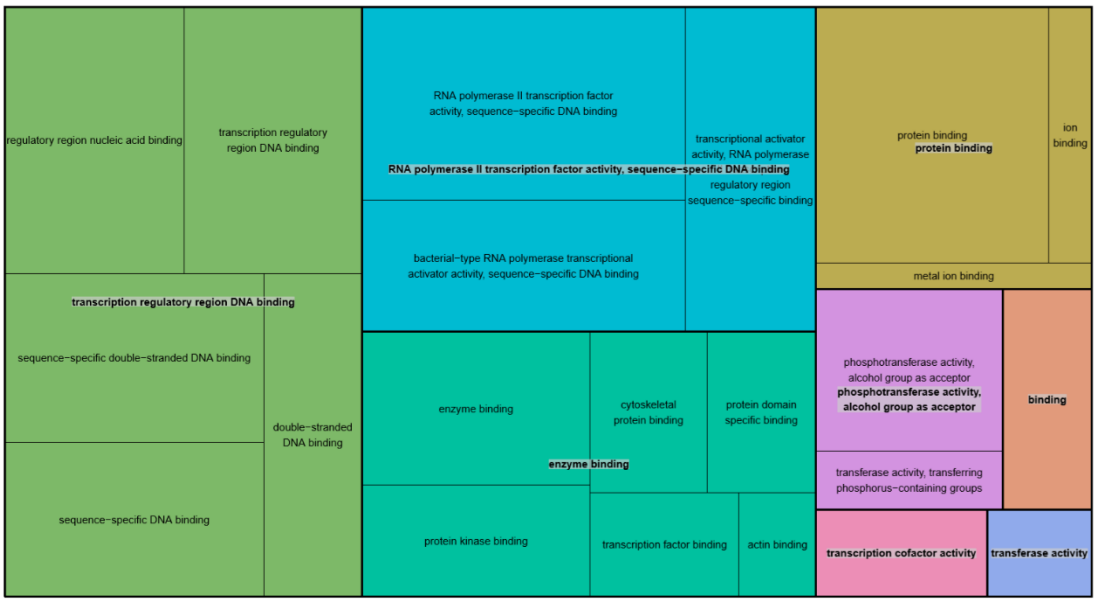

Appendix 39: Tree map of biological process GO terms functionally enriched within the predicted gene list associated with differentially expressed extracellular miRs in ciGEnC medium under both the 5mM glucose + 10 ng/mL TNF-α, and 25mM glucose + 10 ng/mL TNF-α treatment conditions.

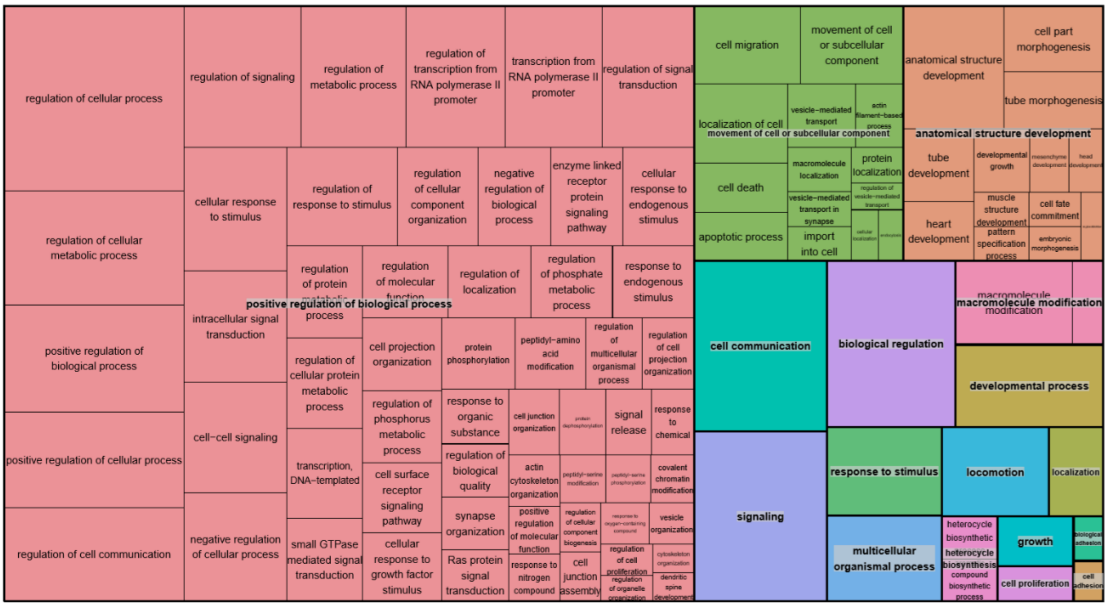

Appendix 40: Tree map of cellular component GO terms functionally enriched within the predicted gene list associated with differentially expressed extracellular miRs in ciGEnC medium under both the 5mM glucose + 10 ng/mL TNF-α, and 25mM glucose + 10 ng/mL TNF-α treatment conditions.

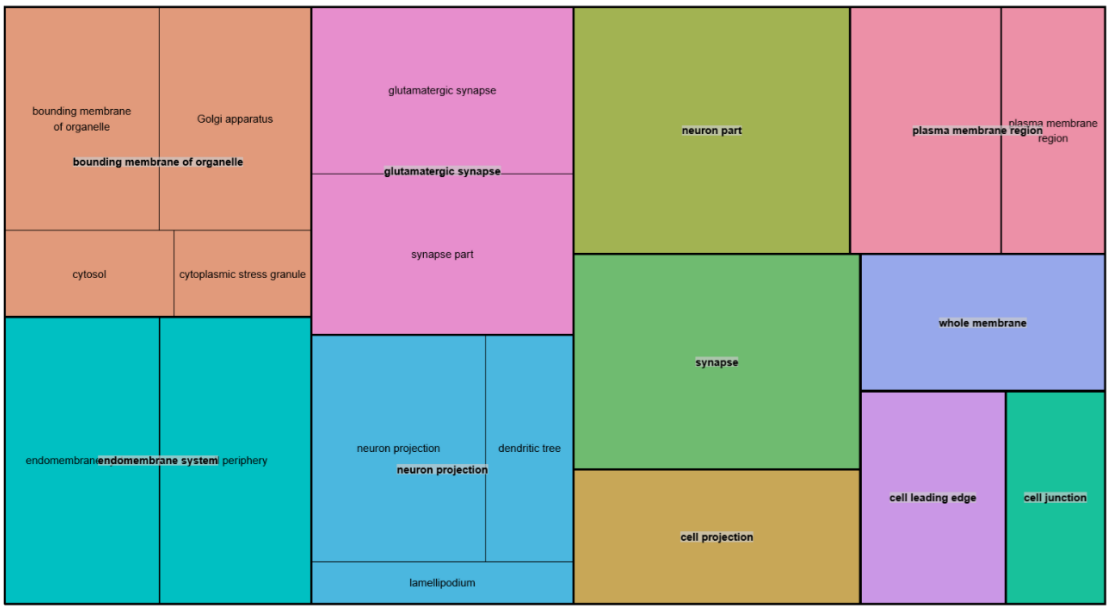

Appendix 41: Tree map of molecular function GO terms functionally enriched within the predicted gene list associated with differentially expressed extracellular miRs in ciGEnC medium under both the 5mM glucose + 10 ng/mL TNF-α, and 25mM glucose + 10 ng/mL TNF-α treatment conditions.

Appendix 42: Tree map of biological process GO terms functionally enriched within the predicted gene list associated with differentially expressed extracellular miRs in ciGEnC medium under the 25mM glucose + 10 ng/mL TNF-α cell treatment condition.

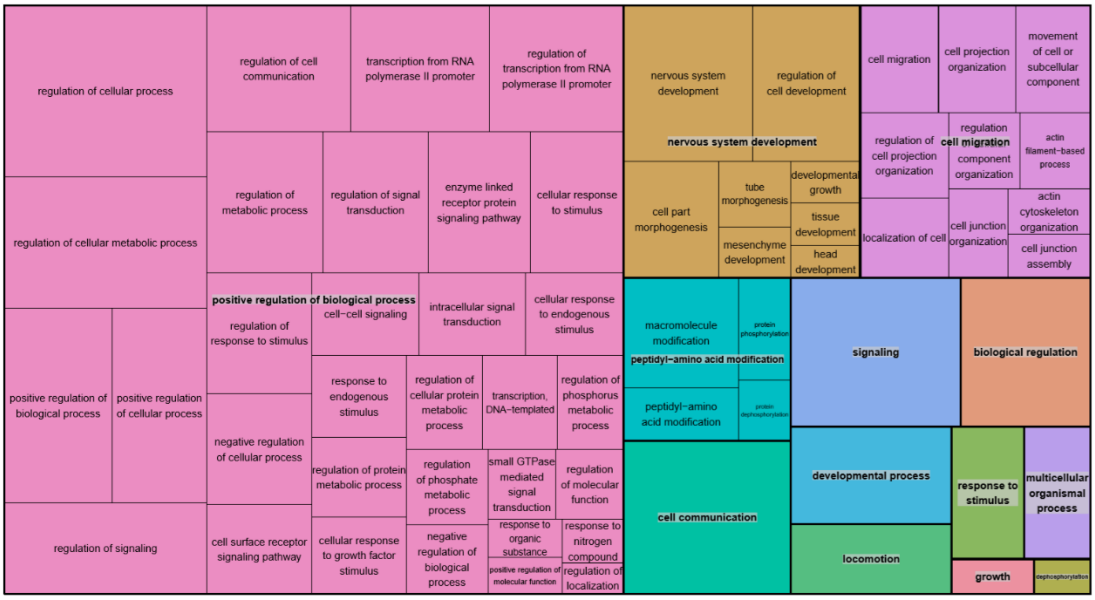

Appendix 43: Tree map of cellular component GO terms functionally enriched within the predicted gene list associated with differentially expressed extracellular miRs in ciGEnC medium under the 25mM glucose + 10 ng/mL TNF-α cell treatment condition.

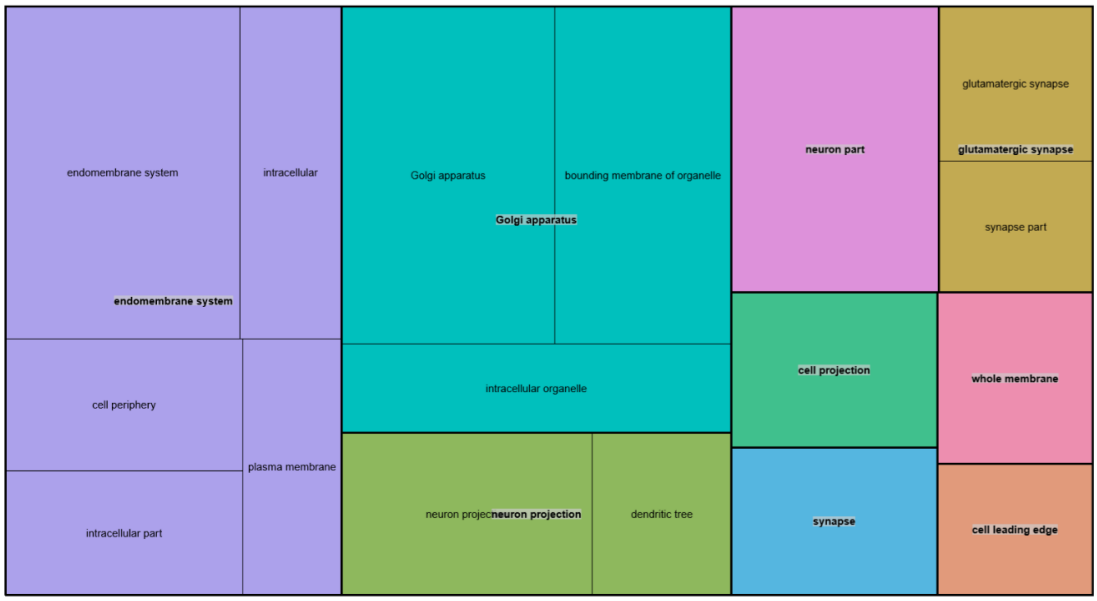

Appendix 44: Tree map of molecular function GO terms functionally enriched within the predicted gene list associated with differentially expressed extracellular miRs in ciGEnC medium under the 25mM glucose + 10 ng/mL TNF-α cell treatment condition.

Appendix 45: Tree map of biological process GO terms functionally enriched within the predicted gene list associated with differentially expressed extracellular miRs in ciGEnC medium under the 25mM glucose cell treatment condition.

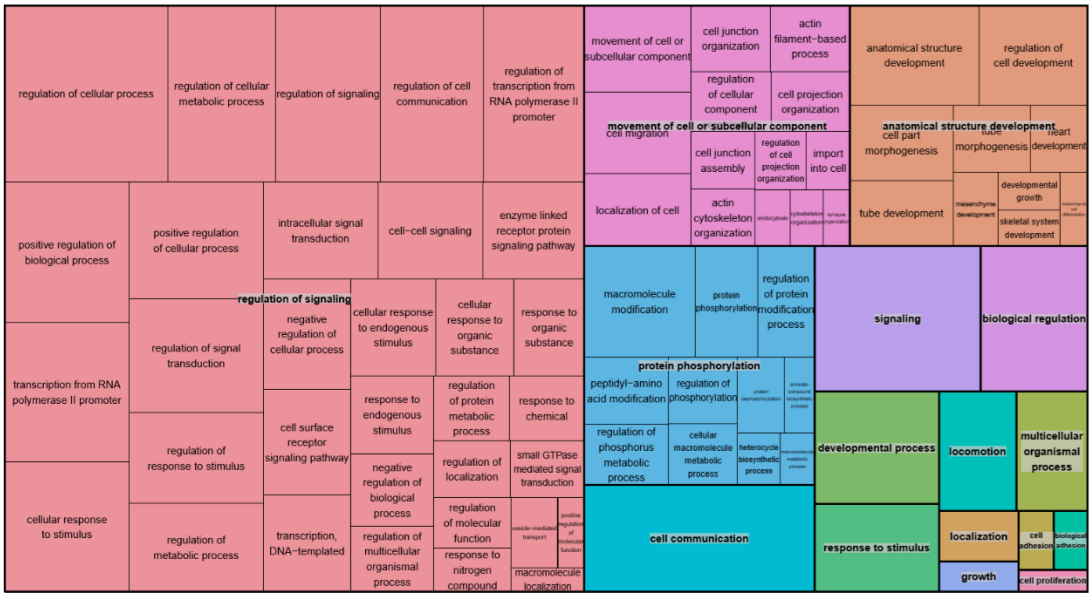

Appendix 46: Tree map of cellular component GO terms functionally enriched within the predicted gene list associated with differentially expressed extracellular miRs in ciGEnC medium under the 25mM glucose cell treatment condition.

Appendix 47: Tree map of molecular function GO terms functionally enriched within the predicted gene list associated with differentially expressed extracellular miRs in ciGEnC medium under the 25mM glucose cell treatment condition.

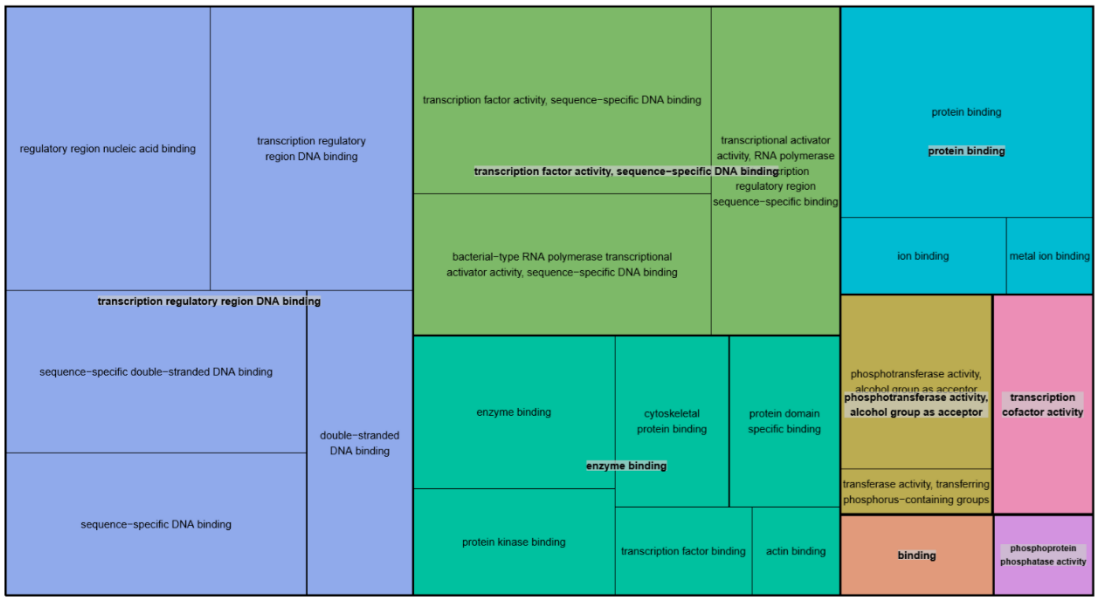

Appendix 48: Tree map of biological process GO terms functionally enriched within the predicted gene list associated with differentially expressed extracellular miRs in ciGEnC medium under the 5mM glucose + 10 ng/mL TNF-α cell treatment condition.

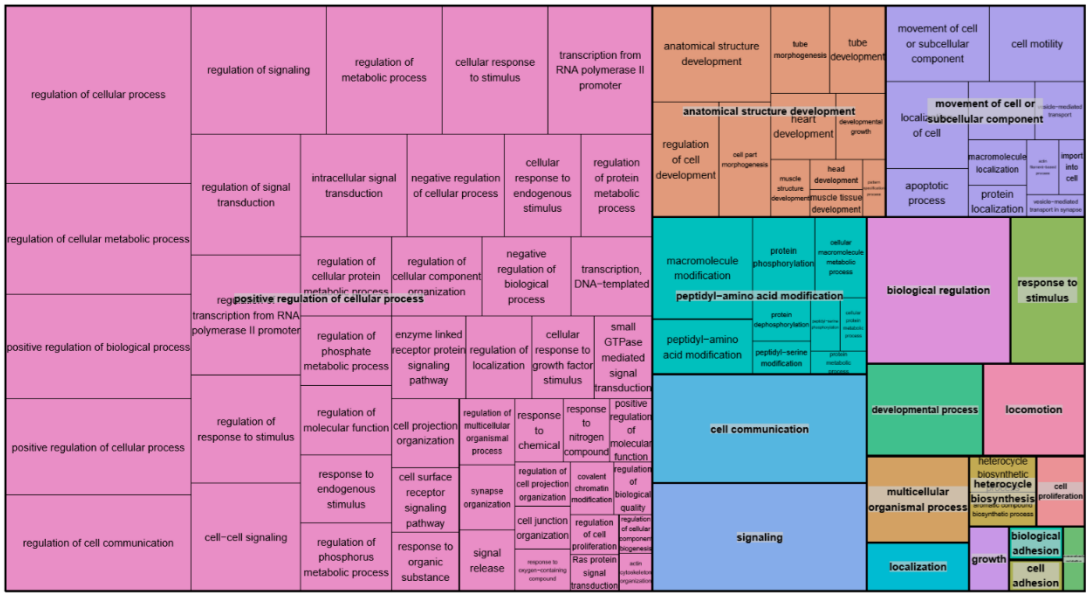

Appendix 49: Tree map of cellular component GO terms functionally enriched within the predicted gene list associated with differentially expressed extracellular miRs in ciGEnC medium under the 5mM glucose + 10 ng/mL TNF-α cell treatment condition.

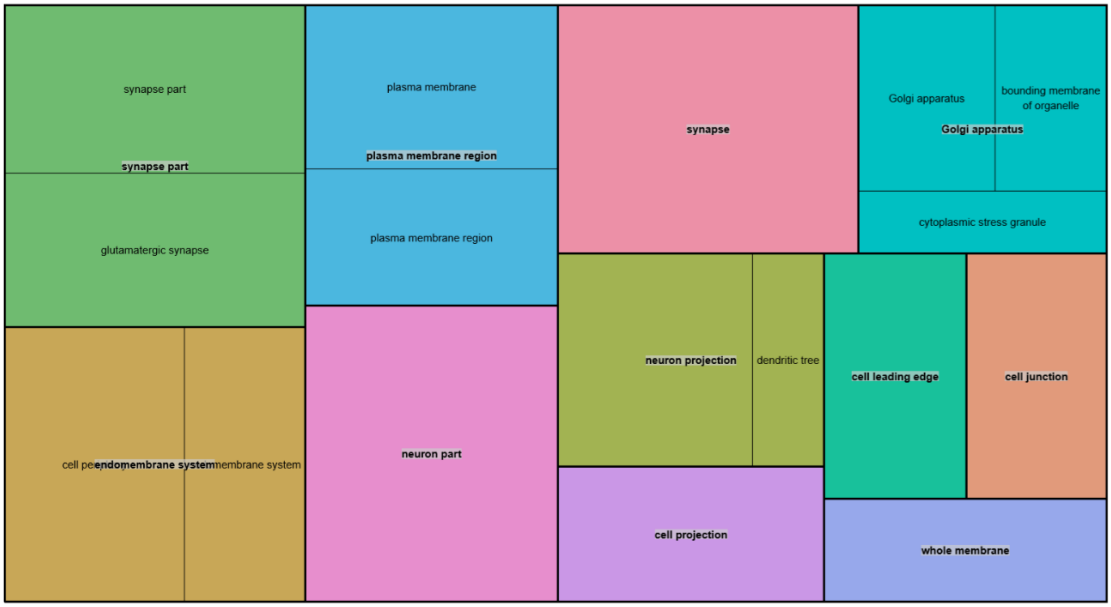

Appendix 50: Tree map of molecular function GO terms functionally enriched within the predicted gene list associated with differentially expressed extracellular miRs in ciGEnC medium under the 5mM glucose + 10 ng/mL TNF-α cell treatment condition.